

In-vitromodellering van de linkerhelft van het hart

In-Vitro Modelling of the Left Heart

Benjamin Van Der Smissen

Promotoren: prof. dr. ir. P. Segers, prof. dr. ir. P. Van Ransbeeck
Proefschrift ingediend tot het behalen van de graad van
Doctor in de industriële wetenschappen: industrieel ontwerpen

Vakgroep Elektronica en Informatiesystemen
Voorzitter: prof. dr. ir. R. Van de Walle
Faculteit Ingenieurswetenschappen en Architectuur
Academiejaar 2015 - 2016



ISBN 978-90-8578-913-0
NUR 964
Wettelijk depot: D/2016/10.500/45

Supervisors:

Prof. dr. ir. Patrick Segers Faculty of Engineering and Architecture, UGent
Prof. dr. ir. Peter Van Ransbeeck Faculty of Science and Technology, HoGent

Research lab:

Institute Biomedical Technology (IBiTech)
Biofluid, Tissue and Solid Mechanics for Medical Applications (bioMMeda)
Ghent University
De Pintelaan 185 - Blok B
B-9000 Gent
BELGIUM

Members of the exam committee:

Chairman:

Prof. dr. ir. Rik Van de Walle Faculty of Engineering and Architecture, UGent

Secretary:

Prof. dr. ir. Tom Claessens Faculty of Engineering and Architecture, UGent

Reading committee:

Prof. dr. ir. Marcel Rutten Dept. of Biomedical Engineering, TU Eindhoven
Prof. dr. ir. Pieter Vandervoort Faculty of Medicine and Life Sciences, UHasselt
Dr. ir. Peter Verschueren Materialise, Leuven
Prof. dr. ing. Jelle Saldien Faculty of Engineering and Architecture, UGent

Other members:

Prof. dr. ir. Pascal Verdonck Faculty of Engineering and Architecture, UGent
Prof. dr. ir. Marc Vanhaelst Faculty of Engineering and Architecture, UGent

This research was funded by the University College Ghent.

Dankwoord

Dit proefschrift was niet mogelijk geweest zonder de inbreng van velen. Mijn dank gaat dan ook uit naar al degenen die zowel van dichtbij als van op afstand een bijdrage leverden aan het tot stand komen van dit werk.

Op de eerste plaats wil ik mijn promotor prof. Patrick Segers bedanken voor zijn gedreven, bemoedigende en leerrijke begeleiding doorheen de verschillende fasen van dit project. Bedankt voor alle kansen die ik kreeg, de vrijheid om dit project een eigen invulling te geven, de aanbreng van nieuwe ideeën en waardevolle suggesties, de motiverende en constructieve feedback en, niet in het minst, het nauwgezet nalezen van alle teksten. Uw deur stond steeds voor me open (letterlijk) en als ik langs kwam, nam u steeds ruim de tijd. Ik heb bijzonder veel van u geleerd en vind het een eer om met u te mogen samenwerken.

Ook mijn promotor van de Hogeschool Gent, Peter Van Ransbeeck: enorm bedankt voor uw steun en om steeds in mij te (blijven) geloven. Naast uw promotorschap bent u er ook steeds als een vriend geweest waar ik steeds op kon rekenen, in het bijzonder ook tijdens de finale fase van dit proefschrift. Ik herinner me nog het eerste telefoongesprek waarin u me warm maakte om op de Hogeschool te komen werken en een doctoraat te beginnen. We hebben doorheen de jaren een heel kostbare samenwerking én vriendschap opgebouwd en ik hoop van ganser harte dat we dit nog vele jaren kunnen verderzetten.

Ook prof. Pascal Verdonck wil ik hartelijk danken om mij de gelegenheid te geven om te doctoreren en om me steeds weer uit te dagen om grenzen te verleggen. Ook wil ik u specifiek danken voor het aanbrengen van dit intrigerende en relevante onderwerp van het modelleren van de mitralisklep en voor de wijze raad op het juiste moment.

Prof. Marc Vanhaelst en Marc Wouters wil ik bijzonder bedanken om me zowel de tijd en ruimte te geven, als ook de steun om te doctoreren en de opleiding te volgen tot burgerlijk ingenieur biomedische ingenieurstechnieken. Daniel Vanhercke, hartelijk dank voor uw diepe en praktische kennis over de mitralisklep waardoor ik concreet aan de slag kon gaan. Ook dank aan prof. Damien Coisne voor het duiden op de juiste draairichting van de torsiemodellen in een vroege fase van dit project ☺. Ook prof. Guido Van Nooten en prof. Filip De Somer wil ik bedanken voor het bijwonen van experimenten en om te wijzen op de relevantie van mitralisklepmoedellering. Prof. Joris De Grieck en Dr. Frank Dewaele, bedankt voor uw verfrissende ideeën rond (composiet)materialen. Prof. Tom Claessens, dank u wel voor uw nuchtere en doordachte opmerkingen. Mathias

Vermeulen, bedankt voor het meebouwen aan modellen en het mee begeleiden van thesisstudenten. Ook dank aan Jurgen Deviche voor de tips & tricks bij het verwerken van siliconen en het aansluiten van specifieke druksensoren. Ten slotte, gaat mijn dank ook in het bijzonder uit naar David Mester (voormalig CEO van ViVitro, Victoria, British Colombia) voor zijn concreet advies over de noden in de markt van linkerharthelftmodellen.

Mijn thesisstudenten (Ben, Ruben, Jo, Mathias, Ludo, Arend, Johny, Isabelle, Alexander, Lieselot, Nicolas, Joren en Laurens) wil ik bedanken voor de fijne samenwerking en hun bijdrage aan mijn project. Verder dank ik mijn collega's van BioMMeda, IBiTech (Abigail, Bram, Benedict, Charlotte, David, Denis, Dieter, Dries, Francesco, Frederic, Gianluca, Guillermo, Guy, Hicham, Iris, Jan, Joris, Koen, Liesbeth, Lieve & Seba, Luis, Matthieu, Michele, Mirco, Nic, Peter, Rado, Sander, Saskia, Sofie, Sunny, Thomas, Tomas en Wouter) voor de aangename sfeer en voor de leuke gesprekken. Mijn dank gaat ook uit naar mijn collega's van de vroegere INWE vakgroep mechanica (Annemieke, Antoine, Armand, Cédric, Charles, Christian, Kim, Frederic, Frank, Jan, Guy, Ingrid, Luc, Ludwig en Marc) als ook naar mijn huidige collega's van de FNT vakgroep mechatronica (Caroline, Frank, Hilde, Hubert, Johan, Koen, Luc, Marianne, Mathias, Mandy, Mauricette, Marieke, Michel, Patrick, Patrick, Peter, Philippe, Piet, Stefan, Ruddy, Tom, Wim, Veerle, Yvan, Yves en Yves) voor hun steun, interesse en betrokkenheid. Een speciaal woord van dank ook aan Muriel Vervaeke en Veerle Delrue, decanaatsmedewerkers FEA, voor het supersonisch in orde brengen van mijn dossier.

Aan al onze vrienden en familie, geloof me, er is een (sociaal) leven na het finaliseren van dit doctoraat! Peter, Gina, Monique, Nelly, Albert, Dina, Gudrun, Matthieu, Dries, Marieke, Paul, Iris, Tim, An, Tim, Gerlinde, Chris, David, jullie horen tot de club van de allergrootste supporters voor het afwerken van dit doctoraat ☺. Ook speciale dank aan de vele babysitters-vrienden tijdens de eindspurt: Evi, Stefan, Cindy, Stefan, Naomi, Bart, Sara, Eefje, Yves, Manu, Nele, Dirk en Els. Ook mijn (schoon)broers en (schoon)zussen wil ik danken voor hun betrokkenheid. Mijn grootste dank gaat uit naar mijn hemelse Vader, die me leidt en keer op keer moed en de nodige kracht geeft.

Mama, bedankt voor uw bemoedigende teksten en de hulp en zorg voor onze kids. Moma en bopa, bedankt dat onze kapoenen ook bij jullie mochten komen spelen en logeren. Jullie zijn schatten! Bedankt voor jullie gebed, steun en voorbeeld!

Hoeveel werk en tijd ik ook gestoken heb in het maken van harten binnen dit doctoraat, het resultaat blijft nog steeds een sterke vereenvoudiging van de werkelijkheid. Wat blijft het een hemelsbreed verschil met de vier ‘echte’ hartjes die ik mocht helpen realiseren tijdens dit doctoraatstraject. Ruben, Bram, Anna en Baby, jullie zijn het mooiste geschenk dat ik ooit mocht ontvangen en ik ben zo dankbaar voor jullie!

Saartje, ik herinner me de woorden van het liedje van onze openingsdans 10 jaar geleden (Everything About You, Darlene Zschech). Hoewel de woorden van het liedje dezelfde zijn gebleven, heeft de betekenis een diepere dementie – oeps, dat is voor nu nog niet, ik bedoelde dimensie ☺ - gekregen. Op dat moment zongen we van wat we droomden, maar nu kunnen we ook zien wat al uitgekomen is. Want schat, jij realiseert het bijna onmogelijke in deze uitdagende en intense periode van ons leven (You'd catch a falling star if I asked you), jij geeft al wat je bent, elke dag, en maakt het leven mooi, elke dag. Ik hou gewoon helemaal van wie je bent. Jij was en bent voor mij onmisbaar, niet in het minst bij het realiseren van deze hartmodellen en het schrijven van dit proefschrift, of bij het zorgen voor onze vier ‘echte’ hartjes ☺.

Saartje, Ruben, Bram, Anna en Baby, ik kijk uit om meer van onze tijd en harten met elkaar te delen, en dat zal nu makkelijker zijn na deze laatste zin van dit proefschrift ☺.

Benjamin Van Der Smissen, April 2016

“Above all else, guard your heart,
for everything you do flows from it.”

King Solomon, ca. 900 B.C.

Samenvatting

INLEIDING

Hart- en vaatziekten vormen wereldwijd een van de belangrijkste doodsoorzaken. In het bestuderen van dit probleem wordt door onderzoekers zeer veel belang gehecht aan de rol van de linkerhartcirculatie (grote bloedsomloop). In dat onderzoek vormt experimentele simulatie een onmisbaar instrument, naast computermodellering en dierexperimenteel onderzoek. Zo blijft experimentele simulatie onder andere een onmisbare tool om cardiovasculaire procedures en medische hulpmiddelen uit te testen en te verbeteren. Voordat dergelijke cardiovasculaire toepassingen in klinische omgeving gebruikt kunnen worden, moeten deze voldoen aan extreme eisen, vastgelegd in strenge certificaten die door regelgevende instanties zoals de FDA en ISO worden uitgereikt. Dergelijke certificaten kunnen pas verkregen worden als cardiovasculaire procedures voldoen aan strikte protocollen. Deze protocollen omvatten richtlijnen voor prestatiekenmerken, maar benadrukken ook het belang van bench tests, virtuele tests, in-vivo tests en klinische studies. In dit verband stelt de FDA dat klinisch relevante benchtop modellen, en bij voorkeur de best mogelijke, dringend nodig zijn om vooruitgang te boeken bij het in-vitro testen.

In de afgelopen 55 jaar werd er veel aandacht besteed aan het ontwikkelen en verfijnen van in-vitro benchtop modellen van de linkerharthelft en de bijhorende experimentele opstellingen. In deze evolutie, werden in-vitromodellen steeds uitgedaagd om de complexe anatomische en fysiologische kenmerken van de menselijke linkerharthelft alsmear nauwkeuriger na te bootsen. Ook zijn deze modellen in recente jaren door de opkomst van nieuwe technologieën (zoals medische beeldvorming, 3D-printtechnologie, software-gebaseerde regulering van actuator systemen) sterk verbeterd. Echter, nog steeds ontbreken er een aantal opmerkelijke, elementaire anatomische kenmerken en fysiologische mechanismen in de huidige in-vitrosimulatoren van de linkerharthelft.

In deze context formuleren we binnen dit proefschrift drie doelstellingen. Als eerste doel willen we de uitdagingen binnen de huidige in-vitro benaderingen identificeren, om van daaruit praktische richtlijnen te formuleren hoe in-vitromodellen moeten worden geoptimaliseerd om tot meer anatomische en fysiologische getrouwheid te komen. Het tweede doel van dit onderzoek is om effectief meer natuurgetrouwe modellen van het linkerventrikel (LV) en de mitralisklep te ontwerpen en te ontwikkelen. Het derde doel is dan om deze nieuw ontwikkelde componenten te integreren tot

een meer accuraat en meer natuurgetrouw in-vitromodel van de linkerharthelft.

Dit proefschrift heeft de volgende opbouw. Deel I start met een overzicht van de belangrijkste anatomische en fysiologische aspecten van de linkerharthelft. Daarna volgt een gedetailleerde bespreking van de bestaande in-vitromodellen van de linkerharthelft. Vervolgens volgt een kritische evaluatie van deze huidige modellen. Op basis daarvan worden praktische richtlijnen voor de optimalisatie van deze modellen geformuleerd. Daaropvolgend wordt een ontwerpmethodologie beschreven en toegepast waarbij nieuwe ideeën worden gegenereerd, geselecteerd en verder ontwikkeld om te komen tot innovatieve concepten die aan de specifieke praktische richtlijnen voor meer optimale in-vitromodellen voldoen. In de volgende drie delen worden deze concepten in meer detail besproken. Deel II beschrijft drie nieuw ontwikkelde in-vitromodellen van het linkerventrikel terwijl Deel III twee nieuwe in-vitroklepmodellen beschrijft, nl. van de mitralisklep (en bijhorende structuren) en van de veneuze klep als nevenproject. In Deel IV, worden deze gemodelleerde, individuele componenten geïntegreerd in twee omvattende linkerharthelftmodellen. Van deze modellen werd zowel een monolithische versie (in één stuk) als een modulaire, bilithische versie (in twee stukken) ontwikkeld. Deze laatste maakt de (her)plaatsing van diverse LV modellen in experimentele opstellingen mogelijk. Deel V geeft ten slotte een overzicht van de belangrijkste bevindingen van dit proefschrift, samen met de methodologische beperkingen, innovaties, en perspectieven voor verder onderzoek. Een algemeen overzicht van doctoraat wordt gegeven in Figuur 121 en Tabel 8. Hieronder wordt de inhoud van elk hoofdstuk kort samengevat.

DEEL I. DE LINKERHARTHELFT: VAN ANATOMIE TOT MODEL

HOOFDSTUK 1. DE STRUCTUUR EN FUNCTIE VAN HET LINKERVENTRIKEL

Hoofdstuk 1 behandelt de anatomie en fysiologie van de linkerharthelft. Ten eerste beschrijft dit hoofdstuk de bloedsomloop, de hartcyclus, de algemene fysiologie en de determinanten van de diastolische functie van de linkerharthelft. Ten tweede concentreert dit hoofdstuk zich op de macro- en microscopische structuur van de hartwand. Bijzondere aandacht gaat hierbij uit naar de manier waarop de unieke, uniaxiale cellulaire beweging van

cardiomyocyten wordt overgebracht naar de driedimensionale wandvervormingspatronen van het LV die op macroscopisch niveau waargenomen worden tijdens systole en diastole. Tot slot focust dit hoofdstuk op de functie en de structuur van de cardiovasculaire kleppen, met een meer diepgaande bespreking van het kleppenvlak en de mitralisklep, omdat deze een centrale rol vervullen in dit proefschrift.

HOOFDSTUK 2. IN-VITROMODELLEREN VAN DE LINKERHARTHELFT: STATE-OF-THE-ART

Hoofdstuk 2 beschrijft de ontwikkelingsgeschiedenis van cardiovasculaire simulatoren over de afgelopen 55 jaar. Dit overzicht illustreert enerzijds de grote vooruitgang en anderzijds de brede waaier van methoden die gebruikt werden om in-vitrohartmodellen te ontwerpen en te ontwikkelen. In deze review, worden een dertigtal in-vitrosystemen besproken die een belangrijke rol speelden in de geschiedenis van cardiovasculaire modellen. Drie belangrijke evoluties kunnen hierbij onderscheiden worden. Ten eerste is er een geleidelijke progressie in het nabootsen van de complexe anatomie van de linkerharthelft. Ten tweede is er duidelijke vooruitgang in het simuleren van fysiologische events in de linkerharthelft. Ten derde is er een significante evolutie in het afstemmen van deze in-vitromodellen om (klinische) validatie en onderzoekstechnieken mogelijk te maken. Tot slot benadrukt deze review de veelzijdige toepassingen waarvoor cardiovasculaire simulators tot op vandaag gebruikt worden en beklemtoont het de complexiteit van het moderne in-vitromodelleren.

HOOFDSTUK 3. KRITISCHE EVALUATIE EN PRAKTISCHE RICHTLIJNEN VOOR HET OPTIMALISEREN VAN LINKERHARTHELFTMODELLEN

De reviewinformatie van Hoofdstuk 2 is een waardevolle inspiratiebron om ontwerpcriteria te definiëren om de optimalisatie van cardiovasculaire simulatoren te bevorderen. Hoofdstuk 3 evalueert kritisch de tekortkomingen van de huidige in-vitrobenaderingen. Tegelijkertijd formuleert dit hoofdstuk praktische richtlijnen die de leidraad vormen voor de optimalisatie van in-vitromodellen van de linkerharthelft in dit proefschrift. Deze praktische richtlijnen (practical guidelines, PG) concentreren zich rond drie thema's.

Ten eerste blijkt er dringend nood aan het ontwikkelen van meer natuurgetrouwe linkerventrikel (LV) modellen. Bijna alle huidige cardiovasculaire simulatoren bootsen momenteel de wand van de linkerventrikelwand na door een dunwandig membraan, wat niet overeenstemt met de fysische realiteit. Ontwerpen van meer anatomisch en fysiologisch accurate LV modellen zouden zich minstens op vijf doelen moeten richten, nl. op het realiseren van een dikwandige benadering van de LV wand (PG1), op het includeren van de anisotrope eigenschappen van de natuurlijke LV wand (PG2), op het modelleren van de LV wandcontractie door het integreren van actieve contractiele elementen in de LV wand (PG3), op het simuleren van de verschillende globale vormveranderingen van de LV wand, zoals de longitudinale, circumferentiële en radiale vervorming (PG4a-c), en, op het realiseren van de torsiebeweging van het LV (PG5).

Ten tweede blijkt er uit Hoofdstuk 2 een belangrijke behoefte aan het ontwikkelen van een natuurgetrouwe mitralisklep. Tot op vandaag blijken er nauwelijks in-vitromodellen van de mitralisklep te bestaan, aangezien cardiovasculaire simulatoren voornamelijk mechanische, bioprothetische of post-mortem mitraliskleppen in hun modellen integreren. Een in-vitro ontwerp van de mitralisklep is echter zeer interessant omdat het zich kan richten op het modelleren van de meer gedetailleerdere anatomische kenmerken van de mitralisklep en het bijhorende mitralisklepapparaat (PG6a-e), zoals de flexibele en zadelvormige annulus, de twee klepbladen (anterior en posterior), de chordae tendinae en de papillaire spieren (zowel anterolateraal als posteromediaal).

Ten slotte blijkt uit Hoofdstuk 2 dat huidige cardiovasculaire simulatoren twee belangrijke beperkingen vertonen met betrekking tot de integratie van de mitralisklep in het kleppenvlak van linkerharthelftmodellen. Wanneer men zo'n mechanische, bioprothetisch of post-mortem mitralisklep integreert in een linkerharthelftmodel, valt op dat het kleppenvlak steeds gemodelleerd wordt met een rigide benadering, terwijl een meer anatomische natuurgetrouwe versie best een flexibel kleppenvlak zou implementeren (PG7). Zo'n flexibel kleppenvlak garandeert immers de ophanging van een flexibele mitralisring, terwijl ook de LV contractiefunctie intact blijft. Daarnaast zorgen de huidige starre benaderingen van het kleppenvlak er ook voor dat huidige modellen van de linkerharthelft niet in staat zijn om de apicale-basale bewegingen van het natuurlijke kleppenvlak te simuleren. Het verdient dus aanbeveling dat toekomstige in-vitromodellen zich richten op nieuwe, innovatieve ventrikelcontractiemechanismen die deze flexibele, neerwaartse bewegingen van het kleppenoppervlak kunnen toelaten (PG8).

HOOFDSTUK 4. DE ONTWERPMETHODOLOGIE

Hoofdstuk 4 bespreekt de algemene ontwerpstrategie van dit proefschrift die gebruikt werd om ideeën op een gestructureerde manier te genereren en om deze ideeën op een zo effectief mogelijke manier te realiseren. De toegepaste ontwerpmethodologie bestaat uit twee opeenvolgende divergentie-convergentiefasen. De eerste divergentie-convergentiefase start met een brede en diepgaande verkenning van de literatuur die vervolgens wordt geanalyseerd om de noden en praktische richtlijnen scherp te stellen. De toepassing van deze eerste divergentie-convergentiefase omvat het literatuuronderzoek over de anatomie en fysiologie van de linkerharthelft (Hoofdstuk 1) en de huidige state-of-the-art van linkerharthelftsimulatoren (Hoofdstuk 2). Op basis van deze verkenning van de literatuur, worden dan de onderzoeksnoden en bijhorende praktische richtlijnen gedefinieerd om cardiovasculaire simulatoren te optimaliseren (Hoofdstuk 3). De tweede divergentie-convergentiefase omvat het proces waarbij eerst meerdere nieuwe ideeën worden gegenereerd om aan de vooropgestelde noden en praktische richtlijnen tegemoet te komen, en waarbij vervolgens de beste conceptideeën geselecteerd en verder ontwikkeld worden in een iteratief proces. Hoofdstuk 4 geeft meer details over deze ontwerpprocessen die de basis vormen van de gerealiseerde in-vitro modellen die voorgesteld worden in Hoofdstukken 5 tot en met 12. Dit hoofdstuk illustreert dat elk in-vitro model van dit proefschrift niet enkel gebaseerd is op afgelijnde ontwerpcriteria maar ook het resultaat is van een breed scala aan gegenereerde ideeën en uitgevoerde hands-on experimenten.

DEEL II. IN-VITROMODELLEN VAN DE LINKER VENTRICULAIRE SPIER

HOOFDSTUK 5. EEN DIKWANDIG MODEL VAN DE LINKER VENTRICULAIRE SPIER

Hoofdstuk 5 beschrijft het ontwerp en de ontwikkeling van een eerste innovatief LV model (LV1). Dit model werd uitgerust met een dikwandige modellering van de LV spier om zo een meer realistische weergave van het LV te benaderen. Huidige dunwandige, passieve experimentele ventrikelmodellen bestaan uit een silicone membraan in een gesloten kamer, dat passief wordt samengeperst door een extern gekoppelde zuigerpomp. Hoewel deze modellen over het algemeen een goede pompfunctie vertonen, blijven de vervormingen van het membraan onvoorspelbaar en kunnen deze dus niet gelden als een goede nabootsing van de natuurlijke wandvervorming

van het LV. In dit hoofdstuk ontwierpen we daarom een experimenteel hydraulisch LV model waarbij de vervormingen van de linkerventrikelwand wel gecontroleerd kunnen worden. De praktische realisatie van dit model bestond uit een gecombineerde toepassing van rapid prototyping technieken. Ook testten we de werking van dit model om de wandvervorming en pompfunctie te valideren. Onze experimenten tonen aan dat dit model zowel circumferentiële als longitudinale vervorming realiseert, en dat dit model vrij fysiologische, realistische waarden van druk en debiet kan genereren. Dit model realiseert dus twee van de vijf gespecificeerde praktische richtlijnen voor nieuwe in-vitroventrikelmodellen: het implementeert een dikwandige benadering van de linker ventriculaire spier (PG1) en het modelleert twee wandvervormingspatronen, namelijk, longitudinale en circumferentiële vervorming (PG4a-b).

HOOFDSTUK 6. EEN MODEL VAN DE ACTIEVE WANDCONTRACTIE EN TORSIEBEWEGING VAN HET LINKERVENTRIKEL

Hoofdstuk 6 beschrijft het ontwerp en de ontwikkeling van een tweede innovatief LV model (LV2). Dit model integreert contractiele elementen in de ventrikelwand om zo zowel het effect van spiercontractie als van meer natuurgetrouwe wandvervormingspatronen na te bootsen, in termen van longitudinale, circumferentiële en radiale vervorming, maar ook in termen van torsie. Om deze verschillende wandvervormingspatronen in onze actuator te reproduceren, ontwierpen we een nieuw soort artificieel LV "spierweefsel", dat bestaat uit meerdere actieve contraherende cellen. De contractie van zo'n cel baseert zich op een mechanisme waarbij perslucht, in zo'n cel, in één richting contractie veroorzaakt en loodrecht op deze richting expansie veroorzaakt. Door middel van een uitgekiende organisatie en geometrie van deze contractiele cellen binnen één kunstmatige LV spier, de toegepaste druk in de cellen, en de heersende LV belastingcondities (voor- en nabelasting) is het mogelijk om de globale wandvervorming van het LV te bepalen. Een experimentele versie van dit principe werd gebouwd op basis van een eenvoudige plastic zak. Deze werd vervolgens gekoppeld aan een hydraulisch circulatiemodel van het vaatstelsel (inclusief compliantie en weerstand). De wandvervormingspatronen van dit model werden visueel gevalideerd en de pompprestatie werd geëvalueerd in termen van LV volume, druk en hartritme. Onze experimentele resultaten demonstreerden dat de globale beweging van dit LV de beweging van een natuurlijk LV relatief goed benaderde. Ook toonden ze een nauwe samenhang aan tussen dit experimentele model en een natuurlijk LV in termen van eind-systolisch volume en druk, eind-diastolisch

volume en druk, slagvolume, ejectiefractie en druk-volume relatie. Deze veelbelovende resultaten suggereren dat dit model een grote vooruitgang betekent tegenover de huidig gebruikte actuator mechanismen. Verdere optimalisaties van dit model dragen het potentieel om meer fysiologische intracavitair bloedstromingspatronen te genereren. Dit model komt tegemoet aan alle vijf praktische richtlijnen om meer natuurgetrouwe LV modellen te ontwikkelen: het implementeert een dikwandige benadering van de linker ventriculaire spier (PG1), het includeert anisotrope wandeigenschappen door middel van de toepassing van opblaasbare cellen (PG2), het integreert actieve contractiele wandelementen (PG3), het modelleert drie wandvervormingspatronen, zowel longitudinale, circumferentiële als radiale vervorming (PG4a-c) en het slaagt er ook in om torsie te genereren (PG5). Bovendien laat het nieuw ontwikkelde, innovatieve actuatormechanisme van het LV de neerwaartse beweging toe van het kleppenoppervlak (PG8).

HOOFDSTUK 7. MODELLEREN VAN DE TORSIEBEWEGING VAN HET LINKERVENTRIKEL DOOR MIDDEL VAN DE INTEGRATIE VAN ANISOTROPE MATERIAALEIGENSCHAPPEN

Hoofdstuk 7 beschrijft het ontwerp en de ontwikkeling van een derde LV model (LV3), welke geïnspireerd werd door de draaibeweging van het kunstmatige spiermodel LV2 uit Hoofdstuk 6. Dit LV3-model omvat geen dikwandige modellering van de LV spier, maar voegt in plaats daarvan vezels toe aan de huidig courant gebruikte, dunwandige LV modellen om op die manier de natuurlijke torsiebewegingen te simuleren. Het doel van dit model is om een breder fysiologisch bereik van torsieparameters te verkrijgen dan wat gerealiseerd werd door het LV2 model uit Hoofdstuk 6, dat een maximale torsiewaarde van ongeveer 13° bereikte. Daarnaast wenst dit model ook de circumferentiële en de longitudinale wandvervormingen van het natuurlijke LV na te bootsen. Het vervormingsconcept van dit model is gebaseerd op het uitrekken van een anisotroop membraan waarbij vezels ingebed werden in een flexibele matrix. Door deze inbedding wordt een composietstructuur gevormd. Om dit werkingsprincipe te bewijzen en om nieuwe inzichten te verkrijgen in de relatie tussen torsiegedrag en vezeloriëntatie, werden drie verschillende anisotrope LV modellen met verschillende vezeloriëntatiehoeken (20° , 35° en 45°) gebouwd. Deze experimentele modellen werden in de bestaande cardiovasculaire ViVitro-simulator gemonteerd en getest, waar ook de torsiehoeken tijdens de hartcyclus geregistreerd konden worden. Deze experimenten tonen aan dat elk van deze drie modellen een homogene wandvervorming produceert met duidelijke torsie-, circumferentiële en ook longitudinale bewegingen. Bovendien tonen

de experimenten aan dat de mate van torsie merkkelijk gerelateerd is aan de vezeloriëntatie van het LV model. Hierbij leiden de hogere vezeloriëntatiehoeken tot hogere torsiehoeken. De fysiologische torsiehoek van ongeveer 17° wordt gegenereerd door het model met een vezeloriëntatiehoek van 20° . Dit model voldoet aan drie beschreven praktische richtlijnen voor meer natuurgetrouwe LV in-vitromodellen: het includeert anisotrope wandeigenschappen (PG2), het modelleert twee globale wandvervormingspatronen, nl. longitudinale en circumferentiële vervorming (PG4a-b), alsook torsie (PG5). Een belangrijke beperking van dit model is echter dat het gebaseerd is op een vereenvoudigde geometrie van het LV en niet op de natuurlijke vorm van het LV. Daarom werd een meer natuurgetrouwe geometrie op dit LV3-model toegepast in een latere fase van dit proefschrift. Dit aangepaste LV3-model zal geïntegreerd worden in het uiteindelijke linkerharthelftmodel LH2 (Hoofdstuk 11).

DEEL III. IN-VITROMODELLEN VAN DE MITRALISKLEP (EN DE VENEUZE KLEP)

HOOFDSTUK 8. EEN MODEL VAN DE MITRALISKLEP OP BASIS VAN EEN VEZELHOUDEND COMPOSITMATERIAAL

Hoofdstuk 3 identificeerde een sterke nood aan het ontwikkelen van meer natuurgetrouwe in-vitromodellen van de mitralisklep, welke ook de complexe anatomische eigenschappen van het mitralisklepapparaat zouden kunnen modelleren. In dit hoofdstuk, stellen we een nieuwe methode voor het modelleren van de mitralisklep voor. Deze maakt gebruik van een vezelhoudend composietmateriaal (met dezelfde materiaalsamenstelling als het LV3-model uit Hoofdstuk 7) om een mitralisklep te realiseren met een nog steeds vereenvoudigde, maar meer natuurgetrouwe geometrie. De vooropgestelde methode maakt het mogelijk om de belangrijkste anatomische structuren van het mitralisklepapparaat, zoals de flexibele en zadelvormige annulus, de voorste en achterste klepbladen, de chordae tendineae en de anterolaterale en posteriomediale papillaire spieren (PG6a-e) na te bootsen. In het kader van deze studie realiseerden we twee werkende prototypes. Het eerste mitralisklepmodel (MV1) toonde vooreerst de werkzaamheid van het productieproces aan, terwijl het tweede mitralisklepmodel (MV2) een verdere geoptimaliseerde versie is van het eerste model met het oog op een meer natuurgetrouwe benadering van de geometrie en van de vezels in de tip van het klepblad. Het interessante van de in dit hoofdstuk ontwikkelde methode is

dat deze het mogelijk maakt om de nieuw ontwikkelde mitralisklepmodellen te integreren in de integratieve linkerharthelftmodellen, zoals beschreven wordt in Hoofdstuk 10. Deze integratie maakt het mogelijk om ook de prestaties van deze klepmodellen experimenteel te evalueren binnen de context van deze linkerharthelftmodellen. Hoofdstuk 8 geeft alvast een beknopte samenvatting weer van de resultaten over de functionaliteit van de ontwikkelde klepmodellen. Onze testen tonen hierbij aan dat het MV2-model relatief goed voldoet aan de doelstelling om fysiologische waarden van mitralisklepprestaties te genereren, in termen van ‘effective orifice area’ en transmitrale drukgradiënten. Ook het MV1-model blijkt interessant omdat het een vernauwde mitralisklep blijkt na te bootsen, met hoge transmitrale drukgradiënten, lage ‘effective orifice area’s’ en terugstroom (regurgitatie). Kortom, de nieuw ontwikkelde prototypes van de mitralisklep tonen aan dat deze nieuwe methode gebruikt kan worden om zowel normale als pathologische mitraliskleppen in-vitro te modelleren.

HOOFDSTUK 9. INNOVATIEF ONTWERP VAN EEN PIV-COMPATIBEL MODEL VAN DE VENEUZE KLEP

Er blijkt bij het in-vitromodelleren van cardiovasculaire kleppen een groeiende belangstelling voor het gebruik van Particle Image Velocimetry (PIV), om zo computermodellen experimenteel te valideren en stromingspatronen langsheen de kleppen te simuleren. In het licht van deze recente evoluties zouden nieuwe ontwerpen van cardiovasculaire simulatoren dus idealerwijs PIV-compatibel moeten zijn en voldoen aan de strenge vereisten om PIV-metingen mogelijk te maken. Dit betekent dat cardiovasculaire modellen volledig transparant moeten zijn, terwijl ze toch hun functionaliteit blijven behouden (zie PG9). In dit proefschrift hebben we deze praktische richtlijn niet gerealiseerd in de context van in-vitromodellering van de linkerharthelft, maar we ontwikkelden wel een PIV-compatibel prototype van de veneuze klep (VV) in het kader van het optimaliseren van in-vitromodellen voor hemodialyse gerelateerd onderzoek. Toekomstig onderzoek moet evalueren in hoeverre deze concepten bruikbaar zijn om een geheel, volledig transparant, PIV-compatibel linkerharthelft te bouwen. Hoofdstuk 9 beschrijft het innovatieve ontwerp van een PIV-compatibele veneuze klepmodel die zijn functionaliteit behoudt bij minimale drukverschillen en die tevens in staat is om waardevolle PIV-data te genereren. Ons ontwerp is gebaseerd op de transparante en buigzame kenmerken van polymeerfilm. Op basis hiervan werd een operationele klep gerealiseerd die gevoelig is voor vloeistofbewegingen en die zijn functionaliteit behoudt, zelfs bij lage drukverschillen. Dit prototype voldoet

dus aan de vooropgestelde praktische richtlijn om een PIV-compatibele veneuze klep te ontwerpen (PG9). Bovendien tonen de preliminaire resultaten aan dat de PIV-metingen niet enkel de stromingspatronen rond de klep, maar ook in de klep zelf, in kaart kunnen brengen. Dit opent de intrigerende mogelijkheid dat men op basis van dit soort in-vitromodellen experimentele studies kan opzetten om intravalvulaire vloeistofpatronen verder te onderzoeken.

DEEL IV. MODELLEN VAN DE LINKERHARTHEFT: EEN INTEGRATIEVE BENADERING

HOOFDSTUK 10. MODELLEREN VAN DE LINKERHARTHEFT: EEN MONOLITHISCHE BENADERING

Hoofdstuk 10 gaat dieper in op het ontwerp en de ontwikkeling van een innovatief monolithisch (in één stuk) linkerharthelftmodel (LH1). Dit model incorporeert het huidig courant gebruikt dunwandige LV model samen met het flexibele, van vezelhoudend composietmateriaal gemaakte mitralisklepmodel MV2 (Hoofdstuk 8). Dit hoofdstuk beschrijft ook het ontwerp en de ontwikkeling van specifiek op maat vervaardigde ophangings- en aansluitingssystemen. Deze maken de integratie van dit linkerharthelftmodel in een bestaand pompsysteem van een hartsimulator mogelijk, nl. de cardiovasculaire ViVitro simulator. Hierdoor kan het model van de linkerharthelft experimenteel getest worden. Dit hoofdstuk rapporteert tenslotte preliminaire maar veelbelovende resultaten van hydrodynamische en echocardiografische metingen van het model van de linkerharthelft. Deze resultaten suggereren dat deze nieuwe benadering van modellering op meerdere manieren een relatief goede benadering geeft van de fysische, anatomische realiteit. Ten eerste is de geometrie van dit in-vitromodel gebaseerd op medische beelden van een echt hart. Dit model omvat niet alleen het linkerventrikel, linkeratrium en de aortaboog, maar ook meer gedetailleerde kenmerken, zoals het hartootje van het linkeratrium en de ingangen van de vier longaders. Ten tweede integreert dit model het eerder beschreven mitralisklepapparaat MV2 (Hoofdstuk 8), welke nog meer anatomisch gebaseerde structuren (PG6a-e) aan het linkerharthelftmodel toevoegt. Ten derde is dit linkerharthelftmodel gemaakt van silicone en vezelhoudende materialen. Hierdoor kunnen zowel de mechanische als de ultrasonische eigenschappen van het biologische zachte hartweefsel worden nagebootst. Ten vierde was het door het innovatieve productieproces mogelijk

om dit complexe model in één stuk te realiseren, wat een meer natuurgetrouwe en compacte versie van het linkerharthelftmodel oplevert. Ten vijfde zorgt het op maat ontwikkelde ophangingssysteem voor functionele compatibiliteit met een standaard cardiovasculaire simulator, terwijl er toch geen afbreuk gedaan wordt aan het flexibele karakter en de complexe anatomische-gebaseerde vorm van het kleppenvlak (PG7). Ten slotte tonen de preliminaire experimenten aan dat dit linkerharthelftmodel in staat is om relatief fysiologisch normale waarden te genereren, maar ook dat de structuren van dit hart zichtbaar gemaakt kunnen worden door ultrageluid. Ook tonen de resultaten dat het model fysiologisch-gerelateerde intraventriculaire stromingspatronen genereert die via kleuren Doppler kunnen worden waargenomen. Samengevat betekenen deze verschillende sterke punten van onze integrale, monolithische benadering een belangrijke stap voorwaarts in het ontwikkelingsproces van in-vitromodellen van de linkerharthelft. Toch blijken er nog steeds een aantal essentiële aanbevelingen voor in-vitromodeloptimalisatie te ontbreken. Het model implementeert immers niet de anisotrope eigenschappen van de natuurlijke ventrikelwand (PG2) en laat het daarom niet toe om de ventriculaire wandvervormingspatronen zoals longitudinale, circumferentiële en radiale vervorming (PG4a-c) of de draaiende torsiebeweging (PG5) te integreren of te controleren.

HOOFDSTUK 11. MODELLEREN VAN DE LINKERHARTHELFT: EEN BILITHISCHE BENADERING EN STUDIE VAN HET EFFECT VAN TORSIE OP INTRACARDIALE DIASTOLISCHE DRUKPARAMETERS

Hoofdstuk 11 beschrijft de ontwikkeling van het innovatief linkerharthelftmodel LH2, dat de unieke kinematische mogelijkheden van het anisotrope model LV3 (Hoofdstuk 7) combineert met het anatomiegetrouwe mitralisklepmodel MV2 (Hoofdstuk 8), en het ophangingssysteem van Hoofdstuk 10, dat de verbinding toelaat tussen het linkerharthelftmodel en het pompsysteem van de standaard cardiovasculaire ViVitro-simulator. Dit LH2-model is gebaseerd op het monolithische linkerharthelftmodel LH1 maar werd aangepast naar een modulair, bilithisch linkerharthelftmodel met een aparte, demonteerbare ventriculaire component. Hierdoor waren we in staat om een innovatieve, experimentele opstelling te bouwen waarbij we vijf ventrikelmodellen met verschillende wandvervormingspatronen met elkaar kunnen vergelijken op vlak van intracardiale drukparameters. In deze set-up worden twee modellen met hoofdzakelijk longitudinale en circumferentiële vervorming, samen met twee modellen met verschillende torsiegraden, vergeleken met een generiek model met algemene deformatiepatronen.

Hiertoe werden vijf verschillende ventrikelmodellen gebouwd op basis van verschillende anisotrope eigenschappen en achtereenvolgens gemonteerd en getest in ons bilithisch LH2-model. De experimentele metingen rapporteren hoe de verschillende globale wandvervormingspatronen en torsie invloed uitoefenen op de transmitrale (TMPDe) en intraventriculaire drukverschillen tijdens de vroeg-diaastolische fase (IVPDe). Opmerkelijk is dat deze resultaten substantiële effecten van de torsiemodellen suggereren: bij toenemende torsie observeren we lagere TMPDe waarden en hogere IVPDe waarden. Deze substantiële effecten kunnen gedeeltelijk worden toegewezen aan de longitudinale vervormings-component, maar de resultaten suggereren tevens dat de torsiebeweging een aanvullend effect heeft bovenop de longitudinale contractiecomponent. Dit integratief model LH2 voldoet aan het grootste aantal praktische richtlijnen zoals voorgeschreven in Hoofdstuk 3. Het kan veelzijdig wandvervormingspatronen genereren door middel van anisotrope wandeigenschappen (PG2) en genereert zowel longitudinale als circumferentiële vervorming (PG4a-b) maar ook torsie (PG5). Verder bevat het LH2-model ook de geïntegreerde mitralisklep model met alle basiseigenschappen van het mitralisklepapparaat MV2 (PG6a-e). Ten slotte wordt ook in dit model de mitralisklepinrichting geïntegreerd in een flexibel kleppenvlak (PG7).

DEEL V. CONCLUSIES EN PERSPECTIEVEN VOOR DE TOEKOMST

HOOFDSTUK 12. CONCLUSIES EN RICHTLIJNEN VOOR TOEKOMSTIG ONDERZOEK

Hoofdstuk 12 biedt een overzicht van de belangrijkste bevindingen en conclusies van dit proefschrift en geeft een gedetailleerd overzicht (zie Tabel 8) in welke mate de ontwikkelde modellen voldoen aan de praktische richtlijnen opgesteld in Hoofdstuk 3. In dit proefschrift, realiseerden we werkende in-vitroprototypes van drie meer natuurgetrouwe LV-modellen, een gedetailleerd model van het mitralisklepapparaat, en een PIV-compatibel model van een veneuze klep. Bovendien slaagden we erin om deze afzonderlijke componenten in twee integratieve linkerharthelftmodellen te integreren, terwijl tegelijkertijd ook een flexibele kleppenvlak behouden kon worden. We vervaardigden zowel een monolithische versie van dit integratieve hartmodel, als een bilithische versie met een aparte, demonteerbare ventriculaire component.

Globaal genomen kan men deze set van modellen als een belangrijke stap voorwaarts beschouwen in het vervaardigen van meer realistische in-vitromodellen van de linkerharthelft. Ook zijn deze modellen veelbelovend omdat ze belangrijke instrumenten kunnen worden in in-vitro experimentele studies om de kennis over klepgerelateerde of wandvervormingsgerelateerde fysiologische gebeurtenissen te vergroten. Uiteindelijk zouden geoptimaliseerde versies van deze modellen ook gebruikt kunnen worden voor cardiovasculaire toepassingen in klinische context. Om dit ultieme doel te realiseren, zou toekomstig onderzoek zich moeten richten op drie belangrijke thema's van methodologische beperkingen bij de huidige modellen. Ten eerste zouden optimalisaties van de in dit proefschrift ontwikkelde modellen gericht moeten zijn op het modelleren van een aantal belangrijke fysiologische gebeurtenissen, waaraan niet (voldoende) tegemoetgekomen wordt in de huidige, voorgestelde modellen. Ten tweede zouden optimalisaties van deze modellen kunnen streven naar nog nauwkeurigere geometrische benaderingen van het natuurlijke hart. Ten derde erkennen we dat dit proefschrift in de eerste plaats gericht is op het aantonen van de 'proof-of-concept' van de ontwikkelde modellen en dat het belangrijk is om de voorgestelde modellen door meer uitgebreide experimenten en metingen verder te evalueren en te valideren. Ten slotte bespreken we in dit hoofdstuk drie belangrijke uitdagingen (nl. om in te zetten op 'actieve wand', 'integratie' en 'transparantie') die - volgens ons - het in-vitromodelleren van de linkerharthelft naar de volgende fase van innovatie kunnen brengen. Hiervoor formuleren we tevens vier suggesties voor nieuwe ontwerpen (linkerventrikelmodellen LV4 en LV5 alsook volledige hartmodellen FH1 en FH2) die we ontwikkelden tijdens het denken ontwerpproces van dit doctoraatstraject. We geloven dat de realisatie van de voorgestelde modellen kunnen helpen om de drie geïdentificeerde uitdagingen in toekomstig in-vitromodelleringsonderzoek aan te gaan.

Summary

INTRODUCTION

Cardiovascular diseases are one of the leading causes of death worldwide. To address this global problem, the left heart circulation is extensively studied. Despite recent advances in computational modelling and the availability of animal models, experimental simulation of the left heart circulation remains an indispensable tool for continually advancing cardiovascular procedures and medical devices. Before such cardiovascular appliances can be implemented in clinical settings, they need to meet extreme requirements to attain the stringent certificates provided by regulatory agencies such as the FDA and ISO. Attaining such certificates include compliance with strict protocols for performance characteristics, bench testing, virtual testing, in-vivo tests, and clinical studies. In this respect, the FDA postulated in 2011 that clinically relevant benchtop models, preferably the best possible, are urgently needed to advance in-vitro testing.

In-vitro benchtop models and mock circuits simulating the left heart (circulation) have been developed and refined over the past 55 years. In this process, benchtop models have been continuously challenged to more accurately mimic the complex anatomical and physiological features of the human left heart. Even though advances in engineering methods (such as medical imaging, 3D print technology, and software-based regulation of actuator systems) have significantly improved the design of these models, there remain a number of elementary anatomical features and physiological events that are not included in current in-vitro simulators.

The first research objective of this dissertation is to identify challenges within current in-vitro approaches and to formulate practical guidelines towards in-vitro model optimization in terms of anatomical and physiological likeness. The second research objective is to design and develop more realistic models of the left ventricle and the mitral valve. The third research objective is to integrate these novel components to attain a more nature-like model of the left heart.

The structure of the dissertation is as follows: Part I presents a background overview of the anatomy and physiology of the left heart, the state-of-the-art of left heart in-vitro modelling, and a critical discussion of the challenges in optimizing current models. Based on this critical evaluation, practical guidelines for a new generation of models are formulated. Subsequently, the design methodology of this dissertation is described by which new ideas are generated, selected and further developed into innovative

design concepts that meet the specified practical guidelines towards attaining more optimal in-vitro models. The resulting final concepts are described in more detail in the next three Parts. More particularly, Part II describes three newly-developed in-vitro models of the left ventricle (LV) whereas Part III presents novel concepts for the in-vitro modelling of the mitral valve apparatus and of the venous valve as a side project. In Part IV, the modelled individual components are integrated into two entire left heart models: a monolithic version and a modular, bilithic version which allows the (re)placement of various LV models in experimental set-ups. Part V (Chapter 12) concludes this dissertation by listing the key findings, methodological considerations, innovations, and future perspectives. A global overview of this dissertation is shown in Figure 121 and Table 8. Below, the content of each chapter is summarized.

PART I. THE LEFT HEART: FROM NATURE TO MODEL

CHAPTER 1. THE LEFT HEART STRUCTURE AND FUNCTION

Chapter 1 discusses the anatomy and physiology of the left heart. Firstly, it describes the circulatory system, the cardiac cycle, the general physiology and determinants of diastolic function in the left heart. Secondly, this chapter concentrates on the macro- as well as microscopic structure of the cardiac wall, with a specific focus on how the unique uniaxial cellular motion of cardiomyocytes is transferred to the three-dimensional wall deformation patterns that can be observed at the macroscopic level of the left ventricle during systole and diastole. Finally, this chapter directs attention to the function and structure of the cardiovascular valves, providing a more in-depth discussion of the valve plane and the mitral valve apparatus, which play a central role in this dissertation.

CHAPTER 2. IN-VITRO MODELLING OF THE LEFT HEART: STATE-OF-THE-ART

Chapter 2 describes the history of cardiovascular simulator development, which took place over the past 55 years. This history illustrates the major progression and the wide range of approaches that has been taken to design and develop in-vitro cardiovascular systems. This review presents more details on about thirty in-vitro approaches that played a significant role in cardiovascular modelling history. Three key areas of development can be

distinguished. First, there is a gradual progression in mimicking the complex anatomy of the left heart. Second, there is a noted progress in the duplication of physiological events. Third, there is a significant evolution in the adaptation of these in-vitro models to (clinical) validation and examination techniques. This review also underscores the versatile applications for which cardiovascular simulators are used and highlights the complexity of in-vitro modelling today.

CHAPTER 3. CRITICAL EVALUATION AND PRACTICAL GUIDELINES FOR OPTIMIZING CURRENT MODELS

The state-of-the-art information in Chapter 2 serves as a valuable source of inspiration to define design criteria to advance cardiovascular simulator optimization. Chapter 3 critically evaluates the shortcomings of the current in-vitro-approaches. Concomitantly, this chapter formulates practical guidelines to form the basis for the in-vitro left heart model optimization in this PhD project. These practical guidelines (PG) are centered around three themes. First, designs of more anatomically and physiologically accurate LV models should be directed towards realizing a thick-walled approach of the left ventricular wall (PG1), towards including the anisotropic properties of the natural wall (PG2), towards modelling the LV wall contraction by means of active contractile elements (PG3), towards mimicking multiple global ventricular wall patterns such as longitudinal, circumferential, as well as radial deformation (PG4), and importantly, towards including torsional motion (PG5). Second, as current cardiovascular simulators relied upon mechanical, bioprosthetic or even post-mortem mitral valves to include in their models, there is a strong need for developing more natural and anatomically correct in-vitro mitral valve models. These designs should include more detailed anatomical features of the mitral valve apparatus (PG6), such as the flexible and saddle-like annulus, anterior and posterior leaflets, the chordae tendineae, and the anterolateral papillary and posteromedial papillary muscles. Finally, in the context of integrating left ventricular and mitral valve models in entire left heart models, current models show two major limitations at the level of the valve plane. This valve plane is typically modelled by a rigid approach, whereas a more natural and anatomically correct valve plane would be obtained by implementing a flexible valve plane (PG7). This should allow the suspension of a flexible mitral valve plane, while keeping the actuation functionality. Also, due to this rigid valve plane approach, current left heart models are not able to include the apical-basal movement of the natural valve plane. Therefore, new designs should search for opportunities to allow the motion of the valve plane by inventing novel ways of ventricle actuation mechanisms (PG8).

CHAPTER 4. DESIGN METHODOLOGY

Chapter 4 discusses the overall design strategy that was used in this dissertation to produce original ideas in a structured way and to realize these ideas in an effective manner. The applied design methodology consists of two paired convergence-divergence phases. The first divergence-convergence phase starts with a broad and in-depth exploration of the literature which is subsequently analyzed to define the needs and accommodating practical guidelines. The implementation of this first phase includes literature reviews about the anatomy and physiology of the left heart (Chapter 1), the current state-of-the-art cardiovascular simulators (Chapter 2) and the distillation of the needs and definition of practical guidelines for optimization (Chapter 3). The second divergence-convergence phase includes the process whereby first, several new ideas are generated that meet the established practice guidelines, and then, the further development via iterative processes of the best concept ideas into the actual in-vitro models. Chapter 4 provides more details on these design processes that form the basis of the realized in-vitro models that are Presented in Chapters 5 to 12. This chapter illustrates that each in vitro model of this PhD project is not only based on delineated practical guidelines, but is also the result of a wide range of generated ideas and concepts and the effectuation of numerous hands-on experiments.

PART II. IN-VITRO MODELLING OF THE LEFT VENTRICULAR MUSCLE

CHAPTER 5. MODELLING THE LEFT VENTRICULAR MUSCLE BY A THICK WALL

Chapter 5 describes the design and development of a first novel LV model (LV1) equipped with a thick wall. This is a more realistic representation of the natural LV wall in comparison with the generally-used thin-walled passive experimental models, consisting of a silicone membrane in a closed box, which is squeezed passively by an externally connected piston pump. Although the pump function of these models has already been well established, the membrane deformation remains unpredictable and hence natural wall deformation cannot be simulated. Therefore, this study describes the design of an experimental hydraulic left ventricular model in which left ventricular wall deformation can be controlled. This model was built by a combination of rapid prototyping techniques and tested to demonstrate its wall deformation and pump function. Experiments in this study show that circumferential and longitudinal deformation can be attained and that this

model can generate fairly physiological values of pressure and flow. This model meets two specified practical guidelines: it models the ventricular wall by a thick-wall approach (PG1) and mimics two global wall deformation patterns, i.e., longitudinal and circumferential deformation (PG4a-b).

CHAPTER 6. MODELLING THE ACTIVE WALL CONTRACTION AND TORSIONAL MOTION OF THE LEFT VENTRICLE

Chapter 6 describes the design and development of a second novel LV model (LV2) which integrates active contractile elements into the left ventricular wall in order to mimic the effect of muscle contraction as well as more nature-like left ventricular wall deformation patterns, in terms of circumferential, radial and longitudinal deformation, as well as torsion. In order to reproduce these basic wall deformation patterns in our actuator device, we designed a novel kind of artificial LV “muscle” composed of multiple actively contracting cells. Its contraction is based on a mechanism by which pressurized air, inside such a cell, causes contraction in one direction and expansion perpendicular to this direction. The organization and geometry of the contractile cells within one artificial LV muscle, the applied pressure in the cells, and the governing LV loading conditions (preload and afterload) together determine the global deformation of the LV wall. Starting from a simple plastic bag, an experimental model based on the above-mentioned principle was built and connected to a lumped hydraulic model of the vascular system (including compliance and resistance). The wall deformation pattern of this device was validated visually and its pump performance was studied in terms of LV volume and pressure and heart rate. Our experimental results revealed a global LV motion resembling a real LV, and a close correlation between our model and a real LV in terms of end-systolic volume and pressure, end-diastolic volume and pressure, stroke volume, ejection fraction and pressure-volume relationship. Our model appears promising and it can be considered as a step forward when compared to currently applied actuator mechanisms, as optimizations of this model will likely result in more physiological intra-cavity blood flow patterns. This model meets all five practical guidelines specified to attain more naturally correct LV models: it models the ventricular wall by a thick-wall approach (PG1), includes anisotropic wall properties by means of the inflatable cells (PG2), integrates active contractile wall elements (PG3), and mimics the global wall deformation patterns, such as longitudinal, circumferential as well as radial deformation (PG4a-c), and includes torsion (PG5). Moreover, due to its novel ventricle actuation mechanism, it also allows the downwards motion of the valve plane (PG8).

CHAPTER 7. MODELLING THE TORSIONAL MOTION OF THE LEFT VENTRICLE BY INTEGRATION OF ANISOTROPIC MATERIAL PROPERTIES

Chapter 7 describes the design and development of a third novel LV model (LV3) which is inspired by the twisting motion of the artificial muscle model LV2 (Chapter 6). This model does not include a thick-wall approach but adds fibers to the currently commonly used thin-walled LV models in order to mimic natural torsional motion. The aim of this model is to attain torsion parameters within a wider physiological range than the Chapter 6 model which is limited to a maximal value of about 13° , while also mimicking the circumferential as well as longitudinal deformation components of the natural LV. The deformation concept is based on the stretching of an anisotropic membrane, which is realized by embedding fibers into a flexible matrix, forming a composite structure. For the proof of concept and to obtain more insights of the torsional behavior in function of the fiber orientation, three different anisotropic left ventricular models are developed with different fiber orientation angles (20° , 35° , and 45°). These models are mounted into a cardiovascular simulator and torsional angles are captured during the heart cycle. Our experiments show that each model displays homogenous wall deformation with torsional, circumferential, as well as longitudinal wall motion. Moreover, the experiments show that the degree of torsion clearly relates to fiber orientation angle, with higher fiber orientation angles resulting in higher torsional angles. The physiological torsional angle of about 17° is generated by the model with a fiber orientation angle of 20° . This model meets three specified practical guidelines: it includes anisotropic wall properties (PG2), mimics two global wall deformation patterns, i.e., longitudinal and circumferential deformation (PG4a-b), and includes torsion (PG5). One important limitation of this model is that it is based on a simplified geometry and not on the natural shape of the LV. A modified version, applying a more natural geometry, of this third left ventricular model will be integrated into the left heart model LH2 (Chapter 11).

PART III. IN-VITRO MODELLING OF THE MITRAL (AND VENOUS) VALVE

CHAPTER 8. MODELLING THE MITRAL VALVE USING A FIBER-BASED COMPOSITE MATERIAL

Chapter 3 identified a strong need for developing more natural and anatomically correct in-vitro mitral valve models that incorporate detailed features of the mitral valve apparatus (PG6). In this chapter, a novel approach of modelling mitral valves is proposed that (1) makes use of a fiber-based composite material with a similar material composition as the LV3 model (Chapter 7), and (2) provides a valve with a (simplified) natural mitral valve geometry. This approach enables us to include core anatomical structures of the mitral valve such as the flexible and saddle-like annulus, the anterior and posterior leaflets, the chordae tendineae as well as the anterolateral papillary and posteromedial papillary muscles (PG6). Within the context of this study, two working prototypes were realized. The first one (MV1) demonstrated the proof of concept of the production process, whereas the second one (MV2) is a further optimized version of the valve model in terms of geometry and leaflet tip fiber. Interestingly, our methodology allows for the integration of these mitral valve models into the integrative left heart models as described in Chapter 10, allowing experimental tests of their performance within this left heart model. This chapter already briefly summarizes these experimental results to provide a first evaluation of the valves' functionality. Our tests showed that while MV2 meets our goal to generate more physiology-like values of mitral valve performance providing reasonable performance in terms of effective orifice area (EOA) and transmitral pressure gradients, MV1 is also interesting as it reflects a model of a stenosed mitral valve, exhibiting high transmitral pressure differences in early diastole, low EOA, and regurgitation. Overall, these mitral valve prototypes demonstrate that this new approach can be used to model normal as well as pathological mitral valves.

CHAPTER 9. INNOVATIVE DESIGN OF A PIV COMPATIBLE VENOUS VALVE MODEL

There is a growing interest in in-vitro cardiovascular valve modelling to enable experimental validation of computer models by using Particle Image Velocimetry (PIV) for simulation of flow fields. Hence, ideally, new designs of cardiovascular models should meet the stringent requirements to allow PIV measurements, i.e., to be fully transparent while keeping their functionality

(see PG9). In this PhD work, this practical guideline was not realized in the context of in-vitro left heart modelling, but a PIV compatible prototype of the venous valve (VV) was developed for optimizing in-vitro modelling research in the context of hemodialysis-related research. Chapter 9 describes the innovative design of a PIV compatible venous valve model which has the ability to function at minimal pressure differences and which is able to generate valuable PIV data. Our design uses the transparent and pliable features of polymer film which resulted in an operational valve that is sensitive for fluid motion and able to function at low pressure differences. As such, this model meets the proposed practical guideline towards designing a PIV compatible venous valve model (PG9). Moreover, our preliminary results show that PIV measurements are not only available for flow patterns adjoining the valve but also within the valve itself. This opens the intriguing possibility for experimental assessments and examinations of intra-valvular flow patterns, making this valve design a promising tool for use in experimental validation studies of computational models of valve configurations. Future research should evaluate to what extent these concepts are applicable towards building an entire, fully transparent, PIV compatible left heart.

PART IV. MODELLING THE LEFT HEART: AN INTEGRATIVE APPROACH

CHAPTER 10. MODELLING THE LEFT HEART BY A MONOLITHIC APPROACH

Chapter 10 elaborates on the design and development of an innovative monolithic left heart model (LH1) that incorporates a currently commonly used thin-walled LV model together with the flexible fiber-based mitral valve model MV2 (Chapter 8). This chapter also describes the design and development of tailored suspension and connection systems that enable the integration and experimental testing of the left heart model into an existing pulse duplicator system, i.e., the ViVitro mock circulatory loop. Finally, preliminary but promising results of the left heart model based upon hydrodynamic and echocardiographic measurements are reported. Results suggest that this novel approach of left heart modelling more closely approximates real anatomic features in multiple ways. First, the geometry of the in-vitro left heart model is based on medical images from a real heart, and includes the left ventricle, left atrium and the aortic arch, but also more detailed features, such as the auricle and the entrances of the four pulmonary veins. Second, the previously described mitral valve apparatus MV2 (Chapter 8) has been integrated into the model, which adds even more anatomical-like

structures (PG6a-e). Third, the left heart model is made of silicon and fiber materials to mimic the mechanical as well as the ultrasonic characteristics of the biological soft tissue of the heart. Fourth, the innovative production process enabled the realization of this complex model in one single piece, resulting in a more anatomical-like and compact left heart model. Fifth, the newly developed suspension system ensures compatibility with a standard (Type I) cardiovascular simulator, while preserving its flexible appearances and complex anatomical-like shape of the valve plane region (PG7). Finally, the preliminary benchtop experiments show that the model is able to generate normal values of left heart performance, the structures are visible using ultrasound, and the model generates physiologically relevant intraventricular flow patterns that can be observed via color Doppler. These multiple strengths of our integrative monolithic approach can be considered a significant step forward in in-vitro modelling of the left heart. Nevertheless, some essential recommendations for in-vitro model optimization are still lacking: the model does not implement the anisotropic properties of the natural ventricular wall (PG2); hence control of ventricular wall deformation patterns, such as longitudinal, circumferential, and radial deformation (PG4) or including the twisting motion (PG5) is not possible.

CHAPTER 11. MODELLING THE LEFT HEART BY A BILITHIC APPROACH: FEASIBILITY STUDY OF THE EFFECT OF TORSION ON INTRACARDIAC DIASTOLIC PRESSURE PARAMETERS

Chapter 11 describes the development of an innovative left heart model, which combines the unique kinematic abilities of the anisotropic model LV3 (Chapter 7), with the anatomical-like mitral valve model MV2 (Chapter 8), and the suspension system of Chapter 10, allowing the connection to a broadly used standard cardiovascular simulator. Moreover, by modifying the monolithic to a modular bilithic left heart model with a separate and demountable ventricular component, it was possible to build an innovative, experimental set-up enabling an experimental feasibility study relating five different wall deformation patterns to diastolic parameters. Two models with predominantly longitudinal or circumferential deformation, and two models with different degrees of torsion, were compared to a general model without a global deformation pattern. To this end, five different ventricular models were built based upon different anisotropic properties, and mounted successively into our bilithic model. Initial experimental measurements report how global wall deformations and torsion affect the transmitral (TMPDe) and intraventricular pressure differences during early diastole (IVPDe). Notably, these results show lower TMPDe and higher IVPDe values in models with increasing torsional angles. These high effects may be partly allocated to its longitudinal component, but results suggest that the torsional motion has an

additional effect on top of the longitudinal deformation component. This integrative model complies with the greatest number of practical guidelines. It is able to generate versatile wall deformation patterns by the anisotropic wall properties (PG2) in terms of torsional motion (PG5) as well as longitudinal and circumferential deformations (PG4a-b). Also, the integrated mitral valve model includes all basic features of the mitral valve apparatus MV2 (PG6a-e). Finally, the mitral valve apparatus is integrated into a flexible valve plane (PG7).

PART V. CONCLUSIONS

CHAPTER 12. CONCLUSIONS AND FUTURE DIRECTIONS

Chapter 12 reviews the key findings and most important conclusions of this PhD project, giving a detailed overview (see Figure 121 and Table 8) to what extent the developed models meet the practical guidelines of Chapter 3. Working prototypes of three more realistic LV models, a detailed mitral valve apparatus model, and a PIV compatible venous valve model were realized in this dissertation project. Moreover, these individual components were successfully integrated into two integrative left heart models, while incorporating a flexible valve plane, producing a monolithic version as well as a bilithic version with a separate and demountable ventricular component. Overall, this set of models can be considered a major step forward towards attaining more realistic in-vitro modelling of the left heart. Also, these models bear promise to become important tools in expanding knowledge of valve or wall deformation-related physiological events in in-vitro experimental studies. Eventually, optimized versions of these models may be used to test cardiovascular applications in clinical settings. To realize this ultimate goal, three important themes of methodological limitations should be addressed by future research. First, optimized in-vitro models should account for important physiological events which are not (sufficiently) met in the proposed models. Second, optimized in-vitro models should aim to attain even more accurate geometrical approximations of the natural heart. Third, it is acknowledged that this dissertation primarily demonstrates the proof of concepts which need deeper evaluation and validation by more extensive experiments and measurements. Finally, three challenges are highlighted to bring left heart benchtop models to a next level of innovation. This chapter concludes by formulating four suggestions (left ventricle models LV4 and LV5, and full heart models FH1 and FH2) – developed during the thinking and design process for this PhD work – that we believe may help to accomplish this three-fold ambition, i.e., *‘to go for an active wall, to go for an integrative approach and to go for a transparent model’* in future in-vitro modelling research.

Contents

Dankwoord	3
Samenvatting	11
<i>Inleiding</i>	11
<i>Deel I. De linkerharthelft: Van anatomie tot model</i>	12
<i>Deel II. In-vitromodellen van de linker ventriculaire spier</i>	15
<i>Deel III. In-vitromodellen van de mitralisklep (en de veneuze klep)</i>	18
<i>Deel IV. Modellen van de linkerharthelft: Een integratieve benadering</i>	20
<i>Deel V. Conclusies en perspectieven voor de toekomst</i>	22
Summary	25
<i>Introduction</i>	25
<i>Part I. The left heart: From nature to model</i>	26
<i>Part II. In-vitro modelling of the left ventricular muscle</i>	28
<i>Part III. In-vitro modelling of the mitral (and venous) valve</i>	31
<i>Part IV. Modelling the left heart: An integrative approach</i>	32
<i>Part V. Conclusions</i>	34
Contents	35
Abbreviations	41
Introduction	43
Context	43
Research goals	44
Structure of the PhD thesis	45

Part I. The left heart: From nature to model	47
Chapter 1 The left heart structure and function	49
1.1 Introduction	49
1.2 The left heart.....	50
1.2.1 The circulatory system.....	50
1.2.2 The cardiac cycle.....	52
1.2.3 Diastolic function.....	55
1.3 The cardiac wall.....	60
1.3.1 Macrostructure of the cardiac wall	61
1.3.2 Microstructure of the myocardium	61
1.3.3 From uniaxial cellular motion to 3D wall deformation	65
1.4 Cardiovascular valves	71
1.4.1 The valve plane	72
1.4.2 The mitral valve	72
Chapter 2 In-vitro modelling of the left heart: State-of-the-art	81
2.1 Introduction	81
2.2 Three major developments during history.....	82
2.2.1 Mimicking the complex anatomy	82
2.2.2 Duplicating physiological events.....	83
2.2.3 Compatibility to measurement techniques	84
2.3 Pulse duplicator systems before the 1960s.....	85
2.3.1 Oxygenated animal hearts.....	85
2.3.2 Postmortem human hearts actuated by a piston pump	86
2.4 Pulse duplicator systems after the 1960s	87
2.4.1 Department of Thoracic Surgery, Uppsala, Sweden (1962)	87
2.4.2 Engineering Science Group, Oxford (1972).....	88
2.4.3 Mechanical Engineering Group, Berkeley, California (1977)	90
2.4.4 Cardiothoracic Surgery Unit, New York (1978).....	91
2.4.5 ViVitro Labs Inc., Victoria (1979 – present).....	92
2.4.6 Cardiovascular Fluid Mechanics Lab, Atlanta (1984 - present).....	96
2.4.7 Cardiovascular Engineering Group, Aachen (1981 and 1988)	98
2.4.8 Department of Mechanical Engineering, British Columbia (1985).....	101
2.4.9 Dynatek Laboratories Inc., Galena, Missouri (1990 – present)	102
2.4.10 University of Sheffield, UK (1991)	104
2.4.11 IBiTech-BioMMeda Group of Ghent, Belgium (1992 – present)	106
2.4.12 Cardiovascular Biomechanics Group of Marseille (2000 - present).....	109
2.4.13 Department of Mechanical Engineering, Blacksburg (2004).....	111
2.4.14 Kheradvar Research Group, Pasadena (2006 - present)	112
2.4.15 Department of Mechanical Engineering, Bari, Italy (2006)	115
2.4.16 Vascular Simulations, Stony Brook, New York (2013 - present)	116
2.4.17 Materialise NV, Leuven (2013 – present).....	117
2.5 Conclusion.....	119

Chapter 3	Critical evaluation and practical guidelines for optimizing current models.....	121
3.1	<i>Introduction.....</i>	121
3.2	<i>Limitations and practical guidelines related to left ventricular muscle modelling.....</i>	122
3.2.1	A more realistic thick-wall.....	122
3.2.2	Anisotropic wall properties.....	123
3.2.3	Modelling active contractile wall elements.....	123
3.2.4	Modelling multiple global wall deformation patterns.....	123
3.2.5	Including the twisting motion.....	124
3.3	<i>Limitations and practical guidelines related to the mitral valve.....</i>	125
3.3.1	More anatomic features of the mitral valve.....	125
3.4	<i>Limitations and practical guidelines related to valve plane optimization.....</i>	126
3.4.1	A flexible mitral valve annulus and valve plane.....	126
3.4.2	Including the apical-basal movement of the valve plane.....	127
3.5	<i>Conclusion.....</i>	128
Chapter 4	Design methodology.....	133
4.1	<i>Introduction.....</i>	134
4.2	<i>Global design strategy and application.....</i>	136
4.2.1	Key-Diamond I: Discover and Define.....	138
4.2.2	Key-Diamond II: Develop and Deliver.....	138
4.3	<i>Conclusion.....</i>	153
Part II. In-vitro modelling of the left ventricular muscle.....		155
Chapter 5	Modelling the left ventricular muscle by a thick wall.....	157
5.1	<i>Introduction.....</i>	157
5.2	<i>Physiological background.....</i>	158
5.3	<i>Contraction principle.....</i>	160
5.4	<i>Design and composition of the model.....</i>	162
5.4.1	Thick wall.....	162
5.4.2	Valve plane.....	166
5.5	<i>Rapid prototyping materials and methods.....</i>	168
5.6	<i>Experiments and preliminary results.....</i>	170
5.7	<i>Conclusion.....</i>	174

Chapter 6	Modelling the active wall contraction and torsional motion of the left ventricle.....	175
6.1	<i>Introduction.....</i>	176
6.2	<i>Physiological background.....</i>	176
6.3	<i>Contraction mechanism.....</i>	177
6.4	<i>Realization of the artificial LV muscle.....</i>	180
6.5	<i>Preliminary functional tests.....</i>	180
6.6	<i>Conclusion.....</i>	181
Chapter 7	Modelling the torsional motion of the left ventricle by integration of anisotropic material properties.....	183
7.1	<i>Introduction.....</i>	183
7.2	<i>Background.....</i>	184
7.3	<i>Deformation mechanism.....</i>	186
7.4	<i>Design and composition of the model.....</i>	186
7.5	<i>Materials and methods.....</i>	189
7.6	<i>Preliminary experiments and results.....</i>	190
7.7	<i>Discussion.....</i>	190
7.8	<i>Limitations.....</i>	192
7.9	<i>Conclusion.....</i>	193
Part III. In-vitro modelling of the mitral (and venous) valve.....		197
Chapter 8	Modelling the mitral valve using a fiber-based composite material.....	199
8.1	<i>Introduction.....</i>	199
8.2	<i>Model design.....</i>	200
8.3	<i>Model composition.....</i>	201
8.4	<i>Materials and methods.....</i>	202
8.5	<i>Experiments and results.....</i>	204
8.6	<i>Discussion and conclusion.....</i>	206
8.7	<i>Limitations and future directions.....</i>	207

Chapter 9	Innovative design of a PIV compatible venous valve model.....	209
9.1	<i>Introduction</i>	209
9.2	<i>Materials and methods</i>	210
9.2.1	<i>Practical guidelines for building the venous valve model.....</i>	210
9.2.2	<i>Experimental setup.....</i>	212
9.3	<i>Results.....</i>	212
9.4	<i>Discussion and conclusion.....</i>	215
9.5	<i>Limitations and future research</i>	215
Part IV. Modelling the left heart: an integrative approach.....		217
Chapter 10	Modelling the left heart by a monolithic approach	219
10.1	<i>Introduction, design and composition.....</i>	219
10.2	<i>Realization of the monolithic left heart model.....</i>	222
10.2.1	<i>Preparation of the CAD heart model</i>	223
10.2.2	<i>Production of a sacrificial core by rotational molding</i>	224
10.2.3	<i>Creation of the left heart model and integration of the MV model</i>	227
10.2.4	<i>Model realizations.....</i>	228
10.3	<i>Connection with the ViVITRO simulator</i>	230
10.3.1	<i>Configuration of the original ViVITRO suspension system</i>	231
10.3.2	<i>Design and realization of a new suspension system.....</i>	232
10.3.3	<i>Connection to the ViVITRO mock circulatory loop.....</i>	238
10.4	<i>Experimental test setup.....</i>	238
10.5	<i>Preliminary results.....</i>	239
10.6	<i>Discussion and conclusion.....</i>	241
10.7	<i>Limitations and further directions.....</i>	242
Chapter 11	Modelling the left heart by a bilithic approach: Feasibility study of the effect of torsion on intracardiac diastolic pressure parameters.....	247
11.1	<i>Introduction</i>	247
11.2	<i>Left heart model design</i>	249
11.3	<i>Left ventricular model design.....</i>	250
11.4	<i>Experimental protocol</i>	254
11.5	<i>Preliminary results.....</i>	258
11.5.1	<i>Transmitral pressure differences during early diastole.....</i>	258
11.5.2	<i>Intraventricular pressure differences during early diastole</i>	258
11.6	<i>Discussion of results.....</i>	261
11.7	<i>Conclusions</i>	263
11.8	<i>Limitations and further directions.....</i>	264

Part V. Conclusions and future directions 267

Chapter 12 Conclusions and future perspectives 269

12.1 General discussion 269

 12.1.1 Key findings 270

 12.1.2 Methodological considerations..... 272

 12.1.3 Innovations 277

12.2 Future directions..... 279

 12.2.1 To go for an active wall 280

 12.2.2 To go for an integrative approach..... 282

 12.2.3 To go for a transparent model 282

References 285

List of figures..... 301

List of tables 311

Abbreviations

ESP	End-systolic pressure
ESPVR	End-systolic pressure-volume relation
ESV	End-systolic volume
FDA	Food and Drug Administration
FEM	Finite element method
FH1	Full heart model 1
FH2	Full heart model 2
FIH	First in humans
HVMB	Helical ventricular myocardial band
IDE	Investigational Device Exemptions
ISO	International Organisation for Standardization
IVPDe	Intraventricular pressure difference during early diastole
LA	Left atrium
LAP	Left atrial pressure
LDA	Laser Doppler anemometry
LH1	Left heart model 1
LH2	Left heart model 2
LV	Left ventricle
LV1	Left ventricular model 1
LV2	Left ventricular model 2
LV3	Left ventricular model 3
LV4	Left ventricular model 4
LV5	Left ventricular model 4
LVP	Left ventricular pressure

ABBREVIATIONS

MRI	Magnetic resonance imaging
MV	Mitral valve
MV1	Mitral valve model 1
MV2	Mitral valve model 2
MVPHT	Mitral valve pressure half time
P	Phosphate
PG	Practical guideline
PIV	Particle image velocimetry
PML	Posterior mitral leaflets
PMMA	Polymethyl methacrylate
PMPM	Posteromedial papillary muscles
PV	Pulmonary valve
PVA	Polyvinyl alcohol
PV-loop	Pressure-volume loop
RA	Right atrium
RPT	Rapid prototyping techniques
RV	Right ventricle
SLA	Stereolithography apparatus
SLS	Selective laser sintering
THV	Transcatheter heart valves
TMPDe	Transmitral pressure differences during early diastole
TV	Tricuspid valve
US	Ultrasound
VIA	Viscoelastic impedance adapter
VV	Venous valve

Introduction

CONTEXT

Cardiovascular disease is one of the leading causes of death worldwide [1]. To tackle this worldwide problem, substantial research effort is devoted to continually advance cardiovascular procedures and medical devices. These cardiovascular devices need to meet extreme functional and quality requirements and are subjected to a set of extended tests before such appliances can be implemented in clinical settings. These requirements are defined by regulatory agencies, such as the Food and Drug Administration (FDA) and International Organization for Standardization (ISO), in certificates that are needed before these medical devices can be launched on the market. Attaining such certificates includes compliance with strict protocols for performance characteristics, bench testing, virtual testing, in-vivo tests, and clinical studies. The FDA mentions in a guideline draft document [Draft Guidance for Industry and Food and Drug Administration Staff, Investigational Device Exemptions (IDE) for Early Feasibility Medical Device Clinical Studies, Including Certain First in Human (FIH) Studies, November 10, 2011][2] that clinically relevant benchtop models, preferably the best as possible, are urgently needed for in-vitro testing.

Although the pump function of current in-vitro modelling approaches for the human (left) heart has already been well established, literature shows that there remain a number of elementary anatomical features and physiological events that are not included in current in-vitro modelling. For instance, current cardiovascular simulators do not account for the natural left ventricular twisting motion and active muscle contraction, nor do these models include the basic structure of the biological mitral valve apparatus. In the context of mimicking the anatomical and physiological conditions of the human heart as accurately as possible, it is clear that there is an urgent need for novel concepts which include these key features and are capable of modelling their interrelationships.

RESEARCH GOALS

Throughout this dissertation, multiple innovative methods for more advanced modelling of the left heart's anatomical features and physiological events will be developed and subsequently assembled in order to mimic their joint interaction. This work was guided by three major research goals:

Goal 1: *Defining practical guidelines for more realistic in-vitro left heart modelling in terms of anatomical and physiological likeness*

Goal 2: *Designing more realistic models of the left ventricle and the mitral valve apparatus*

Goal 3: *Integrating these novel components to attain a more nature-like model of the left heart*

STRUCTURE OF THE PHD THESIS

This dissertation is divided into five major parts.

Part I gives a background overview and state-of-the-art of current in-vitro modelling approaches. Chapter 1 reviews the left heart anatomy and physiology. Subsequently, Chapter 2 gives a literature overview of previous in-vitro modelling approaches and identifies major challenges in attaining a more nature-like left heart anatomy and physiology. In Chapter 3, these challenges are summarized and practical guidelines are formulated towards the design and development of more nature-like in-vitro left heart models. Chapter 4 describes the design methodology applied in this dissertation by which new ideas were generated, selected and further developed into the new functional prototypes that are presented in Parts II to V.

In Part II, three novel in-vitro left ventricular models are introduced. The first LV model (LV1) is equipped with a thick wall, which is a more realistic representation of the LV wall in comparison with the generally used thin walled membranes (Chapter 5). The second LV model (LV2) includes active contractile elements which enables mimicking natural torsional motion of the wall (Chapter 6). A second technique to generate this twisting motion is by implementing anisotropic wall properties, as demonstrated by the third LV model (LV3; Chapter 7).

Part III presents two concepts of in-vitro valve modelling. The first concept is a basic mitral valve model (MV1 and MV2) which includes all elementary parts of the mitral valve apparatus (Chapter 8). The second concept, an add-on to the left heart work, is a PIV compatible venous valve model (VV) for the validation of Computational Fluid Dynamics (CFD) models (Chapter 9).

Whereas parts II and III focus on the modelling of individual cardiovascular components, part IV integrates these different components into a total left heart model. This integrative approach is applied for two model versions. Chapter 10 deals with the monolithic version (LH1) and focuses on the design, realization and connection to the pump system, whereas Chapter 11 describes the bilitic version (LH2) and applies this model to relate different LV deformation patterns to diastolic parameters.

Finally, part V summarizes the most important conclusions of this dissertation with regard to the research goals and outlines future perspectives and directions for further research.

Part I

The left heart:

From nature to model

The left heart structure and function

Before addressing the research and new concepts of this PhD dissertation (part II-IV), it is important to provide a general background overview. In this chapter, key elements of the anatomy and physiology of the left heart will be discussed.

1.1 INTRODUCTION

The heart is probably the most vital organ of the human body and is a hollow, four-chambered muscular organ. Its function is to rhythmically pump blood throughout the body's blood vessels in order to supply organs and tissues with oxygen- and nutrient-rich blood, while carrying away carbon dioxide and waste products from the organs to the lungs. To transport blood throughout the whole body, the heart muscle has a double pump function: the left side pumps the oxygenated blood throughout the body whereas the right half of the heart pushes the oxygen-depleted blood from the heart through the lungs. The left and right heart pumps work as two independent systems that are anatomically separated from each other by a thick muscular wall (the septum). Each of these pumps consists of two chambers, the atrium and the ventricle. In the atrium, the blood that has returned to the heart is collected and pushed towards the lower positioned ventricle. The ventricle is the discharging

chamber that pumps the blood from the heart. At the bottom of the heart, the ventricles join in the form of a point, which is called the apex. Since the aim of this dissertation is to design a true to nature phantom of the left heart, our discussion in this physiology review is focused on the left side function of the heart.

1.2 THE LEFT HEART

1.2.1 The circulatory system

As a pulsatile pump, the heart shows two distinct phases: systole (contraction) and diastole (relaxation). During systole, the heart pumps blood into the arteries, whereas during the diastole the ventricles are filled with blood. During this process, the performance of the left ventricle depends on the ability to cyclically change phase. In diastole, the left ventricle functions as an elastic chamber to allow the ventricle's filling at low atrial pressure [3]. In systole, the left ventricle operates as a contracting and stiffening chamber to eject blood at arterial pressure. In this manner, the ventricle alternates its function between diastolic filling and systolic ejection. We consider diastole to begin with the closing of the aortic valve. This phase successively includes the pressure drop of the left ventricle, rapid filling, diastasis (a phase that is only clearly discernable when there is a low heart rate) and atrial contraction [4]. Subsequently, the ventricular contraction begins, initiating systole.

The composition of the heart is illustrated in Figure 1, while Figure 2 shows the circulation of the blood through the four heart chambers. The oxygen-depleted blood coming from the organs flows through the venae cavae and through the right atrium (RA) into the right ventricle (RV). The RV then pumps this oxygen-depleted blood via the pulmonary artery into the lungs. Here, the blood takes up fresh oxygen. This oxygen-rich blood flows from the lungs through the four pulmonary veins (i.e., left and right superior, and left and right inferior pulmonary veins) via the left atrium (LA) into the left ventricle (LV). The LV, which is the most powerful chamber, then pumps the oxygenated blood via the aorta to the entire body, except for the lungs. Thanks to the four heart valves, the blood flow can only take place in one direction through the heart, passing successively through the tricuspid valve (TV), the pulmonary valve (PV), the mitral valve (MV), and the aortic valve (AV).

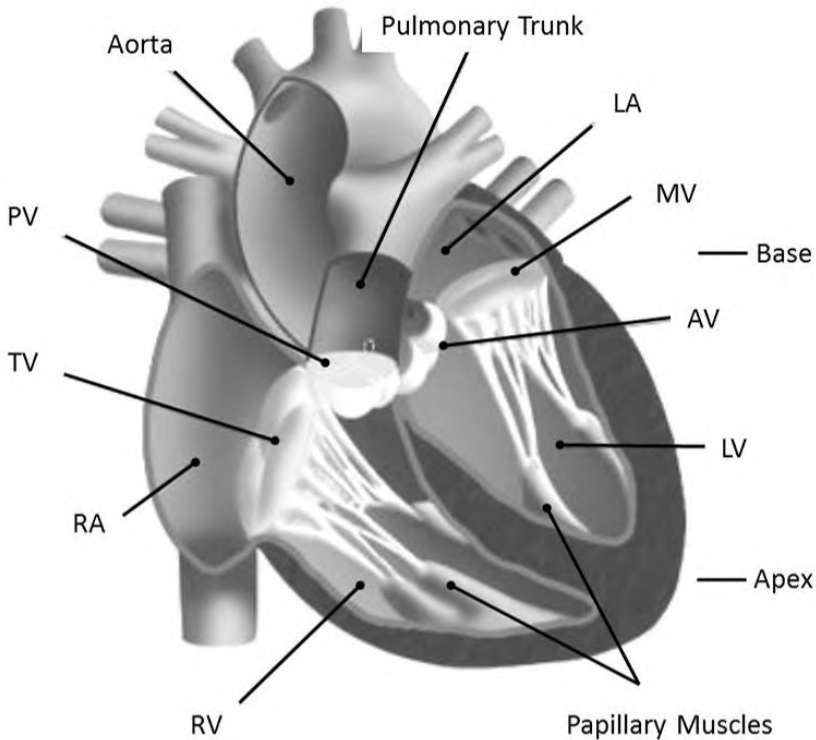


Figure 1: Composition of the heart with Right (RA) and Left Atrium (LA), the Right (RV) and Left Ventricle (LV), the Tricuspid Valve (TV), the Pulmonary Valve (PV), the Mitral Valve (MV) and the Aortic Valve (AV). Adapted from [5].

Looking in more detail to the left heart circulation, we see that oxygen-rich blood flows through the pulmonary veins from the lungs into the left atrium. The left atrium is separated from the left ventricle through the mitral valve. This mitral valve consists of two leaflets, one anterior and one posterior that close while the ventricle contracts (systole). The mitral valve leaflets are connected to the heart wall with papillary muscles that go over into tendon strings. These papillary muscles ensure that the leaflets of the mitral valve cannot invert or displace toward the atrium. As such, these muscles prevent the backflow of blood from the left ventricle into the left atrium of the heart (see §1.4.2 The mitral valve).

During systole, the left ventricle pushes the blood through the aortic valve towards the aortic arch. The aortic valve normally consists of three leaflets that seal off the blood flow during diastolic relaxation. The aortic arch is the first segment of the aorta, the main artery of the body. Three major arteries originate from this aortic arch, from left to right: the brachiocephalic

artery (supplying blood to the brain and head), the left common carotid artery, and the left subclavian artery. Once the blood passes the arteries and arterioles, it leaves the arterial system at the level of the capillaries. Flowing through the venules and veins, the blood enters the venous system. In contrast to the arteries that contain no valves, some veins contain valves, the so called venous valves. These prevent the backflow of venous blood and are key features for propelling the blood towards the venae cavae and the right heart. After that, the right heart pumps the blood into the lungs back into the left heart.

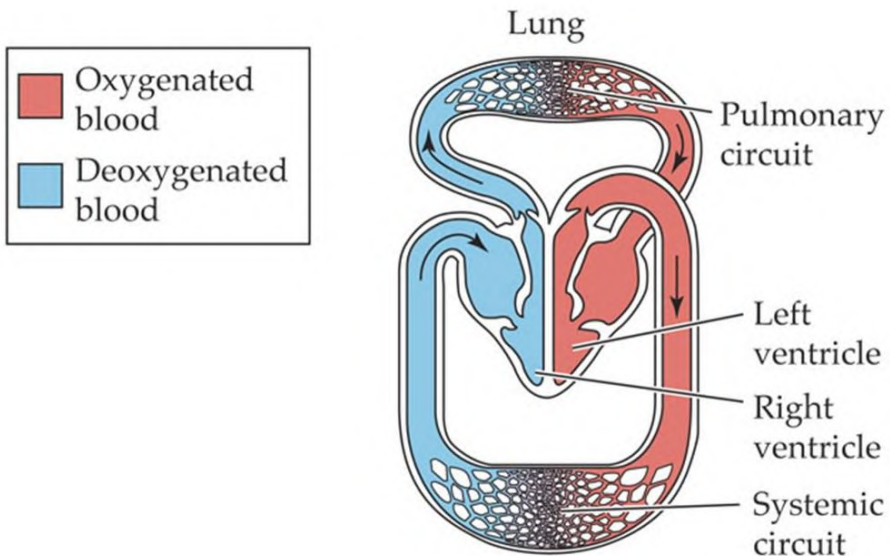


Figure 2: The blood flow through the four heart chambers. Adapted from [6].

1.2.2 The cardiac cycle

The cardiac cycle in the left ventricle can be described as a function of pressure and volume, also known as the Pressure-Volume loop (PV-loop) and shown in Figure 3. Starting the loop at the end of diastole with a filled LV, ventricular systole begins with the isovolumic contraction and the closing of the mitral valve, which is indicated as point A of the PV-loop. Then, during this isovolumic contraction, the ventricular pressure rises very quickly to point B of the loop. At this time point, the aortic valve opens and the ejection phase of the systole starts. The left ventricle volume swiftly decreases until the left ventricular pressure drops below the aortic pressure, which is shown as point C. At this time point, the left ventricle has reached its minimal or end-systolic

volume (ESV), causing the aortic valve to close. At this point, the isovolumic relaxation begins. Due to a constant volume, the ventricular pressure speedily decreases to the point where the pressure in the left ventricle is lower than that in the LA (point D in Figure 3). At this point, the mitral valve opens, the ventricle starts filling and quickly reaches its maximum or end-diastolic volume (EDV), to point A, which corresponds with the starting point of where the next cardiac cycle begins.

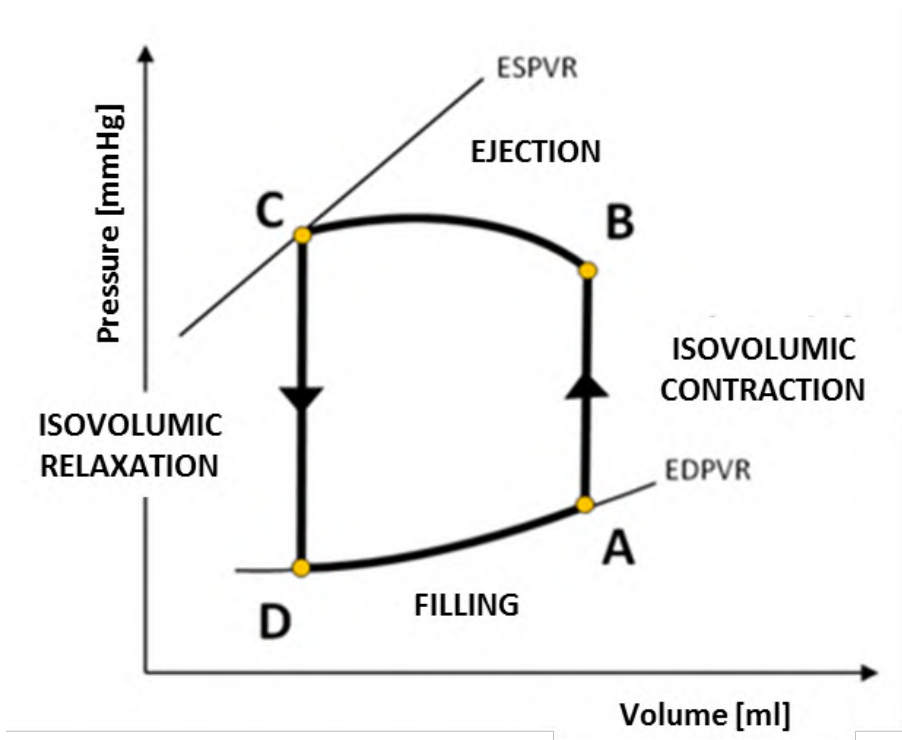


Figure 3: Ventricular pressure-volume relation during a cardiac cycle with ESPVR: end-systolic pressure-volume relation and EDPVR: end-diastolic pressure-volume relation.

On the one hand, the filling phase proceeds according to the End-Diastolic Pressure-Volume Relation (EDPVR) which is also known as the passive filling curve of the left ventricle. The slope of the EDPVR is the equivalent of passive ventricular stiffness (or the reverse of ventricular compliance). On the other hand, the maximum pressure which the left ventricle can supply at a given volume is defined by the End-Systolic Pressure-Volume Relation (ESPVR) which is a measure of the inotropic state

(contractility) of the ventricle. On the basis of this pressure-volume relation, the cardiac cycle is divided in the two phases of systole (A-B-C) and diastole (C-D-A).

Figure 4 illustrates the pressures, flow rates, and volumes in the cardiovascular system during one cardiac cycle. In addition, the above described points A, B, C, and D are displayed as a function of time.

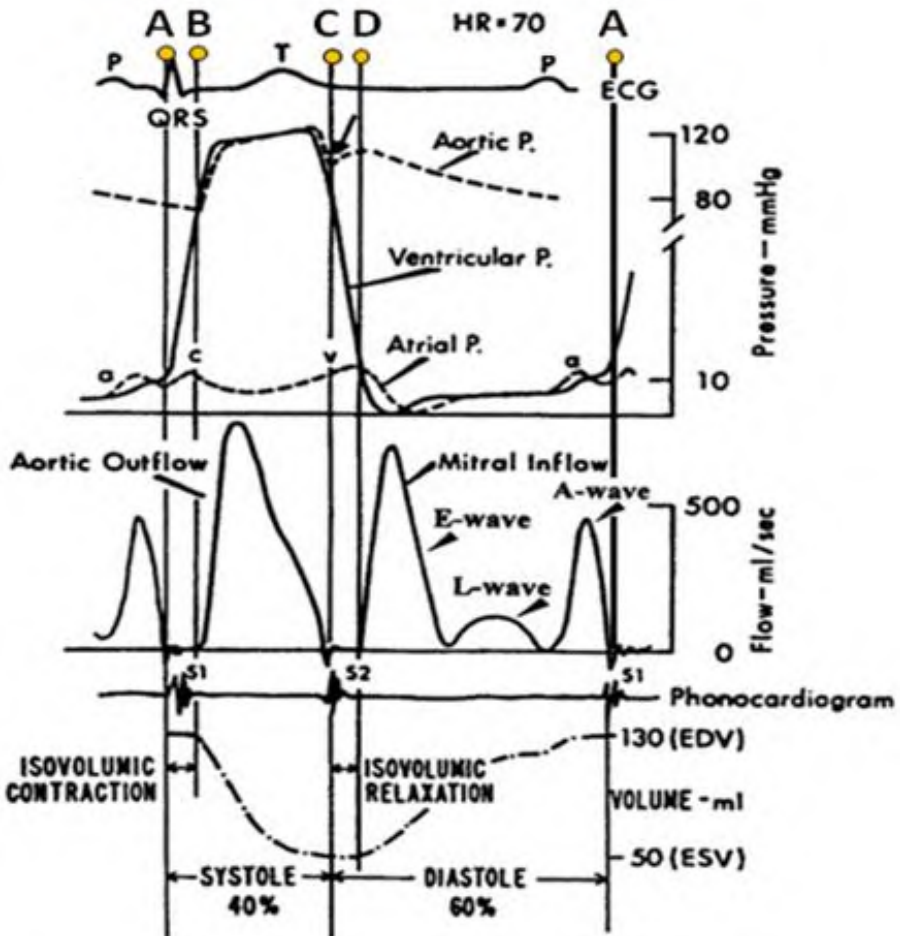


Figure 4: Changes in pressure, flow, and volume in the left heart during a cardiac cycle. The points A, B, C and D indicate the start of the following stages: A, isovolumic contraction; B, ejection; C, isovolumic relaxation; and D, filling. Adapted from [7].

1.2.3 Diastolic function

1.2.3.1 Physiology of diastolic filling

During the filling phase of the diastole, three stages are distinguished based on the characteristic pattern of the blood flow rate through the mitral valve. These three stages, shown in Figure 5, are labeled as (1) the early filling or rapid filling phase, (2) the diastasis or slow filling phase, and (3) the filling during atrial contraction.

The early filling phase

The early filling phase occurs immediately after the ejection phase of the left ventricle, where energy is stored in the myocardium by the compression and/or deformation of the elastic elements in the muscular wall [8]. During early filling, active myocardial relaxation and elastic recoil cause a rapid drop in the left ventricular pressure throughout the isovolumic relaxation [3].

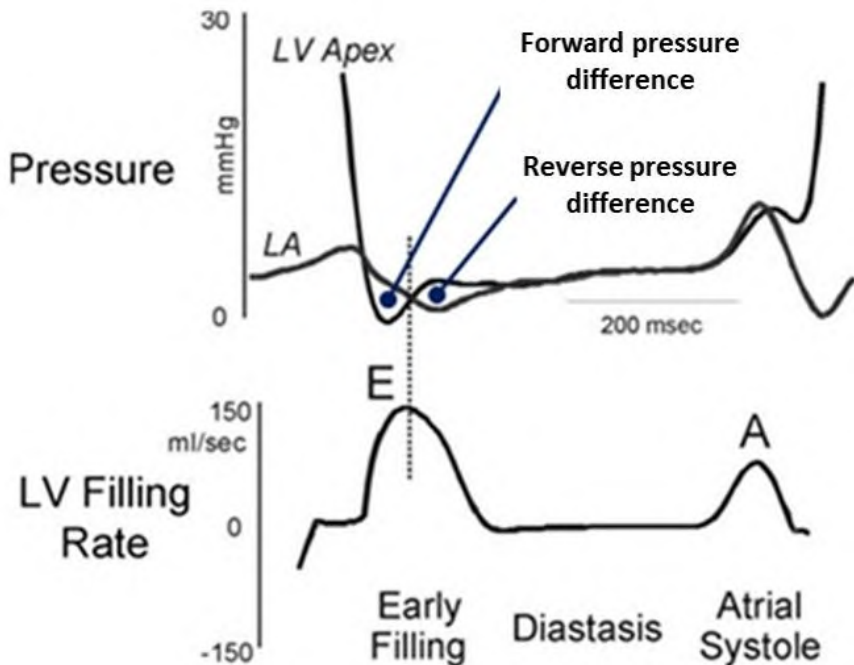


Figure 5: Top panel: Pressure measurement at the level of the LV apex and in the LA. Bottom panel: Accompanying LV filling rate, as assessed in a dog. Adapted from [9].

This decrease in pressure in the left ventricle causes a pressure difference during early diastole [10] (Figure 5) which begins from the LA and then spreads towards the LV apex [11]. This pressure difference accelerates the blood coming from the LA and causes a rapid inflow which is carried on towards the left ventricular apex and then again upwards, opening the mitral valve. This diastolic pressure difference draws the blood into the left ventricle and hence can be regarded as a measure of left ventricular relaxation [3].

The LV pressure drop is so fast that - during the first 40ms after the opening of the mitral valve - the pressure continues to drop in spite of the rapid increase of the LV volume [9, 12]. This phenomenon, i.e., the continuing decline in the LV pressure despite the rapid filling during early diastole, was already observed by Katz in 1930 [13]. He inferred from this phenomenon that a ventricle during relaxation has not only the ability to lead blood into the chamber, but is also effectively pursuing an active suction on the blood. This is why this stage is also called the ‘active filling’ or ‘active suction’ phase.

The transmitral flow rate of this early diastole filling is determined by the cross-sectional area of the valve orifice and by the pressure difference between the LA and the LV apex (shown as the "forward pressure difference" on Figure 5): the lower the early diastolic pressure is in the LV, the greater the pressure difference is for the filling. In this way, the LV has the ability to fill itself without really depending on an increase in the LA pressure. Following the start of the filling of the LV, the pressure difference between the LA and the LV apex drops and briefly reverses its direction (shown as the “reverse pressure difference” on Figure 5).

These findings were also confirmed by Courtois et al. [11] in dogs. The pressure difference between LA and LV apex (defined as $p_{LA} - p_{apex}$) here is measured in two portions by measuring an additional pressure between the LA and the LV apex, namely at the base level. The total pressure difference is thus composed of the transmitral pressure difference (Equation 1) and the intraventricular pressure difference (Equation 2). During early diastole (subscript ‘e’), they observed that the LV pressure rise (or decrease of the pressure difference) first occurs at the level of the apex, and only later at the level of the base. From this observation, they concluded that the filling action near the apex is finished earlier than the filling action near the base. This makes that the blood at the level of the apex is slowing down sooner than the blood at the height of the base, causing the blood to first accumulate near the apex.

$$TMPDe = p_{LA} - p_{base} \quad \text{Equation 1}$$

$$IVPDe = p_{base} - p_{apex} \quad \text{Equation 2}$$

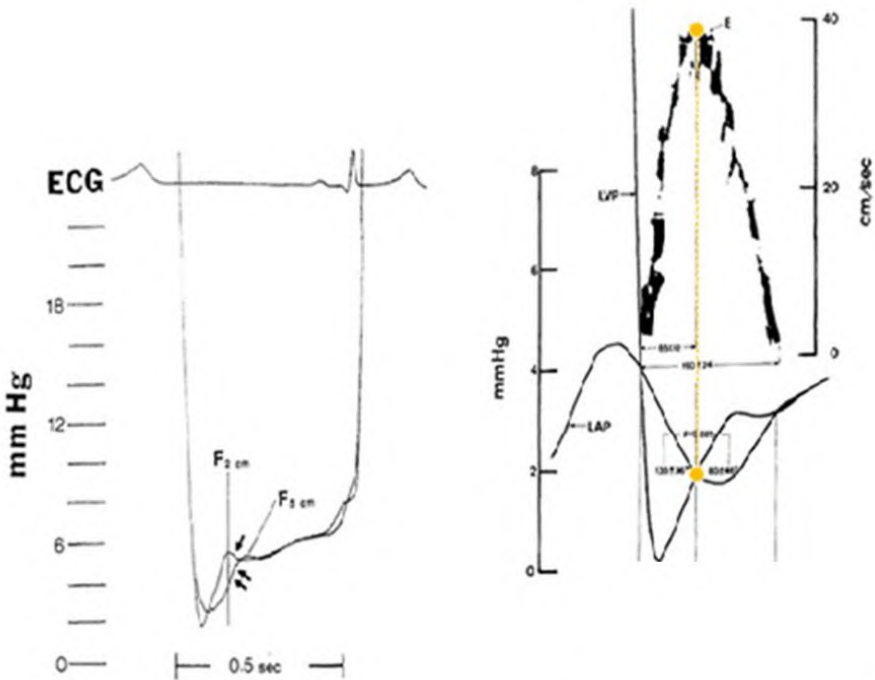


Figure 6: Left: Simultaneous intraventricular pressure measurement 2 and 5 cm away from the apex towards the base, respectively. Right: simultaneously measured transmitral pressures, in the middle of the atrium and the center of the ventricle, respectively. Adapted from [11].

From the TMPDe measurements they observed that the beginning, the maximum and the end of the E-wave occur simultaneously with the three intersections of the atrial (Left Atrial Pressure, LAP) and LV pressure (Left Ventricular Pressure, LVP), respectively. On the basis of these findings, they made the association between the forward transmitral pressure difference and the acceleration of the blood flow, while the opposite transmitral pressure difference is related to the delay of blood flow, such as illustrated in Figure 6 (right panel). From this study, we can deduce that pressure differences play an important role in the acceleration/deceleration of the blood flow.

The brief reversal of the transmitral pressure difference (from “forward pressure difference” to “reverse pressure difference” on Figure 5) has first been observed by Ling et al. in 1979 and is considered to be physiologically normal [10]. Due to this reversed pressure difference, the blood inflow is slowing down, causing the mitral valve to close and the rapid filling to end. The time which is needed for this blood inflow is strongly determined by the functional stiffness of the LV wall. This time indication

hence is used as a non-invasive measurement of the stiffness of the LV diastolic function [14-16].

Diastasis or slow filling phase

Diastasis is the time interval between the early filling phase and the atrial contraction phase. Throughout this phase, the pressures in the LA and the LV attain an equilibrium so that there is almost no transmitral blood flow. During diastasis, the mitral valve remains predominantly closed.

Filling during atrial contraction

Whereas the LV produces an under-pressure during early diastole by active relaxation and recoiling, the LA generates an over-pressure during late diastole by means of contracting. This atrial contraction causes a second positive pressure difference between the LA and the LV apex, which - on its turn - pushes the blood towards the LV [3, 11]. After this atrial contraction, the LA relaxes, the atrial pressure drops below the LV pressure and the mitral valve begins to close. The subsequent onset of the LV systole generates a sudden increase in pressure in the LV, so that the mitral valve closes completely. This point in time denotes the end of the diastole.

1.2.3.2 Determinants of diastolic function

The three major determinants of diastolic function are preload, isovolumic relaxation, and passive ventricular properties [17].

Preload

The blood flow from the LA to the LV strongly depends on the pressure difference across the mitral valve (and on the resistance the mitral valve is exerting to the blood flow). Therefore, the pressure in the LA (the filling pressure or “*preload*”) plays an important role in diastolic function. This LA pressure varies according to the functions the LA is fulfilling throughout one heart cycle. During ventricular systole, the LA operates as a reservoir, while during diastase, the LA functions as a conduit. Finally, during diastole, the LA works as a pump. The *resistance* of a healthy mitral valve is minimal because the valve leaflets offer very little resistance to the flow and open wide. This resistance is largely determined by the geometry of the valve relative to the geometry of the LA and LV [18].

Isovolumic relaxation

The rate of pressure decline in the LV is also determined by the rate of *relaxation* of the muscle fibers (this is termed *lusitropy*). At the molecular level, the cyclic phase changes between contraction and *relaxation* are the result of interactions between myofilaments. Relaxation is the process of the myocardium returning to its strainless/strain-free and slackened state. This relaxation is directly dependent on calcium transport and is regulated largely by the sarcoplasmic reticulum of the cardiomyocytes, which are responsible for rapidly re-sequestering calcium following contraction. This myocardial relaxation results in an exponential pressure drop from the end-systolic pressure to the minimum LV pressure. Elastic recoil is regarded to promote this myocardial relaxation [19-21].

Under normal conditions, ventricular *relaxation* starts already in the second half of the systole, and is completed at the minimal LV pressure during the early filling. Relaxation depends on load: an increased load slows the myocardial relaxation [22]. In addition, relaxation is also conditional upon heart rate, body temperature, and neuro-hormonal stimulation [23]. The onset, velocity and intensity of this myocardial relaxation are important determinants of diastolic filling.

Passive Ventricular Properties

Finally, an optimal diastolic filling is importantly determined by the passive characteristics of the chambers. These passive structural features comprise *elasticity* (change of the muscle cell length at a given change in strain) and *compliance* (change in volume at a given change in pressure) [23]. These passive characteristics are quantified and graphically illustrated by the passive pressure-volume relation (EDPVR such as illustrated in Figure 3) and are particularly important immediately after the early filling phase. At this point in the cardiac cycle, it is assumed that the pressure within the LV is the result of the balance between the pressure forces within the LV cavity on the one hand, and the resistive forces due to the elasticity of the myocardium on the other hand [7].

During systole, potential energy is stored within the myocardium in the form of elastic energy (analogous to compressing a coil spring) which is returned during the early diastolic filling phase (analogous to releasing a coil spring). This energy storage and release assists adequate ventricular filling, even at low filling pressures [24]. This phenomenon is also known in the literature as 'elastic recoil' [19-21].

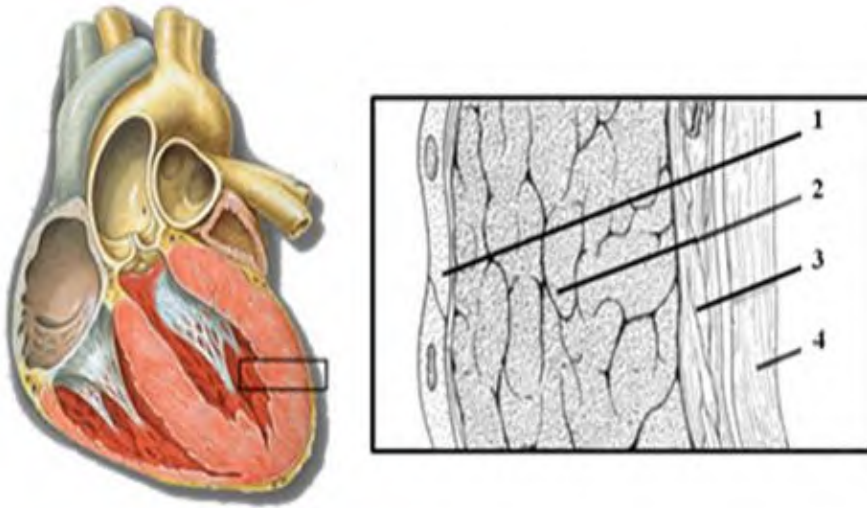


Figure 7: The cardiac wall comprises 1) the endocardium, 2) the myocardium, 3) the epicardium, and 4) the pericardium. Adapted from [25, 26].

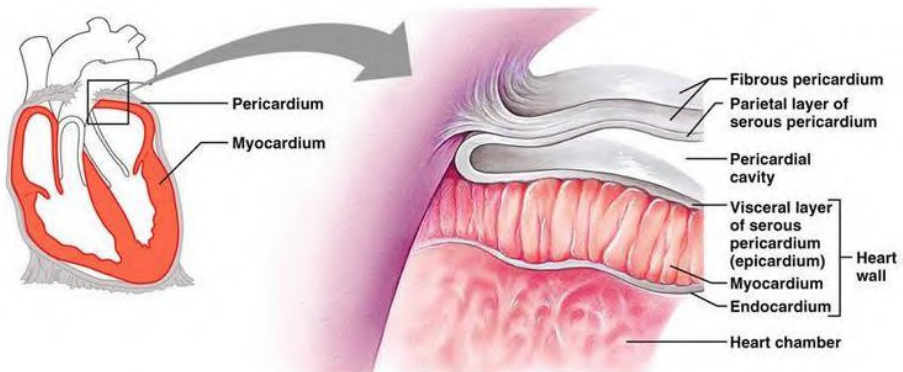


Figure 8: Macrostructure of the cardiac wall. Adapted from [27].

1.3 THE CARDIAC WALL

The pumping function of the heart is realized by the rhythmic contraction and relaxation of cardiac muscle cells (cardiomyocytes) under the stimulation of electrical currents. These cardiomyocytes, embedded in an extracellular matrix (ECM), compose the myocardium of the cardiac wall.

1.3.1 Macrostructure of the cardiac wall

As described above, the pressure development and ejection of blood are the results of the tension generated by the heart muscle tissue. This dynamic tension is realized by the rhythmic contraction and relaxation of the myocardium. The cardiac wall consists of four functional layers: the endocardium, the myocardium, the epicardium, and the pericardium (Figure 7). The *endocardium* is the inner layer of the heart that covers the inner surfaces of the ventricles, atria, and cardiac valves, and is composed of endothelial cells. The *epicardium* and *pericardium* are the two outer layers of the heart, forming together a fibrous protective sac. The epicardium (or visceral pericardium) is the elastic layer covering the outer surface of the heart whereas the pericardium (or parietal pericardium), mainly consisting of connective tissue, is the outer layer that holds the heart firmly in place. A thin film of lubricating fluid separates the epicardium from the pericardium and allows the heart to move easily in the fibrous sac. The fibrous pericardium not only holds the heart in place, it also protects the heart and anchors it to the surrounding structures.

The *myocardium* is the actual muscle tissue, lying between the endocardium and epicardium (Figure 8). This layer is composed of muscle fibers, collagen fibers, and elastin fibers. The muscular component is important for the active properties of the heart, whereas the collagen and elastin components are essential for the passive elastic properties of the heart. The muscle layer of the heart is thickest in the left ventricle (10 mm during diastole), while it is only 3 to 4 mm thick (during diastole) for the right ventricle. This difference is related to the fact that the pressure development in the left ventricle is much larger (120 mmHg) than in the right ventricle (20 mmHg) due to the much higher hydraulic resistance of the systemic circulation in comparison with the pulmonary circulation.

1.3.2 Microstructure of the myocardium

1.3.2.1 Microscopic structure of cardiomyocytes

Cardiomyocytes are specialized cardiac muscle cells with an elongated, branched, and cylindrical shape, a diameter of about 12-20 μm and a length of about 50-100 μm [28]. These specialized cells are joined end-to-end by *intercalated disks*, which contain gap junctions. These junctions support the

electrical continuity between cells, so that nervous pulses can easily spread to all the cardiac muscle cells.

Cardiomyocytes show striations similar to those on skeletal muscle cells, but unlike multinucleated skeletal cells, they have only one, unique nucleus (see Figure 9). Their contraction proceeds in a synchronized, rhythmic, powerful and autonomous manner.

Examining the microscopic structure of a cardiomyocyte, one can distinguish the nucleus in the center of the cell from the striation. This striation, comprising darker A-bands and lighter I-bands, is mainly formed by alternating segments of the protein filaments myosin and actin. Myosin filaments are thicker than actin filaments, and this causes the darker appearance of A-bands (largely composed by myosin) and the lighter appearing I-bands (mainly containing actin) (Figure 10). Just like skeletal muscle, the cardiac muscle cell is made up of *myofibrils* (Figure 10), comprising *myofilaments*. These myofilaments comprise a series of structured contractile elements, the *sarcomeres*. The sarcomere is the fundamental contractile unit of striated cardiac muscle and is defined as the area of the myofilament between two Z-lines that bisect the I bands. In the human heart, the length of one sarcomere varies between 1.6 to 2.2 μm (in resting state).

The molecular structure of the sarcomere can be further investigated with an electron microscope. Just as in skeletal muscle, the primary structural proteins of cardiac muscle are actin and myosin. The thinner actin filaments can be easily distinguished with the electron microscope from the thicker myosin filaments. In one sarcomere, zones with myosin correspond to the A-band. I-bands, on the other hand, comprise the thin filaments that run from the Z-lines towards the center of the sarcomere (M-line). These zones are mainly made of actin and the troponin-tropomyosin complex.

The biochemical and physical interactions between the thinner actin and thicker myosin filaments cause a shortening of the length of the sarcomere, so that active tension development and shortening of the cardiomyocytes can occur. This proceeds according to “*the sliding filaments principle*” [29]. This principle is the “engine” of the contraction of the heart muscle cell, and will be further explained in detail in the next section. To understand its working mechanism, we first need to consider the chemical structure of these filaments.

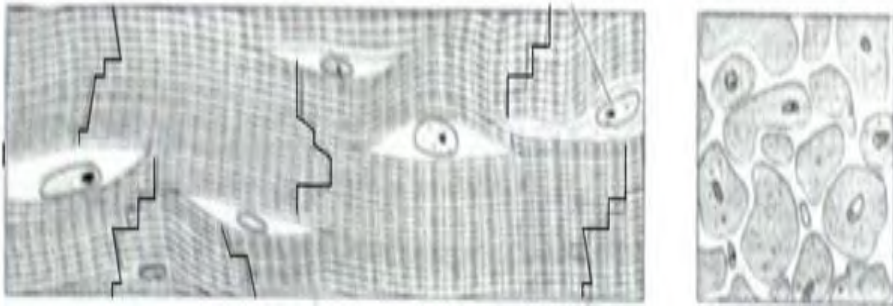


Figure 9: Microscopic structure of cardiomyocytes: mononuclear, striated muscle cells. Adapted from [26].

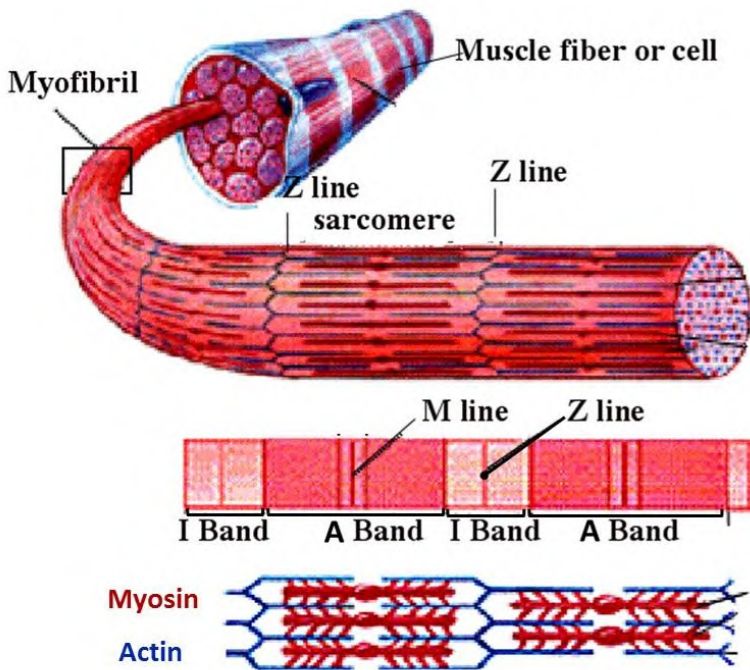


Figure 10: Myofibrils of the cardiomyocyte. Adapted from [30].

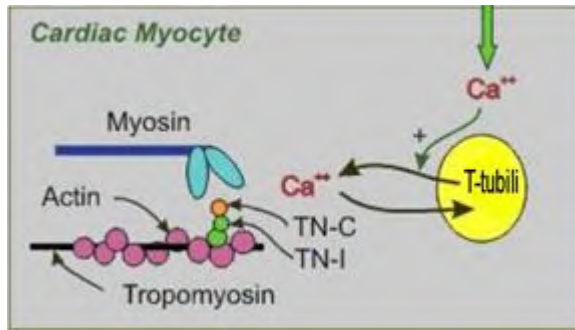


Figure 11: Myosin filaments are composed of myosin proteins; each protein has two heads that are connected via the neck to the tail portion. Actin filaments comprise three different types of protein: actin, tropomyosin, and troponin. Adapted from [31].

Myosin filaments (see Figure 11) are composed out of more than 300 myosin proteins, each having a molecular weight of about 470.000 Daltons. Each myosin protein contains two heads that are connected via the neck to the tail portion. Actin filaments, on the other hand, consist of three different types of proteins: actin, tropomyosin and troponin. Actin consists of globular proteins, labeled G-actin, which are spirally wound to form filamentous fibers, labeled as F-actin. These fibers are surrounded by tropomyosin. On tropomyosin, the troponin units are located. In addition, the cardiac muscle cell also comprises other structures, such as mitochondria (for the energy supply), and blind-ending pouches, T-tubules (for the calcium supply). The latter are part of the cell membrane.

1.3.2.2 Contraction and relaxation of cardiomyocytes

To perform their pumping function, the cardiomyocytes must be able to shorten but also to lengthen their fibers. The shortening of the myofilaments corresponds to the development of active tension (contraction principle) whereas the lengthening of the fibers corresponds to the relaxation of the cardiomyocytes (relaxation principle).

Active tension development – contraction principle

When an action potential arrives at the cardiomyocyte, the polarity of the cell membrane changes. Hence, also the polarities of the T-tubules change, causing the T-tubule to release calcium ions. These Ca²⁺ ions bind with the troponin units (Troponin C). As a result, the troponin units drop down between the filamentous fibers of the F-actin, which releases the G-actin units of the actin filaments. Then, the G-actin makes direct contact with the myosin heads (Figure 12 step 1). ATP (adenosine triphosphate) provides the energy for

cross-bridge cycling and is during the process converted to ADP (adenosine diphosphate) and P (phosphate).

This released energy is used for the conformational change of the myosin protein, more particularly for bending the neck portion of the myosin molecule (Figure 12, step 2 and 3). This bending process generates power which is then transferred, due to the very close contact between the myosin heads and the actin filaments. In this manner, the myosin filaments move (slide) relative to the actin filaments, causing the sarcomere of the cardiomyocyte to shorten, i.e., to contract. The point in time when myosin and actin interconnect, is also known as the formation of ‘*cross-bridges*’.

Relaxation principle

During the relaxation of the heart muscle cell, the actin-myosin bond is broken down (Figure 12, step 4) and the calcium-ions are pumped back into the T-tubules, waiting for the next action potential to arrive. This cross-bridge cycling occurs in all involved cardiomyocytes and repeats itself as long as power is required. This phenomenon is hence also referred to as ‘cross-bridge cycling’ or ‘sliding filament theory’. The whole process by which depolarization at the cell surface initiates interaction between actin and myosin so that cardiomyocytes can produce tension and shorten, is also referred to as *excitation-contraction coupling*.

1.3.3 From uniaxial cellular motion to 3D wall deformation

1.3.3.1 Myocardial macrostructure

The myocardium comprises a heterogeneous complex network of myocardial fibers that are chemically, mechanically, and electrically connected to one another. One of the most intriguing issues in cardiac physiology is to understand how the above described uni-axial force generation at the microscopic level of the cardiomyocytes is transferred to the three-dimensional wall deformation at the macroscopic level of the ventricles during systole and diastole. Notwithstanding more than five decades of research, the relationship between cardiomyocyte mechanics and ventricular mechanics still remains a much debated subject. Below, we give a brief overview of four different prominent visions (Figure 13) on the three-dimensional nature of myocardial macrostructure in relation to the myocardial microstructure and fiber organization. A more in-depth state-of-the-art of different concepts and their link to 3D wall motion has been described by Buckberg et al. [32].

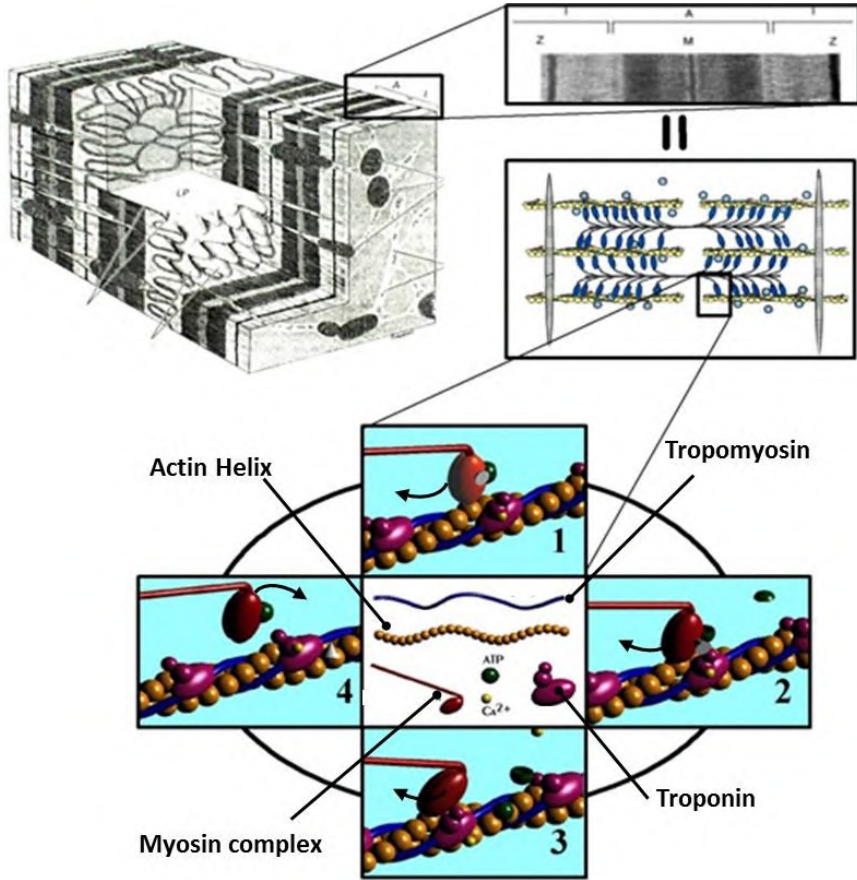


Figure 12: The organization of actin and myosin filaments is represented by formation of cross-bridges in a myocyte. Adapted from [26, 33].

The first view, expressed by Robb et al. [34], is built on the presumption that the heart contains a slanted clockwise as well as a slanted counterclockwise muscle architecture that sandwiches a circular transverse layer of muscle at the top level of the LV. The second model, presented by Rushmer et al. [35], describes the LV muscle as consisting of three distinguishable layers of fibers. Their conceptual model shows how the spiral muscle layer at the surface and the deep layer are sandwiching the middle layer and this with a transverse fiber orientation. According to Streeter et al. [36], the third conceptual model, the myocardial wall is an interweaving, continuous network in which the myocyte alignment varies across the wall according to a 60-degree helix, hence forming a doughnut-like (toroidal surfaces) structure. The fourth view was proposed by Torrent-Guasp et al. [37-40] and is based on the so-called *Helical Ventricular Myocardial Band* (HVMB) which is a continuous muscle band for both the RV and LV. This

band can be unfolded by punctilious dissection and consists of two loops, four segments and a central fold which twists the band by 180° . As shown in Figure 14 in more detail, the band starts from the pulmonary artery root and runs via the right and left segments of the basal loop to the oblique fold (at the center) and continues via the descending and ascending segments of the apical loop up to the aortic root. Hereby, the rising segment corresponds to the free wall of the right ventricle, while the left segment represents the free wall of the left ventricle.

Although the concept of Torrent-Guasp's model of the incessant helical band of myocardial fibers has been subjected to doubt [41], the existence of this helical band and its function during the heart cycle has recently been demonstrated by cine-MRI diffusion tensor imaging [42]. Moreover, this theory gives more insights in the mechanisms behind the overall force transmission pathways in the myocardial wall than the others [32].

1.3.3.2 LV wall deformation patterns

As a result of the above described fiber architecture and of the timing and sequence of electrical excitation, the LV deforms as follows. During the LV contraction, (a) the diameter of the LV decreases while (b) the ventricular base is moved in an apical direction (c) in a rotating manner [43]. These global LV wall deformation patterns can be basically described in terms of (a) circumferential, (b) radial and (c) longitudinal deformation, as well as (d) torsion (Figure 15). Due to these patterns and the accompanying "wringing" effect, there is a simultaneous reduction of the cross-sectional area of the ventricular cavity and pressure is efficiently exerted on the blood enclosed within the chamber, thereby directing it upwards to the aortic outflow tract. During the LV relaxation, these actions are supposed to allow the filling of the ventricle.

The downward motion of the valve plane during the systolic phase fulfills a double pump function. First, it results in a diminished enclosed volume of the LV chamber and second, it enlarges the volume of the atrium [28].

Left ventricular torsion is calculated as the difference between rotation at the apical ($\text{rotation}_{\text{apical}}$) and basal level ($\text{rotation}_{\text{basal}}$) and its typical variation during one heart cycle is depicted in Figure 16. LV torsion values of healthy subjects are reported in various studies, and some values are listed in Table 1. According to the Torrent-Guasp's model, it has been suggested that the opposing systolic twisting between base and apex is due to the specific double-helix architecture of the muscle fibers and that the zone where no rotation is observed (neutral plane) corresponds with the junction of the double-helix (see **Figure 13 4a**) [44].

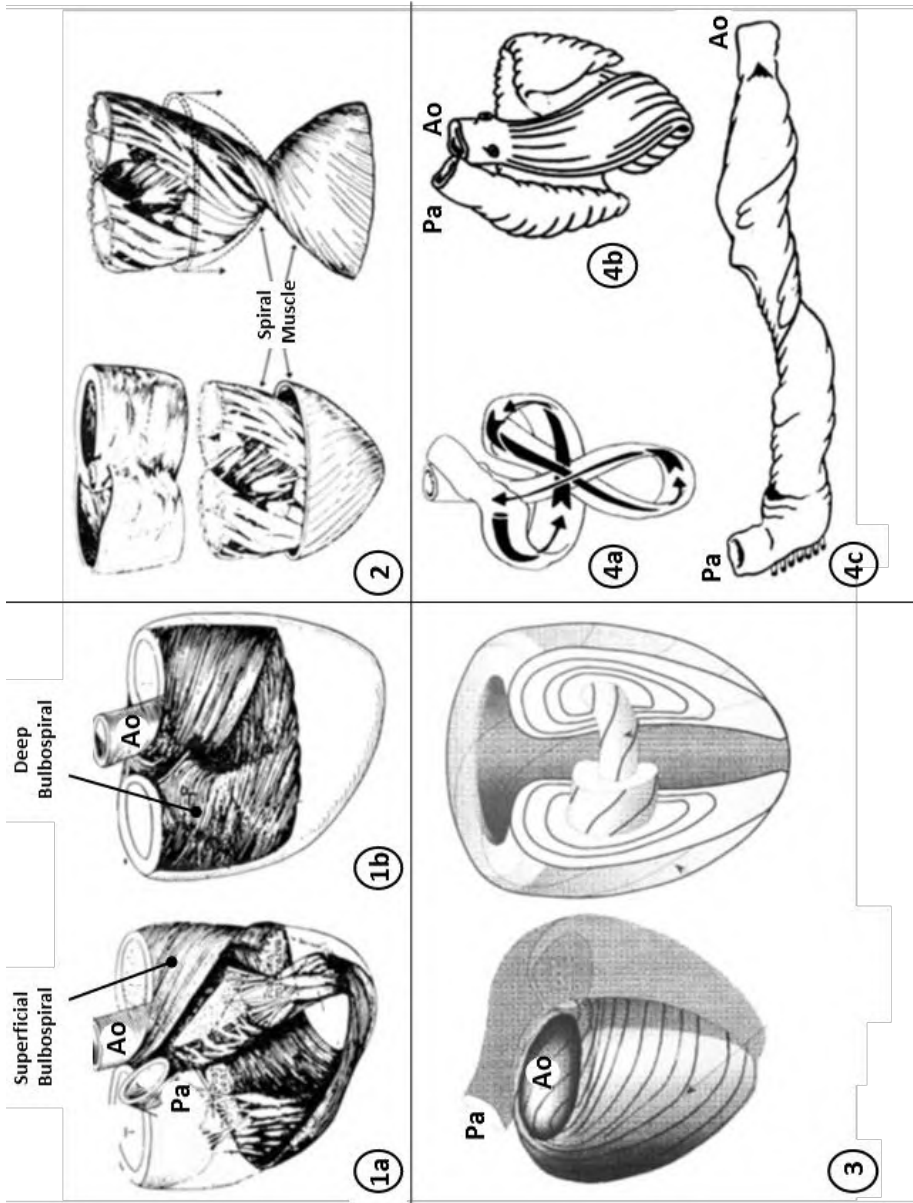


Figure 13: Four concepts of myocardial fiber orientation are given: (1) by Robb et al. [34] with a superficial (1a) and deep bulbospiral (1b), by Rushmer et al. [35] with spiral muscles including opposite fiber orientation, (3) by Streeter et al. [36] with helical fibers which forming doughnut-like surfaces and (4) by Torrent-Guasp et al. [37-40] including a continuous ventricular myocardial band, with (4a) a schematic version of the double-helix, (4c) the unwrapped version of (4b). Ao, Aorta and Pa, Pulmonary artery. Adapted from [32].



Figure 14: A step-by-step procedure to unscroll a heart by dissection according to the Torrent-Guasp's myocardial band model. Starting from the intact heart (1), the Right Segment (RS) is first unwrapped (2), then the Left Segment (LS) (3) and subsequently, the Ascending Segment (AS). At the end, by unfolding the Descending Segment (DS) (4), the complete helical structure is outspread and forms a continuous myocardial band. Note the twisting nature of the oblique fold at the center of the junction of the basal as apical loops. Adapted from [32].

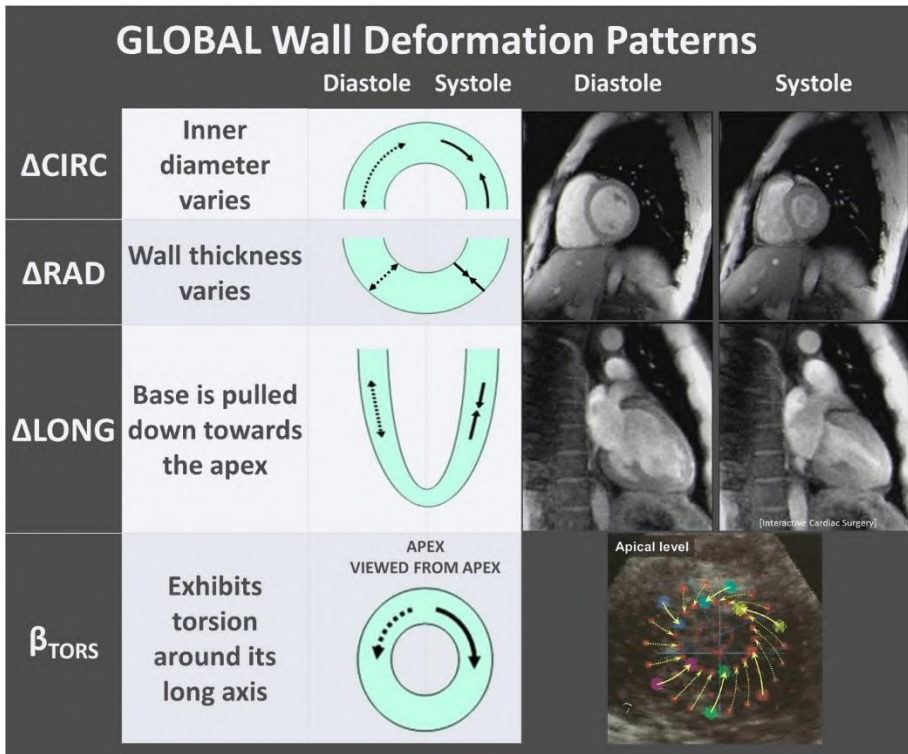


Figure 15: Global wall deformation patterns during systole and diastole. Adapted from [45-47].

Researchers	<i>n</i>	LV torsion (°) (SD)	Age (years) (SD)
Maharaj et al.	127	8.87 ± 2.21	39.7 ± 12.1
Carreras et al.	18	10.48 ± 1.63	30.7 ± 7.5
Helle-Valle et al.	29	16.4 ± 5.5	33 ± 6
Kocabay et al.	194	20.0 ± 7.3	44 ± 16

Table 1: Values of LV torsion in healthy humans [44, 48-50].

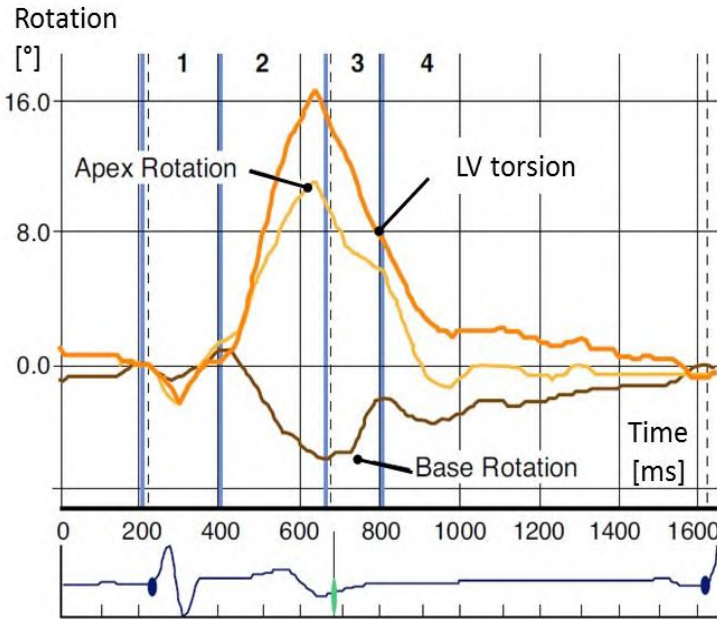


Figure 16: The LV torsion during one heart beat in a normal healthy subject is illustrated.

$LV_{torsion}$ (orange curve) is defined as $rotation_{apex}$ (yellow curve) minus $rotation_{base}$ (black curve). During the isovolumic contraction phase (1), the apex generates a small clockwise twist and the base a small counterclockwise twist. During ejection phase (2), the twisting directions alter and the LV torsion values are significantly higher. During the isovolumic relaxation phase (3) and the early diastolic filling phase (4), the twisting direction is changed again and torsional recoil takes place. Adapted from [43].

1.4 CARDIOVASCULAR VALVES

The heart is equipped with four valves (see Figure 1) that ensure the right direction of the blood flow. Two of these valves, the right and left atrioventricular valves, are located in the valve plane which is between the atria and the ventricles. These valves allow the blood to flow from the atria into the ventricles when the atrial pressure is higher than the ventricular pressure (ventricular filling). Another function of these valves is to prevent the backflow to the atrium during ventricular contraction, when the pressure of the ventricle is much higher than the pressure in the atrium. The right atrioventricular valve is also called the tricuspid valve (as it consists of three semi-lunar cusps or leaflets) and the left atrioventricular valve is also called the bicuspid valve (as it consists of two semi-lunar cusps or leaflets) or the mitral valve. These two valves are both supported by fibrous tissue cords, the chordae tendineae, which connect each of the leaflets to papillary muscles

projecting from the ventricular wall. During diastole, the papillary muscles relax and provide little tension on the chordae tendineae, fostering ventricular filing. During systole, the papillary muscles contract along with the ventricle. This creates tension on the chordae tendineae, helping to hold the leaflets of the atrioventricular valves in place and prohibiting the prolapse of the valve leaflets toward the atrium. The third valve, the aortic valve, is located between the left ventricle and the aorta whereas the fourth valve, the pulmonary valve, is located between the right ventricle and the pulmonary artery. These two latter valves are known as the semilunar valves of the heart. Both the aortic and the pulmonary valve have three cusps or leaflets which are not attached to any other structure. Both the aortic valve and pulmonary valve operate in a similar way. Both valves open in ventricular systole, when the pressure in the LV or RV rises above the pressure in the aorta or pulmonary artery, respectively. When the ventricle relaxes, blood flows back into the ventricle from the aorta or pulmonary artery and this flow of blood fills the pocket-like valves. This blood flow presses against the leaflets which close to seal the valves. In addition to the four heart valves, there are also valves located in the veins, the so-called venous valves. These promote the blood flow back to the heart. In this dissertation, we have primarily focused on the mimicking of the mitral valve. Hence, here we focus more in-depth on mitral valve anatomy.

1.4.1 The valve plane

The four cardiac valves are attached to their valve rings or annuli and are located at the base of the heart. These fibrous rings join to form the fibrous frame or the valve plane of the heart (see Figure 17) [51]. The aortic valve forms the center of the cardiac valve plane, and its fibrous extensions are in contact with each of the other three valves, anchoring and supporting them. The cardiac valve plane not only contains the four valve annuli but also the membranous septum and four fibrous trigones of the respective valves [51].

1.4.2 The mitral valve

The mitral valve is located between the left atrium and the LV, in the left atrioventricular groove [52]. The mitral valve apparatus is a very complex three-dimensional assembly of separate anatomic components and comprises the mitral valve annulus, the leaflets and commissures, the chordae tendineae, the papillary muscles, and the left ventricle [53]. This system allows the unidirectional flow of oxygenated blood from the left atrium into the relaxed LV during diastole. Accurate mitral valve function is a complex process that requires the proper interaction of all components, as well as adequate left atrial and left ventricular function [51]. A coordinated interaction of these anatomic components closes the valve against ventricular pressure during systolic

1. THE LEFT HEART STRUCTURE AND FUNCTION

contraction, and widely opens the valve during diastolic relaxation. In what follows, we describe the multiple anatomic components in more detail. The functional opening or orifice of the mitral valve is defined by its narrowest diastolic cross-sectional area, called the effective orifice area (EOA). Three-dimensional imaging of the atrial (surgical view) and ventricular (interventional cardiologist fluoroscopic view) surfaces of the mitral valve is now possible with echocardiography [51]. Typical normal values of EOA are about 3 cm^2 [54]. Another parameter to assess mitral valve performance in this dissertation is the transmitral pressure difference during early diastole (TMPDe). Normal values for this parameter are a few mmHg for normal, and 10-30 mmHg for severe mitral stenosis [55].

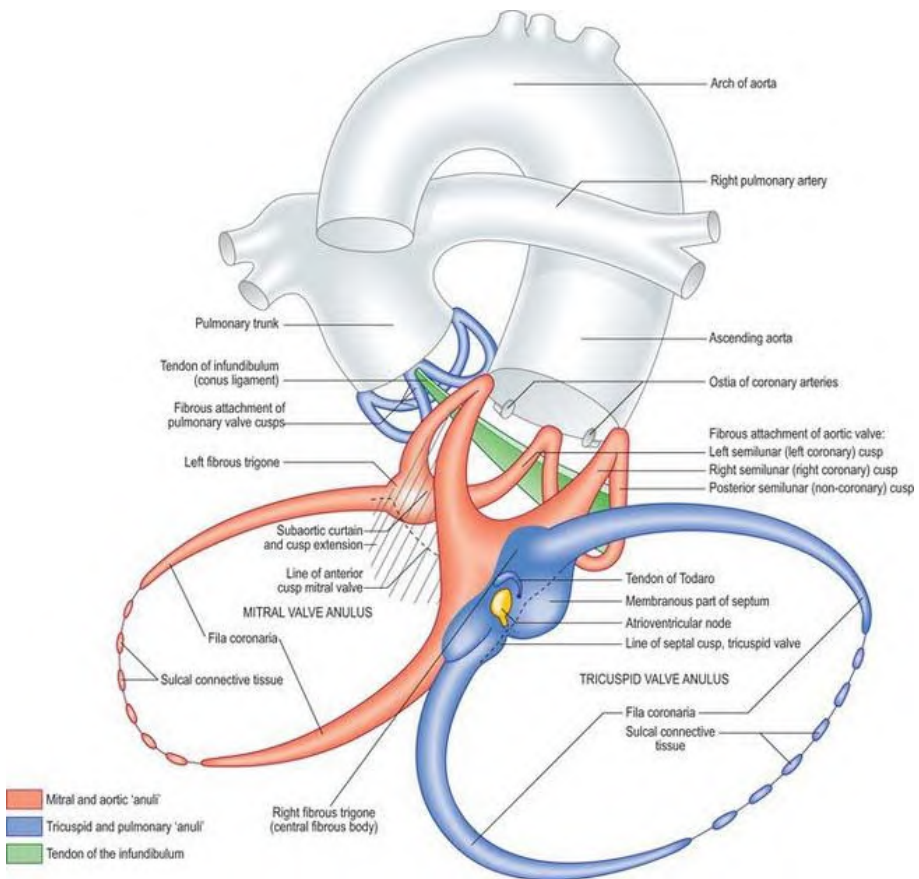


Figure 17: This diagram shows the fibrous cardiac skeleton or valve plane with the four annuli of the cardiac valves. The aortic annulus at the center is the keystone and its fibrous extensions support the other three annuli. Adapted from [51].

1.4.2.1 *The mitral annulus*

The mitral annulus is a fibromuscular structure located in the left atrioventricular groove ring which is firmly anchored along the circumference of the anterior leaflet by the tough fibrous skeleton of the heart [56] (see Figure 17). It operates as a suspension and hinge point for the mitral valve leaflets [52]. The mitral annulus is subjectively separated into anterior and posterior segments based on the attachments of the anterior and posterior mitral leaflets [52]. The anterior portion of the mitral annulus is intertwined with the fibrous skeleton of the heart, identified by the right and left fibrous trigones and the aortic mitral curtain [52]. The normal mitral annulus is kidney bean formed and has a three-dimensional saddle shape. The overall circumference of the annulus may decrease by as much as 20% during systole, aiding leaflet coaptation [57].

1.4.2.2 *Mitral leaflets and commissures*

Unlike the other cardiac valves, the mitral valve comprises only two leaflets, an anterior and posterior leaflet with similar surface areas but distinctly different shapes [58]. The anterior leaflet is longer than the posterior leaflet but with a shorter base, attaching to one-third of the annular circumference between the right and left fibrous trigones (see Figure 17) [52]. The posterior leaflet is wider based and extends along the remaining two-thirds of the annulus with a height which is half the height of the anterior leaflet [56].

Despite their differences in shape, the overall surface areas of the two leaflets are similar. The different positioning of the two leaflets guarantees that - during systole - the closure line of the mitral valve will be situated in the posterior one-third of the valve orifice, which prevents motion of the anterior leaflet tip into the outflow track during systole [59]. Both leaflets present two zone regions from their base to the free boundary: *the clear zone* (smooth and semitransparent) and *the rough zone* (thicker and bumpy due to the attachment of numerous chordae tendineae) [52]. The major chordae supporting a leaflet are inserted into its free edge and rough zone (see Figure 19). During systole, the coaptation regions of the respective leaflets merge to form an overall seal from a few millimeters to a centimeter, ensuring mitral valve closure (see Figure 18 and Figure 20) [52]. Collagen fibers are of key importance for the strength of the leaflets and are generally oriented in parallel with respect to the annulus and become radial close to commissures [60] (see Figure 21).

1. THE LEFT HEART STRUCTURE AND FUNCTION

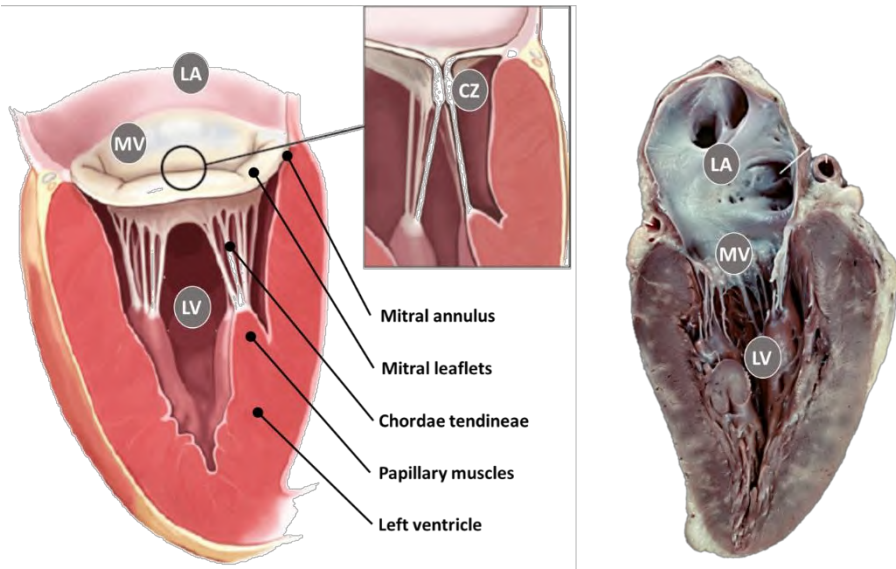


Figure 18: As shown in the drawing (left) and the real heart (right), the mitral valve (MV) apparatus is composed of five elementary components, the mitral annulus, mitral leaflets, chordae tendineae, papillary muscles, and the left ventricle (LV). During systole, the mitral apparatus brings the two leaflets together and establishes the coaptation zone (CZ). Adapted from [51, 61].

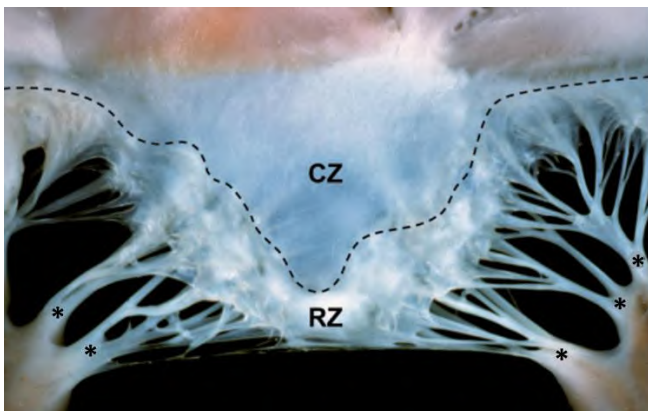


Figure 19: Both mitral valve leaflets have a clear zone (CZ) and a rough zone (RZ) and are separated by a closing edge (dotted line). Note the fanlike array of the commissural chordae tendineae (*). Adapted from [51].

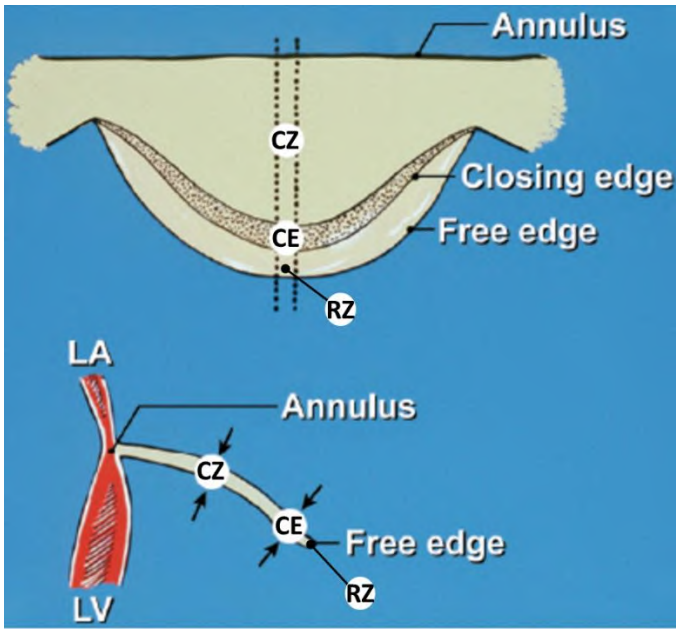


Figure 20: Schematic diagram of the section across the dotted lines clarifies the association between the annulus, the closing edge (CE), the free edge and the left ventricle (LV) and atrium (LA). Also the clear zone (CZ) and the rough zone (RZ) are shown. Modified from [51].

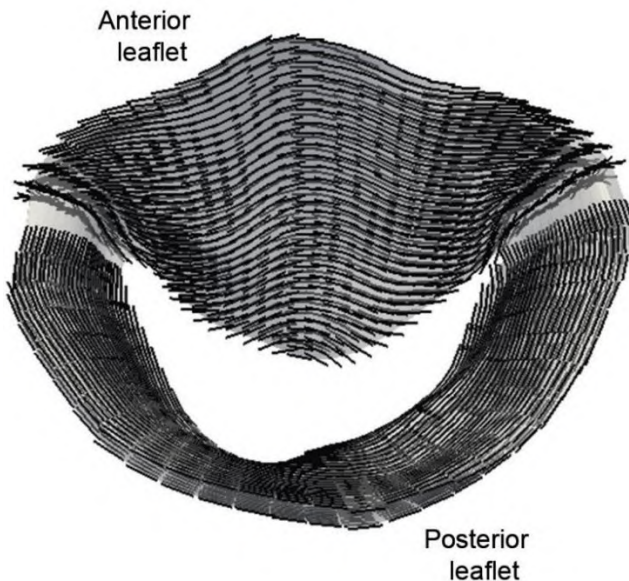


Figure 21: Fiber orientation of the mitral valve. Adapted from [60].

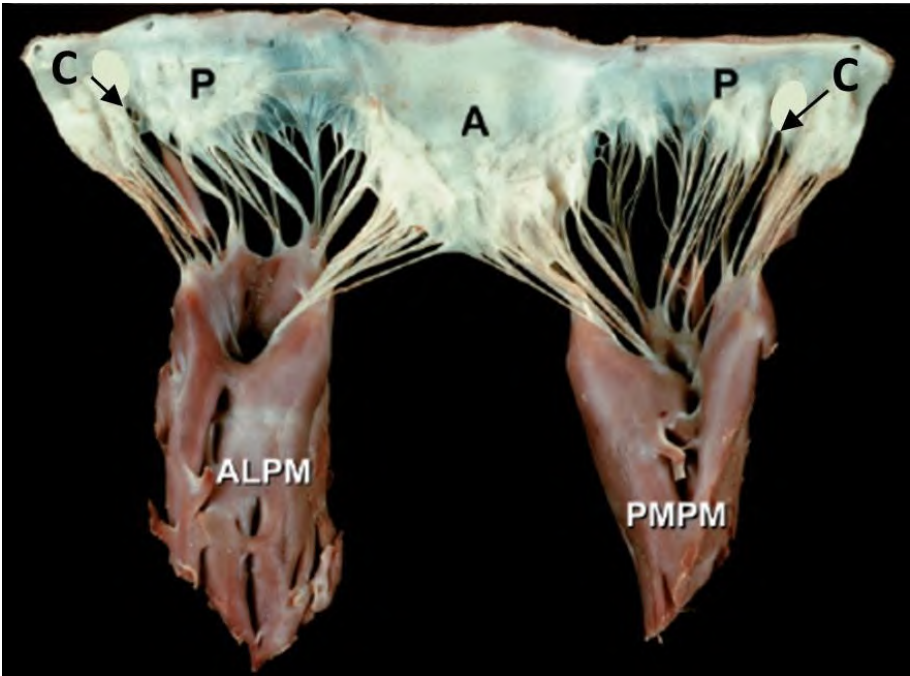


Figure 22: This picture shows an isolated and unfolded mitral valve including the anterolateral (ALPM) and posteromedial papillary muscles (PMPM) with the chordae tendineae and leaflets. Note the commissures (C) of the posterior (P) and anterior leaflets (A). Adapted from [51].

The commissures are splits in the leaflet structure that signify the sites of the leaflet parting (see Figure 22). Beneath the two mitral commissures lie the two underlying papillary muscles, which protrude from the left ventricular free wall (see Figure 18 and Figure 22) [51]. Commissural chords begin from each papillary muscle and extend in a fanlike array to interleave into the free edge of both anterior and posterior leaflets [56] (see Figure 19). In contrast to inherited clefts, a true commissure is always connected with an underlying papillary muscle and a dominant array of chordae tendineae [56].

The leaflets of the mitral valve can be divided into individual borders or scallops based upon the location of the clefts in the posterior leaflet. The central scallop of the posterior leaflet is defined as $P2$, and the neighboring lateral and medial scallops are defined as $P1$ and $P3$, respectively (see Figure 23) [52]. Natural clefts are not typically observed in the anterior leaflet, in this case, the segments are defined according to the opposite segments of the posterior leaflet as $A1$, $A2$, and $A3$ [62].

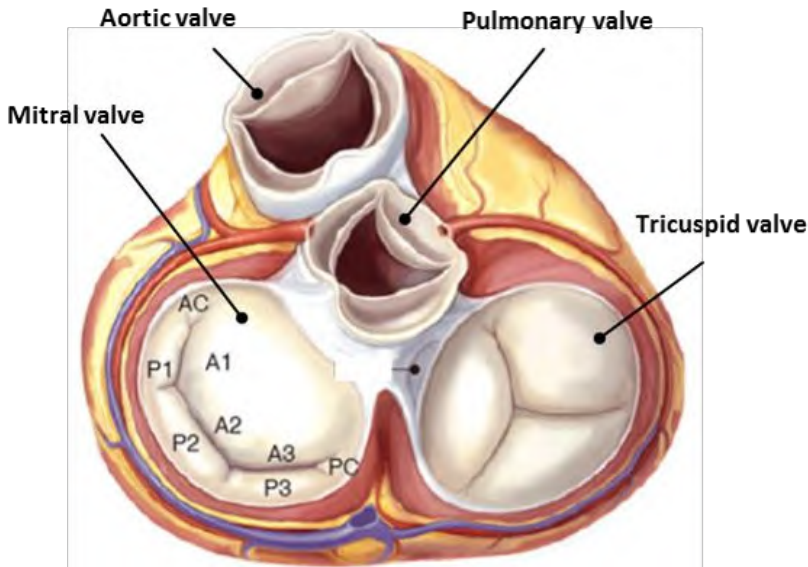


Figure 23: Anatomical section shows the valve plane with the cardiac valves in systole and a detailed composition of mitral valve. The anterior (A) and posterior leaflets (P) are both subdivided into three segments (1 -3) and separated from one another by the anterior (AC) and the posterior commissures (PC). Adapted from [51, 61].

1.4.2.3 Chordae tendineae

The main function of the chordae tendineae, forming a suspension system, is to prevent a displacement of the leaflets above the annular plane, hence avoiding the leaflets to prolapse during systole, as well as to allow a full opening of the leaflets during diastole [51]. Chordae tendineae are categorized according to their connection between the free margin and the base of the leaflets [63]. As such, primary, or marginal, chordae attach along the margin of the leaflets and are crucial to avoid leaflet prolapse and to bring the rough zone of the anterior leaflet into line with the posterior leaflet during systole. Typically, primary chordae implant every 3 to 5 mm along the border of both leaflets [52]. Secondary, or body chordae, connect to the ventricular side of the corpse of the leaflets and establish ventricular annular continuity as well as control of leaflet tension during systole [52]. Tertiary, or basal chordae, attach to the foot of the leaflet hinge and serve as additional connection to the ventricle [64]. Since the chords are responsible for these different functions, rupture of a chord may thus have very different consequences depending upon the type of chord which is involved.

1.4.2.4 Papillary muscles and the left ventricle

Via the chordae tendineae, the entire mitral apparatus is supported by the papillary muscles, which are part of the LV muscle. The papillary muscles differ in the number of heads and precise position in the ventricle, but are generally categorized into two main groups comprising the anterolateral (ALPM) and posteromedial papillary muscles (PMPM) (see Figure 22). Each papillary muscle is identified according to its association with the valve commissures and is equipped with a fan chord to its related commissure as well as to both anterior and posterior leaflets [52]. The anterolateral papillary muscle is generally single whereas the posteromedial papillary muscle normally has multiple heads [65].

In-vitro modelling of the left heart: State-of-the-art

This chapter overviews current in-vitro left heart approaches and identifies the major challenges in approximating normal left heart anatomy and physiology, as described in Chapter 1. In Chapter 3, these challenges are summarized and practical guidelines are formulated towards in-vitro model optimization.

2.1 INTRODUCTION

In-vitro simulation of the human cardiovascular system for hydrodynamic testing of cardiac devices began about 55 years ago, when left heart in-vitro models were first used for testing valve prostheses [66]. Since then, bench models are continuously challenged in order to more accurately mimic the complex anatomical and physiological conditions.

In this chapter, we first start with a general description of the history of heart model development highlighting the major developments during the past decades. Subsequently, we examine this history in more detail by providing a state-of-the-art overview of left heart simulators and distinguish model before and after the 1960s.

There are plenty in-vitro approaches currently available. For our state-of-the-art overview, we aimed to (1) highlight the evolution of continuous improvement during the history of in-vitro modelling, and (2) to illustrate the variety between the different approaches. As a result, only a selected set of models are included. Although it is our intention to give a review as completely as possible, the probability remains that some groups with mock loop systems were not included in this review chapter.

In this overview, the heart models are chronologically ordered and grouped according to the research institute of origin. The first cardiovascular simulators which are being described in this chapter are based on beating animal hearts. Then, the postmortem human hearts are explained which are actuated by a piston pump. After that, a wide range of in-vitro heart models are illustrated which are exclusively made of non-biological materials like rigid and flexible polymers. By this, we illuminate a number of model evolutions concerning geometrical complexity to obtain anatomical likeness, actuation and regulation to mimic physiological events and modifications to enable different validation techniques. Finally, recent innovations are discussed such as multi-material 3D printing to attain anatomical accurate geometries derived from medical images.

This review aims to primarily present and describe the models, only briefly discussing their possibilities and limitations. Chapter 3 will critically evaluate the limitations of these models as a whole, in order to optimize design criteria for a new generation of in-vitro model testing.

2.2 THREE MAJOR DEVELOPMENTS DURING HISTORY

In the history of left heart duplicator systems, we can roughly distinguish three key areas of development. The first area of progression is the mimicking of the complex anatomy. The second field of development is the duplication of physiological events. The third significant area of evolution is the adaptation of these in-vitro models to (clinical) validation techniques. These three fields of cardiovascular simulator development have greatly fostered research in cardiovascular mechanics and the testing of medical devices.

2.2.1 Mimicking the complex anatomy

The first attempts in cardiovascular simulation were performed in 1895. The pioneering efforts of Langendorff [67] used isolated animal hearts which were artificially kept beating with an oxygenated solution. These models have proven to be great research tools advancing our knowledge of physiology and anatomy. Yet, these models are still animal models having only a limited

period of beating time and cardiac parameters which are difficult to control. Interestingly, several research groups have recently picked up this old technique, such as the isolated four-chamber working swine heart model of Chinchoy et al. (2000) [68], the PhysioHeart of de Weger et al. (2010) [69], the passive-heart platform of Leopaldi et al. (2014) [70].

From the mid-1950s on, cardiovascular simulation was achieved using postmortem human hearts which were actuated by hydraulic pumps [71-73]. This procedure allowed more cardiac parameter control and had the advantage of more anatomical-like modelling because of the use of a real human heart. Although the beating time could be prolonged, the preservation time of the postmortem tissue still signified a major issue. Nevertheless, this work proved to be very significant in advancing our knowledge on the cardiovascular system and even today, in specific cases, isolated biological tissues are still used as research tool [5, 74].

Then, since the early 1960s, simulation of the cardiovascular system was generally modelled by mechanical in-vitro pulse duplicators composed of non-biological materials. There are two main reasons for this alternative approach. First, the cardiovascular parameters can be more straightforwardly regulated and second, mechanical models are not (or less) subjected to functional decay and tissue decomposition. However, in contrast to biological models, anatomical likeness relapsed because of the model's relative simple geometrical shapes. For example, the left ventricular geometry has been replicated by a cylinder [75-78], a balloon [66], a truncated cone [79] and a truncated ellipsoid [5, 80-85]. From the 2000s on, more realistic approximations of the natural left heart geometry were obtained by applying 3D reconstructions of the anatomical structures using medical images [86-92] in combination with more advanced manufacturing techniques, such as 5-axis milling [88] and 3D printing [92-94].

Today, research is going even further than only the accurate modelling of the anatomical shape. Recent research explores possibilities to build heart phantoms using multi-material 3D printing to model the different anatomical structures, such as the fabrication of calcified heart valves [92-94].

2.2.2 Duplicating physiological events

In addition to attaining anatomical likeness, the mimicking of physiological events is equally crucial in the context of cardiovascular modelling. Physiological pressure and flow conditions can be obtained by a left heart model which is connected to a vascular model which can be a windkessel model configuration or a (branching) tube-like system. The heart model is equipped with an actuator to realize ventricular contraction. In some models,

ventricular contraction is combined with atrial contraction [88, 95-97]. The actuator systems are equipped with a control unit to induce the generation of prescribed volume and/or pressure waveforms. There are two main actuation approaches which can be distinguished, namely hydraulic and pneumatic systems.

The first hydraulic system was developed in the 1950s and comprises a mechanical actuator which consists of an one-arm rolling pump mechanism acting during systole, and this in combination with a flexible bladder functioning during diastole [66]. This way of activation comprises a more natural way of ventricular suction; yet, the cardiac parameters are relatively cumbersome to control. A more recent and commonly used hydraulic approach is a piston pump which can be either driven by a crankshaft [98, 99] or a ball screw servo motor, powered by either an analogue [5, 77, 79, 87, 98-102] or a digital amplifier [103].

Then, according to the pneumatic actuation approach, one can distinguish two types. The first type is based on two reservoirs containing pressurized air and a vacuum which are controlled using valves to cause a sequential contraction [84, 85, 95, 96]. The second type makes use of an electric motor which drives a pneumatic cylinder to induce a proper actuation [97].

Next to the type of actuator and its control unit, the vascular model is a third important component when modelling replicating physiological events. The windkessel effect of the arteries is generally generated using closed, partly filled reservoirs including fluid and air. A more recent and more nature-like approach of vascular simulation is the use of an anatomical-like vasculature geometry which is made of an elastic material [91]. In this design, custom elastic properties of the vascular wall can be obtained by locally varying the wall thickness, although it is extremely hard to mimic the elastic properties of young, healthy arteries.

2.2.3 Compatibility to measurement techniques

In addition to anatomical and physiological likeness, the setup of cardiovascular simulators is also determined by the specifications required by the signal acquisition, such as measurement of pressure and flow waves, wall deformation patterns, intraventricular flow patterns, etcetera. The model setup involves specific adaptations to enable compatibility with the preferred measurement techniques.

Generally, cardiac simulation systems comprise the ability to connect pressure transducers and flow probes which involves only limited adaptations.

However, more specific modifications are needed for validation techniques such as visual examination using cameras, Ultrasound (US) imaging, Laser Doppler Anemometry (LDA), Particle Image Velocimetry (PIV), and Magnetic Resonance Imaging (MRI).

Visual validation techniques require the use of optical cameras in combination with clear viewing ports and a clear fluidum [72]. Then, in order to obtain US imaging compatibility, the left heart model materials need to approach tissue-equivalent properties to obtain proper ultrasound transmission [95, 96, 101]. Next, LDA compatibility requires a transparent or semi-transparent fluid to allow measurement of a laser beam Doppler shift [79]. Subsequently, concerning PIV measurements, beside optical clearness of the in-vitro model, there is also a need for refractive index match between the fluid media and the solid materials [79, 104, 105]. And finally, regarding MRI compatibility, only non-ferromagnetic materials are allowed in the close proximity of the MRI scanner which often results in a setup length of several meters, bridging the heart model with the actuator and software [92].

In summary, during the past 55 years, cardiovascular duplicators have continuously been improved by a more accurate mimicking of the human anatomy, especially in recent years, by the entrance of medical imaging and 3D print technologies. Other crucial developments have been the implementation of more physiological-like events by using more sophisticated actuator systems and software-based regulation. Moreover, significant strides forward have been made in the area of validation, as models have been made compatible to a wide range of validation techniques, including clinical examination techniques. In the following sections, we cover in more detail the in-vitro simulators that played a significant role in this intriguing part of cardiovascular modelling history.

2.3 PULSE DUPLICATOR SYSTEMS BEFORE THE 1960S

2.3.1 Oxygenated animal hearts

As early as the 1890s, animal models have been used for the study of cardiac physiology. Langendorff introduced an ex-vivo approach to isolate a mammalian heart and allowing it to continue beating for several hours after its removal from the animal [67]. By this ex-vivo approach, he showed the feasibility of restoring physiologic cardiac function on isolated hearts through suitable myocardial perfusion. The biological heart was connected to a benchtop vascular model to replicate the cardiovascular system. In the last decades, many research groups practiced this beating heart approach and

successfully developed testing platforms for numerous applications, in the past [106-110] as well as recently [68-70, 111-118].

The use of real animal hearts has proven to be a great research tool in terms of anatomy and physiology. However, application of these animal models has some major limitations. Firstly, an animal heart does not fully represent a human heart. Secondly, a heart which is artificially kept beating is able to beat only for a limited length of time. Finally, it is a complex task to control cardiac parameters in a biological heart such as heart rate, systole/diastole time ratio and stroke volume. Therefore, future cardiovascular duplicators were more and more built from polymer instead of biological parts.

2.3.2 Postmortem human hearts actuated by a piston pump

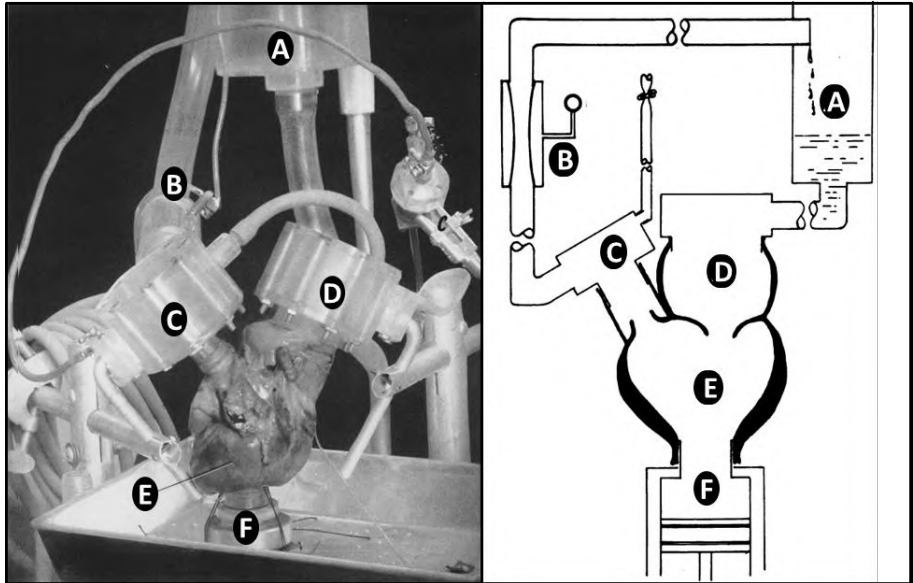


Figure 24: Pulse duplicator using a postmortem human heart actuated by a piston pump. (A) The reservoir, (B) the peripheral resistance, (C) aortic viewing chamber-outflow, (D) atrial viewing chamber-inflow, (E) postmortem heart with left ventricle connected to the pump outflow tube and (F) piston pump. Adapted from [72].

Another approach which has been used to mimic the cardiovascular system is the use of postmortem human hearts. These were connected to a hydraulic pump to realize the pump function of the heart. This methodology was applied by McMillan and colleagues (the Cardiac Department, St. Thomas's Hospital, London) [71] and Davila and colleagues (at the Cardiovascular Research Laboratory at the Presbyterian Hospital, Philadelphia, Pennsylvania) [72] for

cinematographic assessment of cardiac valve movements. Figure 24 illustrates the construction of the pulse duplicator of Davila and colleagues. Duran and colleagues (Nuffield Department of Surgery, Oxford) also applied this approach and presented their pulse duplicator in the literature as a simple, versatile, and inexpensive system [73].

In the context of human cardiovascular modelling, this approach has the advantage of using human hearts instead of animal hearts but still suffers from other major limitations. Although the lifetime of this kind of heart model is prolonged compared to the artificially beating animal hearts, postmortem tissues do have only a limited preservation time. In most of the future approaches, biological parts were therefore replaced by polymer materials such as PMMA (polymethyl methacrylate) and silicones.

2.4 PULSE DUPLICATOR SYSTEMS AFTER THE 1960S

2.4.1 Department of Thoracic Surgery, Uppsala, Sweden (1962)

In 1962, Björk and colleagues [66] invented – to our knowledge - the first mechanical in-vitro pulse duplicator exclusively made from non-biological materials. As shown in the figure below (Figure 25), the system consists of the following components: left atrium (A), mitral valve (B), left ventricle (C), aortic valve (F), compliant aorta (G), and peripheral resistance (H). The pulsatile flow is generated by a roller pump together with an elastic container. During systole, the roller pump forces the liquid from the (E) elastic container into the (D) rigid container (Figure 25 bottom right). During diastole, the roller pump is inactive and the fluid is extracted from the rigid container back into the flexible container (Figure 25 top right). A unique feature of this model is the controllable diastolic suction, obtained by varying the difference in height between (D) and (E). Similar to the system of Davila and colleagues [72], this system is also capable of controlling systolic/diastolic ratio, stroke volume and cardiac rate. Cardiac rate is adjusted by regulating the power delivery of the electric motor which actuates the pump. The motor rotates a one-arm rolling pump mechanism to generate the shape of an average ventricular pressure pulse. In this way, this pulse duplicator is able to generate the physiological dynamics of the left ventricle, aorta and left atrium.

This system has been used by Björk and colleagues for the evaluation of cardiac prosthetic valves, specifically the ball type aortic and mitral valves [66].

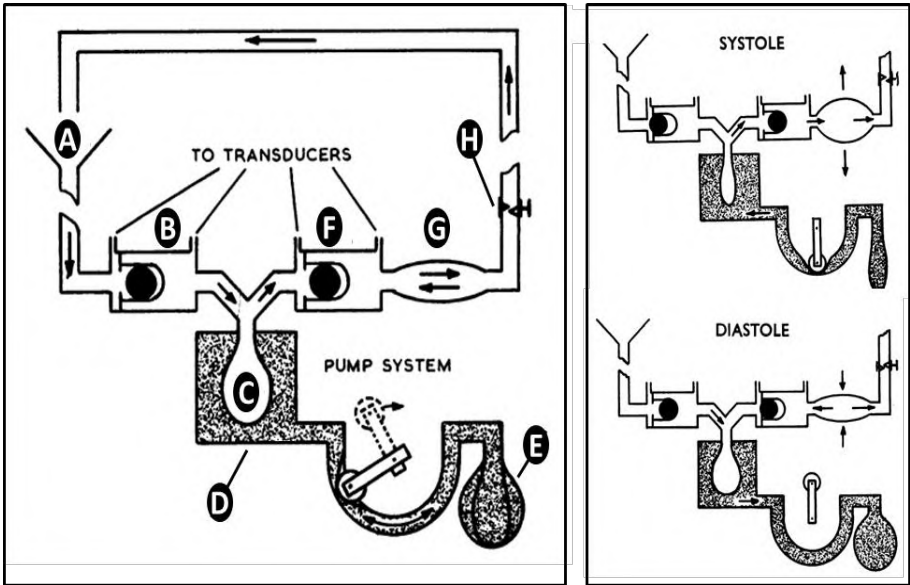


Figure 25: Pulse duplicator system of the Department of Thoracic Surgery at Sweden (1962). Left panel: The pulse duplicator with (A) left atrium, (B) mitral valve (C) left ventricle, (D) rigid container, (E) elastic container, (F) aortic valve, (G) aorta, and (H) peripheral resistance. Right panel: The pulse duplicator at the time of end systole (top) and end diastole (bottom). Adapted from [66].

This apparatus used only mechanical components and has therefore a much longer life time and is also much simpler, smaller and less expensive than biological models used at that time [66].

Compared to more recent systems using piston pump driven heart models (see further), this model actually comprises a more natural way of ventricular relaxation. Thanks to the extraction of the fluid from the rigid to the flexible container during diastole, negative ventricular pressures are limited. By this innovative approach, this model is able to simulate the diastolic phase more physiologically, since only minimal diastolic ventricular suction is present in the human heart. According to the authors, the major limitation of this system is the inability to simulate the annular motion [66].

2.4.2 Engineering Science Group, Oxford (1972)

Bellhouse and colleagues [80] developed an in-vitro model of the left heart, including a more extended set of components to simulate the cardiovascular system. According to Figure 26, the test fluid enters the left heart via the pulmonary veins (A) and then goes into the left atrium (B). The fluid then travels through the mitral valve (C) into the left ventricle model (D). An

external pressure source (E) forces the ventricle to contract, and by this contraction, the fluid is pumped through the aortic valve (F), into the aorta (G), and finally, back to the pulmonary veins (A). Yet, the description of the pulse duplicator gives insufficient detail about the type of pump mechanism.

The authors used this model to study the fluid mechanics of a model mitral valve and left ventricle. Their findings suggest that the mitral valve tends to close during diastasis, particularly if the flow is very low [80]. In this early experimental study, they noticed the existence of three-dimensional flow patterns and showed the existence of a vortex ring in a flexible left ventricular model which aids in the valve closure during diastole [81].

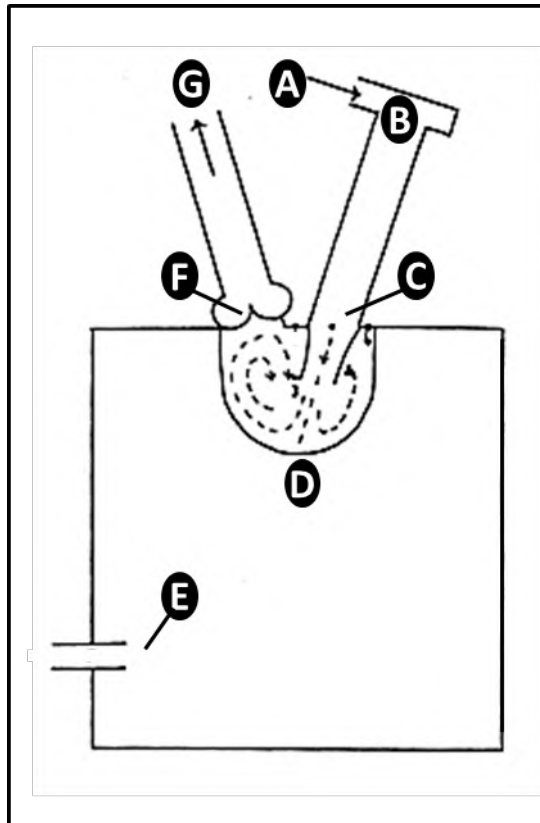


Figure 26: Cardiovascular simulator of the Engineering Science Group at Oxford (1972), including pulmonary veins (A), the left atrium (B), the mitral valve (C), the left ventricle model (D), the external pressure source (E), the aortic valve (F) and the aorta (G). Adapted from [80].

2.4.3 Mechanical Engineering Group, Berkeley, California (1977)

In 1977, Lee developed a heart model to study the fluid mechanics and motion of the ventricular wall and mitral valve [84]. In addition to the basic components of a compliance-resistance mock circulatory network as depicted in the previous model, the simulator was equipped with a high speed cinematographic camera to visualize ventricular wall motion, mitral valve motion and intra ventricular flow using the hydrogen-bubble technique (Figure 27). All components of the left heart model are made of transparent materials to allow clear visualization of the flow. As such, the flexible ventricle model is made of transparent rubber which is surrounded by a rigid box made of PMMA.

Besides the development of the pulse duplicator, Lee also designed an aortic model based on the design of Bellhouse & Bellhouse [81] as well as a mitral valve model. The mitral valve (Figure 27 bottom left) components are also made of a rigid PMMA, such as the two leaflets and the ring on which two parallel supporting triangular walls are mounted. The valve leaflets are hinged by thin flexible plastic sheets which allow the leaflets to smoothly open and close.

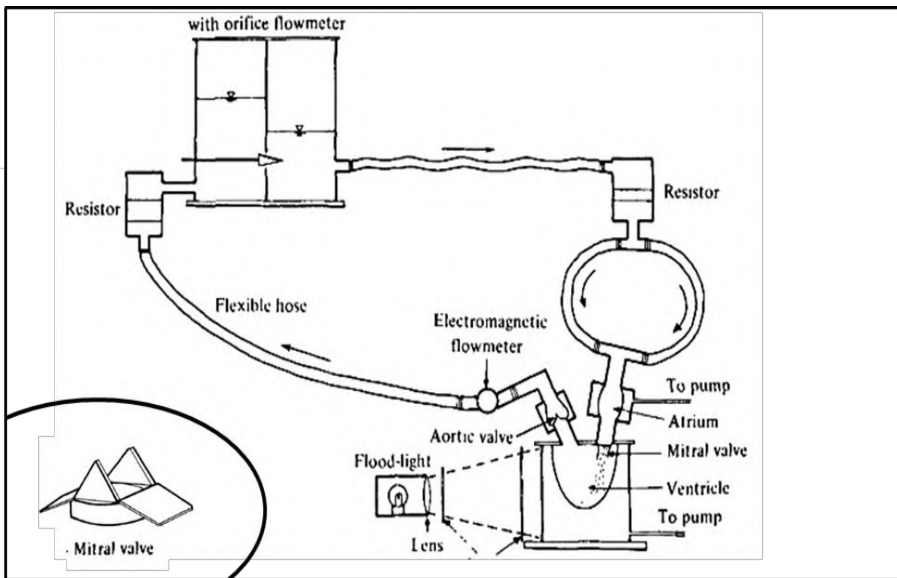


Figure 27: Schematic diagram of the left heart model and circulatory network of the Mechanical Engineering Group at Berkeley, California. Adapted from [85].

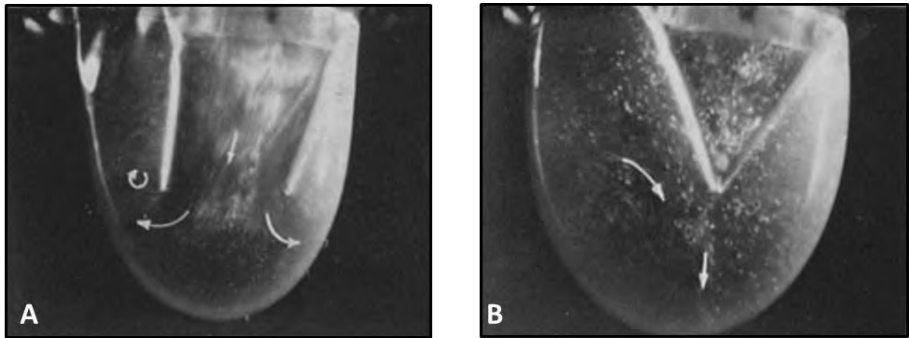


Figure 28: Flow patterns inside ventricle model to explore the nature of pulsatile flow (A) during diastolic filling and (B) just after mitral valve closure. The experiment was performed at a heart rate of 20 beats/min and a stroke volume 80 ml. Adapted from [85].

Another interesting feature of this left heart model is the actuation of both the ventricle as well as the atrial model, by a sequential contraction using compressed air in combination with a vacuum. Moreover, pneumatic heart model parameters are being electronically controlled such as heart rate, systole/diastole time ratio and stroke volume.

As shown in Figure 28, Lee and Talbot used this model to study the fluid mechanics of heart valve closure [85].

2.4.4 Cardiothoracic Surgery Unit, New York (1978)

In 1978, Gabbay and colleagues developed a cardiovascular simulator made of rigid PMMA tubes and two reservoirs [75]. As shown in Figure 29, the left heart model is simulated by the following components: the left reservoir representing the left atrium (1), the mitral valve (2), the left ventricle which is modelled as a stiff walled cylindrical chamber (3), and driven by a piston pump (4). Downstream the aortic valve (5), the mock loop includes two resistances (6, 8) and a compliance (7), which is connected to the second reservoir, in which the fluid is collected (9). Finally, the mock loop is closed by connecting the two reservoirs. Flow measurements are realized downstream the left ventricle (10) and at the aortic valve position (11). Pressure was measured in the atrium and ventricle using tip catheter transducers.

This heart simulator was used for the in-vitro hydrodynamic comparison of mitral valve prostheses [75] as well as for bio prostheses [76]. A major limitation of this left heart model is the simplified simulation of the left ventricle by a stiff walled cylindrical chamber.

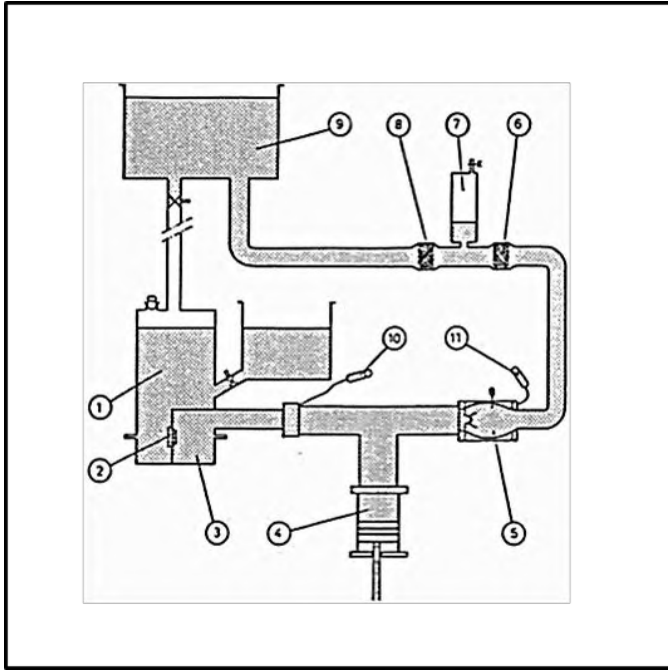


Figure 29. Pulse duplicator system of the Cardiothoracic Surgery Unit, New York [75].

2.4.5 ViVITro Labs Inc., Victoria (1979 – present)

In 1979, Scotten and Walker (Victoria, CA) presented the construction and performance of their cardiovascular simulator for the assessment of mitral valve prostheses [82]. In the mid-1970s, this research initiated the foundation of the company ViVITro Systems and the commercialization of the Pulse Duplicator in 1984. Today, ViVITro Labs is a global provider of prosthetic heart valve test equipment, laboratory testing, consulting, and engineering services. The ViVITro pulse duplicator is developed according to ISO 5840 (Cardiovascular implants - Cardiac valve prostheses) and FDA requirements.

The simulation fluid of the first ViVITro simulator is pumped (Figure 32) from a left atrial reservoir (1) through the mitral valve (2) into the left ventricle (3), and subsequently, through the aortic valve (4), the aorta (5), a compliance (6) and a resistant (7), and finally flows back into the left atrial reservoir. Although there are similarities with the heart simulator of Gabbay and colleagues [75], Scotten and Walker came up with two significant innovations. First, the left ventricle model (8) is shaped as a truncated ellipsoid which is more similar to the natural ventricle than the stiff walled cylindrical chamber of Gabbay et al. [75]. Second, the pump is more sophisticated and can generate more physiologically relevant flows.

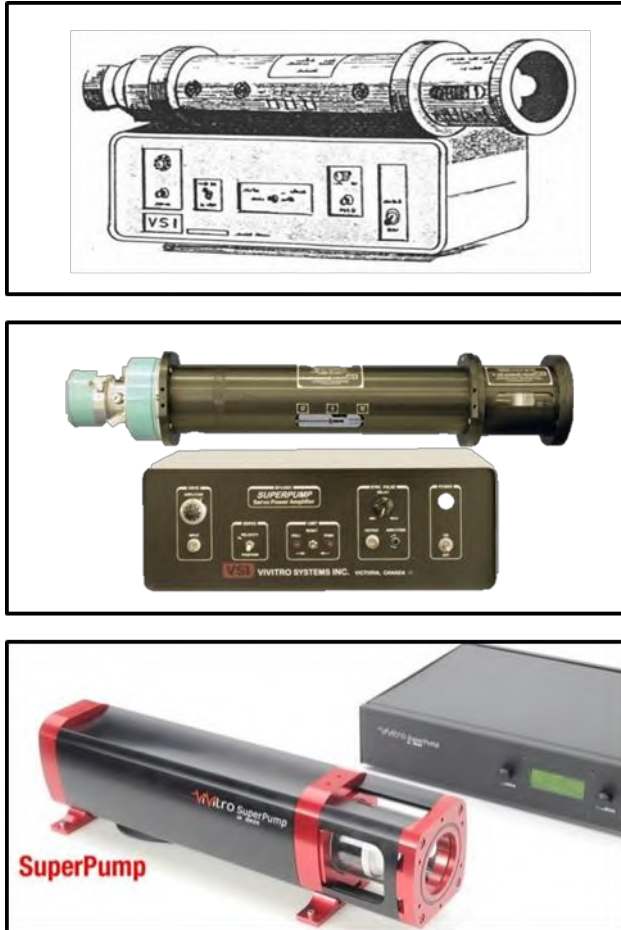


Figure 30: The Superpump system SPS 3891 of ViVITRO Lab Inc. This pump was commercially available from the 1984 (top), for a period of almost 30 years (middle: latest version of the analog pump), until the electronic pump (bottom) came in place.

Figure 30 shows the three versions of the ViVITRO Superpump that have become available throughout the past three decades. The first two super pump systems (10) (Figure 30 top and middle) consist of a piston-in-cylinder pump head driven by a low inertia DC electric motor. The rotary motion of the DC motor is converted to a linear piston displacement using a ball-screw mechanism. The motor is driven by a power amplifier which is controlled by a wave form generator (9). Complex waveforms can be loaded to the wave form generator to realize the desired oscillatory physiological flows. The frequency of playback for each waveform can be set to values between 30 -

200/minute. Moreover, not only the peripheral compliance (6), but also the aortic compliance (5) is replicated in this model. Pressure can be measured at mitral (11) and aortic position (12), as well as inside the left atrium, the left ventricle and the aorta. Upstream the mitral (13) and aortic (14) valves, flow is measured using electromagnetic sensors. Three pressure and two flow signals can be simultaneously processed and visualized by the ViVitro software.

The more recent ViVitro systems (such as the left heart system used for this doctoral dissertation which was purchased in 2009; Figure 31 left panel), are equipped with a wave form generator (Type VG2001) which can generate form frequencies of 1 - 500/minute. Another new feature is the ViVitro software ViViTest which is developed to monitor, acquire and analyze the data of the pulse duplicator system. This software is particularly designed for heart valve characterization. An additional new feature is the Viscoelastic Impedance Adapter (VIA) which can produce more realistic waveforms by replicating the viscoelastic properties of the ventricle in terms of resistance and compliance. The VIA is located between the piston pump and left heart model.

The latest version of the ViVitro heart model is also equipped with a digital motor (Figure 30 bottom and Figure 31 right panel) instead of an analogue motor to provide more control with precision accuracy by a high torque to inertia ratio. Another new feature is the integrated design of ventricle, two heart valves and the piston pump, called the ViVitro Pump Head (Figure 33).

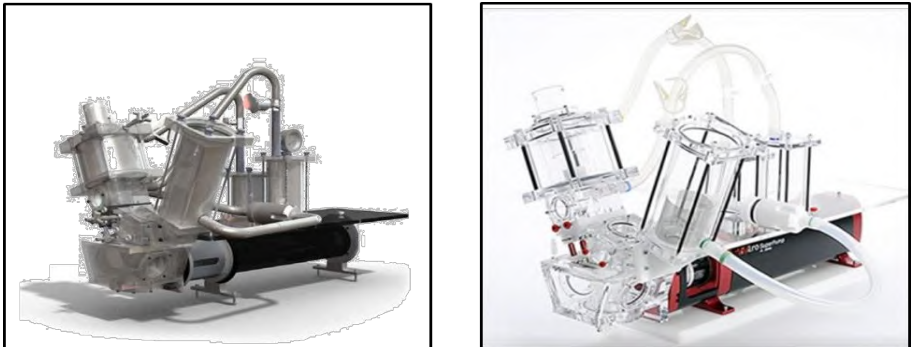


Figure 31: The ViVitro Left Heart Simulator: version 'Model SD 2001-1' of 2009 (left panel) and version 'AR Series' of 2014 (right panel). Adapted from [103, 119].

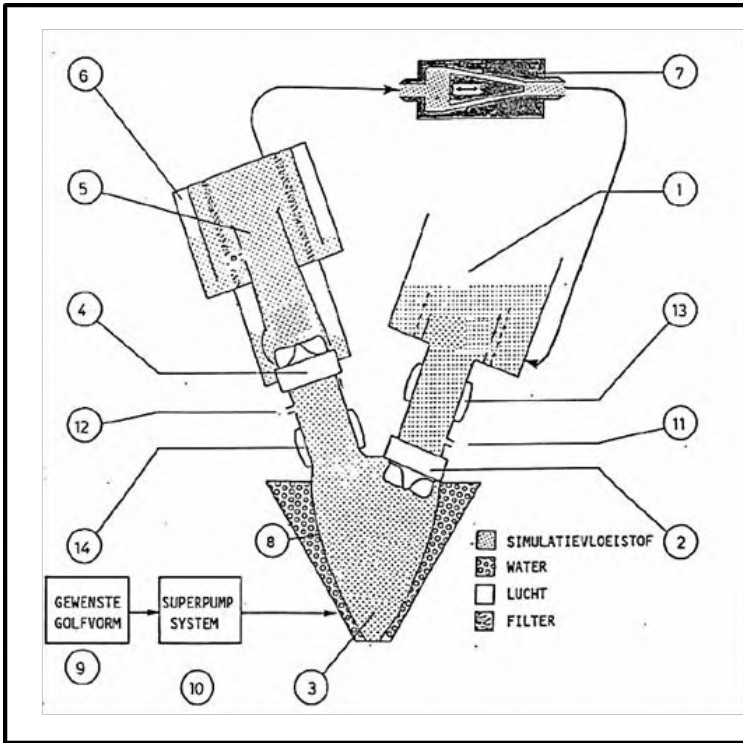


Figure 32: The Heart Simulator according to ViVibro Labs Inc., Victoria (1992) [100]. The model is composed of a left atrial reservoir (1), mitral valve (2), left ventricle (3), aortic valve (4), the aorta (5), peripheral compliance (6), resistant (7), ventricle membrane model (8), wave form generator (9) and super pump system (10). Pressure sensors can be placed at mitral (11), aortic (12), left atrial, left ventricular, and aortic position. Electromagnetic flow sensors are positioned upstream the mitral (13) and aortic (14) valves.

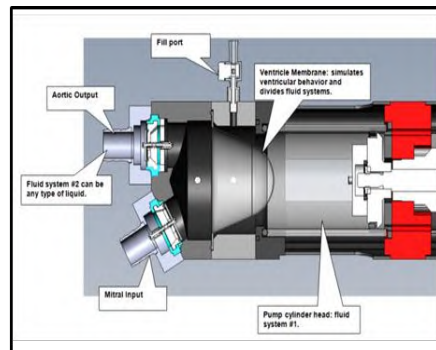
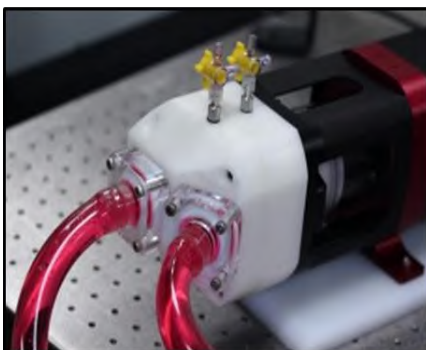


Figure 33: The ViVibro electronic Superpump AR Series can be provided with a pump head including a ventricle membrane and two heart valves to simulate physiological flows.

This ViVitro left heart model was first used for an in-vitro study of a mitral valve prostheses [82, 83] and is currently mostly used for hydrodynamic testing of heart valves, such as mechanical heart valves [104, 105, 120]. At this moment, this commercial system is the most applied and cited pump for simulating cardiac flows [103].

2.4.6 Cardiovascular Fluid Mechanics Lab, Georgia Institute of Technology, Atlanta (1984 - present)

In 1984, Yoganathan developed an aortic valve test equipment at the Georgia Institute of Technology (Figure 34 left panel) for the in-vitro hydrodynamic characterization of heart valves, such as bileaflet, tilting disc and porcine aortic valve substitutes [121]. Then, in the late 1990s, Hashim and colleagues developed a left heart model with a modular mitral valve mounting device, in which biological valves can be mounted. This left heart model was used for the assessment of three-dimensional forces applied by the papillary muscle on the left ventricular wall [74, 122]. In 2008, Padala and colleagues called this apparatus the “Georgia Tech Left Heart Simulator” [123].

After that, Rausch and colleagues majorly improved this simulator in the late 2000s by replacing the rigid ventricle by a flexible bag model to simulate wall motion. They also changed the compressible bladder type pump into a piston pump driving system to obtain more physiological and versatile transmitral pressures and flow curves [5]. Figure 35 illustrates both configurations of the Georgia Tech Left Heart Simulator: the left panel before and after right panel after the revision of Rausch and colleagues.

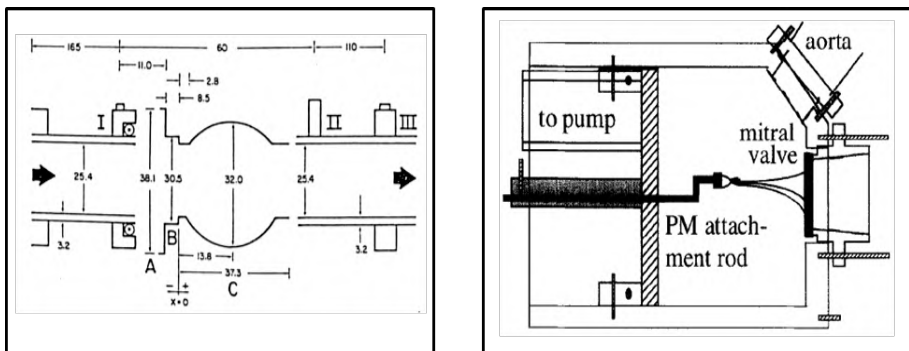


Figure 34: Left panel shows the aortic valve test apparatus developed by Yoganathan in 1984 [121]. Right panel illustrates the left heart model build by Hashim and colleagues in 1997 [74], also called the “Georgia Tech Left Heart Simulator” [123].

In more detail, the left heart model is driven by a piston pump system (type SPS 3891 [124]) with the capability of simulating isolated annular dilatation by a custom made dynamic annulus plate. The left ventricle is made of a polyurethane bag which is immersed in a closed transparent box which is, on its turn, connected to the piston pump. The ventricular chamber comprises a mechanical aortic heart valve and a native mitral valve. The papillary muscles of the native mitral valve are inventively attached to a papillary muscle positioning system by permanent magnets which avoid puncturing of the left ventricular model. The positioning system allows a three-dimensional adjustment to accurately obtain the natural position of the papillary muscles. The Georgia Tech Left Heart Simulator was used for the study of mitral valve (dys)function with focus on the mitral annulus [5].

Despite the improvements by Rausch et al., the authors consider it as a limitation that the left ventricle model is not able to mimic the natural apical-basal movement and twisting motion [5].

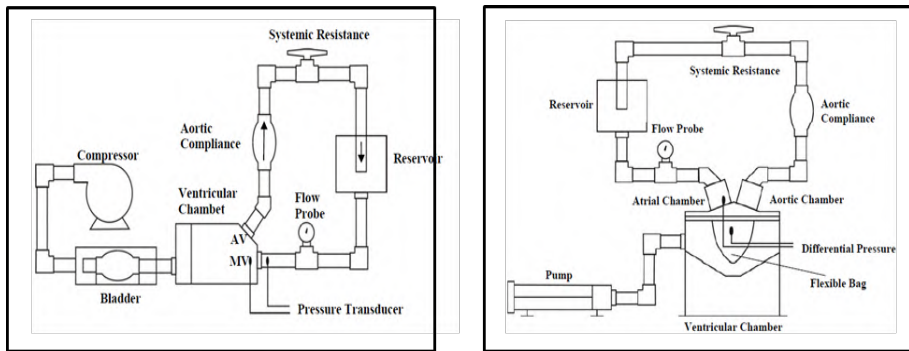


Figure 35: Left, the original Georgia Tech Left Heart Simulator (2007) including a rigid left ventricle which is driven by a compressible bladder type pump. Right, the simulator revised by Rausch and colleagues (2009) including a flexible ventricle model which is driven by a ViVitro linear piston pump [5].

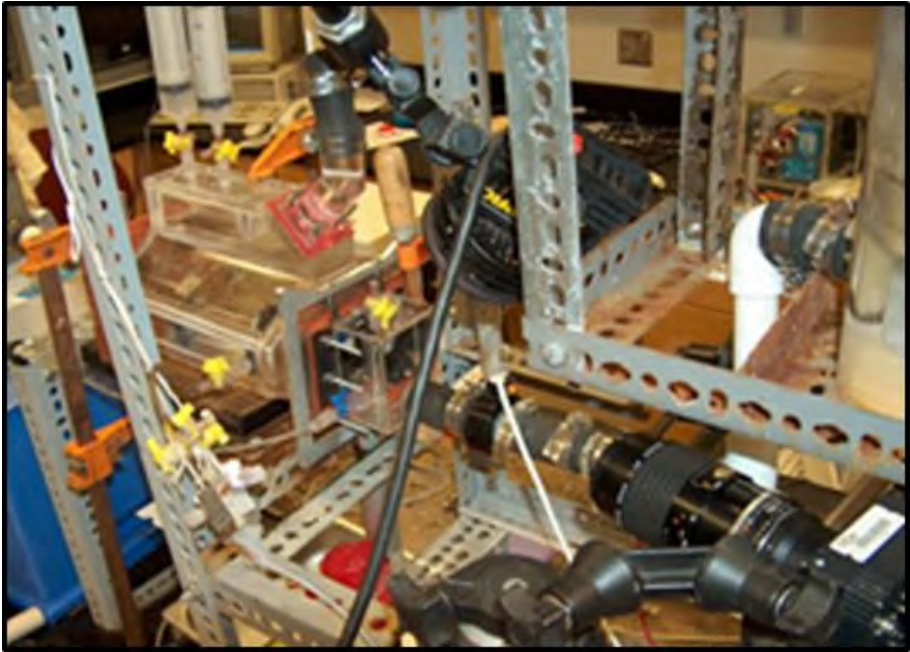


Figure 36: The latest version of the Georgia Tech Left Heart Simulator (2013). Adapted from [125].

2.4.7 Cardiovascular Engineering Group, Aachen (1981 and 1988)

In the early-1980s, Reul and colleagues [86] developed a cardiovascular simulator to study the fluid mechanics of natural and bioprosthetic heart valves. The mock loop is similar to the latter described system, as it also includes an elastic ventricular model as well as a volume controlled actuation by a piston pump. Later, in the late-1980s, Knott and colleagues [87] rebuilt the system and added some extra features, such as an air compartment between the ventricular sac and the ventricular rigid box. These two cardiovascular simulators contain the following similar components (Figure 37 A and B). An atrial reservoir (1) is connected to an atrial chamber (3) which includes an atrial elastic sac (2). The atrial chamber is separated from the ventricular chamber (6) by a flow meter (4) and a mitral valve (5). Both models include an elastic ventricular model (7) which is positioned in a rigid transparent box (6) and a fluid which fills the space in between. However, only in Knott's model, this space is partly filled with fluid (6b) and air (6a). Downstream the aortic valve (8), in both models, there is an elastic aorta (9) placed in a rigid chamber (10) with on top of it, a pressure regulation (11), a flow meter (12),

a resistance (13) and a compliance (14). The peripheral resistance (15) is adjustable by a valve mechanism (16). The actuation system (17) is volume controlled by an electromagnetic valve (17c) and consists of two hydraulic pistons, one for low (17a) and one for high pressures (17b). Pressure is measured at the left atrium (2), the left ventricular apex (7) and the aorta (9), using tip catheter transducers. According to Knott's model, transmitral (4) and aortic (12) flows are measured using two electromagnetic flow sensors. In Reul's model, only aortic flow is measured using a hot wire anemometer. Figure 37 C shows a photo of the model of Knott and colleagues.

Unique features of these two simulators are first, the left atrium and aorta which are made of a flexible silicone material, and second, the implementation of an aortic and ventricular compliance.

The cardiovascular simulator of Reul and colleagues was used to study the fluid mechanics of a natural mitral valve [102], for the comparative in-vitro evaluation of porcine and pericardial bioprostheses [126], and for the in-vitro comparison of bileaflet aortic heart valves [127]. Furthermore, this heart model was used by Hasenkam and colleagues for velocity visualizations of aortic valves [128]. Even though most of the in-vitro dynamic studies of flow through prosthetic heart valve were limited to two dimensions, they were able to visualize three-dimensional velocity fields downstream the mechanical aortic valves, using suspended particles in an aqueous glycerol solution. The system of Knott and colleagues was applied for in-vitro comparisons of series aortic heart valve prostheses [87] and for assessing velocity and shear-stress distribution of mechanical heart valves [129].

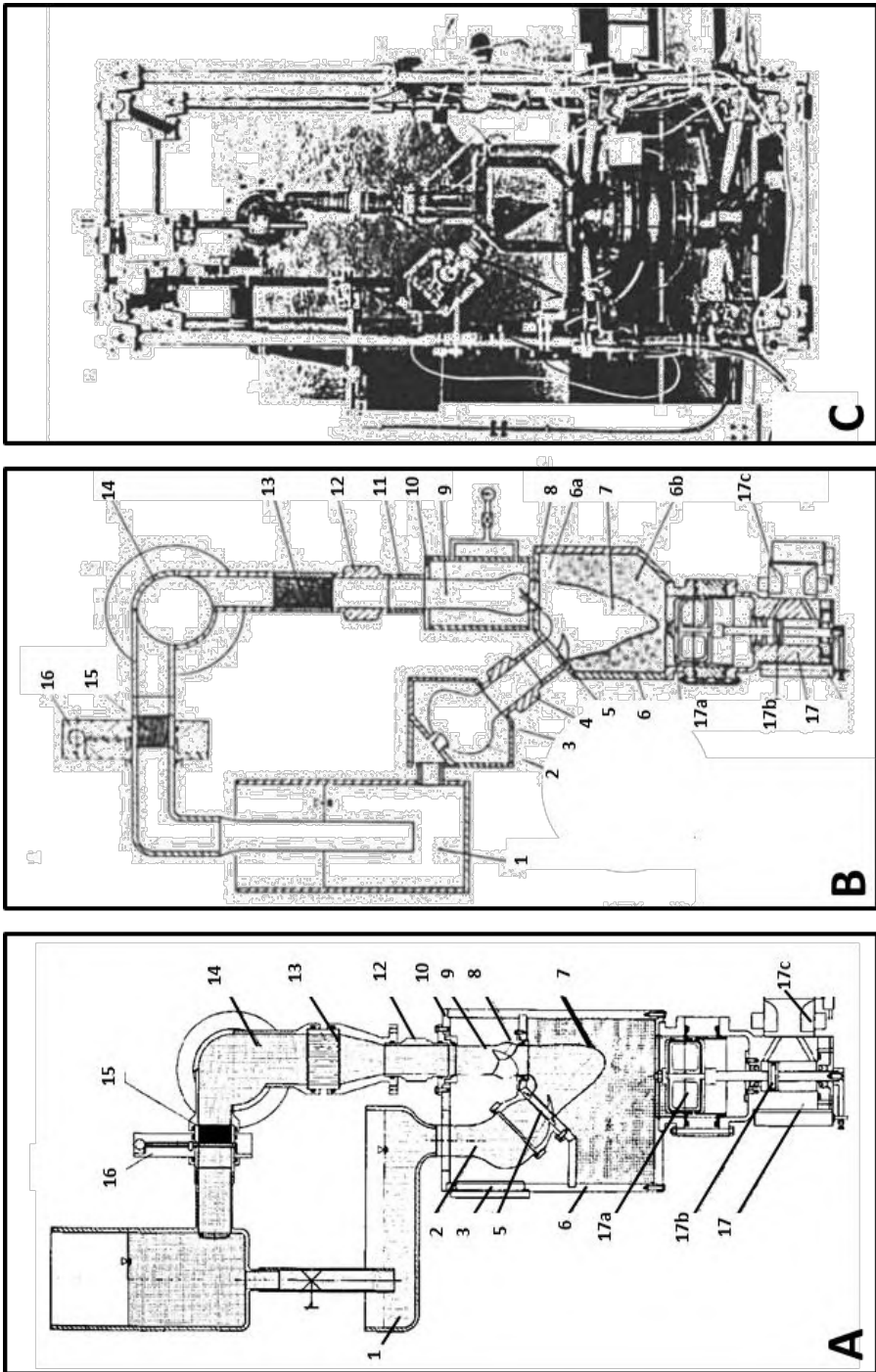


Figure 37: Schematic overview is shown of the cardiovascular simulator of Reul and colleagues (A) and of Knott and colleagues (B). Panel (C) shows a photograph of Knott's model. Adapted from [86, 87].

2.4.8 Department of Mechanical Engineering, British Columbia (1985)

In 1985, Akutsu designed a cardiovascular simulator to assess hydrodynamic performance of both aortic and mitral valves [79]. As illustrated in Figure 38, this heart model consists of a valve support block which holds the atrium, aorta, cardiac valves and ventricle model and is mounted on a PMMA box which is connected to a piston pump. This system is actuated by a stepping motor and controlled by a microprocessor.

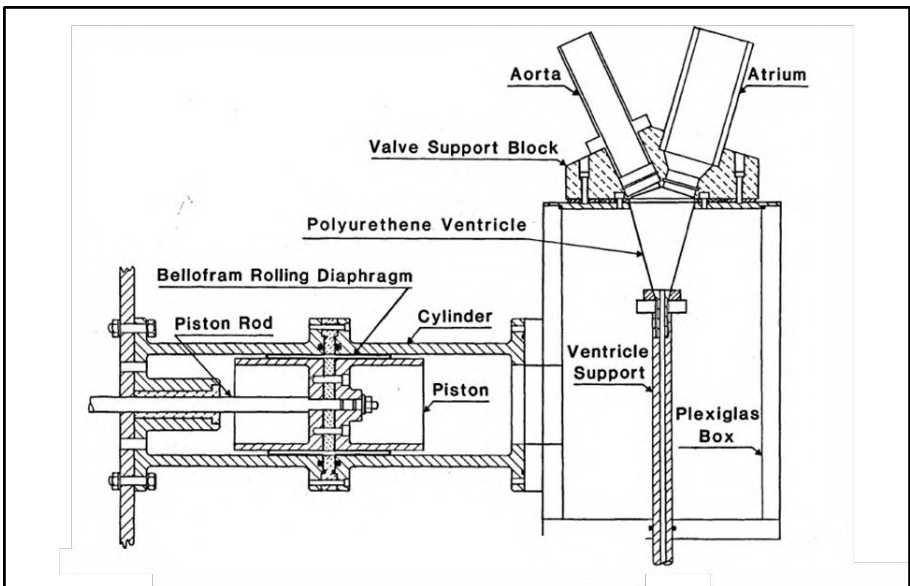


Figure 38: The cardiovascular simulator according to Akutsu (1985) with a conically shaped transparent ventricle [79].

This cardiovascular simulator was used for the assessment of hydrodynamic performance of mechanical [79, 130-142] and biological prosthetic heart valves [142] in relation to valve orientation [131] and design [131, 132]. Flow fields were analyzed using LDA (Laser Doppler Anemometer) [79, 130, 134, 141, 142] and PIV (Particle Image Velocimetry) [131-140] inside the simulated ventricle [131, 132] and through the model aorta [139, 140].

Although this basic design follows the model developed by Scotten et al. and Reul et al., this left heart model has some unique features. First, the ventricle model is made of a transparent polyurethane sheet material which allows flow measurement and visualisation by optical methods, such as LDA and PIV. Akutsu approached the anatomical shape of the natural ventricle by a truncated cone and the natural flexible character using a flexible material. Another unique feature is the Ventricle Support (Figure 38) which artificially connects the ventricle model apex to the PMMA Box. Although this support rod is responsible for a smooth wall deformation during the pump cycle, it has the disadvantage that natural apex movements of the ventricle are restricted which in turn artificially affects velocity patterns inside the ventricle model [79].

2.4.9 Dynatek Laboratories Inc., Galena, Missouri (1990 – present)

Dynatek Laboratories Inc. is a research company located in Galena, Missouri, launched in the early 1990s. Since then, the company develops medical device testing equipment, such as for heart valve and stent testing. They also developed a series of left heart models, such as the MP1 Anthropomorphic cardiac ultrasound phantom, the MP3 Pulse Duplicator and most recently the MP4 – Robotic Cardiovascular Pulse Duplicator. We suppose that there has been also a MP2 system, however, no information could be retrieved on this system.

The MP1 system was the first ultrasound compatible pulse duplicator. Previous cardiac simulators were not apt for ultrasound imaging for multiple reasons: setup components sensitive to reverberations and ultrasound reflections, test fluid which did not contain ultrasound contrast agent, and/or the fluid reservoirs lacking viewing windows. In contrast, the MP1 phantom is the first left heart simulator which is made suitable for ultrasound studies, as illustrated in Figure 39. First, the container contains three membrane-covered viewing ports (32, 34 and 36) which allow ultrasonic examination. These chambers are oriented according to the three conventional cardiac ultrasound views, i.e., the long axis (LA), short axis (SA) and apical (AP) views. Second, the phantom contains a blood-mimicking fluid (28) for the circulatory system as well as a tissue-mimicking medium (46) to ultrasonically simulate the human tissue. An ultrasound transducer (44) is shown as well as the three examination windows (32, 34 and 36). Apart from ultrasound related features, the MP1 is also equipped with a compressible tubing (26) to fine-tune the pump flow output. The pulsatile flow in this pulse duplicator is

realized by a piston pump (24) which pushes the fluid through a compressible tubing (26) into the viewing chamber (30). The piston pump is driven by an adjustable DC motor (48) via a variable stroke drive (50).

The MP1 was used by Barbara and colleagues to study the data comparability with the system developed by the University of Sheffield in the context of in-vitro evaluation of prosthetic heart valves [143]. Although the same prosthetic heart valve and settings (HR, SV, systole/diastole time ratio and afterload) were used, the authors observed high discrepancies in experimental valve performance data (such as the closing and leakage volume) between these two pulse duplicator systems. Barbara et al. stressed the need for standardization in in-vitro evaluation of heart valves.

The later developed MP3 pulse duplicator is also an ultrasound compatible system but with special attention for transparency of the setup to provide full visibility of the device during experiments. This system is coupled with a programmable pumping system and was used for durability testing of stent bars [144].

The newest system which Dynatek developed (2004) is called the MP4 Robotic Cardiovascular Pulse Duplicator and is illustrated in Figure 41 [145]. This model includes an updated version of data acquisition, a computer controlled rolling piston to actuate the ventricle, and a silicone mock aorta which is fabricated from MRI data.

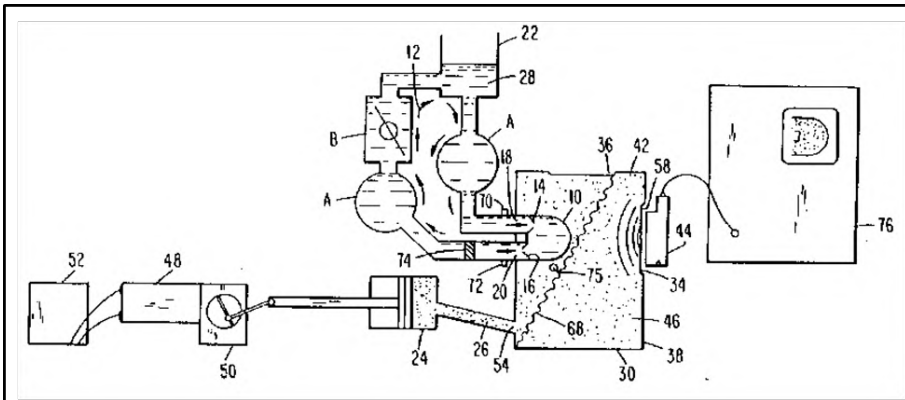


Figure 39: The Dynatek MP1 Pulse Duplicator (1990). The simulated circulatory loop 12 includes the following successively components: a reservoir 22, a variable compliance chamber (A), mitral valve port 18 including the mechanical prosthetic mitral valve 14, a flexible left ventricular sac 10, aortic valve port 20 including the mechanical prosthetic aortic valve 16, flow meter 74, variable compliance chamber (A) and a variable resistance manifold (B). Adapted from [101].

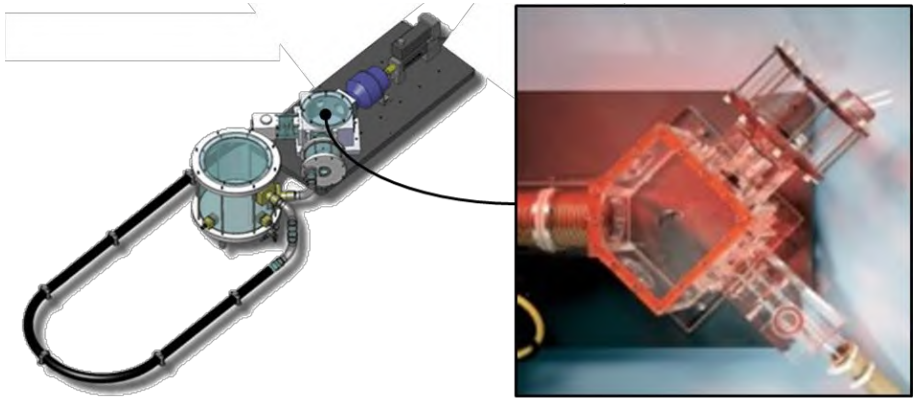


Figure 40: The Dynatek MP3 Pulse Duplicator: the circulatory system is given (left) together with a close-up of the left heart model (right). The ventricle model is not shown on the pictures. Adapted from [144].

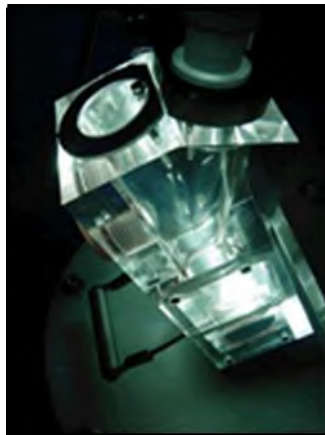


Figure 41: The Dynatek MP4 Robotic Cardiovascular Pulse Duplicator [145].

2.4.10 University of Sheffield, UK (1991)

The Sheffield heart simulator was first reported on in 1991. Unique feature of this simulator are its straightforward control of the piston pump using a microcomputer and the flow straighteners at mitral and aortic valve sites. The system is equipped with valve mounting blocks to enable valve tests in either mitral position or in aortic position. Pressures have been measured at both the ventricle and aorta site, while flow has been measured directly by electromagnetic flow meters at both mitral and aortic valve sites. Pressure and flow data can be loaded to the computer and processed automatically.

The simulator has been used for the validation of the Gorlin orifice formula, more specifically for the assessment of the heart valve effective orifice area (EOA) [78], and for a comparative study of steady and pulsatile flow within the context of in-vitro validation of heart valves [146].

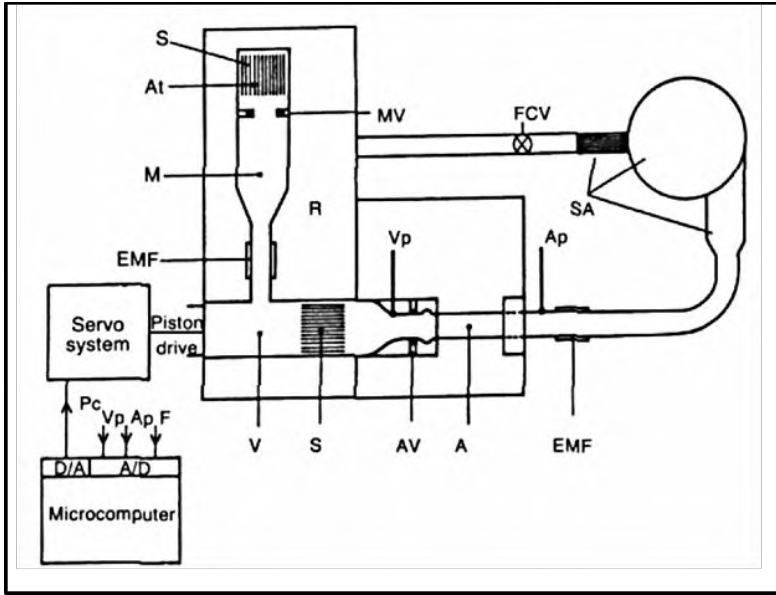


Figure 42: Schematic drawing of the Sheffield pulse duplicator (1991) consisting of the following components [78]: fluid container (R), electromagnetic flow meter (EMF) and flow straighteners at both mitral and aortic valve sites (S), left atrium (At) and a mitral valve plane (Mv), mitral chamber (M), left ventricle (V), mitral (MV) and aortic valve (AV), aorta (A), a model of the systemic circulation (SA). Systemic arterial compliance is realized by a volume of trapped air and the peripheral resistance is controlled by a flow control valve (FCV).

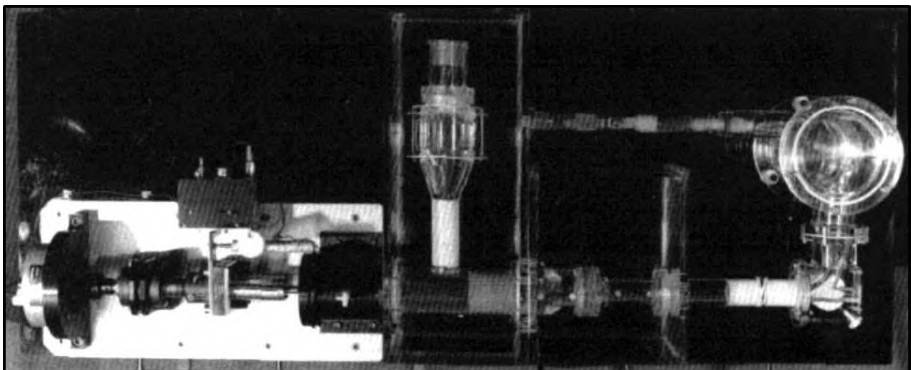


Figure 43: Photograph of the pulsatile flow simulator of Sheffield (1991) [78].

2.4.11 IBiTech-BioMMeda Group of Ghent, Belgium (1992 – present)

From the early 1990s onwards, multiple cardiovascular simulators have also been developed and tested at the IBiTech-BioMMeda group of Ghent University. First, Verdonck and colleagues developed a revolutionary, computer controlled cardiovascular simulator in the early 1990s [95, 96] which was extended in the late 1990s by Segers and colleagues with a full arterial system [147]. In the mid-2000s, Claessens and colleagues developed a thick-walled left ventricular model [98].

The original model was a computer controlled cardiovascular simulator which was developed in collaboration with the Norwegian Technical University of Trondheim [95, 96] to study the influence of the several determinants of the left heart performance on transmitral flow. This left heart simulator was one of the first in-vitro models which allowed an echographic study of transvalvular mitral and aortic flow [96]. Also, the natural geometric representation together with the separate activation of the atrium and ventricle made this left heart simulator state-of-the-art for that time. Up to date, a modified version of this simulator is still currently and routinely used as a simulation platform for cardiovascular research in the IBiTech-BioMMeda Group.

Originally, the simulator was a pressure controlled system (Figure 44 left and top panel). In a later stage, the simulator was redesigned to a volume controlled system using a hydraulic piston pump system (Figure 44 right panel). The hydraulic part of the simulator consists of a PMMA reservoir holding a Latex model of the left heart and is connected to models of the pulmonary veins, the left atrium, the left ventricle and the aortic arch. Parts are modularly designed in order to easily mount mitral and aortic valves. The electronic part allows control and monitoring of the cardiac cycle in terms of heart rhythm, atrial as well as ventricular pressures and flows. In addition, the model also allows for differentiation of several left heart performance determinants on transmitral flow, such as preload, compliance of the left atrium and ventricle, peripheral resistance (afterload) and heart rate. Ultrasound evaluation has been made possible from both atrial and ventricular windows.

This heart simulator has been used for a very wide range of applications, such as (among others) testing heart valves [148-150], in-vitro simulation of the arterial system [151], and more recently, assessment of blood-wall interaction [98], testing assist devices [152, 153], and evaluation of aortic valve matrices for tissue engineering [154].

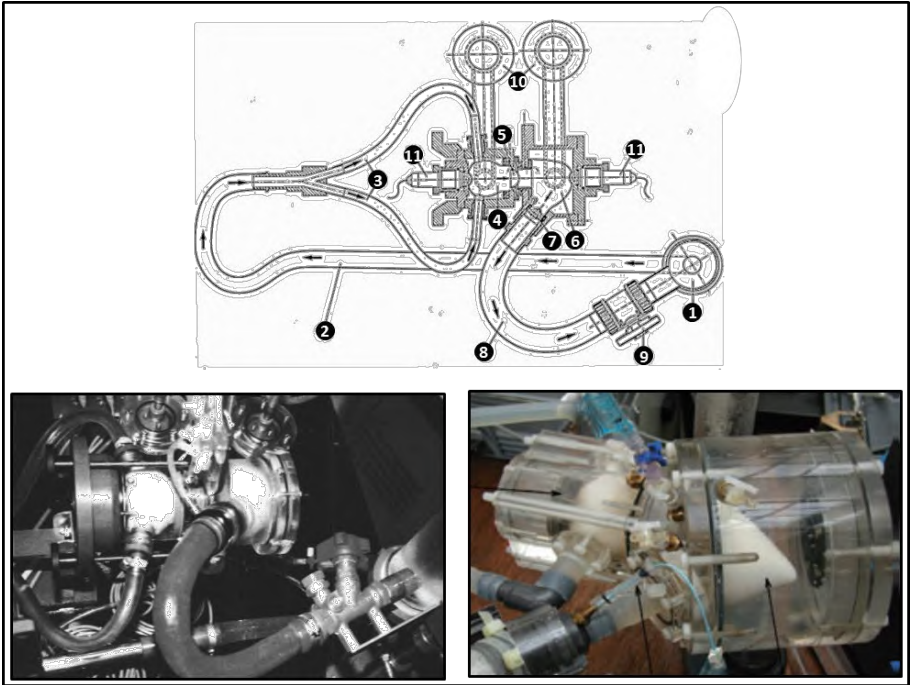


Figure 44: The cardiovascular left heart simulator of Verdonck and colleagues. The left panel shows a photograph and the top panel shows a technical drawing of the original pneumatically driven model (1992) and the right panel illustrates the revised hydraulically actuated model (2006). The system is equipped with (1) reservoir, (2) tube, (3) two pulmonary veins, (4) left atrium, (5) mitral valve, (6) left ventricle, (7) aortic valve, (8) aorta, (9) resistance, (10) volume measurement reservoirs and (11) ultrasound probes. Adapted from [95] and [154].

In 1997, Segers extended the left heart model of Verdonck and colleagues to a cardiovascular simulator by adding a model of the arterial system [99]. The arterial tree model was made of latex rubber and included the aorta, the upper and lower limb arteries, the carotid arteries and the major branches to the abdominal organs. Accurate simulation of physiological and pathological conditions was realized by a representative anatomical geometry (matching the arterial tree of a male subject of 1.75 m and 75 kg) and by terminating the arteries with adjustable resistances and compliance chambers. This model was, among other applications, used for the non-invasive assessment of arterial compliance [99], for studying the role of tapering in aortic wave reflection [155], the impact of an abdominal aortic aneurysm on aortic pressure and flow [156], and for the validation of a mathematical 1D arterial network model [157].

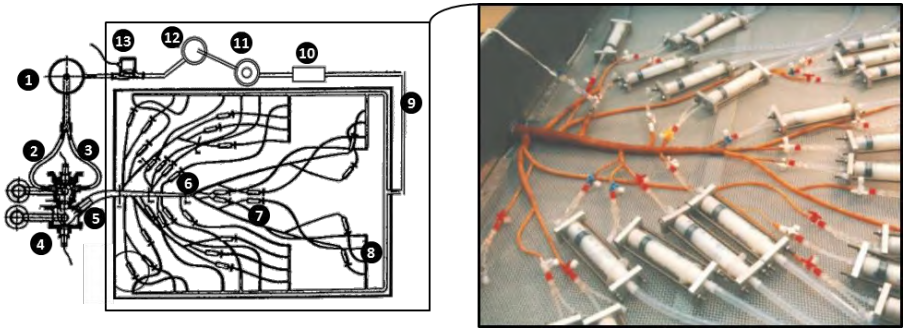


Figure 45: The extended version by Segers and colleagues (1997) comprises the left heart model of Verdonck and colleagues (at the outer left side) which is connected to an extensive model of the arteries (middle and right panel). The left heart model comprises 1) lung reservoir, 2) pulmonary veins, 3) left atrium, 4) left ventricle and a partial aorta. The arterial tree model includes 5) the larger part of the aorta, 6) aorto-iliac bifurcation, 7) peripheral model, 8) veins, 9) venous return conduit, 10) electromagnetic flow meter, 11) venous overflow, 12) buffering reservoir and 13) pump. Adapted from [99, 155].

In 2004, Claessens and colleagues [98, 158] developed a LV model [96] by implementing a thick-walled left ventricular model to reveal more fundamental insights in left ventricular isovolumic relaxation and early filling dynamics. They developed a unique left ventricular phantom mimicking the mechanical and acoustic myocardial tissue properties of the human heart. Variation in phantom compliance was obtained by using a Polyvinylalcohol (PVA) solution which allows systematical wall stiffening with the number of freeze-thaw cycles during preparation. Suitable acoustic properties were realized by adding graphite powder to the PVA solution to enable appropriate backscatter of the ultrasonic waves. Unfortunately, the systolic phase was not modelled in this study; therefore, we categorized this model not as a cardiovascular simulator but as a side project to the work of Verdonck et al. and Segers et al.

The model was used to individually adjust clinically obvious parameters concerning depressed diastolic function such as end-systolic pressure, active relaxation rate, passive myocardial properties, and preload [98].

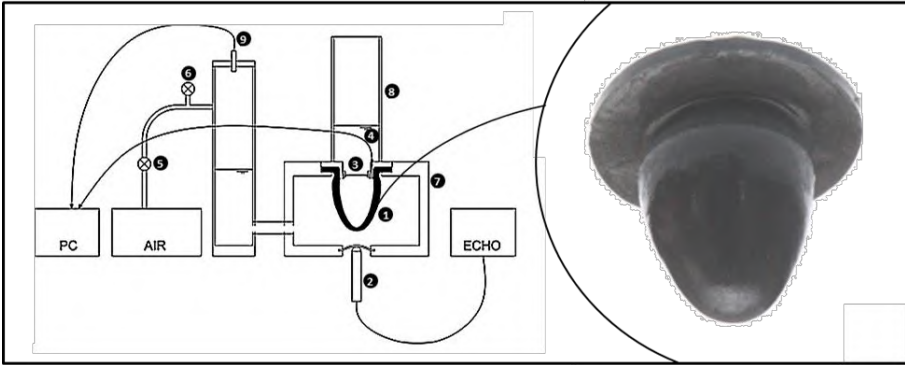


Figure 46: Overview of the experimental setup of Claessens and colleagues: (1) Left ventricular phantom (close up right), (2) Doppler transducer, (3) mitral valve, (4) pressure transducer, (5) proportional valve, (6) valve, (7) PMMA chamber, (8) preload reservoir and (9) device to measure ventricular volume. Adapted from [98].

2.4.12 Cardiovascular Biomechanics Group of Marseille (2000 - present)

In Marseille, France, the research group of prof. Régis Rieu has had an interest in developing cardiovascular models for several decades.

In 2000, Mouret and colleagues developed the “Dual Activation Simulator (DAS)” (Figure 47) including an independent hydraulic activation of the left atrium and left ventricle [88]. Because the left atrium and left ventricle model shapes are based on medical data, this model represents an anatomical shape of the human left heart. In order to build the cardiac chambers, first an aluminum core was manufactured using a 5-axis milling machine. Subsequently, this core was coated by successive layers of silicon (see Figure 48).

In 2010, Tanné and colleagues developed a cardiovascular simulator with a more detailed anatomical-shaped left atrial and a left ventricular model [89] (see Figure 48 and Figure 49 left). This cardiovascular simulator was made by transparent materials and also equipped with a PIV system.

This pulse duplicator was used to measure and describe the complex 3D flow dynamics inside a realistic left atrium geometry [89], and more recently, to study local transvalvular pressure gradients in bileaflet mechanical heart valves [159] (see Figure 49 right). This cardiovascular simulator is also employed for valve testing services by the company Protomed Labs which is also located in Marseille.



Figure 47: The Dual Activation Simulator (DAS) setup (left panel) and the left heart model of Mouret and colleagues (2000) [88].

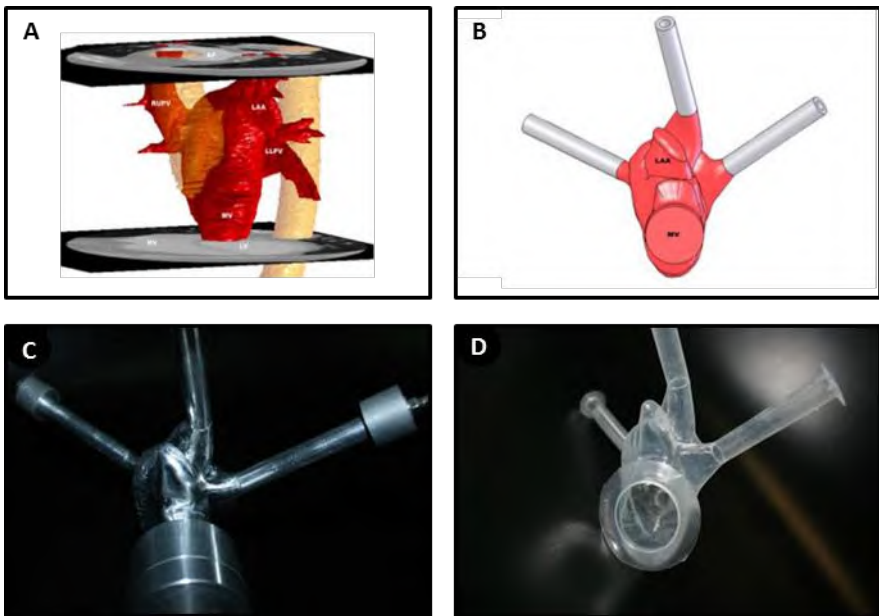


Figure 48: Workflow to obtain an anatomical-shaped left atrial and a left ventricular model: first, medical images are segmented (A), then a virtual solid model is created (B), next an aluminum core is milled (C) and finally a silicone model is produced (D). Adapted from [89].

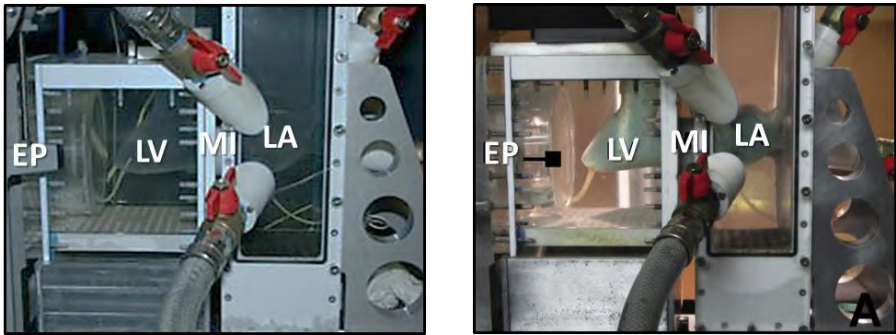


Figure 49: Two versions of the cardiovascular simulator of Marseille are shown. Left panel illustrates the PIV compatible version (2010) and right panel demonstrates the ultrasound compatible version (2013). The following components are indicated: echocardiographic probe (EP), left ventricle (LV), mitral valve (MI) and left atrium (LA). Adapted from [89] (left) and [159] (right).

2.4.13 Department of Mechanical Engineering, Virginia Tech, Blacksburg (2004)

In 2004, Pierrakos and colleagues of Virginia Tech, developed a cardiovascular simulator for the analysis of the hemodynamic characteristics of blood flow through heart valves, but also of intraventricular blood flow (see Figure 50). The system is equipped with a piston pump with an adjustable travel in order to generate physiological pressure and flow waveforms. The ventricular model is made of transparent silicone in order to allow PIV examination.

A unique feature to highlight is the presence of a flexible valve plane which is an innovative way of ventricle model suspension, allowing clear flow assessment of the valve inflow and outflow regions.

To date, this left ventricular model has been used to analyze intra ventricular vortex dynamics through porcine and mechanical heart valve prostheses [160] and to study the effect of vortex formation on ventricular filling and mitral valve performance [161].

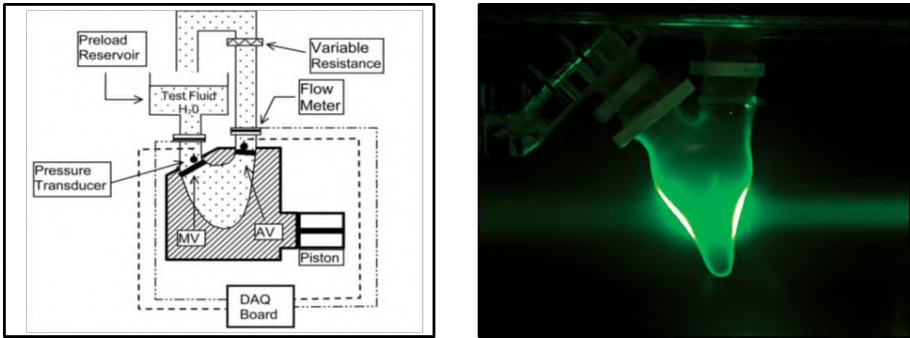


Figure 50: The Virginia Tech heart simulator (2004), a schematic setup overview (left panel) [160] and a photo (right panel) of the left heart model are shown [162].

2.4.14 Kheradvar Research Group, California Institute of Technology, Pasadena (2006 - present)

Also in the United States, in 2006, Kheradvar et al. developed a cardiovascular simulator which is called the ‘Caltech’s left heart pulsed flow simulator system’ [90]. This system comprises a left ventricle and valve plane which are made of transparent flexible silicone to allow flow measurements by optical techniques, such as a custom-designed high-resolution high-speed PIV equipment.

The Caltech’s left heart pulsed flow simulator system (Figure 51 A) is connected to a ViVibro hydraulic pump system (Superpump system, VSI, SPS3891, ViVibro systems Inc., Victoria, BC, Canada) and controlled by a VSI Wave Generator VG2001 (ViVibro Systems Incorporated, Victoria, BC, Canada) to generate pulsatile flow in the circulatory system. The ventricular model (Figure 51 B-D) comprises a geometry which is based on a 3D reconstruction of a normal adult heart using cardiac MRI in systolic state and is realized via dip-molding of a transparent, flexible silicone material. The left ventricular model is suspended in a cubic container made from PMMA to which the hydraulic pump system is connected (Figure 51 A) and connected to the circulatory system via inlet and outlet tubes (Figure 51 B). Prosthetic as well as bioprosthetic heart valves can be mounted in both mitral and aortic positions.

Just like in the model of Pierrakos et al. [160, 161], this model is equipped with a special valve plane feature. While all other left heart models are equipped with a rigid valve housing block which suspends the left ventricle model in a fixed way, these models include a flexible valve plane which holds the left ventricle model by the in- and outlet tubes at the aortic and mitral sites

(Figure 51 B). This innovative way of ventricle model suspension allows movement of the valve plane as well as a clear flow assessment of the valve inflow and outflow regions. In comparison with the left heart model of Pierrakos et al, this model has a smaller travel between the two valves, which seems more anatomically and physiologically correct (Figure 51).

There are, however, some limitations to this experimental setup [163]. In their validation study, Falahatpisheh and Kheradvar note that “the silicone LV model cannot generate the twisting motion similar to the left ventricle, which may affect the flow-field”. This limitation applies to all (as far as we know) current in-vitro left heart models since there are no left heart models which include this twisting motion to date.

The Caltech's left heart pulsed flow simulator system is primarily designed and used for in-vitro study of intraventricular flow fields and this in relation to mitral valve dynamics [90]. As such, Kheradvar and colleagues examined the effect of varying the profile height of mitral bioprostheses on flow [90]. Also, they validated the so-called ‘Echocardiographic Particle Image Velocimetry’ which is a technique being applied, for example, to quantify blood vorticity patterns in the left ventricle [164]. Another study with this in-vitro setup considered the fluid dynamics downstream of a novel mitral bioprosthesis [165] (Figure 52). The authors determined the effect of mitral saddle annulus and leaflet length on peak leaflet stress and transmitral flow pattern by using a new design of a bileaflet bioprosthetic valve. It was found that the movements of the mitral saddle annulus, together with the leaflet length, are critical factors which decrease stress distribution at the leaflet tips.

Recently, Kheradvar and colleagues also developed a bileaflet mitral bioprosthesis which imitates the mitral valve’s saddle annulus motion (Figure 52) [165]. The bioprosthesis comprises a saddle-shaped Nitinol core on which the leaflets were sutured. The leaflets were made of bovine pericardial tissue with a thickness of 0.5 mm. In the mitral valve prosthesis, they did not include the natural supporting structures such as the chordae tendineae and papillary muscles which avoid the valve leaflets being prolapsed toward the atrium. Instead, they realized the supporting function of the mitral valve prosthesis by suturing the leaflet to each other by means of two supporting prongs which extend from the annulus along with the valve leaflets, in this way improving the robustness of the prosthesis.

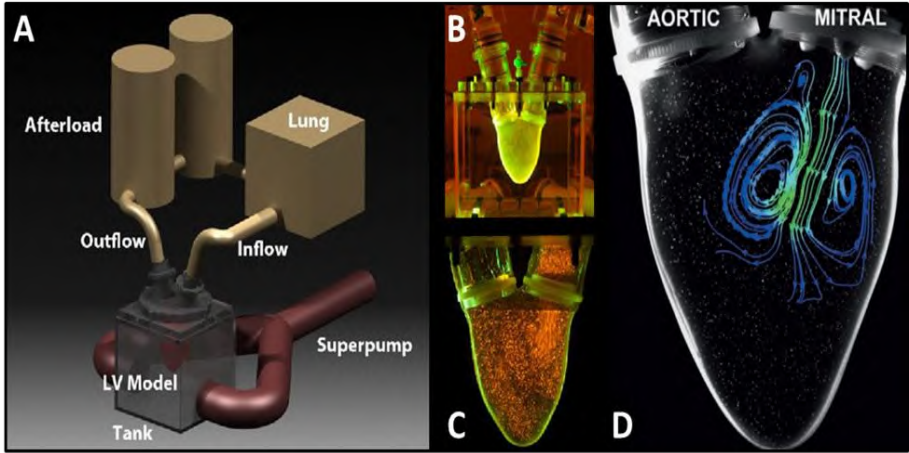


Figure 51: The Caltech's left heart pulsed flow simulator system (2006): A) Composition of the in-vitro setup, B) left ventricular model suspended in a transparent box full of water, C) close up of the ventricular model, the aortic and mitral valves and the inflow and outflow tract. Intraventricular flow patterns which are visualized by fluorescent microparticles which are illuminated by a laser sheet. D) Intraventricular streamlines of a transmittal jet which are obtained by PIV. Figures A, B and C are adapted from [163] and D from [166].

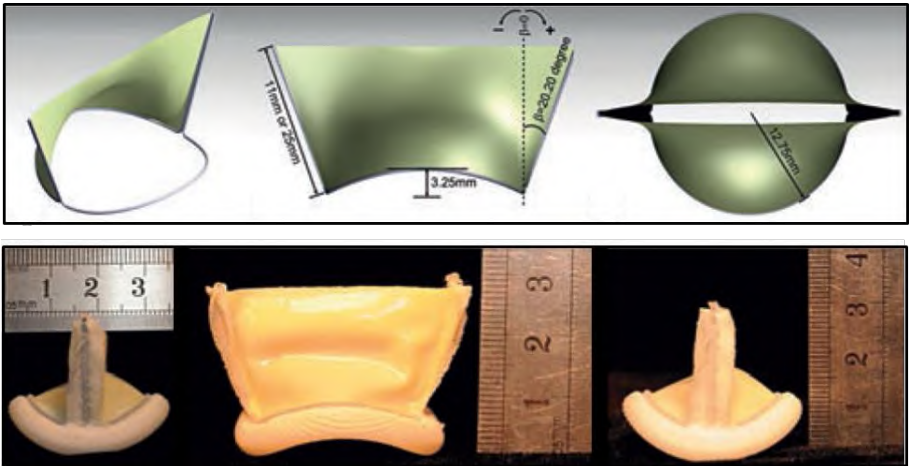


Figure 52. Design of a bi-leaflet mitral bioprosthesis (top panel) composed of a saddle shaped annulus made of Nitinol and two leaflets made of pericardial tissue (bottom panel). Adapted from [165].

2.4.15 Department of Mechanical Engineering, Bari, Italy (2006)

In Italy, Rasponi and colleagues developed a left ventricular model with special attention to mimic natural wall deformation [167]. Generally, left ventricular models are made of a flexible sac with a truncated ellipsoid shaped geometry and suspended in a rigid transparent outer box which is connected to a piston pump. When water is extracted from the outer closed box, the flexible sac expands to its end diastolic state and contracts to its end systolic state when the water is pumped back. Although it is well demonstrated that these models provide adequate pump function, none of these models particularly mimic the physiological wall deformation patterns for it is difficult to predict the wall deformation patterns of the model.

Rasponi and colleagues are the first to pay attention to modelling morphological variations which may be expected to influence the hemodynamics. They designed a novel heart simulator with a ventricular model which deformed in a more physiological mode, by using a composite structure composed of a silicone sac reinforced by circumferential bands. As a result of this material composition, the ventricular deformation was forced in a longitudinal direction, which is illustrated in Figure 53.

The ventricular sac was designed using structural FEM analyses and was prototyped for experimental validation of mitral valve surgical corrections [167].



Figure 53: The left ventricular model of Rasponi and colleagues (2006). This figure illustrates the fair agreement between numerical model (left panel) and the ventricle prototype (right panel) at the end diastolic phase. A prominent longitudinal deformation is realized using reinforcement of the silicone wall by circumferential bands. Adapted from [167].

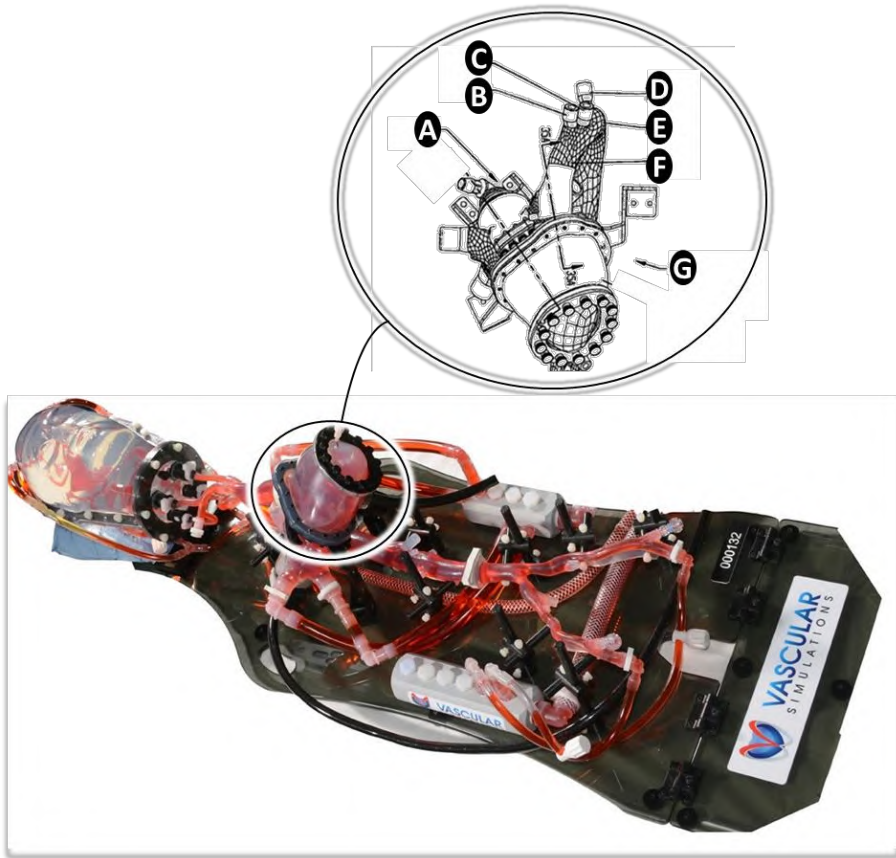


Figure 54: The Vascular Simulations Replicator developed by Carson and colleagues (2013) with (A) left atrium assembly, (B) brachiocephalic artery, (C) right common carotid artery, (D) subclavian artery, (E) aortic arch, (F) aorta and (G) left ventricle assembly. Adapted from [91, 97].

2.4.16 Vascular Simulations, Stony Brook, New York (2013 - present)

In 2013, Carson and colleagues patented an anatomically accurate left cardiac simulation device to replicate normal and diseased state cardiac function, the “Vascular Simulations Replicator”, illustrated in Figure 54 [97]. The invention of this cardiovascular simulator and the development of anatomically accurate vascular models recently lead to the foundation of the company Vascular Simulations in Stony Brook, New York.

The system comprises a functional left atrium and ventricle, two mechanical valves at a mitral and aortic sites and a vascular model. Ventricle

and atrium contractions are realized by a pneumatic actuator module, powered by an electric motor. This actuation system allows accurate simulation of a wide range of heart states, going from normal to severely pathological heart conditions.

Unique for this system is that it duplicates the cardiac cycle and blood flow in a patient specific vasculature including the great vessels arising from the aortic arch and the cerebrovasculature, as shown in Figure 54. Another exclusive feature is the silicone aorta with a built-in compliance which allows replication of the natural pressure waveforms in the aorta.

The system is developed for cardiovascular training and testing medical devices, for example for interventionists who can train their procedures with the identical anatomy and pathology that they will ultimately treat in clinical practice.

2.4.17 Materialise NV, Leuven (2013 – present)

The current digital revolution brings forth a wide range of new applications which also foster the creation of benchtop models. As such, the ability of 3D reconstruction of anatomical structures from medical images, the fast development of 3D printing techniques and anatomically-like 3D printing materials are leading to more advanced and anatomically accurate cardiovascular benchtop models.

Recently, Materialise NV, Leuven, one of the leading companies in this field, started a 3D printing service for patient-specific cardiovascular anatomical models, the so-called HeartPrint®. These models can be used to assist in the pre-operative planning, in planning complex interventional procedures, and as functional benchtop models for testing medical devices. Figure 55 illustrates two recent realizations. The first realization is a transparent rigid heart model which is an anatomically realistic and accurate representation of a human heart. The second example is realized by multi-material 3D printing (using the Objet Connex 3D printer, Stratasys Ltd., Minnesota), which is a calcified model of the aortic valve. This valve model is composed of both the tissue, which is a flexible material, as well as the calcification, which is a rigid material. In order to 3D print patient-specific highly flexible and tear-resistant cardiovascular models [93], Materialise developed the HeartPrint® Flex process.

In 2012, Little and colleagues developed a patient-specific cardiovascular simulator at the Methodist Hospital in Houston, Texas in

collaboration with Materialise, the so-called the ‘Heart Beat Simulator™’ [92]. This pulse duplicator is equipped with a functional calcified model of Materialise and is made cardiac MRI-compatible using a long drive shaft and a flow loop which does not contain any ferrous metals, as illustrated in Figure 56. To date, the Heart Beat Simulator has been used to get more insight in risk factors of deployed Transcatheter Heart Valves (THVs) [94].



Figure 55: The left panel illustrates a transparent rigid anatomically realistic and accurate representation of a human heart. The right panel illustrates a printed calcified aortic valve. Adapted from [168].

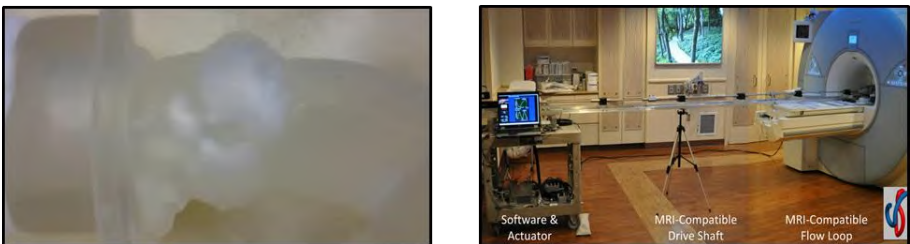


Figure 56: The left panel illustrates a functional multi-material 3D printed calcified aortic valve which was built in the Heart Beat Simulator. The right panel shows the MRI compatible set up including the software and actuator, the MRI-compatible drive shaft and the MRI-compatible flow loop. Adapted from [92].

2.5 CONCLUSION

This chapter describes the history of cardiovascular simulator development which took place over the past 55 years. This history illustrates the major strides forward and the wide range of approaches that has been taken to make in-vitro cardiovascular systems. Also, in briefly reviewing their versatile applications, it can be concluded that such in-vitro cardiovascular models have become an indispensable tool to enhance cardiovascular insights, to advance procedures and to develop medical devices, not only in the past and the present, but that it will only become even more important in the (near) future. Finally, our review also highlights the complexity of in-vitro cardiovascular modelling. As a consequence, this state-of-the-art information is a valuable source of inspiration to define design criteria for new cardiovascular simulators. In the following chapter, we discuss the limitations of the current models in order to optimize design criteria for a new generation of models.

Critical evaluation and practical guidelines for optimizing current models

This chapter formulates practical guidelines to accommodate for the challenges in present in-vitro left heart modelling, as described in the state-of-the-art overview of Chapter 2.

3.1 INTRODUCTION

In Chapter 2, we presented a state-of-the-art overview to demonstrate the wide range of in-vitro approaches and models that were developed during the past 55 years of cardiovascular simulator history. In this chapter, we critically evaluate the current approaches and their accompanying concepts in light of what (we believe) the field needs to further optimize such in-vitro models. We summarized these possibilities and general shortcomings of the current state-of-the-art of in-vitro cardiovascular modelling in Table 3. We tried to summarize the limitations across the different models in one overview table. In the discussion of this chapter, we will hence also describe these limitations across the different models, instead of separately for each of the discussed models. This wide range of limitations clearly reflects the complexity of in-vitro cardiovascular modelling. However, this list of limitations also provides

us with valuable information and design challenges to define clear practical guidelines to advance cardiovascular simulator optimization.

In this chapter, the critical evaluation and definition of practical guidelines are first described for left ventricular muscle modelling, then for mitral valve apparatus modelling, finally for valve plane optimization in the context of integrating ventricular and mitral valve models into a left heart model. We will close this chapter with a schematic summary of the various practical guidelines (PG1 – PG8 Table 2). These guidelines will form the well-informed basis for the in-vitro left heart model optimization steering this dissertation project.

3.2 LIMITATIONS AND PRACTICAL GUIDELINES RELATED TO LEFT VENTRICULAR MUSCLE MODELLING

In this section, we describe five major limitations of the current left ventricular models and translate these limitations into corresponding guidelines that should be targeted in order to attain more realistic ventricular models. Such models should be primarily designed to accomplish a more realistic anatomy (limitations 1 to 3) of the complex left ventricular wall anatomy. This left ventricular wall is in reality thick-walled, (1) and is physiologically characterized by anisotropic wall properties (2) and a composition of contractile elements (3). Moreover, such models should be assigned to achieve a more accurate mimicking of the physiological events of the natural left ventricle (limitations 4 and 5). These include – among others – the complex wall deformation patterns in terms of longitudinal, circumferential and radial deformation (4), and the twisting motion (5).

3.2.1 A more realistic thick-wall

The first major limitation of the current collection of cardiovascular simulators is that almost all in-vitro cardiovascular simulators have modelled the natural thick left ventricular muscular wall by a thin-walled membrane. The left ventricular wall, however, is more anatomically correctly modelled by a thick-walled approach. One exception to the common use of thin-walled membranes is the phantom designed by Claessens et al. [98], who designed a thick-wall made from a Polyvinylalcohol solution. Unfortunately, the systolic phase was not modelled in this study, therefore, we categorized this model not as a cardiovascular simulator but as a side project to the work of Verdonck et al. and Segers et al. (see § 2.4.11). Hence, we identify **the implementation of a**

thick wall as a first practical guideline (**PG1**) that should be taken into account when searching to optimize in-vitro models of the left ventricle.

3.2.2 Anisotropic wall properties

The second limitation of current left ventricular models relates to the use of isotropic wall materials (e.g. silicone). The natural cardiac wall, however, consists of interweaving bundles of cardiac muscle fibers leading to anisotropic wall properties. To our knowledge, only one study has used anisotropic material, i.e., the study of Rasponi et al. [167]. This model was unique in modelling anisotropy by integrating fibers into the thin-walled silicone left ventricular model, yet performed less at optimizing anisotropy towards the modelling of the natural global wall deformation patterns. Therefore, the second guideline (**PG2**) for optimizing cardiovascular simulators to attain more anatomically correct left ventricle models is to **try including the anisotropic wall properties of the natural ventricular wall**. These anisotropic wall properties are also directly related to the wall deformation patterns, and are hence also closely intertwined with the following limitations.

3.2.3 Modelling active contractile wall elements

As a third limitation, the present left heart simulators are all confined to modelling the muscular contraction by a passive membrane. These passive movements stand far away from the natural active movements of the human ventricular wall. Hence, the natural muscular contraction and relaxation of the ventricle are important active phenomena which remain un-modelled in current left heart models. Therefore, our third practical guideline (**PG3**), needed to mimic natural wall contraction, is **to invent left ventricular models which include an active contractile wall containing contractile elements**.

3.2.4 Modelling multiple global wall deformation patterns

Closely related to the use of passive thin-walled membranes made of isotropic material, is that no simulator to date has been able to simultaneously model the global wall deformation patterns in terms of longitudinal, circumferential, and radial deformation. Hence, we identify this issue as a fourth major limitation. As can be inferred from Table 3, longitudinal or circumferential deformation is not entirely absent in most models, yet these processes remain rather limited because they occur mainly uncontrollable. More particularly, though the general thin-walled membrane models include a circumferential as well as longitudinal deformation, the wall deformation remains uncontrolled, as also mentioned in the first limitation. For the thin-walled left ventricular

models, differences in wall thickness are negligibly small. Therefore, radial deformation can be considered absent in these models. This issue of physiological likeness in terms of morphological variations of the left ventricular wall has only received little attention in the history of cardiovascular simulator development. This is surprising given that wall movements are found to be sensitively related to the hemodynamics of ventricular filling [167]. Therefore, our fourth practical guideline (**PG4**) for optimization left heart models is the **mimicking of global ventricular wall deformation patterns including longitudinal, circumferential as well as radial deformation**. To date, we identified only one study which gave attention to the controllable modelling of one of these three wall deformation patterns. Rasponi et al. [167] were able to model the longitudinal component, in a controlled manner, by integrating circumferential reinforcements. However, to the best of the author's knowledge, no report so far reported modelling the circumferential or radial components in a controlled manner, nor the combination of all three global wall deformation patterns together.

3.2.5 Including the twisting motion

Finally, the twisting motion is a fourth deformation pattern of the natural left heart that – to our knowledge – has not been implemented in current cardiovascular simulators. In contrast to the previous aspect, many authors have commented and cited this limitation. Rausch, for example, did mention this limitation in his doctoral dissertation (2009) as following: “even though the Flexible Bag Model has been shown to model wall motion, its “left ventricle” does not undergo the typical ... twisting motion that has been visualized in-vivo” ([5] page 90). Also, Claessens et al. mentioned this limitation for their thick-walled left ventricular model: “we did not account for the myocardial preferential fiber direction which makes a real ventricle heterogeneous and transversely isotropic. Therefore, an untwisting motion during diastole could not be simulated.” ([98] page 336). Also more recently, Falahatpisheh et al. noted this limitation about the Caltech's Left Heart Pulsed Flow Simulator in a study to assess cardiac fluid dynamics in-vitro by high-speed particle image velocimetry. These authors noted that “the silicone LV model cannot generate the twisting motion similar to the left ventricle, which may affect the flow-field” ([163] page 6). The identification of this need by several research groups highlights that there remains a great challenge for new left heart models to simulate the natural torsional motion. Hence, we identify the inability to simulate the twisting motion which is present in the natural left heart (and involves a complex wall deformation pattern) as a fifth and final major limitation. Correspondingly, our fifth practical guideline (**PG5**) for optimizing future left heart models is to take on the challenge to **include the twisting motion**.

3.3 LIMITATIONS AND PRACTICAL GUIDELINES RELATED TO THE MITRAL VALVE

In this section, we discuss the limitations concerning mitral valve models and formulate corresponding guidelines for the optimization of these models. The biggest limitation in this regard relates to the absence of modelling the most relevant anatomical features of the mitral valve, such as the two main leaflets, a saddle-like annulus, the chordae tendineae and the two main papillary muscles. Hence, this is translated in one important practical guideline.

3.3.1 More anatomic features of the mitral valve

As described in the previous chapter, one critical application of left heart simulators today is to test new prosthetic heart valves. In case of aortic valve testing, the setup is generally equipped with a mechanical prosthetic heart valve at the mitral site [66, 75, 78, 79, 82, 84, 87-89, 91, 92, 95, 99, 100, 103, 124, 145, 160, 165]. This approach benefits the setup durability, which is of crucial importance in durability-heart valve testing settings that have no special attention for the mitral valve apparatus. However, such mechanical prosthetic heart valves are in general not great representatives of anatomically correct mitral valve models.

In recent years, we identify a slow but steady growing interest in modelling more natural and anatomically correct in-vitro mitral valve models as an alternative for using mechanical prostheses. The study of interactions of flow and movements with a more natural valve plane is important as it may foster advanced insights in the working of a natural left heart. For example, in 2006, Kheradvar et al. developed a more natural accurate mitral valve prosthesis by modelling the saddle-like annulus and the flexible leaflets. However, when looking into more details to this model - in the context of more natural in-vitro mitral valve modelling - this model still lacks elementary features of the natural valve, such as the chordae tendineae and the papillary muscles, and as such, the dearth of these elements can be considered essential when pondering about natural mitral valve functioning. Knowing that the papillary muscles are mostly expressed by rough anatomical left ventricular wall structure, it may be expected that the papillary muscle movements will sensibly influence the hemodynamics of ventricle filling. Therefore, we identify it as necessary to account for these anatomical features to attain a more accurate modelling of the mitral valve.

More insight in the design of the mitral valve comes from studies with special emphasis on the mitral valve functioning [5, 74, 89, 169, 170]. In these studies, also the chordae tendineae and papillary muscles are modelled, but this modelling is generally restricted to the use of post-mortem mitral valves. As noted in the previous chapter, such post-mortem models do well in accounting for anatomically correct mitral valve models but have major limitations towards preservation time. Also, the limited accessibility to human post-mortem mitral valve models and the inability to vary model parameters, such as geometry and material properties, are important drawbacks of this approach.

These limitations of current mitral valve models emphasize that there is a great need for **an in-vitro mitral valve apparatus model with a parametrized geometry which includes elementary features of the mitral valve apparatus**. The need for such an in-vitro and more naturally accurately mitral valve model has been asserted to the author of this dissertation by several key experts in the field [171-173]. Therefore, we identify **the optimization of more natural, in-vitro mitral valve models** as the sixth practical guideline (**PG6**). This involves the anterior and posterior leaflets (**PG6a**) which are hinged by a saddle-like annulus (**PG6b**) and made from a fiber-based material (**PG6c**), the chordae tendineae (**PG6d**), the anterolateral papillary and posteromedial papillary muscles (**PG6e**).

3.4 LIMITATIONS AND PRACTICAL GUIDELINES RELATED TO VALVE PLANE OPTIMIZATION

In the context of integrating left ventricular and mitral valve models in current left heart models, two other limitations are that the naturally flexible valve plane is typically modelled by a rigid approach and that current simulators do not model the longitudinal motion of the valve plane towards the apex. These two limitations should also be addressed when optimizing integral left heart models.

3.4.1 A flexible mitral valve annulus and valve plane

The first limitation is a consequence of a rigid valve plane which leads to a rigid instead of a flexible fixation of the mitral valve annulus. Rausch et al. reported this limitation by the following quote: “the annulus plate could not simulate the dynamic changes in geometry and stiffness throughout the cardiac cycle” ([5] page 90). Therefore, as seventh practical guideline (**PG7**) (also related to mitral valve model optimization), we identify that future

models should take into account **a flexible instead of a rigid valve plane which allows the suspension of a flexible mitral annulus, while keeping the actuation functionality**. Such a more flexible suspension could be realized in two ways. The first way is to implement a flexible valve plane, instead of the rigid valve plane of the current left heart models, while keeping the actuation functionality intact. This method was applied by Kheradvar et al. [165, 166]. Although this approach allowed the integration of a flexible mitral annulus, the authors made use of mechanical prosthetic heart valves which involves a rigid annulus. The second way would be to invent an alternative actuation principle which allows the integration of a flexible valve plane. We will take up both challenges in the current dissertation.

3.4.2 Including the apical-basal movement of the valve plane

A second limitation related to the current state-of-the-art left heart models, is the hindered longitudinal motion of the valve plane towards the apex. For example, Rausch et al. mention that "... even though the Flexible Bag Model has been shown to model wall motion, its 'left ventricle' does not undergo the typical apical-basal movement ... that has been visualized in-vivo" ([5] page 90). This typical apical-basal movement refers to the valve plane movement in the direction of the apex during systole. Also Claessens et al. observed a similar limitation in their model: "due to technical reasons, the phantom is required to be attached at its basal side, while in a real ventricle, the atrioventricular plane moves up and down." ([98] page 336).

As mentioned before, Rasponi et al. were able to simulate a apical-basal movement by a longitudinal deformation of their left ventricular model [167]. However, the longitudinal valve plane motion towards the apex during systole was hindered by the rigid valve plane suspension, resulting in a non-physiological apex-to-valve-plane movement.

The technical reasons that Claessens et al. mention are about the suspension assembly, which is commonly used in current left heart simulators. The suspension assembly generally comprises a rigid valve plane which suspends a thin walled flexible ventricular sac and mounted to the rigid container [5, 66, 79-84, 87-92, 96, 99, 127, 145, 160]. The heart cycle is realized by changing the volume (volume driven systems) and/or pressure (pressure driven systems) by an external power source. To enable stable control of the left ventricular actuation during the heart cycle, the left ventricular model is rigidly suspended to the closed box, which hinders the motion of the valve plane and prohibits annuli dynamics. As such, it is not possible for current left heart models to model the typical apical-basal motion of the valve plane. In order to allow motion of the valve plane, **new left heart**

models need to be invented with novel ways of ventricle actuation mechanisms. This is the eighth guideline (**PG8**) and is hence related to the previous practical guideline about valve plane optimization of left heart models.

3.5 CONCLUSION

In this chapter, we critically highlighted the possibilities and limitations of the current state-of-the-art of cardiovascular simulators. These critical remarks were formulated across models, yet, they are summarized and listed for each of the discussed studies in Table 3.

The wide variety of heart models and accompanying model limitations emphasizes that - even in these advanced technological times - it is still extremely challenging to accurately simulate the complex physiological conditions that occur in the human left heart and arterial system with a cardiovascular simulator [95]. Because the mimicking of anatomical structures and physiological events are crucial for advancing medical device testing (and our knowledge of human heart functioning), there remains however great value in developing in-vitro test models which mimic the reality as closely as possible. For this reason, the development of more realistic in-vitro test models is a well-defined recommendation of the FDA in their guideline document about medical device testing [2].

We distinguish two major challenges in designing and attaining such more realistic in-vitro models. The first challenge is to mimic the anatomical structures as closely as possible. The second challenge is to attain the duplication of physiological events, to attain a more accurate mimicking of the physiological events in their natural settings. Relevant design criteria for both research challenges are mentioned in Table 3.

The overview in Table 3 enables multiple conclusions regarding the current state-of-the-art of cardiovascular simulators. First, it appears that the current cardiovascular models do account for only a few of the anatomical features and physiological events that are mentioned in the table. Once again, this underscores the need for designing and developing more naturally accurate left ventricular models.

Second, as of yet, no study has been found that describes an in-vitro mitral valve model that includes the elementary features which are listed in the table. Once there will be more naturally correct models of the left ventricle and mitral valve, an integrative approach combining these models, such an in-vitro naturally correct left heart model will be of great value, since it is well

known that there is a close physiological interaction between the left ventricle and the mitral valve.

Third, Table 3 shows that, concerning the left ventricular models, there is a lack of studies that account for the radial wall contraction and twisting motion of the left ventricular wall, nor are the thick-walled structure and contractile elements included. There are four studies [74, 75, 78, 121] which did not include a thin-walled left ventricular model and therefore, none of the left ventricular anatomical features nor physiological events of Table 3 were present. All other studies did implement a thin-walled model and mimicked the longitudinal as well as the circumferential deformation components of the left ventricle; however this wall deformation remains unpredictable. Only one study accounted for the anisotropic wall properties and the longitudinal component of left ventricular wall contraction [167]. In addition, it is noteworthy to see that the more recent studies are making use of medical images to define their ventricular model geometries.

Fourth, regarding the mitral valve models, Table 3 shows that none of the in-vitro mitral valve models includes all elementary parts of the mitral valve apparatus. The models which are generally used are post-mortem valve models; however, functional decay and tissue decomposition of postmortem tissue, together with the inability to vary model parameters, still denote an important issue potentially jeopardizing the applicability of this approach.

From the various limitations described in this chapter, we can isolate three general needs related to cardiovascular in-vitro modelling: (NEED 1) **there is a need for more naturally correct left ventricular models**, (NEED 2) **there is a need for in-vitro mitral valve models including the basic anatomical features**, (NEED 3) **there is a need for in-vitro left heart models integrating a left ventricular model and a mitral valve model including the basic anatomical features**. An overview of these needs and the corresponding practical guidelines are summarized in Table 2. This set of practical guidelines is crucial for the invention and optimization of cardiovascular in-vitro models to bring cardiovascular modelling to the next level. Based on this overview, new in-vitro models of the left ventricle, the mitral valve, and the left heart are developed and presented in the following chapters.

Guidelines towards designing a more naturally correct in-vitro model of the left heart

NEED 1. More naturally correct left ventricular models

- PG1** The left ventricular wall is more naturally correctly modelled by a thick-walled approach
- PG2** Models of the left ventricle are more anatomically correctly represented by including the anisotropic wall properties of the natural wall.
- PG3** Natural left ventricular wall contraction can be modelled by integrating active contractile elements into the left ventricular wall model.
- PG4** Left heart models can be optimized by mimicking the global ventricular wall deformation patterns such as longitudinal (**PG4a**), circumferential (**PG4b**) as well as radial deformation (**PG4c**).
- PG5** The global natural wall deformation of the left ventricular wall is better represented by the inclusion of the twisting motion which is present in the in-vivo left heart.
-

NEED 2. An in-vitro mitral valve model including the basic anatomical features

- PG6** The requirements of a basic in-vitro mitral valve can be described as a reproducible mitral valve apparatus model with a parametrized geometry and including all basic features of the mitral valve apparatus, such as the anterior and posterior leaflets (**PG6a**), the saddle-like annulus (**PG6b**), fiber-based material (**PG6c**), the chordae tendinae (**PG6d**) and the anterolateral and posteromedial papillary muscles (**PG6e**).
-

NEED 3. An integrative approach, combining the left ventricular and the mitral valve models, including the basic anatomical features

- PG7** A more naturally correct valve plane approach for mitral valve modelling is obtained by implementing a flexible instead of the rigid valve plate which allows the suspension of a flexible mitral valve plane, while keeping the actuation functionality.
- PG8** A left heart model is more naturally correctly represented by allowing the motion of the valve plane by the invention of novel ways of ventricle actuation mechanisms.
-

Table 2: Overview of the practical guidelines for designing a more natural accurate in-vitro left heart model.

3. CRITICAL EVALUATION AND PRACTICAL GUIDELINES FOR OPTIMIZING CURRENT MODELS

PART I. The left heart: from nature to model														
Chapter 1. The left heart structure and function	LV						MV					VP		
	Thick wall	Anisotropic wall	Contractile elements	Longitudinal contraction	Circumferential contraction	Radial contraction	Twisting motion	Posterior & anterior leaflets	Saddle-like annulus	Fiber-based leaflets	Chordae tendinae	Papillary muscles	Flexible annulus & valve plane	Longitudinal valve plane motion
Chapter 3. Needs (1-3) and practical guidelines (PG1-8)	LV model						MV model					VP model		
	NEED 1						NEED 2					NEED 3		
	PG1	PG2	PG3	PG4a	PG4b	PG4c	Type	PG6a	PG6b	PG6c	PG6d	PG6e	PG7	PG8
Chapter 2. In-vitro modelling of the left heart: State-of-the-art														
Year	Authors / Company	Origin	Section											
1962	Björk et al.	Uppsala SE	\$2.1	-	-	-	-	-	-	-	-	-	-	-
1972	Bellhouse et al.	Oxford UK	\$2.2	-	-	-	-	-	-	-	-	-	-	-
1977	Lee	Berkeley USA	\$2.3	-	-	-	-	-	-	-	-	-	-	-
1978	Gabbay et al.	New York USA	\$2.4	-	-	-	-	-	-	-	-	-	-	-
1979	Scotten and Walker	Victoria CA	\$2.5	-	-	-	-	-	-	-	-	-	-	-
1981	Reul et al.	Aachen DE	\$2.7	-	-	-	-	-	-	-	-	-	-	-
1984	Yoganathan	Atlanta USA	\$2.6	-	-	-	-	-	-	-	-	-	-	-
1985	Akutsu	Vancouver CA	\$2.8	-	-	-	-	-	-	-	-	-	-	-
1988	Knott et al.	Aachen DE	\$2.7	-	-	-	-	-	-	-	-	-	-	-
1990	Dynatek Laboratories Inc., MP1	Missouri USA	\$2.9	-	-	-	-	-	-	-	-	-	-	-
1991	Cochrane et al.	Sheffield UK	\$2.10	-	-	-	-	-	-	-	-	-	-	-
1992	VIVitro Labs Inc.	Victoria CA	\$2.5	-	-	-	-	-	-	-	-	-	-	-
1992	Verdonck et al.	Ghent BE	\$2.11	-	-	-	-	-	-	-	-	-	-	-
1997	Hashim et al.	Atlanta USA	\$2.6	-	-	-	-	-	-	-	-	-	-	-
1997	Segers et al.	Ghent BE	\$2.11	-	-	-	-	-	-	-	-	-	-	-
1999	Dynatek Laboratories Inc. MP3	Missouri USA	\$2.9	-	-	-	-	-	-	-	-	-	-	-
2000	Mouret et al.	Marseille FR	\$2.12	-	-	-	-	-	-	-	-	-	-	-
2004	Dynatek Laboratories Inc. MP4	Missouri USA	\$2.9	-	-	-	-	-	-	-	-	-	-	-
2004	Claessens et al.	Ghent BE	\$2.11	-	-	-	-	-	-	-	-	-	-	-
2004	Pierrakos et al.	Virginia USA	\$2.13	-	-	-	-	-	-	-	-	-	-	-
2006	Kheradvar et al.	Pasadena USA	\$2.14	-	-	-	-	-	-	-	-	-	-	-
2006	Rasponi et al.	Bari IT	\$2.15	-	-	-	-	-	-	-	-	-	-	-
2009	VIVitro Labs Inc.	Victoria CA	\$2.5	-	-	-	-	-	-	-	-	-	-	-
2009	Rausch et al.	Atlanta USA	\$2.6	-	-	-	-	-	-	-	-	-	-	-
2010	Tanné et al.	Marseille FR	\$2.12	-	-	-	-	-	-	-	-	-	-	-
2012	Kheradvar et al.	Pasadena USA	\$2.14	-	-	-	-	-	-	-	-	-	-	-
2013	Vascular Simulations Inc.	New York USA	\$2.16	-	-	-	-	-	-	-	-	-	-	-
2013	Materialise NV. & Little et al.	Leuven BE	\$2.17	-	-	-	-	-	-	-	-	-	-	-
2014	VIVitro Labs Inc.	Victoria CA	\$2.5	-	-	-	-	-	-	-	-	-	-	-

Table 3: An overview of cardiovascular simulators is given in the context of practical guidelines. Different types of mitral valves are applied, mechanical (M), bioprosthetic (B) and post-mortem (P), but no in-vitro valve model yet. Index: ‘-’ absent, ‘~’ present but limited, ‘v’ present, ‘ ’ not applicable.

Design methodology

This chapter discusses the general design process that was used in this dissertation to produce original ideas in a structured manner and to realize these ideas in an effective way. The applied design methodology is based on the Double Diamond Model [174] which consists of two paired divergence-convergence phases. The first divergence-convergence phase starts with a broad and in-depth exploration of the literature which is then subsequently analyzed to identify the design needs and to define practical guidelines that provide an answer to these needs. The second divergence-convergence phase entails the process in which multiple new ideas are generated to accommodate the identified design needs and from which, in a subsequent step, the best ideas are selected to become realized in final concepts.

In Chapters 1, 2, and 3 (literature reviews on the natural left heart and current state-of-the-art of cardiovascular simulators; distillation of research needs and practical guidelines), we extensively described the first divergence-convergence phase of this Double Diamond Model. In this Chapter, we provide more details on the second divergence-convergence phase, i.e., the generation of new ideas and selection of best concepts, respectively.

From these chosen concept ideas, solutions are further developed into the actual in-vitro models, as described in Chapters 5 to 12.

4.1 INTRODUCTION

The engineering design process is a tool that engineers use in creating functional products according to a structured method. A more comprehensive understanding of engineering design processes can help creative designers to achieve more creativity, to make faster decisions and to boost the innovation process [175]. To date, a wide array of different models on engineering design processes is available. Most dominant in the literature is the ‘linear style’ model, in which a design engineer is assumed to follow a number of predetermined steps [175]. These steps are labeled in various ways across models but generally involve (1) the establishment of a need phase, (2) an analysis of task phase, (3) a conceptual design phase, (4) an embodiment design phase, (5) a detailed design phase, and (6) an implementation phase [175].

In this dissertation, we applied a ‘divergent-convergent type’ of engineering design model. This model slightly differs from the described traditional ‘linear style’ model as it assumes an integrated evaluation of multiple design ideas and a subsequent selection of these ideas and concepts [175]. This model hence separates a period of generating ideas from a period of evaluating ideas. In the idea generating period, creativity is explicitly encouraged by processes as brainstorming, horizontal imagination (i.e., generating many ideas being unconcerned with the detailed implementation of them), and lateral thinking (i.e., solving problems using reasoning that is not immediately obvious nor obtainable by only using traditional step-by-step logic).

More precisely, the design methodology applied in this dissertation closely resembles the so-called ‘Double Diamond’ design process model, created by the British Design Council [174]. The Double Diamond model is based on case studies of industrial design procedures applied by eleven global brands and is proposed "to champion great design that improves lives and makes things better" [176]. The Double Diamond model graphically represents the design process by two diamonds (i.e., rhombuses) in a line (Figure 57), with each diamond reflecting both a divergent and convergent phase.

The Double Diamond model identifies three critical points (Problem – Problem Definition – Solution) and four main stages (Discover – Define – Develop – Deliver) across the whole engineering process. The design process is initiated by a problem, question or hypothesis, which is the first critical point, ‘Problem’, the starting point of the first diamond. The divergence-

convergence phase of this first diamond results in the second critical point, 'Problem Definition', which is a clear description of the problem to be solved. This 'Problem Definition' is the starting point of the divergence-convergence phase of the second diamond which finally results in the 'Solution', which is the output that meets the design criteria of the Problem Definition.

Each diamond has two stages. The first stage of the first diamond is the 'Discover' phase and marks the start of the project. This begins with an initial problem (critical point 'Problem'), idea or inspiration, often sourced from a discovery phase in which user needs are identified. The Discover stage is a phase of divergent thinking. The second stage of the first diamond is the 'Define' phase, in which interpretation and alignment of the identified needs create a clearer definition of the problem. The Define stage is a phase of convergent thinking resulting in the critical point 'Problem Definition'.

The third stage is the 'Develop' phase and denotes the divergent thinking phase of the second diamond. It marks a period of development focusing on multiple concepts through creative thinking, brainstorming and iteration. This 'Develop' stage includes a large number of iteration loops which are characterized by three phases: (1) prototyping a concept or idea, (2) testing the prototype, and (3) refining the prototype based on testing. This iteration loop is repeated until a satisfactory result is achieved. Prototyping and testing can occur virtually, e.g., by using CAD and CAE, or physically, e.g., by using rapid production techniques. The iteration process of physical prototyping can be done via a hands-on approach through trial and error because this generates quick solutions during a process of doing. The final stage of the second diamond is the 'Deliver' phase, where the final concept is chosen and further refined by the process of iteration. The Deliver phase is a phase of convergent thinking in a structured manner that typically occurs in close communication with the expert-stakeholder panel. A frequently used tool hereby is the trade-off table, which is a form of a prioritization matrix in which alternative concepts are scored against the formulated design criteria. The scoring is obtained by the summation of the scores of the different criteria, either in symbol form (for example: ++, +, +/-, -, --) or numerical form (with an additional weight factor). Trade-off tables are suitable for evaluation of alternative concepts and for illustrating the evolution of the iterative design process. Based on this 'Deliver' process, one or more concepts are selected, which is then denoted as the critical point 'Solution' in the Double Diamond model.

4.2 GLOBAL DESIGN STRATEGY AND APPLICATION

Figure 58 shows the general design strategy of this dissertation project which closely follows the logic of the described Double Diamond model. While the original Double Diamond model is about the design and creation process of one tangible object solution, this dissertation designed and developed various solutions at multiple levels of the problem definition. Hence, an adapted version of the Double Diamond model is needed to provide an adequate framework of the applied design methodology in this dissertation.

This adapted version also represents two main diamonds in one line and contains the same three critical points and four stages of thinking. Notably, in our approach, the two convergence phases of the Double Diamond Model resulted in more than one outcome: the first diamond resulted in the formulation of three needs (Problem Definition) and the second diamond resulted in multiple in-vitro models (Solutions). As a result, the right-hand parts of the two diamonds in our model are flattened (which is actually a more realistic representation of a diamond than the original rhombuses from the Double Diamond model).

The first diamond (Key-Diamond I) represents one divergence-convergence loop, while the second diamond (Key-Diamond II) is a collection of many iteration loops and sub loops, because the ‘Develop and Deliver’ processes were completed at multiple levels of the problem definition (needs). This is visualized in Figure 58 by three sub-diamonds (Sub-Diamonds I, II, III), denoting the first generation of concepts developed to accommodate each identified need from Key-Diamond I. From these first generation ideas, seven concepts were selected for further iterative developments. These second generation concepts are visualized by blue rhombuses in Figure 58, with the rhombus shape representing the convergence to one single solution. For the first sub-diamond, three concepts were chosen from the second generation for further iterative developments. These third generation concepts are visualized by pink rhombuses in Figure 58. All sub-diamonds in Key-Diamond II comprised a number of iterations (ranging from one up to twenty-five), resulting in a total of 64 iteration loops across the various design solutions.

In what follows, the methodology applied in each diamond of this adapted Double Diamond framework is described in more detail.

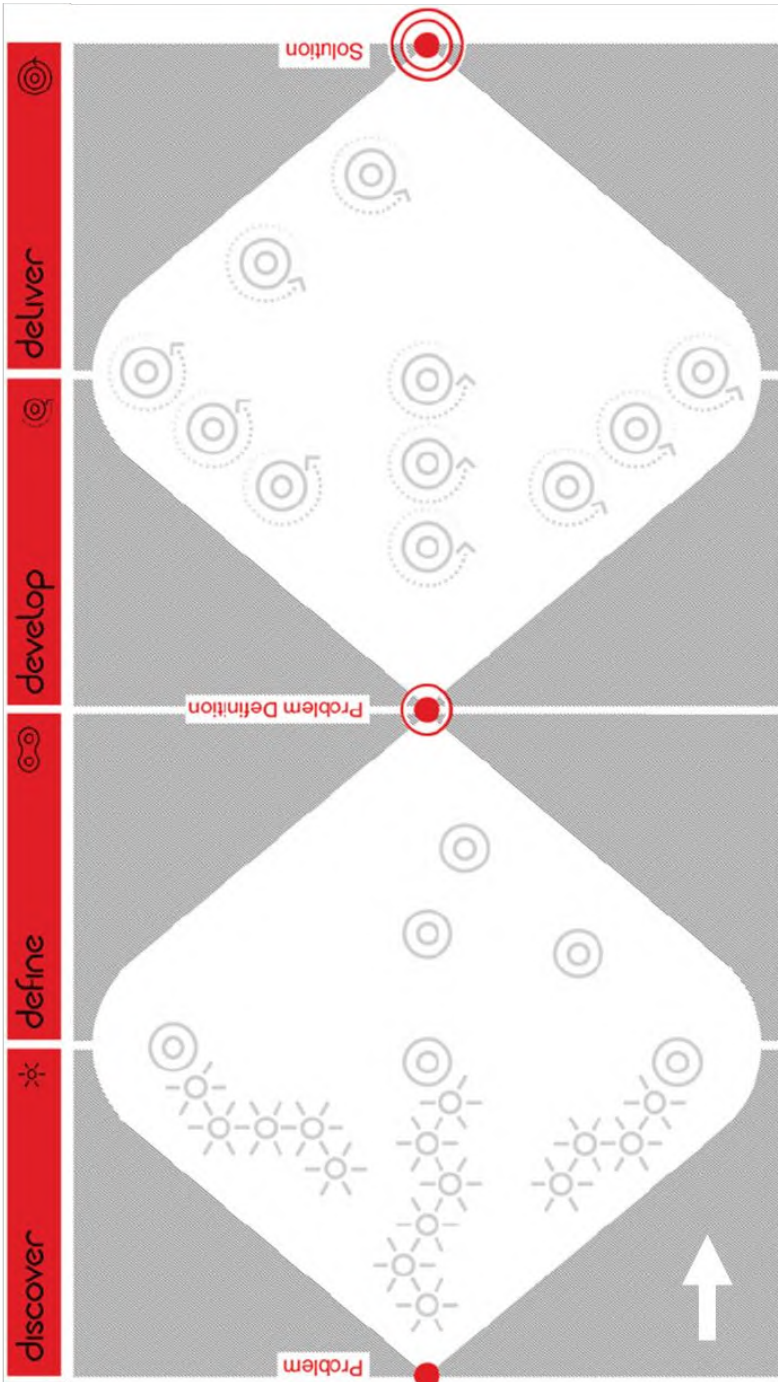


Figure 57: The Double Diamond engineering design process. The red dots represent the following critical points: ‘Problem’, ‘Problem Definition’ and ‘Solution’. Adapted from [177].

4.2.1 Key-Diamond I: Discover and Define

Applied to this dissertation, Key-Diamond I starts from the first critical point ‘Problem’. This includes the context and general need for more realistic modelling of left heart dynamics and is described in the Introduction section. Subsequently, the ‘Discover phase’ (first stage) demands an in-depth exploration of the literature and the market, to gather a divergent collection of ideas and inspiration around the ‘Problem’ from which design needs can be detected. The literature reviews of Chapters 1 and 2 serve this purpose by describing the natural left heart structure and function and by providing a state-of-the-art of cardiovascular simulator history. Next, the ‘Define’ phase (second stage) includes the critical evaluation of this ‘Discover’ phase and the distillation of the research needs and corresponding practical guidelines (PG’s). This convergence phase is extensively described in Chapter 3 and has resulted in a clear definition of three research needs and eight design requirements for new in-vitro models (summarized in Table 2). This corresponds to the second critical point ‘Problem Definition’ of the Double Diamond framework.

4.2.2 Key-Diamond II: Develop and Deliver

From this Problem Definition point on, the Key-Diamond II continues with the ‘Develop’ phase (third stage), which includes the generation of multiple in-vitro model concepts by means of iterative loops. Consequently, the ‘Deliver’ phase (fourth stage) takes place where the final in-vitro model concepts are chosen and iterated. Finally, the Double Diamond process ends with the critical ‘Solution’ points, representing the proof-of-concepts of left ventricle models LV1 – LV3, mitral valve models MV1 – MV2 and left heart models LH1 – LH2, as well as the possible future concepts (LV4 – LV5, FH1 – FH2). These concept solutions are extensively described in the following chapters of this doctoral dissertation (Chapter 5 to 12) and are also summarized in Table 8. In the next sections of this Chapter, more details are provided about the iterative processes that resulted in these concept solutions.

4.2.2.1 Sub-Diamond I: Iteration loop towards LV models

In this section, we describe the iteration loop that forms the root of all LV in-vitro models (LV1 – LV5) developed in this dissertation. It first aims to diverge to a wide range of ideas and subsequently to converge to a selection of ideas with the highest potential to become proof-of-concepts. This approach is primarily focused on the integration of contractile wall elements (PG3) – which are generally anisotropic (PG2) – in a thick wall (PG1) in order to generate natural wall deformation patterns (PG4 – PG5).

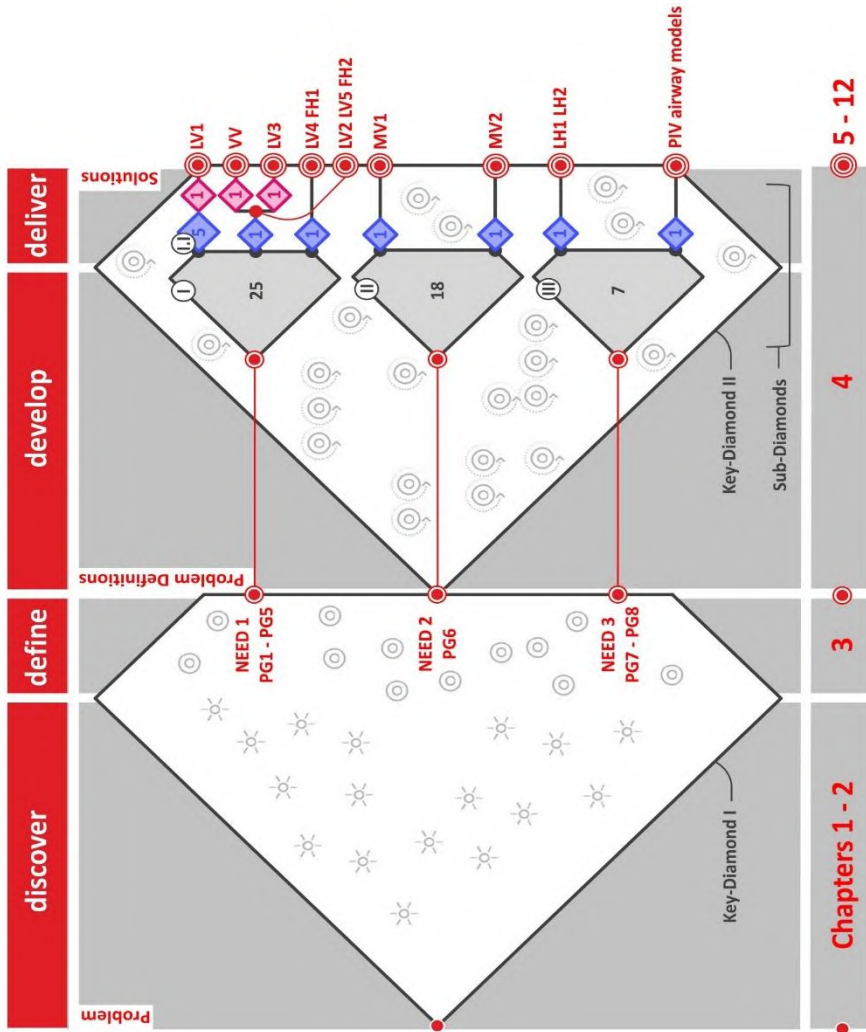


Figure 58: Global design strategy of this dissertation following the Double Diamond design logic.

This sub-design process started with a brainstorm of all kinds of contractile elements which can be assembled to eventually form an artificial LV muscle. This brainstorm (also including horizontal imagination and lateral thinking processes) resulted in twenty-five ideas by which force is induced based upon different principles, including hydraulics/pneumatics, electric and thermal systems. Subsequently, these ideas were virtually prototyped using CAD (SolidWorks, Dassault Systèmes SolidWorks Corp., Concord, MA) and subdivided into groups, as summarized in Figure 59 and Figure 60.

After this divergence phase, the convergence phase took place. This resulted in a general design decision to focus only on the hydraulic/pneumatic models. This decision is based upon the fact that in general, hydraulic models are more compatible with common measurement techniques (Ultrasound, PIV and MRI). This decision was made rather early in the design process, after consulting an expert panel of cardiovascular simulator designers as well as experts in cardiovascular mechanics and material sciences.

From this subset of hydraulic concepts, a subsequent convergence phase was applied by selecting the three most promising ideas for further development. These three models are referred to as (1) the Honeycomb model, (2) the model with Ellipsoid shaped chambers, and (3) the Stent Fiber model. All of the five LV models which are described in the current dissertation (LV1 – LV5) , covering the whole range of the proposed practical guidelines concerning more realistic LV models (PG1 – PG5), as summarized in Table 8, have their roots and/or inspiration within at least one of these three ideas.

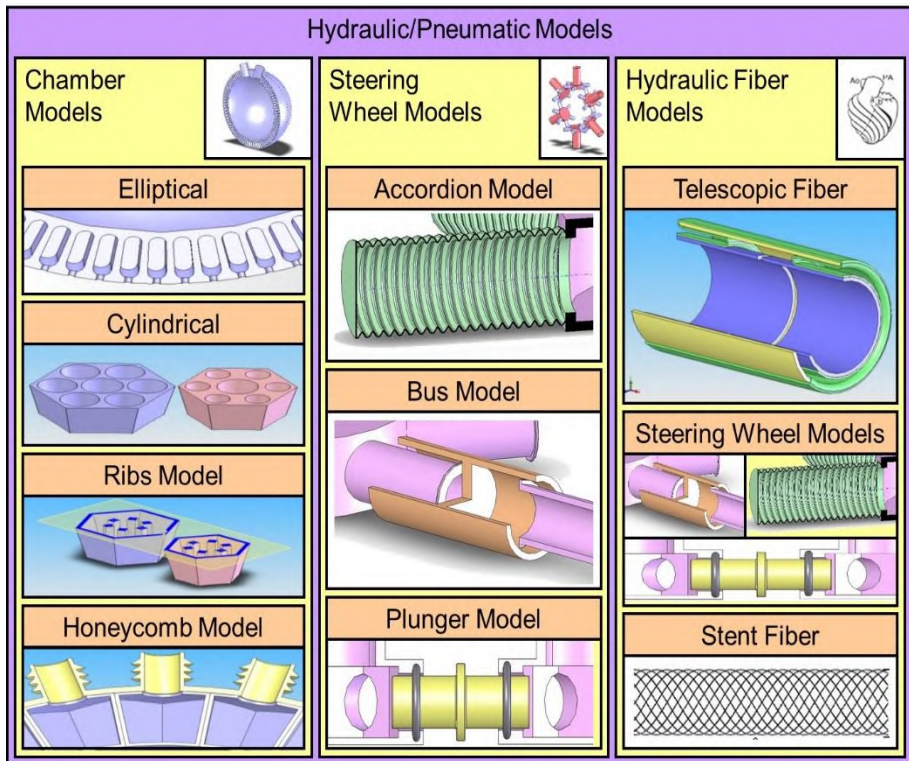


Figure 59: Hydraulic/Pneumatic Models of the general design approach as basis for the actuation mechanism of a LV model.

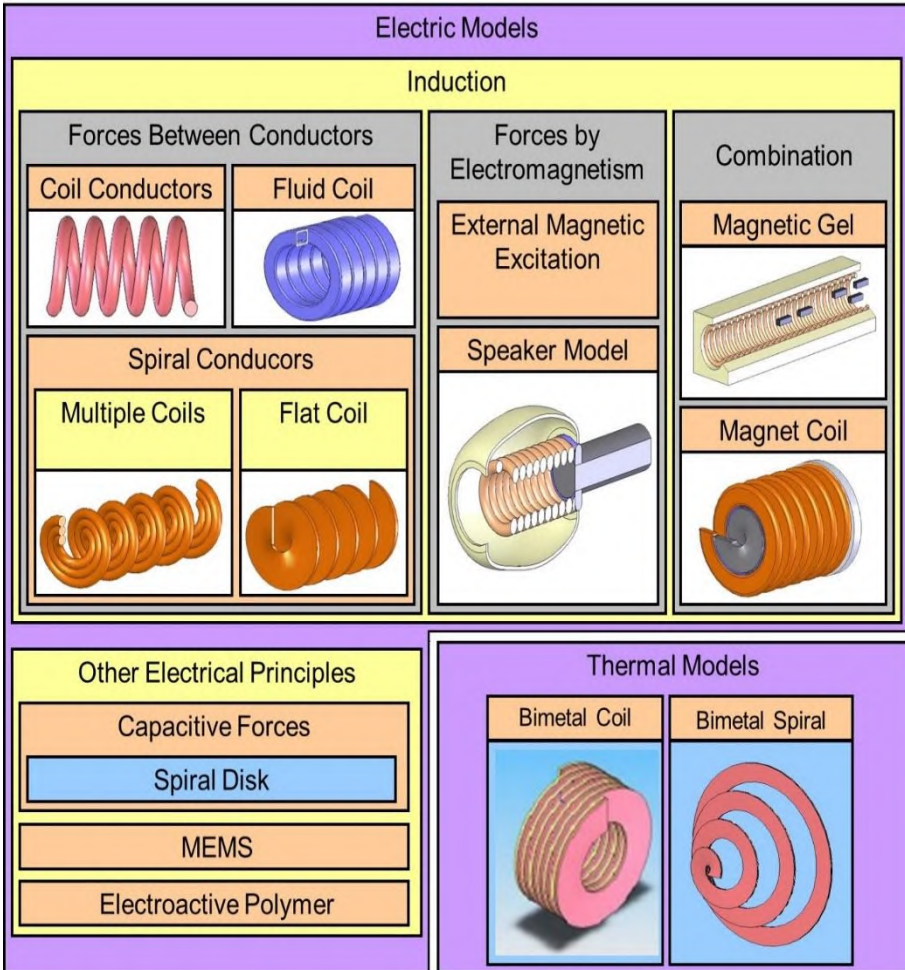


Figure 60: Electric and Thermal Models of the general design approach as basis for the actuation mechanism of a LV model.

More particularly, the first idea of the Elliptical Chambers has been directly used for the development of the active walled LV2 (presented in Chapter 6). This LV2-model is also based upon a set of parallel oriented inflatable chambers, but with the difference that this model is made of a welded polymer multiple layer sheet instead of the silicone material as proposed in this earliest Elliptical Chamber model. Further ideas based upon this original concept led to two other models, i.e., the conceptual model LV5 (described in Chapter 12) which is a PIV compatible version of LV2 by using a transparent type of polymer sheet material and the more extensively explored LV3-model

(presented in Chapter 7) which is made of an anisotropic composite material. The deformation mechanism idea behind the LV3 has been inspired by that of the LV2-model, as such that the active cell elements, which are bordered by weldments, are replaced by flexible regions, which are also bordered but now by a fiber component. These design evolutions illustrate that new divergence-convergence or ‘develop and discover’ phases can sprout from earlier design ideas and hence can produce multiple iteration loops.

The second idea which advanced the design process is the Honeycomb model, which went through an evolution process of five iterations and finally led to the design of LV1 (presented in Chapter 5). This design process is described in more detail in the following sections as it exemplifies the design methodology used throughout this dissertation work.

Finally, the third selected idea is the Stent Fiber model. This concept has been further explored while designing the conceptual models LV4 and FH1, which are described in the future directions section of Chapter 12.

4.2.2.1.1 Example: Sub-Diamond I.I: Iteration loop towards the design of LV1

As a more fine-grained illustration of the design evolution process used in this dissertation, more details are provided on the iteration loop towards the design of LV1. As noted above, the Honeycomb model idea was selected – among others – for further design development. Consequently, it went through a design evolution process of five further models, which were labeled as the ‘Inner Tire model’, the ‘16 Segment model’, the ‘PorQpine model’, the ‘Marionette model’, and eventually, the ‘Frame model’. Each of these six models was equipped with specific design characteristics. The design evolution process is illustrated by the Trade-off table in Figure 61, showing the comparison and evolution of models in function of design criteria. It includes the Honeycomb model as baseline model and identifies the Frame model as most promising model. As a result, this model was selected for physical realization, which led to the development of model LV1 (as described in Chapter 5). This design evolution was based on four specific design criteria: well-functioning in terms of controlled wall deformation (1), practical feasibility in terms of the hydraulic/pneumatic control (2) and production aspects (3), and finally, a simple and straightforward (dis)assembly during experiments (4).

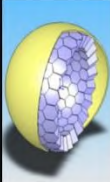
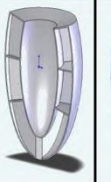
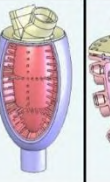
MODELS		Honey-comb Model	Inner Tire Model	Sixteen Segment Model	PorQpine Model	Marionette Model	Frame Model
		DESIGN-CRITERIA					
Working Principle		++	+/-	+	+	+	+
Practical Feasibility	Regulation	--	+	-	++	++	++
	Production	-	+	+/-	-	++	++
(Dis)Assemblage		--	--	--	--	+/-	++

Figure 61: Trade-off table shows the comparison and evolution in function of the design criteria. It starts from the Honeycomb model and designates the Frame model as most favorable model (which led to the LV1 model of Chapter 5).

In the following sections, we provide more details on the specific characteristics of each model developed in an iterative process, in order to attain a more realistic left ventricle.

The Honeycomb model

The composition of the original base model, the Honeycomb model, is shown in Figure 62. It consists of a rigid outer shell and an inner flexible wall (membrane). This wall is thick-walled and is made of hexagon-shaped chambers, so that its structure looks similar to that of a honeycomb. By means of over-pressure within in the chambers, the inner membrane becomes compressed. As a result, the ventricular cavity changes its shape and more particularly, this implies a reduction in volume of the ventricular cavity. In contrast with currently thin walled LV models (see Chapters 2 and 3), this model would allow the change in shape of the inner membrane in a controlled manner, because the segments, from which the membrane is built up, can be individually controlled. The higher the resolution of this segmentation, the more accurate the achieved control of the shape change of the inner membrane would be. In this Honeycomb concept, we realized the control of the inner membrane by dividing the ventricular wall in about 100 chambers, which are individually driven by compressed fluid/air. The control of these individual chambers, however, is large, complex and expensive, since it requires a

separate control valve for each single chamber. Practically, this is not feasible, so we looked for more simple models such as the Inner Tire model, which is the first iteration model.

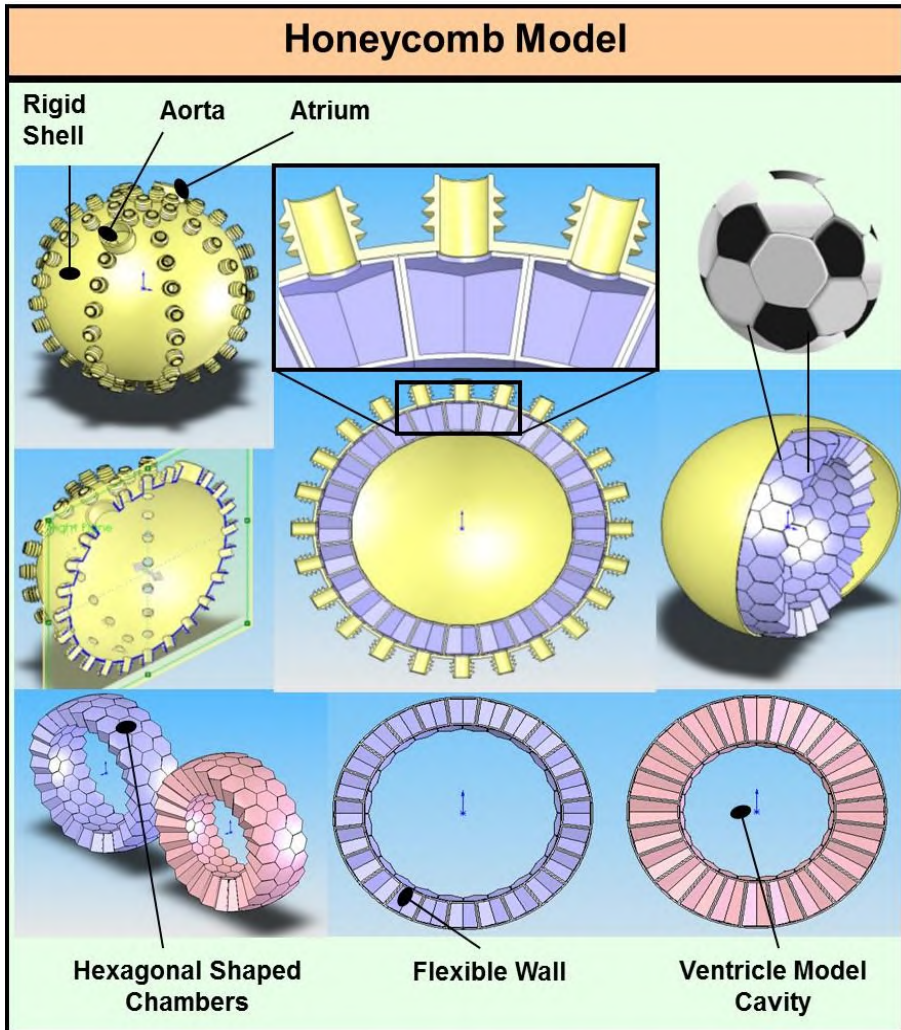


Figure 62: The Honeycomb model.

The Inner Tire model

Figure 63 shows the second model, the Inner Tire model, which is composed out of a rigid shell, similar to the Honeycomb model, with an ellipsoid cavity shape that more closely resembles the natural LV than the spherical shape applied in the Honeycomb model. The model is equipped with three toroid shaped inner cavities (inner tubes) which can be controlled with only three valves. Therefore, this Inner Tire model involves a much simpler control system than the previous model that needed about 100 valves. Yet, on the other hand, wall control is drastically diminished in this model which is a disadvantage that needs to be overcome. This brings us to the next model, the Sixteen Segment model, which is the second iteration model.

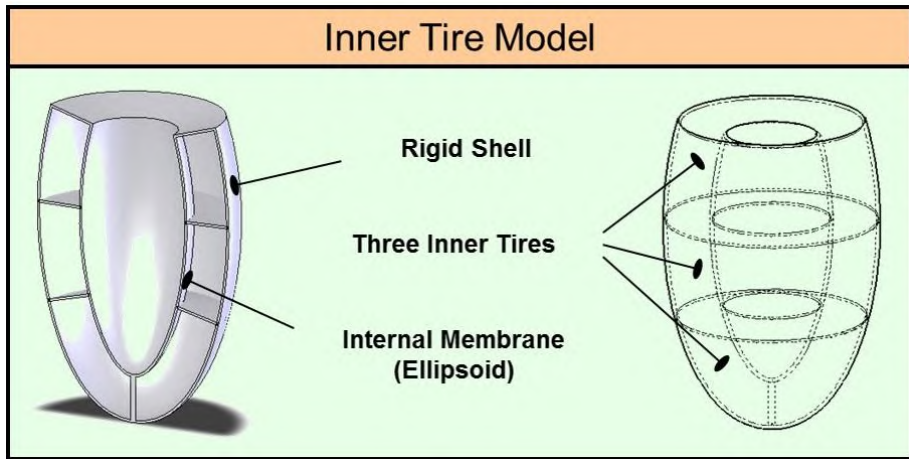


Figure 63: The Inner Tire model.

The Sixteen Segment model

Figure 64 shows the third model, the Sixteen Segment model. In order to report the location of pathology in the left ventricle, cardiologists have divided the ventricular wall in 16 segments [178]. We opted to implement this classification into the chamber geometry of this new model. The control then consists of 16 valves, which is still far more feasible than the 100 valves of the original Honeycomb model. Nevertheless, the number of valve controls remains a thorny issue. Although this number of valves can be reduced to 3 (Inner Tire model) or 16 (Sixteen Segment model), we reckoned that the control by one single control valve would be much easier and more cost efficient. The challenge is thus to develop a model which is controlled by only one control valve, while keeping the ability to control the shape change of the inner membrane. The solution to this challenge was conceived in the following model, the PorQpine model, which is the third iteration model.

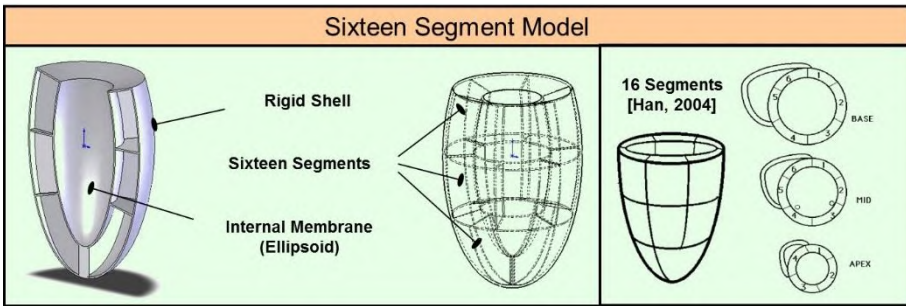


Figure 64: The Sixteen Segment model.

The PorQpine model

Figure 65 presents the fourth model, which was labeled as the PorQpine model as it is reminiscent of the appearance of a porcupine by the numerous bars which are spread over the inner membrane surface. In this model, the ribs of the individual chambers from the Sixteen Segment model have been replaced by sticks because of two reasons. First, all segments (chambers in the former models) are now connected to each other and the compressed fluid/air can penetrate to all segments. As a consequence, this model contains only one chamber that requires only one single control valve, which simplifies the control system and lowers the cost, while still keeping control over the 16 segments. The second reason is that the firming action of the separate sticks is less than the firming action of the ribs in all previous chamber models. This enhances the control over the LV model wall deformation. Nonetheless, this PorQpine design is quite complex in terms of practical feasibility. Hence, the next challenge is to design a model that, in addition to the controlled deformation and control through a single control valve, enhances the practical feasibility towards materializing the model and to allow straightforward (dis)assemblies during experiments. A solution is found in the next model, the Marionette model, which is the fourth iteration model.

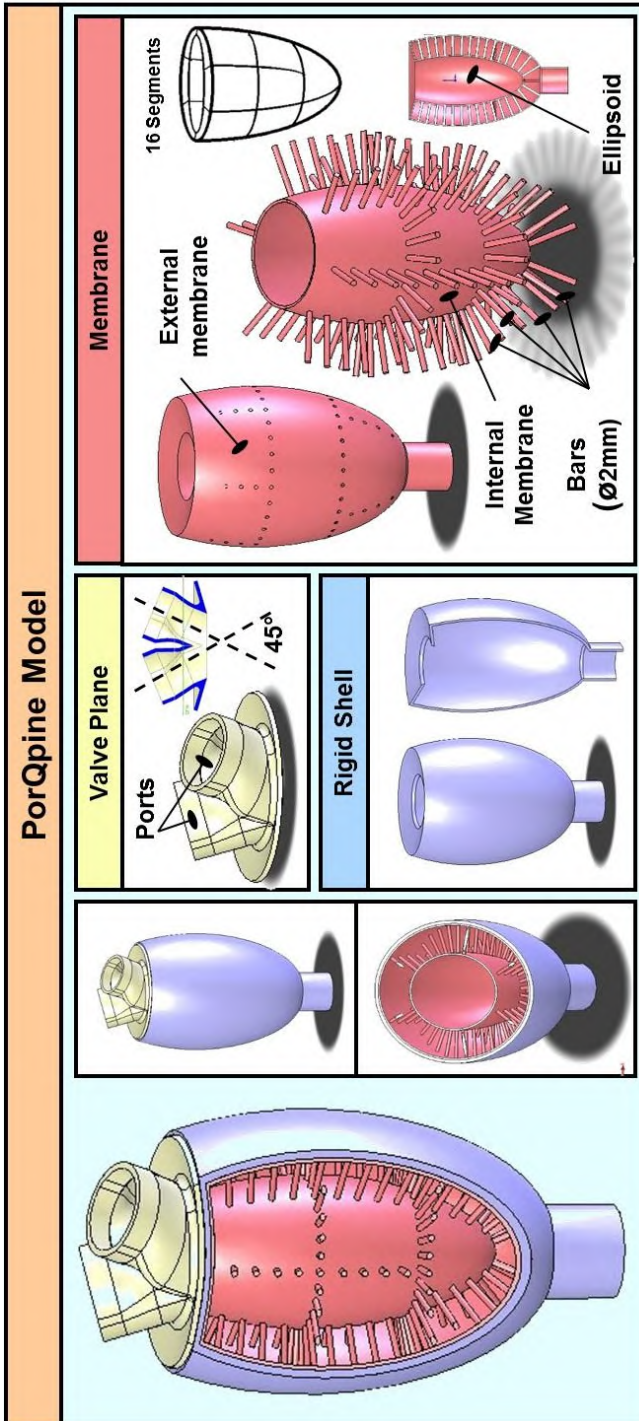


Figure 65: The PorQpine model.

The Marionette model

Figure 66 depicts the fifth model, which was labeled the Marionette model. In contrast to the PorQpine model which is not (de)mountable, this new model is modularly designed. This model owes its name to the operating principle, as it resembles that of a marionette (movement of the puppet controlled by strings). In this model, the control of movement also occurs by means of cords, or more accurately, flexible rods. In this model, the membrane portion of the PorQpine model is replaced by a separate inner membrane. Individual flexible rods serve as the connection between the membrane and the rigid outer shell. A strong and simple connection of the rods is possible as a result of the integrated anchor points, which are present both in the rigid shell and in the membrane. The latter are called buttons. The openings in the rigid shell which have been created in front of the anchor points, are to be sealed by end caps which are either pushed in a bus or screwed. These buses are integrated or screwed into the rigid shell. The actual seal between a bus and a closure cap is carried out by means of an O-ring. In this design, the ventricular cavity is closed at the top by screwing a valve plane in which mechanical heart valves can be mounted. As such, the modular design greatly simplifies the practical feasibility as it is largely confined to routine construction with the aid of 3D printing techniques such as SLS and SLA. However, a complication could occur in the sealing of the compressed fluid/air at the level of the 31 buses, which makes chance of leakage relatively high. Also, the assembly and disassembly of these rods will be a time-consuming occupation. So we have to continue looking for a model that is easier to (dis)assembly during experiments. This brings up the next model, the Frame model, which is the final iteration model in this design evolution process.

The Frame model

Figure 67 presents the sixth and final model, the Frame model, which was eventually chosen for practical realization (LV1, Chapter 5). Whereas in the previous Marionette model, the rigid shell provides strength and stability to the anchor, we considered that the function of this one part could be better fulfilled by two separate pieces. In this model, we replaced the rigid shell with integrated anchors and buses, by two components, i.e., an simplified rigid shell and an anchor frame, from which the label Frame model is derived. This approach offers the following advantages. First, the mounting of the rods is much simpler and can be done much faster. Whereas in the Marionette model, the mounting of the rods occurs through the small openings in the rigid shell, the assembly in this model is simpler because we can move our fingers freely through the anchor frame. Second, there is less risk of leakage. While the

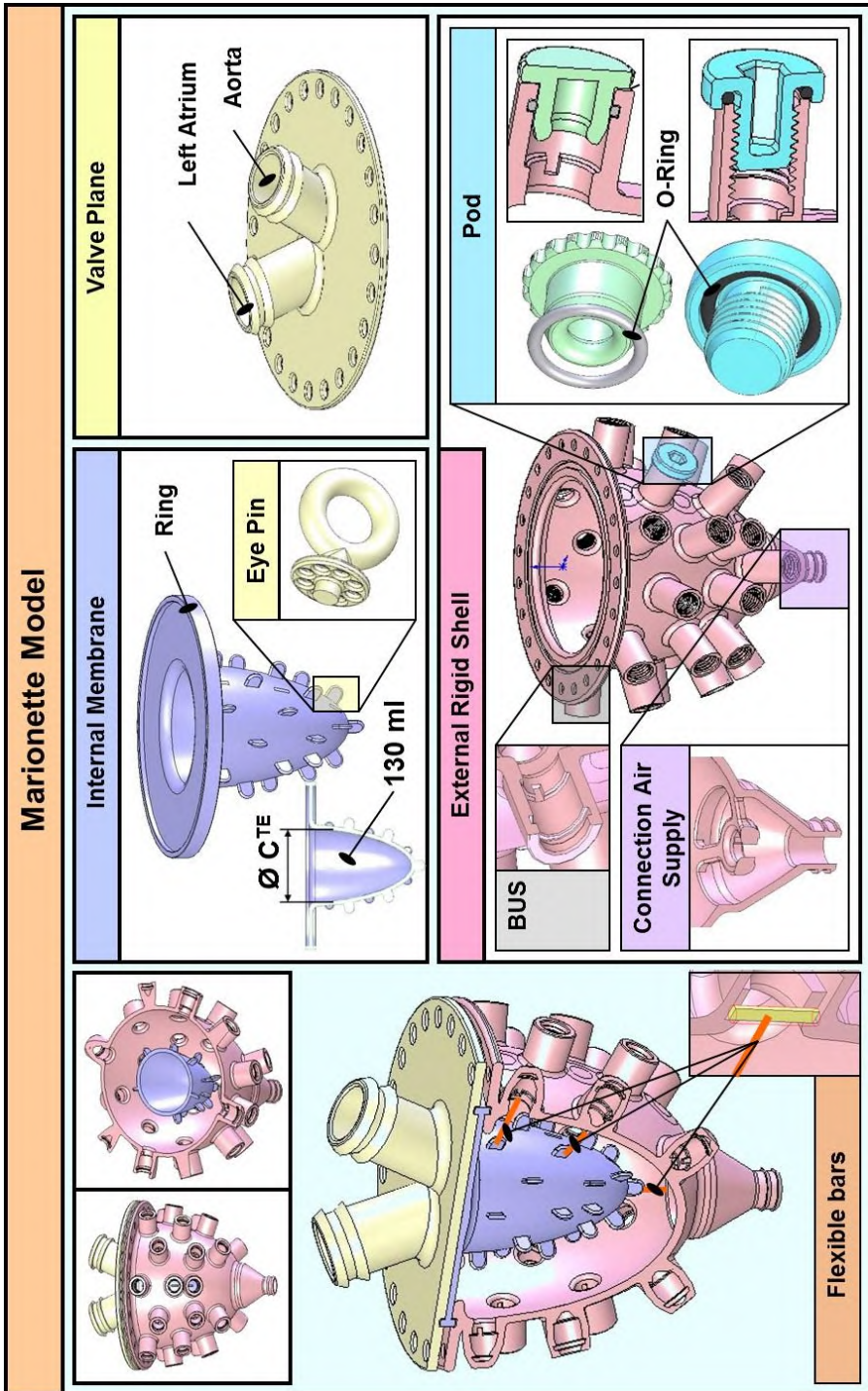


Figure 66: The Marionette model.

Marionette model needed to be sealed at the level of about 31 buses, this new model requires the sealing by means of only one O-ring which is located between the valve plane and the shell. Finally, if there is a need to change the anchor points geometry during experiments, one can rebuild the frame which is less expensive than rebuilding the entire rigid shell of the Marionette model.

In conclusion, the iterative evolution of this sub-design process transformed the initial Honeycomb model into the Frame model, which scores the highest in terms of the proposed design criteria. This model was then chosen to be physically prototyped as LV1 and was implemented in experiments. This realization process and experimental results are extensively described in Chapter 5.

4.2.2.2 Sub-Diamond II: Iteration loop towards MV models

This section describes the iteration loop that forms the basis for the development of the mitral valve models MV1 – MV2. This design process is primarily based upon a hands-on approach. The process started with a logical choice to imitate the anatomical material composition and properties of the biological mitral leaflets. From this choice, a hands-on approach was applied by varying three parameters – first, by means of 2D substrates, and later on, by means of the actual 3D mitral valve geometry. These parameters were different types of silicone and fiber materials (1) and thickness (2), and different fiber structures (such as knitted and woven fiber patterns) (3). In addition, we varied several production techniques (4), such as vacuum casting (using a silicone or 3D printed mold) and dip coating of a kernel. Hereby, three different kernel materials were used in function of smoothness and the non-sticking properties, Acrylate via 3D printed (1), polyurethane via vacuum casting (2) and aluminum via 5-axis milling (3). The total number of iterations during this hands-on approach was about eighteen before we obtained a functional in-vitro mitral valve model.

The first required criterion in this case is the ability of the valve model to combine a firm leaflet structure to withstand high blood pressures with leaflet bend flexibility to diminish transvalvular flow resistance (PG6a). These requirements were preliminary validated by tactile and visual inspection and by leakage and pressure tests after mounting the valve models into a custom made valve housing. This design process formed the basis for the development of the valves MV1 and MV2 (Chapter 8). The second set of requirements are the practical guidelines related to the implementation of anatomical structures (PG6b – PG6e) into the left heart models LH1 and LH2 (Chapters 10 and 11).

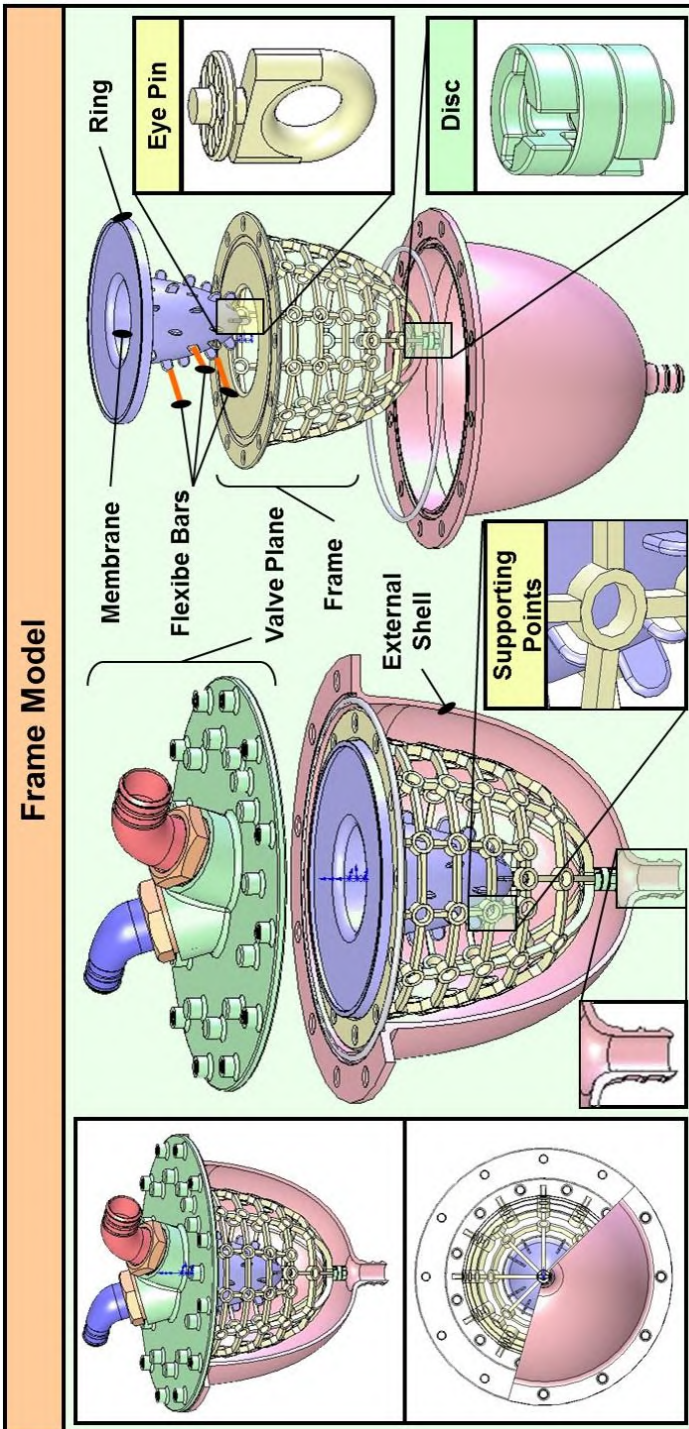


Figure 67: The Frame model (LVI of Chapter 5).

4.2.2.3 *Sub-Diamond III: Iteration loop towards LH models*

In this section, we describe the iteration loop that forms the origin of the left heart models. It is based on the production process development for manufacturing thin walled flexible in-vitro models with high geometrical complexity and an accuracy which is as good as possible. During this design process, seven methods are developed based on different kinds of sacrificial cores, which can be removed after the building process of the in-vitro model. This design process included seven iterations which can be categorized into four methods according to how the core is sacrificed. The first method is based on the melting of a massive core made by vacuum casting of wax (Green Casting Wax, Kerr Ltd, Peterborough, UK, melting point 75°C) (1) and a low melt fusible metal alloy (Bismuth Based Ingot 203, RotoMetals, CA, melting point 95 °C) (2). The second method includes the crushing of a hollow core made by rotational molding of wax (3), plaster (4) and polyurethane (5). Then, the third method is based on the washing out of a water solvable (hollow) core made of sugar glass (brittle transparent form of sugar often used to simulate glass in movies and for sugar sculptures) (6), and finally, the fourth method comprises the mechanical fragmentation of a thin-walled 3D printed core (7).

After this divergence phase, a convergence phase took place in which two methods were selected for application in this dissertation. The first is the hollow wax core approach and is applied for the realization of LH1 (Chapter 10) and the upper half of LH2 (Chapter 11). This approach allowed the meeting of the practical guidelines PG2, PG4a, PG4b, PG5 – PG7 in one model. This selection is based upon three criteria: (1) its minimal damage to the actual model during the removal of the core, (2) the straightforward fragmentation of the core, and (3) its effortful way of producing a series of cores that was needed to optimize the production process of the monolithic LH1.

The second selected method is the one that is based upon the mechanical fragmentation of a thin-walled 3D printed core. The selection criterion in this case is the accuracy due to skipping intermediate steps during the production process by direct 3D printing. This approach is applied for the creation of the highly detailed in-vitro models of the upper airways as shown in Figure 111, and therefore proposed as a promising approach to enhance geometrical complexity and accuracy of the next generation of in-vitro models, as described in Chapter 10.

4.3 CONCLUSION

This doctoral dissertation is based upon a diverging-converging type of engineering design strategy and closely follows the logic of the Double Diamond design process, proposed by the British Design Council. In a first diverging-convergence phase, clear research needs were defined based upon a broad literature review. In a second diverging-convergence phase, creative ideas were catalyzed, selected and developed in response to the identified research needs in order to deliver proper solutions.

This chapter provides the general design strategy and goes deeper into the design roots behind all in-vitro models which are described in the following chapters of this dissertation. It demonstrates that every single concept has been developed within the broader context of a structured design methodology and is based upon a wide range of ideas and numerous hands-on experiments.

Part II

In-vitro modelling of the left ventricular muscle

Modelling the left ventricular muscle by a thick wall

This chapter is based on “Modelling the left ventricle using rapid prototyping techniques”, as published in the IRBM journal (2013) by Van Der Smissen B., Claessens T., Verdonck P., Van Ransbeeck P., and Segers P. [179].

It describes the first of the three new left ventricular models, namely LV1. In this model, the natural left ventricular muscular wall is modelled by a thick-walled approach instead of a thin-walled membrane. A render of this model is shown in Figure 68 [180].

5.1 INTRODUCTION

Heart failure is an increasingly important health problem in most developed countries [181]. Research of biomechanical processes in congestive heart failure primarily concentrates on the assessment of blood flow in the left ventricle. However, at present, the focus shifts towards the role of the deformation of the ventricular wall in the interaction with the blood flow. In previous experimental investigations wall deformation was studied by means of thin-walled passive experimental models, consisting of a silicon membrane in a closed box that is passively squeezed by an externally connected piston pump. Experimental models relying upon this deformation mechanism have been used to study the influence of the different determinants of left heart

performance on transmitral flow [95], to test the hydrodynamic performance of heart valves [182-185] or to investigate LV diastolic filling using color M-mode Doppler echocardiography [186]. Although the pump function of these models has already been well established, the membrane deformation remains unpredictable and the effect of muscle contraction - and hence natural wall deformation - cannot be simulated.

In this study, we propose a new design of an experimental hydraulic LV model (LV1) in which LV wall deformation can be controlled. We built this model by a combination of rapid prototyping techniques and tested it to demonstrate its wall deformation and pump function by measuring aortic flow and ventricular pressure. This described model is the result of an optimization process in which we gradually improved previous designs based on different design criteria, such as deformation mechanism, practical feasibility and the ease of (dis)assemble. However, in this chapter, we exclusively describe the design and composition of the final model that was also physically realized.

5.2 PHYSIOLOGICAL BACKGROUND

As described in Chapter 1, the heart is a four-chambered, muscular organ that continuously pumps blood through the body's extensive network of arteries and veins. The LV can be considered as its most important and powerful pumping chamber, and is therefore probably its most frequently studied chamber. The LV wall consists of three layers: the epicardium, the myocardium, and the endocardium. The endocardium is the thin inner layer of endothelium while the epicardium is an external visceral layer covering the heart. The myocardium, the middle layer, forms the bulk of the LV and is the layer that actually takes care of contraction. It consists mainly of cardiac muscle fibers embedded in connective tissue structure. The myocardium consists of interweaving bundles of cardiac muscle fibers spirally arranged around the circumference of the heart. As a result of this anatomical architecture and of the timing and sequence of electrical excitation, during contraction the LV deforms as follows: (a) the diameter of the LV decreases while (b) the base-apex distance decreases (c) in a rotating manner [43]. As such, global ventricular wall deformation can be basically described in terms of (a) circumferential deformation, (b) longitudinal deformation, and (c) torsion.



Figure 68: Render of the thick-walled left ventricular model LV1 [180].

5.3 CONTRACTION PRINCIPLE

Previous experimental investigations studied wall deformation by means of thin-walled passive experimental models. These models consist of a silicone membrane in a closed box. By using a piston pump, water or pressurized air is applied within the closed box and the internal membrane compresses which consequently results in LV volume reduction. Yet, although it is well demonstrated that these passive models provide adequate pump function, the unpredictability of the membrane deformation prohibits the simulation of the effect of muscle contraction and hence natural wall deformation.

In contrast to this thin-walled conception of the LV, we conceived the LV as a thick-walled hydraulic model which is composed of an inner thin-walled membrane, flexible bars which we assumed to control the wall deformation and an exterior shell. When pressurized air is applied by a piston pump within the thick wall, the internal membrane is compressed and the flexible bars start to stretch. In this way, wall deformation can be controlled while LV volume is reduced.

These three layers of the thick wall can be considered as analogues of the human heart with the thin membrane representing the endocardium, the flexible bars connecting the membrane with a stiff supporting frame representing the middle layer that actually accounts for ventricular contraction, and the exterior shell covering the latter parts representing the epicardium which is the external visceral layer of the heart.

As such, the degree of control over the deformation of the inner membrane is determined by the tension and number of flexible bars arranged over the surface of the membrane. Also, the higher this number, the more accurate the control of the wall deformation will be. In our model, we provided that these bars can be stretched or loosened by means of modular discs in order to control the wall deformation more efficiently. We chose to use 31 bars which represent the corners of the 16 segments that are often used in clinical echocardiography to locate LV pathologies [187].

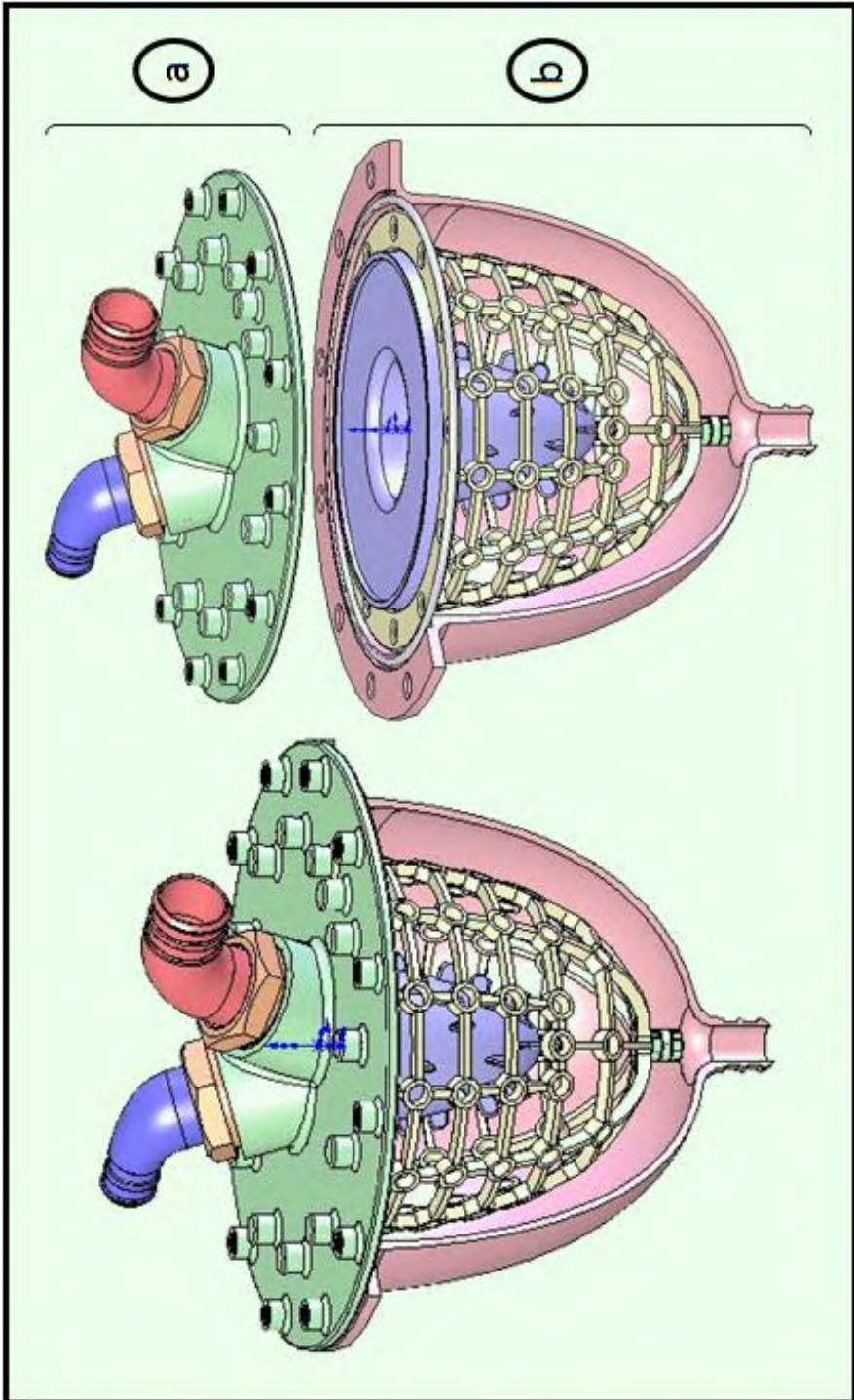


Figure 69: Our model consists of two main parts: (a) a valve plane and (b) a thick wall.

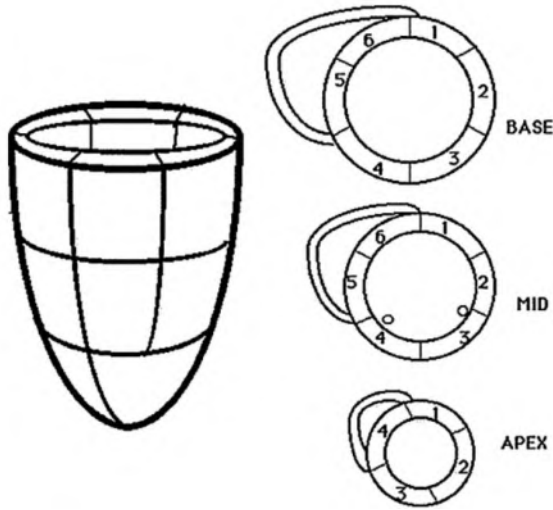


Figure 70: Illustrative drawing of a 16-segment left ventricle model representing the 16 segments, which is often used in echocardiography. The model consists of three slices: (1) the basal and (2) the mid-ventricular slices which are uniformly divided into six segments and (3) the apical slice which is split into four equal segments. Reproduced from Han, 2004 [15].

5.4 DESIGN AND COMPOSITION OF THE MODEL

This contraction principle was further optimized in terms of practical feasibility and resulted in the model shown in Figure 69. This model was modularly designed in order to facilitate experiments and consists of two main parts: a thick wall (Figure 69 b) and a valve plane (Figure 69 a). The thick wall takes care of the ventricular contraction while the valve plane contains the two (mechanical) heart valves.

5.4.1 Thick wall

As depicted in more detail in Figure 71, the thick wall consists of four components: the thin flexible membrane (Figure 71 a), the flexible bars (Figure 71 b), the stiff supporting frame (Figure 71 c) and the exterior shell (Figure 71 e).

First, the thin flexible (E-modulus of 5 MPa) membrane (Figure 71 a) is the inner layer of the thick wall and we modelled it as a truncated ellipsoid with an end diastolic volume of 130 ml, base-apex length of 85 mm, short axis diameter of 45 mm and an overall wall thickness of 3 mm. We also provided the membrane with a sealing ring (Figure 71 f) to prevent leakage between the thick wall and the LV cavity.

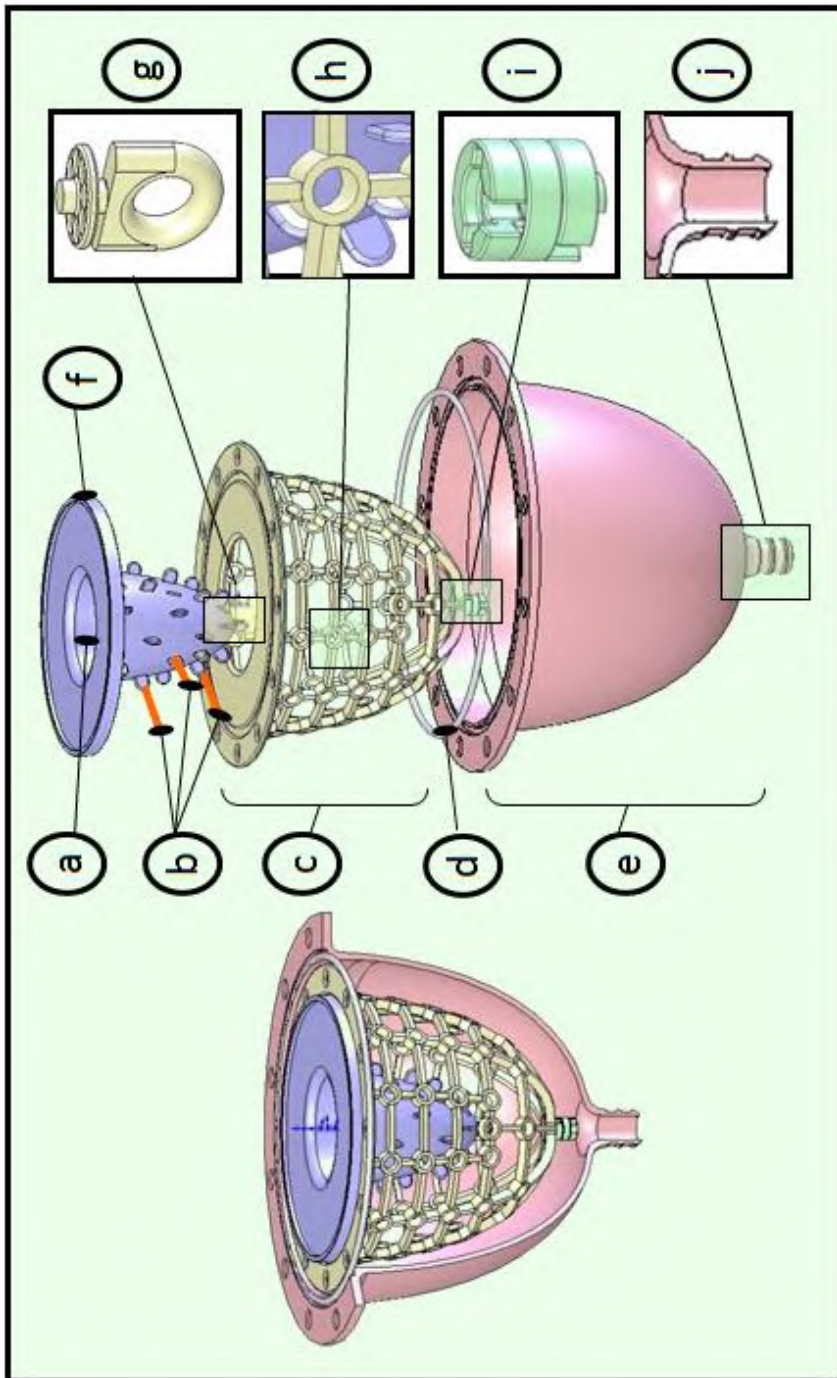


Figure 71: The ventricular part consists of (a) a thin membrane including (f) a sealing ring, (b) flexible bars, (c) a supporting frame, (d) an O-ring, (e) an external shell, (g) eye pins, (h) supporting points, (i) modular discs and (j) connection to the piston pump.

Secondly, the region with the flexible bars (Figure 71 b) connecting the inner and outer layer of the thick wall can be assumed as the middle layer. Importantly, these bars need to be flexible enough to allow deformation of the membrane and stiff enough to exert control over the wall deformation. Empirically, we found the following parameters appropriate to account for these requirements in our model: rubber material (E-modulus of approximately 5MPa) and a cross-section of 4 mm². The flexible bars are connected to the supporting points in the membrane and to the supporting frame: the eye pins (Figure 71 g) and the modular discs (Figure 71 i) respectively. We designed these eye pins (depicted in more detail in Figure 73) with an eye (Figure 73 a) to connect the flexible bars, a perforated flange (Figure 73 d) to assure embedding in a tight connection with the flexible thin membrane, a centering pin (Figure 73 e) to provide a constant membrane thickness, and guiding planes (Figure 73 b) to align them perpendicularly to the membrane (see § 5.5). The modular discs (Figure 74) were designed with a hole (Figure 74 d) and a cut-away (Figure 74 a) in which a transverse spill (Figure 76 c) fits in order to allow easy connection using different types of flexible bars, a cut-away (Figure 74 c) to facilitate tightening and loosening of the flexible bars and an adjusting ring (Figure 74 b) to fit them together (Figure 74 e).

As illustrated in Figure 71 (and in Figure 75 and Figure 76), the third component, the supporting frame (Figure 71 c), is located at the outer side of the middle layer of the thick wall. It provides not only support to the supporting points (Figure 71 h), but also enables visual inspection of the wall deformation as well as an easy assemblage of the flexible bars. We designed its geometry with a constant offset (25 mm) to the membrane. It consists of a wide-meshed structure (beam height and width of 3 and 5 mm respectively) and supporting points which are oriented perpendicular to the eye pins of the membrane. As such, the flexible bars have a constant length and are perpendicularly oriented. In this way, a perpendicular control can be exerted to the membrane surface.

Finally, the exterior shell (Figure 71 e) functions as the exterior box in which pressurized air is applied by a piston pump, as it is used in previous investigations. We designed it to consist of a transparent material to enable visual inspection. Similar to the geometry of the supporting frame, the exterior shell is designed with a constant offset from the membrane in order to facilitate adding modular discs. We opted to supply water or pressurized air at the apex level (Figure 71 j) to simplify the valve plane. Leakage of the pressurized air is prevented using a sealing ring (Figure 71 d) between the exterior shell and the valve plane.

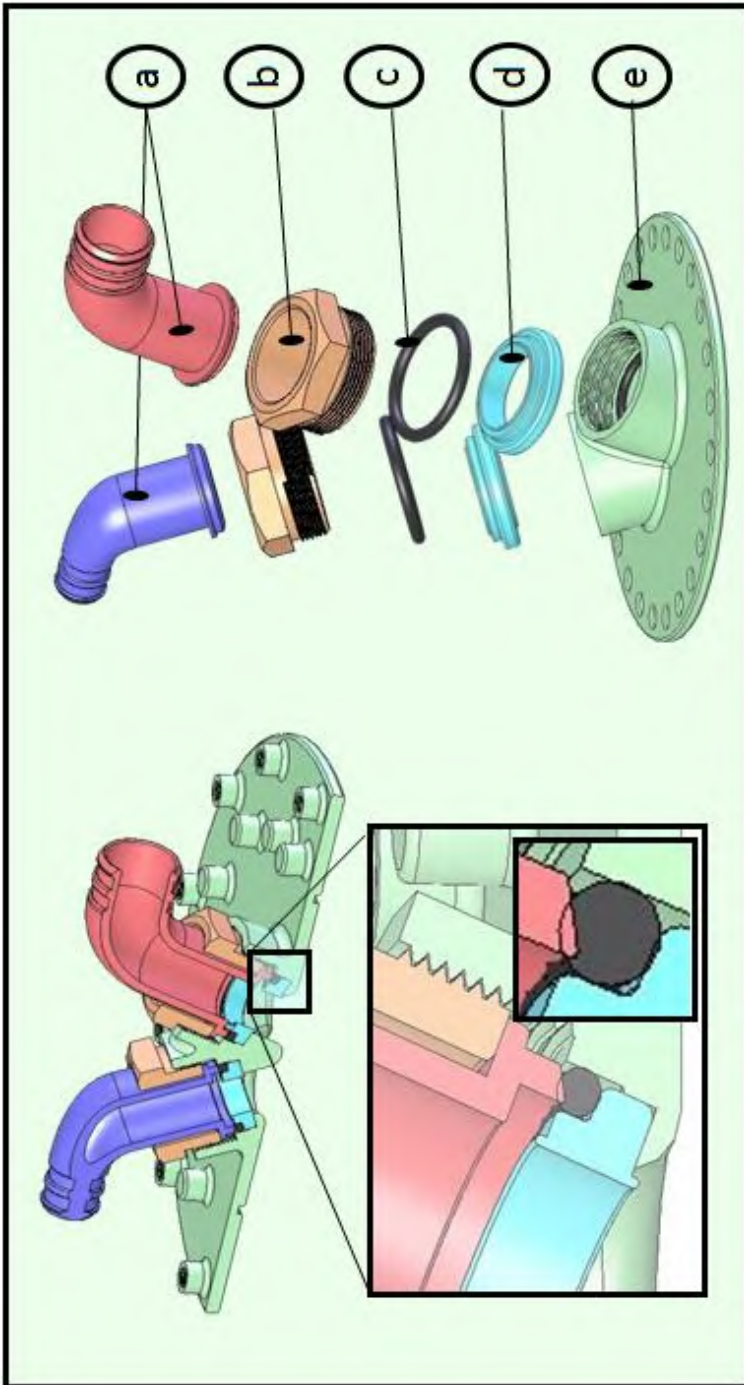


Figure 72: The valve plane contains (e) a valve plane, (a) two gates and positions, (d) two mechanical valves. Leakage between valves and valve plane is prevented by using (c) O-rings which are pressed by (b) a compression nut.

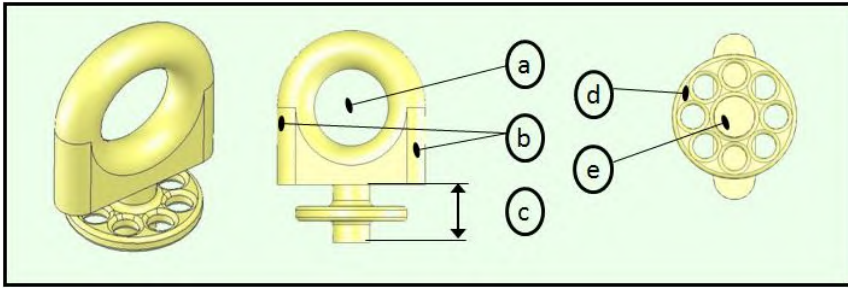


Figure 73: The eye pins are designed with (a) an eye to connect the flexible bars, (d) a perforated flange to assure embedding in a tight connection with the flexible thin membrane, (e) a centering pin to provide (c) a constant membrane thickness of 3mm and (b) guiding planes to align them perpendicular to the membrane.

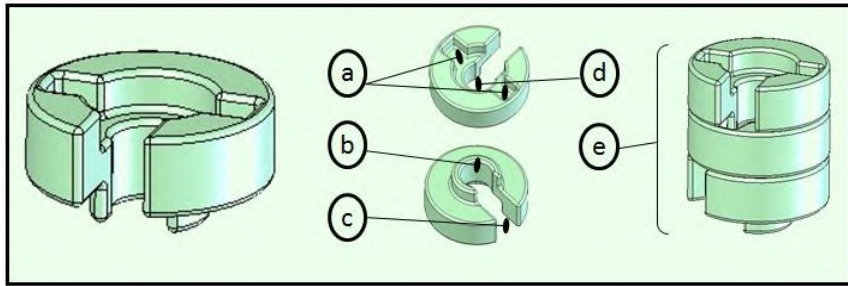


Figure 74: The modular discs are designed with (d) a hole and (a) a cut-away in which a transverse spill (Figure 76) fits to allow easy connection using different types of flexible bars, (c) a cut-away to facilitate tightening and loosening of the flexible bars and (b) an adjusting ring to fit them together (e).

5.4.2 Valve plane

This assembly contains the valve plane itself (Figure 72 and Figure 77) and positions and seals two mechanical valves (Figure 72 d and Figure 77 b and g): the mitral and the aortic valve. The aortic and mitral valves were angled at 135° and leakage between the valve plane and the valves was prevented using an O-ring (Figure 72 c and Figure 77 f) that is pressed by a compression nut (M42 with a pitch of 1.5 mm) (Figure 72 b and Figure 77 c and e).

The valves are positioned as closely as possible to the valve plane to minimize the non-contractile space. However, the limiting factor is the minimal wall thickness at both valves (2 mm in our model). In order to position the valves even closer to the valve plane, we shaped the two canals as following: starting from a crescent-shaped and gradually ending in a circular-shaped cross-section at the level of the valves, as such, keeping the surface area constant.

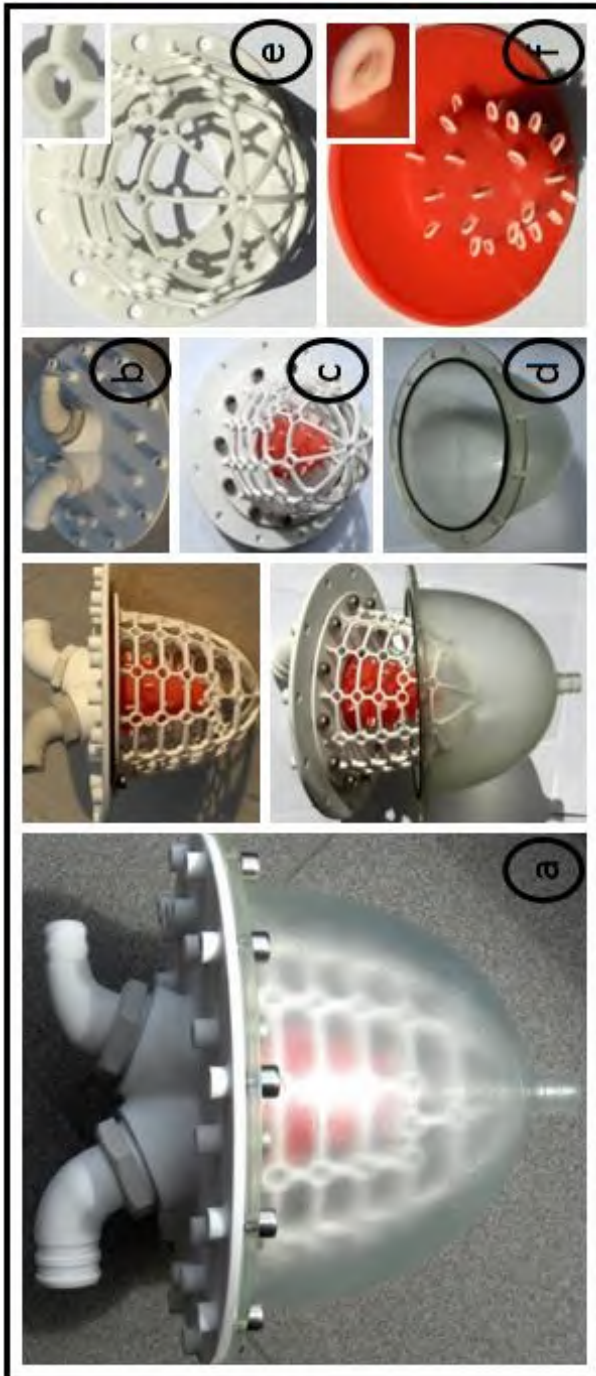


Figure 75: The practical realization of (a) our model, (b) the valve plane, (c) an assembly of the supporting frame and membrane without the flexible bars, (d) the external shell, (e) the supporting frame and (f) the membrane containing the embedded eye pins.

5.5 RAPID PROTOTYPING MATERIALS AND METHODS

Figure 75 shows the final realization of our model based on a combination of the following Rapid Prototyping Techniques: selective laser sintering (SLS), stereo lithography apparatus (SLA) and vacuum casting by using a silicone mold. As these techniques apply different materials, the final model is made of polyamide powder, epoxy and a 2-component polyurethane respectively.

The external shell (Figure 75 d) was built of epoxy using the SLA technique. This technique assures the required transparent and solid properties and hence allows visual inspection while providing enough strength to deal with the pressurized air. In order realize this optical transparency, the shell surface needs to be smoothened by a polishing treatment after the rapid prototyping techniques building process. This smoothing procedure was intended to be done at the design state of our model, but ultimately, as an alternative, we opted to remove the external shell to make even better visualizations, as depicted in Figure 79. However, the latter configuration needs a modification of the validation set up: the pressure gradient, which causes wall deformation, will be realized in this new configuration by applying pressurized air at the inside of the membrane instead of applying vacuum pressure at the outside of the membrane which is valid for the first configuration. Since wall deformation is the result of transmembrane pressure gradient, the direction in which the pressure gradient is applied does neither affect the final wall deformation, nor influence the controlling function of the flexible sticks. For that reason, we can assume that this modified configuration will lead to the same deformation, and therefore we opted this to obtain an improved visualization of the wall deformation.

In contrast to the external shell, the modular discs (Figure 76 c), the supporting frame (Figure 75 e), the valve plane (Figure 77) and the eye pins (Figure 75 f) were built of polyamide (PA) because of the materials tough properties.

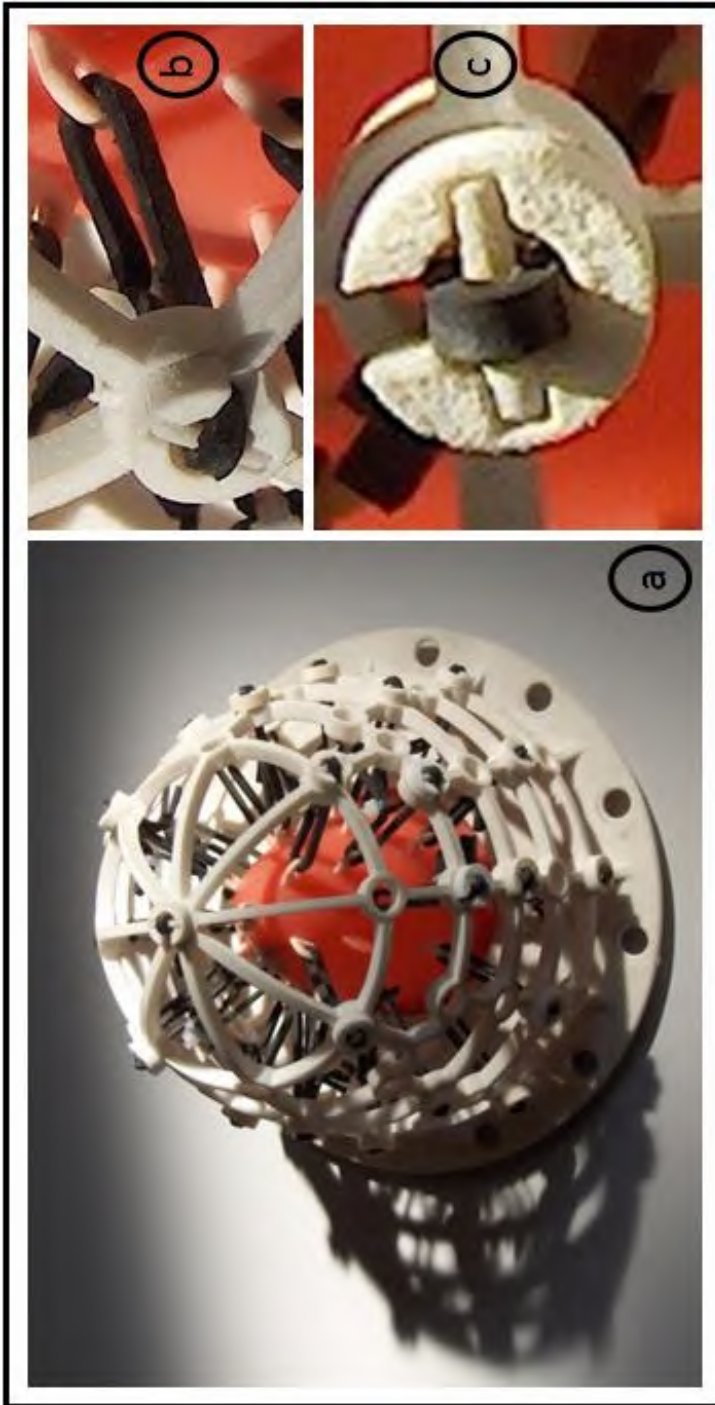


Figure 76: The practical realization of (b) the flexible bars (a) connecting the membrane and the supporting frame by the use of the eye pins and (c) a modular disc.

Whereas these parts could be built directly by RPT-machines, the membrane (Figure 75 f) had to be built in several steps due to its complex practical guidelines: it needs to be flexible (1), the stiff eye pins need to be firmly attached (2) and precisely positioned to it (3), and its wall thickness needs to be consistently constant (4) to avoid irregular wall deformation. The first technique we applied to realize this membrane is vacuum casting: primarily, the membrane was built of epoxy using the SLA technique. Then, this original shape was utilized to produce a silicone mold, and finally, a two-component-polyurethane was vacuum-casted into the silicone mold. The second technique we employed is the insert-technique: the original shape of the membrane was completed with projecting parts that are shaped like the eye pins. When the silicon mold is produced, the corresponding holes were formed in which the eye pins were placed as inserts before casting the membrane. In this way, a correct position of the eye pins was realized according to the 16 segments and the perpendicular orientation to the membrane's surface. Besides a correct position, the stiff eye pins are tightly connected to the flexible membrane, because the liquid (un-polymerized) polyurethane during casting encloses the perforated flange of the eye pin, assuring a close connection with the membrane after polymerization. In addition, the thickness of the membrane is consistently kept constant (3 mm) since the centering pin mutually distances the inner and outer part of the silicone mold during casting.

5.6 EXPERIMENTS AND PRELIMINARY RESULTS

Once our model was built, we activated it (Figure 78 a) using a piston pump (Harvard pump) (Figure 78 f) supplying the pressurized air and connected it to a lumped hydraulic windkessel model of the vascular system (including compliance (Figure 78 b) and resistance (Figure 78 c)) and measured (data acquisition using Labview 7, National Instruments, Austin, TX USA) ventricular pressure (disposable transducer DTX/PLUS, Becton Dickinson Critical Care Systems) and aortic flow (Tubing Flow Sensor ME-PXL, Transonic Systems Inc.).



Figure 77: The practical realization of (a) the valve plane. It contains (d) the valve plane, (a and e) two gates and positions, (b and g) two mechanical valves. Leakage between valves and valve plane is prevented using (f) O-rings which are pressed by (c and e) a compression nut.

In this preliminary study, wall deformation patterns were only visually observed (Figure 79 a and b). These observations fairly nicely demonstrated circumferential and longitudinal deformation. However, torsion was not pronounced. Our experimental results (Figure 80) further showed that this model is able to generate realistic data in terms of end-systolic pressure (120 mmHg) and heart rate (57 BPM). Due to the too high afterload resistance, the aortic flow in our model was low compared to (human) physiological data with a mean aortic flow of 1.6 l/min.

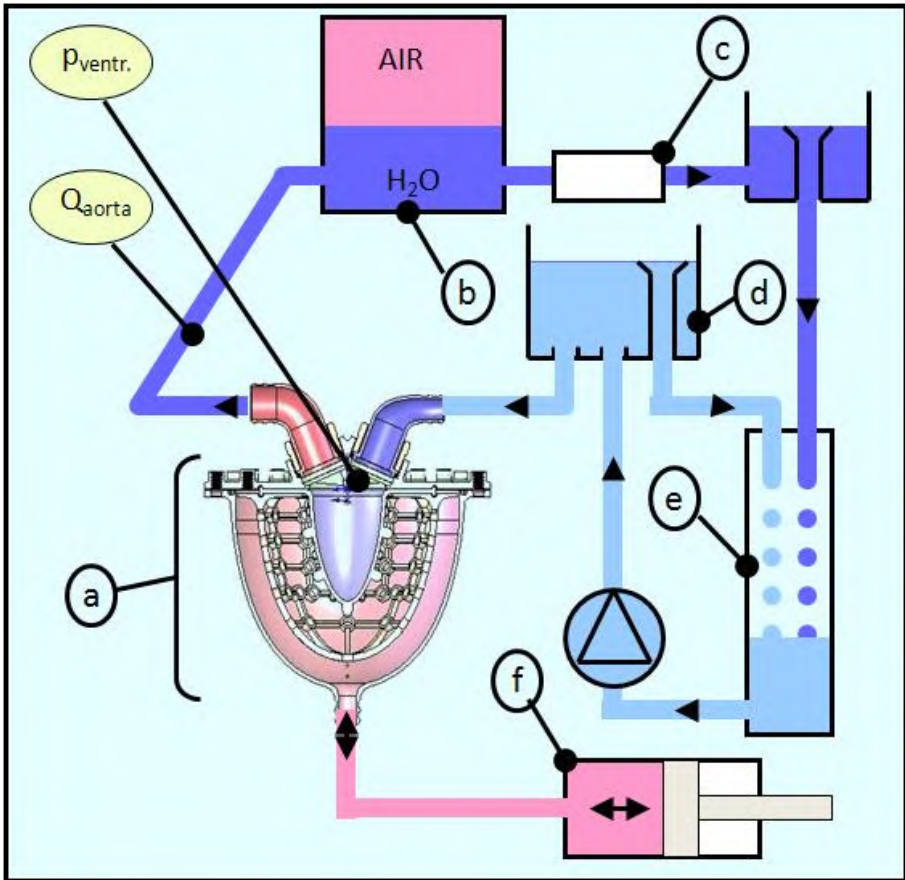


Figure 78: Once (a) our model was built, we activated it using (f) a piston pump and connected it to a lumped hydraulic windkessel model of the vascular system, including (b) compliance, (c) resistance, and (d) preload. After that, ventricular pressure ($p_{\text{ventr.}}$) and aortic flow (Q_{aorta}) were measured. In order to create a closed circuit, (e) an overflow and a circulation pump were added.

5. MODELLING THE LEFT VENTRICULAR MUSCLE BY A THICK WALL

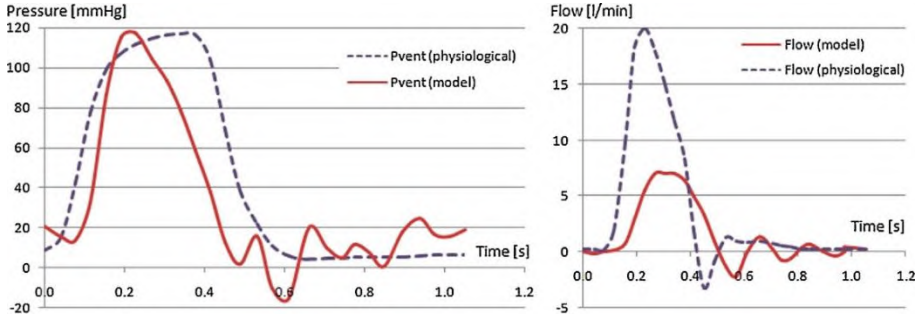


Figure 79: Compared with physiological data (dashed line), the experimental results (solid line) show that the model is able to generate realistic data in terms of end-systolic pressure (120 mmHg). Due to the too high afterload resistance, the aortic flow in our model (solid line) was low compared to (human) physiological data (dashed line) with a mean aortic flow of 1.6 l/min.

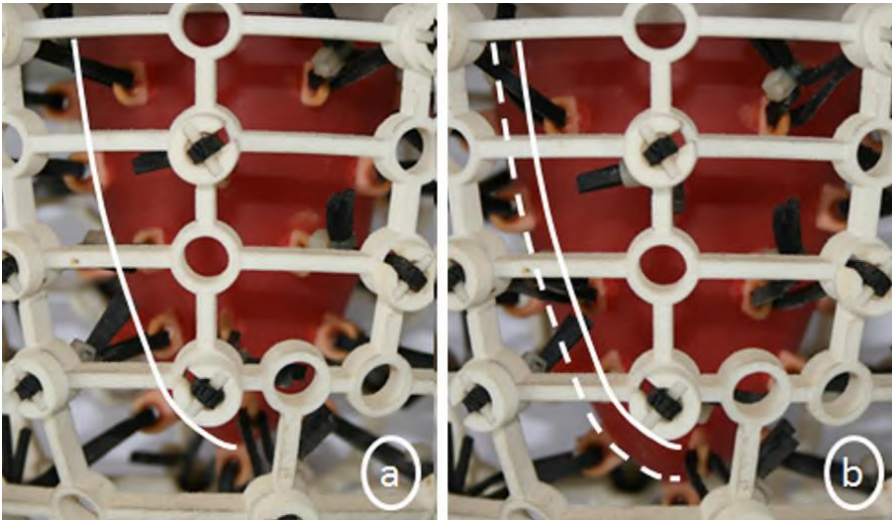


Figure 80: Wall deformation patterns of our model were fairly nicely demonstrated in terms of circumferential and longitudinal deformation: end-systolic (white line) and end-diastolic wall-deformation (white dotted line).

We observed also a few considerable discrepancies regarding human data, such as negative values of pressure and flow which are presumably attributable to the sucking property of the piston pump.

5.7 CONCLUSION

This chapter briefly describes the design and development of a new hydraulic LV-phantom (LV1) aiming to achieve more realistic wall deformation than obtained in the existing thin-walled membrane models. Therefore, we designed a thick-wall model in which control can be exerted on the wall using flexible bars. Our experiments show that circumferential and longitudinal deformation can be attained and that this LV1 can generate fairly normal values of pressure and flow.

Although the wall deformation is controlled in this new model, further work is required to achieve even more realistic wall deformation patterns. Once our experimental setup will be optimized, this new LV model will likely provide useful insights in LV wall deformation and its interaction with blood flow. Nevertheless, the controlled wall behavior of our model is a step forward compared to the unpredictable squeezing of thin walled models.

In the context of the practical guidelines of Chapter 3, this LV model is able to meet the following practical guidelines: modelling the ventricular wall by a thick-walled approach (**PG1**) and mimicking two global ventricular wall deformation patterns, namely longitudinal and circumferential deformation (**PG4 a-b**).

Modelling the active wall contraction and torsional motion of the left ventricle

This chapter is based on “Design of an Artificial Left Ventricular Muscle: an Innovative Way to Actuate Blood Pumps?”, as published in the Artificial Organs journal (2009) by Van Der Smissen B., Claessens T., Verdonck P., Van Ransbeeck P., and Segers P. [188].

This chapter describes the second of three new left ventricular models, namely LV2. By the integration of active contractile elements, this active way of ventricular actuation enables the generation of the left ventricular torsional motion which is present in the natural heart. In the context of the integrative approach of modelling the left heart including the mitral valve and valve plane, this artificial LV muscle model will be further discussed in Chapter 12 (§ 12.2) as it is a possible way of modelling the typical nature-like flexible valve plane and its movements.

6.1 INTRODUCTION

For all in-vitro investigations discussed in Chapter 2, the activation is based upon the passive squeezing of a membrane which is rigidly suspended into a rigid box and connected to a piston pump. Although the function of experimental models relying upon this deformation mechanism has already been proven, these models do not account for realistic wall deformation, nor can intra-ventricular blood flow patterns be realized in these models. As mentioned in Chapter 3 as 3th practical guideline (**PG3**), more nature-like left ventricular wall contraction can be modelled by integrating active contractile elements into the left ventricular wall model.

In this study, we propose an innovative design of the artificial LV muscle (LV2) that mimics fairly realistically global left ventricular wall deformation patterns as it consists of an active wall structure mimicking the heart muscle which efficiently exerts pressure on the blood. To demonstrate the actuation mechanism, we proposed a strategy to build the artificial LV muscle with a simple plastic bag. Next, we built and tested an experimental model to demonstrate the pump performance of this artificial LV muscle.

6.2 PHYSIOLOGICAL BACKGROUND

The heart is a four-chambered, muscular organ that continuously pumps blood through the body's extensive network of arteries and veins. The LV can be considered as its most important and powerful pumping chamber, and is therefore probably its most frequently studied chamber. The LV wall consists of three layers: the epicardium, the myocardium and the endocardium. The endocardium is the thin inner layer of endothelium, while the epicardium is an external visceral layer covering the heart. The myocardium, the middle layer, forms the bulk of the LV and is the layer that actually contracts. It consists mainly of cardiac muscle fibers embedded in connective tissue structure. The myocardium consists of interweaving bundles of cardiac muscle fibers spirally arranged around the circumference of the heart. As a result of this anatomical architecture and the timing and sequence of electrical excitation, during contraction the LV deforms as follows: (a) the diameter of the LV decreases while (b) the base (the atrio-ventricular valve plane) is simultaneously pulled downward in the direction of the apex (c) in a rotating manner (3). Due to this accompanying "wringing" effect, pressure is efficiently exerted on the blood enclosed within the chamber, thereby directing it upwards toward the aortic outflow tract. As such, global ventricular wall deformation can be basically described in terms of (a) circumferential deformation, (b) longitudinal deformation, and (c) torsion.

6.3 CONTRACTION MECHANISM

In order to reproduce these basic wall deformation patterns in-vitro, we designed a novel kind of artificial heart “muscle” composed of multiple actively contracting cells. Contraction is based on a mechanism by which pressure inside such a cell causes expansion in one direction and contraction in another direction. The contraction (systole) and relaxation (diastole) of a biological muscle (Figure 81 a) take place along the cardiac muscle fiber direction, while the contraction (inflation) and relaxation (deflation) in a single contractile chamber (Figure 81 b) of this new artificial LV muscle take place perpendicular to its long axis. The final deformation of the LV wall is determined by the organization and geometry of the contractile cells within one artificial LV muscle, together with the governing LV pressure and the applied pressure in the cells. In the present active LV wall structure, only one layer of artificial muscle was used. However, a well-thought-out configuration of a number and geometry of artificial muscles could be used in future left heart models to produce even more realistic deformations.

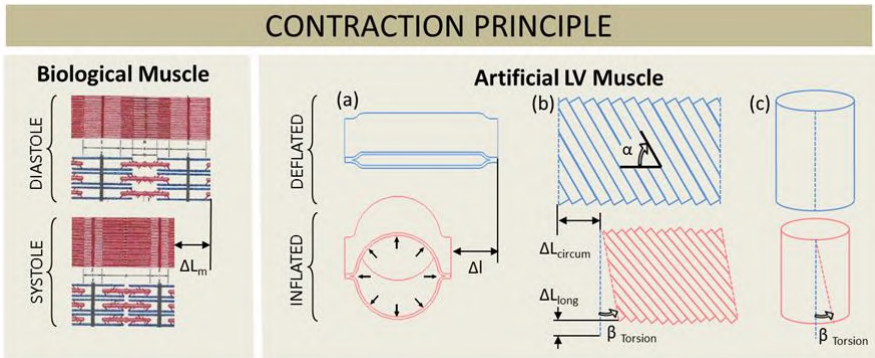


Figure 81: The contraction principles of the biological and the new artificial LV (left ventricle) muscle are illustrated. The contraction (systole) and relaxation (diastole) of a biological muscle take place along the direction of the cardiac muscle fibers, while the contraction (inflation) and relaxation (deflation) in a single contractile chamber of this new artificial LV muscle (a) take place perpendicular to its long axis (L_m : shortening of a biological muscle and $L_{single\ cell}$: shortening of a single contractile chamber). An actual three dimensional (3D) artificial LV muscle can be created by folding the 2D rectangular artificial LV muscle (b) to a cylindrical artificial LV muscle (c). When pressurized air is applied, the muscle cells contract perpendicularly to their longitudinal axis and the rectangular contour transforms into a parallelogram contour (b) with an angle $\beta_{torsion}$, a decrease in length (ΔL_{circum}) and in height (ΔL_{long}). Analogously, if both ends of the artificial muscle are welded together, the 3D cylindrical artificial LV muscle which is initially inactivated, will display torsion (with an angle equal to $\beta_{torsion}$) as well as radial, circumferential, and longitudinal deformation when activated (c).

In its unpressurized state, a basic contractile cell can be considered as a flat cavity with a rectangular ground surface. When pressurized air is supplied to the cell, it inflates and becomes round (Figure 81 a). Because the diameter of the inflated cell is less than the width of the deflated cell, both ends of the chamber move towards each other and the cell starts to contract. The cell shortening $\Delta L_{\text{single cell}}$ then equals the deflated width minus the inflated diameter. As such, the contractile cell shortens and thickens simultaneously, which is to some extent similar to the kinematics of cardiac tissue.

The global deformation patterns of the LV, i.e. longitudinal and circumferential deformation and torsion, can be achieved by arranging the contractile cells under a certain angle (α) relative to the LV long axis (centerline Figure 81 c). As such, exclusively longitudinal deformation (ΔL_{long}), exclusively circumferential deformation (ΔL_{circum}) and torsion in combination with longitudinal and circumferential deformation (ΔL_{long} , ΔL_{circum} and β_{torsion}), are obtained by arranging the contractile cells respectively at an angle $\alpha = 90^\circ$, $\alpha = 0^\circ$ and $0^\circ < \alpha < 90^\circ$ to the long axis of the LV. We found analytically that β_{torsion} reaches a maximum of approximately 13° at an angle $\alpha = 39^\circ$ and, therefore, used this angle in our model (Figure 82 Panel III and Figure 83). Also, the width of the deflated chamber was set to 15 mm.

In order to clarify the principle of the global LV wall deformation in our model, we assume a deflated artificial muscle (Figure 81 b) that is rectangular in shape and consists of a number of contractile cells which are orientated at an angle (α) between 0° and 90° with respect to the LV long axis. By rolling up the rectangular-shaped artificial muscle, a cylindrical LV model is obtained (Figure 81 c) in which the seal (dotted line) is directed parallel to the LV long axis. When pressurized air is applied to each individual cell of the rectangular-shaped artificial muscle, contraction in the cells takes place in a direction perpendicular to its long axis. Because the cell's long axis is orientated at a certain angle (α) between 0° and 90° with respect to the LV long axis, the contraction of the cells results in a transformation of the initial rectangular to a parallelogram contour. In comparison with the rectangular, the parallelogram has become shorter (ΔL_{circum} = circumferential deformation) and less high (ΔL_{long} = longitudinal deformation) and has rotated by an angle β_{torsion} (Figure 81 b). By rolling up the parallelogram-shaped artificial muscle, a cylindrical LV model is created (Figure 81 c) in which the seal (dotted line) is orientated at the angle β_{torsion} to the LV long axis. In this way, a cylindrical LV model is obtained in which longitudinal (ΔL_{long}) and circumferential deformation (ΔL_{circum}), as well as torsion (β_{torsion}) is realized when activated.

6. MODELLING THE ACTIVE WALL CONTRACTION
AND TORSIONAL MOTION OF THE LEFT VENTRICLE

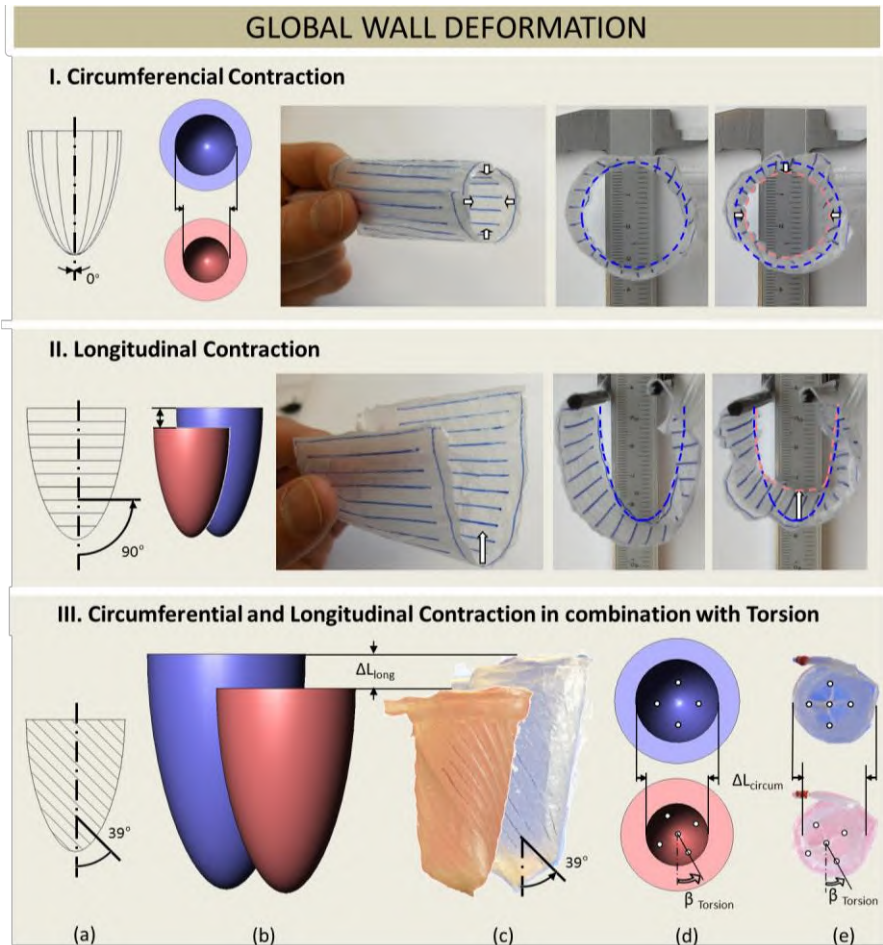


Figure 82 Panel I: Circumferential and radial deformation is obtained by directing the contractile cells parallel to the LV long axis (axis of symmetry). A physical cylindrical 3D model demonstrates circumferential and radial deformation, in top-view at diastole (blue) and systole (red).

Panel II: Longitudinal deformation is obtained by directing the contractile cells perpendicular to the LV long axis (axis of symmetry). A physical 3D model demonstrates the longitudinal deformation in front-view at diastole (blue) and systole (red).

Panel III: A combination of longitudinal, circumferential and radial deformation with torsion can be obtained by organizing the contractile chambers at an angle of about 45 degrees with respect to the LV long axis (axis of symmetry) (a). A physical semi-ellipsoid-like 3D model demonstrates the longitudinal deformation (b and c), circumferential and radial deformation (e) and torsion (e) at diastole (blue) and systole (red).

6.4 REALIZATION OF THE ARTIFICIAL LV MUSCLE

In order to build a cylindrical 3D artificial LV muscle, a step-by-step plan can be followed. First, reform the rectangular contour of the pattern depicted in Figure 81 c (deflated) into a parallelogram with an angle α . Make sure to add at the top a horizontal cell that is connected to every single cell. In this way air can be spread among all the cells in the LV wall. After that, draw the cell pattern on a double film of plastic, for example on a simple plastic bag. Weld the plastic films together according to the cell pattern to obtain the 2D artificial muscle. Then, to achieve a cylindrical artificial LV muscle, fold the 2D artificial muscle and weld the left and right sides together. Next, close the cylindrical artificial LV muscle wall near to the LV apex by bringing the wall together to one point and then welding this all together. Finally, insert an air tube in the top cell. The artificial LV muscle is now ready to be activated. When blowing into the air tube, the artificial LV muscle will contract and the three global deformation patterns can be visually observed.

As the biological LV cavity is better represented by a truncated ellipsoid than by a cylinder, we subsequently built an ellipsoidal artificial LV muscle instead of a cylindrical one. As anticipated, the three basic wall deformation components could also be visually observed in the more realistic ellipsoid artificial LV muscle (Figure 82 Panel III).

Weld quality is crucial for the well-functioning of the active LV wall structure. Weld properties are determined by the type and thickness of the thermoplastic film as well as the welding temperature, pressure and time. The thermoplastic film used in our artificial LV muscle was Polyethylene (PE) with a thickness of 0.05 mm and was welded with a vacuum sealer (Krupps Vacupack 2 Plus). The welding time and pressure were adjusted by trial and error in order to obtain qualitative welds.

6.5 PRELIMINARY FUNCTIONAL TESTS

Besides fairly realistic wall deformation, this new artificial LV can also achieve the pump function performance of a real LV. In order to prove this, we modified the prototype presented above in three aspects. First, in order to obtain realistic performance in terms of pressure and flow, the model was reinforced using 8 instead of only 2 layers of polymer. Secondly, in order to increase the systolic and diastolic speed, we lowered the air flow resistance by modifying the chamber pressure supply: the single collector tube is replaced by a number of individual tubes supplying pressurized air to each chamber individually. Thirdly, in order to simplify the sealing of the experimental model, we opted to supply the pressurized air at the apex instead of at the

atrioventricular valve plane. After the modifications (Figure 83), we connected our pump to a lumped hydraulic windkessel model of the vascular system (including compliance and resistance) and measured pressure (disposable transducer DTX/PLUS, Becton Dickinson Critical Care Systems) and flow (Tubing Flow Sensor ME-PXL, Transonic Systems Inc.). In this preliminary study, wall deformation patterns were only visually observed. Our experimental results show that the model is able to generate realistic data in terms of end-systolic volume (54 ml) and pressure (115 mmHg), end-diastolic volume (156 ml) and pressure (-4 mmHg), stroke volume (102 ml), ejection fraction (65%), mean outflow (6.8 l/min), heart rate (67 BPM), peak positive and negative dP/dt (1072 and -1134 mmHg/s), and pressure-volume relationship. The systolic ejection phase, however, is suboptimal due to the relatively simple afterload model which generates unphysiological reflected pressure and flow waves.

6.6 CONCLUSION

In this chapter, we have developed an innovative left ventricular model that mimics the global kinematics of the LV during the cardiac cycle and produced a demonstrative model by making use of handicraft material and tools. Besides fairly realistic wall deformation, our experimental results show that the LV2 is also able to generate realistic data in terms of volume and pressure.

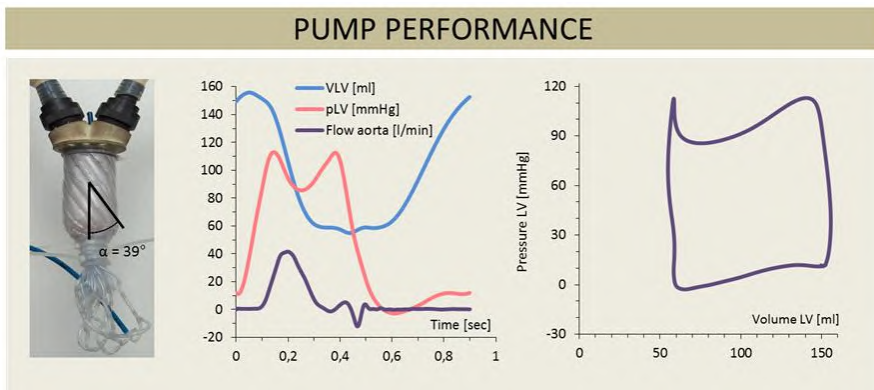


Figure 83: Pump performance. A slightly modified (see text) artificial LV muscle, namely LV2, was built to test the performance of the design as a functional pump. After connecting it to a lumped hydraulic windkessel model of the vascular system (including compliance and resistance), we measured pressure and flow. Our experimental results show that the model is able to generate realistic data in terms of pressure, flow and pressure-volume relationship.

However, unlike the biological system, in which contraction occurs along the muscle fiber direction, the long axis of the contractile chambers in our artificial LV muscle is perpendicular to the shortening direction. Another difference with the biological system is that in our artificial LV muscle air is added during systole and removed during diastole whereas the volume of the biological heart muscle remains virtually constant during the cardiac cycle. It is worth to mention that this limitation is applicable to all of the current heart models, since the actuation is typically realized by water or pressurized air generated by a piston pump. Nevertheless, our proposed artificial LV muscle appears promising and can be considered as a main step forward when compared to currently applied actuation mechanisms, as it will likely result in more physiological intracavity blood flow patterns.

Another limitation is that the LV2 is not based on an image-based patient specific geometry. In this regard, it should be noted that the implementation of a complex three-dimensional shape is only possible to a limited extent because the artificial muscle architecture is merely based on two simple dimensional sheets. Also, although this approach is convenient to account for the flexible nature of the valve plane (**PG7**), it is not implemented yet in this study. Apart from this, this model is able to meet all practical guidelines specified to attain more naturally correct LV models, namely: modelling the ventricular wall by a thick-walled approach (**PG1**), the anisotropic wall properties are included by the inflatable cells (elastic component) which are alternated with welds (fiber component) (**PG2**), integration of active contractile wall elements (**PG3**), mimicking the global ventricular wall deformation patterns such as longitudinal, circumferential, as well as radial deformation (**PG4 a-c**) and inclusion of the twisting motion (**PG5**). By this innovative way of integrating active contractile wall elements, this model achieves the largest number of practical guidelines compared to current LV approaches (Table 3) as well as the other LV models presented in this dissertation. Moreover, due to its novel ventricle actuation mechanism, it also allows the natural downwards motion of the valve plane (**PG8**).

Modelling the torsional motion of the left ventricle by integration of anisotropic material properties

This chapter describes the third of the three new left ventricular models proposed in this dissertation, namely LV3. This model adds fibers to the currently commonly used thin walled ventricular models in order to mimic natural torsional motion. Actually, this anisotropic model is inspired by the latter described artificial muscle model (Chapter 6), where the fibers act as the weld regions (fiber component) and the flexible polymer in between these fibers act as the inflatable cells (elastic component). A modified version (applying a more nature-like geometry) of this third left ventricular model will be integrated into the left heart models LH1 and LH2 (Chapters 10 and 11).

7.1 INTRODUCTION

To date, in-vitro left ventricle models generally mimic the cardiac chamber as a thin walled flexible membrane (called ‘Type-I models’ in this chapter) which is squeezed by an external pressure source to simulate pump function

(see Chapter 2). As such, despite that wall deformation of a natural left ventricle includes circumferential, longitudinal, as well as radial deformations and a twisting motion, current in-vitro left ventricle models only incorporate the circumferential and longitudinal deformation components.

However, a model which is an advancement over current approaches is the in-vitro active-wall left ventricle model (called ‘Type-II models’ in this chapter) which we discussed in the previous chapter (Chapter 6). This model captures the torsional motion of the real left ventricle via a contraction mechanism based on the inflation of contractile elements which are slantly oriented along the circumference of the left ventricular model. Although this in-vitro simulation of torsion is a breakthrough in the context of cardiovascular simulators, the artificial muscle model is only able to generate a torsional angle of maximum 13° , which is significantly smaller than the typical 17° manifested by the real left ventricle [49].

As it is the objective for in-vitro testing to mimic the anatomical and physiological conditions as accurately as possible [2], there is a need to simulate also the torsional motion of the left ventricle, attaining torsion parameters closer to the physiological value of about 17° .

In this chapter, a second torsional in-vitro model of the left ventricle has been developed in which physiological values of torsion are effectively achieved. Besides the torsional motion, this model is able to mimic also the circumferential as well as the longitudinal deformation components of the natural left ventricle. The deformation concept is based on the stretching of an anisotropic membrane, instead of the typical isotropic membrane of current approaches. This anisotropy is realized by embedding fibers into a flexible matrix, forming a composite structure. To evaluate the proof of concept and to obtain more insights of the torsional behavior in function of the fiber orientation, three different anisotropic left ventricular models are developed with different fiber orientation angles. These models are mounted into a cardiovascular simulator and torsional angles are captured during the heart cycle.

7.2 BACKGROUND

This idea has been inspired by the two different deformation mechanisms of existing Type-I and Type-II in-vitro left ventricular models, as well as by the anisotropic composition of the natural heart wall.

The first deformation mechanism, on which the invention is based, is that of the Type-I model. This passive left ventricular model is made of a

silicone material and is the most widely used approach today for in-vitro modelling of the left ventricle [5, 66, 79-84, 87-92, 96, 99, 127, 145, 160], including in the cardiovascular simulator of Verdonck and colleagues which was initially developed to study the blood flow through the mitral valve [95]. As mentioned before in Chapter 2, the membrane mimics the left ventricular wall and is typically represented by a truncated ellipsoid. The space at the inner side of the membrane (compartment 1) represents the left ventricular cavity and is closed at the top by a stiff valve plane that includes valves in the aortic and mitral position. At the outer side of the membrane (compartment 2), a pulsatile volume displacement is generated which deforms the membrane to simulate ventricular wall motion. In this way, this model is able to mimic the circumferential as well as the longitudinal deformation; however, it cannot mimic the torsional wall motion which is present in the natural heart (see Chapter 1). In addition, manufacturing the Type I-model is rather straightforward by a silicone dipping process, and one can account for patient specific geometries [89]. Another issue with Type-I models, is setting the equilibrium volume (which is the volume of the cavity enclosed by the unloaded model) as the end diastolic volume (EDV) or as the end systolic volume (ESV). Most models [5, 66, 79-84, 87-92, 96, 99, 127, 145, 160] choose EDV as the equilibrium volume because of the longer durability of the model. However, this approach implies an unpredictable squeezing of the left ventricular model which prohibits the simulation of natural wall deformation. On the other hand, the approach which uses ESV as the equilibrium volume is only sporadically used [162, 163, 166, 167], but results in a homogenous deformation of the left ventricular model which is a more accurate simulation of the natural left ventricular wall deformation. Although this approach is far more reliable, it is associated with lower model durability due to much higher stresses during the model expansion during the filling phase.

The second deformation mechanism that has inspired the new idea is the active wall Type II-model, described in the previous chapter (Chapter 6, [188]) and which is proposed as an artificial left ventricular muscle in the context of blood pumps actuation systems. In brief, this model consists of a membrane including a number of inflatable cells and is attached to a valve plane which includes two mechanical valves. For this actuation approach, no outer box is required because the ventricular wall motion is generated by a pulsatile flow within the inflatable cells causing the membrane to contract. Although this innovative Type-II model incorporates ventricular torsion in combination with radial, circumferential and longitudinal shortening, the manufacturing process has not been developed yet to account for modelling patient specific left ventricular geometries, nor is it able to generate the typical physiological torsion value of 17° .

The third source of inspiration is obviously the natural left ventricular wall which consists of different components, such as muscle, collagen, and elastin fibers. As described in Chapter 1, the cardiac muscle fibers are arranged in such a pattern that during activation, the ventricular muscle shortens, the diameter reduces and this realizes a twisting movement in order to efficiently eject the blood. These wall deformation patterns are the result of the anisotropic properties of the wall which consists of well-organized fiber structures (muscle and collagen fibers) which are embedded in a flexible matrix (elastin fibers). As mentioned in the literature review of Chapter 2, Rasponi and colleagues introduced anisotropic properties into their model by integrating fibers into a flexible ventricular model, and hereby induced a pronounced longitudinal deformation pattern [167].

7.3 DEFORMATION MECHANISM

The composition of this new left ventricular model is similar to the Type-I model and equally includes a hydraulic box in which a thin walled membrane model is suspended and activated by an external pressure source. However, whereas the Type-I membrane is made of an isotropic wall material, this new model integrates anisotropic wall properties to generate an additional torsional motion. This anisotropic type of membrane is obtained by embedding fibers in an elastic matrix to achieve a composite membrane material. In this way, the membrane material is forced during loading to substantially extend more in the direction perpendicular to the fiber long axis than in the direction parallel to the fiber long axis. The specific arrangement of the fibers is designed according to a well-defined fiber pattern and determines the wall deformation behavior. By varying the fiber angle with respect to the left ventricular long axis between 0° and 90° , we expect a different combination between torsional, circumferential and longitudinal deformations. At the extreme fiber angles of 0° and 90° , stretching of this anisotropic membrane during the heart cycle, no torsion for both cases, and maximal circumferential and longitudinal deformation patterns, respectively, are assumed. In this chapter, we focus on LV models with a slant arrangement of the fibers, whereas in Chapter 11 also perpendicular and parallel fiber directions are applied, as shown in Figure 115.

7.4 DESIGN AND COMPOSITION OF THE MODEL

To evaluate the proof of concept and to gain more insight into the torsional behavior as a function of the fiber orientation angle, three different anisotropic left ventricular models are developed, each featured with a different fiber

7. MODELLING THE TORSIONAL MOTION OF THE LEFT VENTRICLE BY INTEGRATION OF ANISOTROPIC MATERIAL PROPERTIES

orientation angle of 45° , 35° and 20° , respectively, with respect to the left ventricular long axis. The first angle is chosen because we intuitively expect maximum torsion close to 45° , while the values of 35° and 20° are set to outline the torsional range as a function of fiber orientation and to capture the fiber angle which is associated with the physiological torsional angle of 17° .

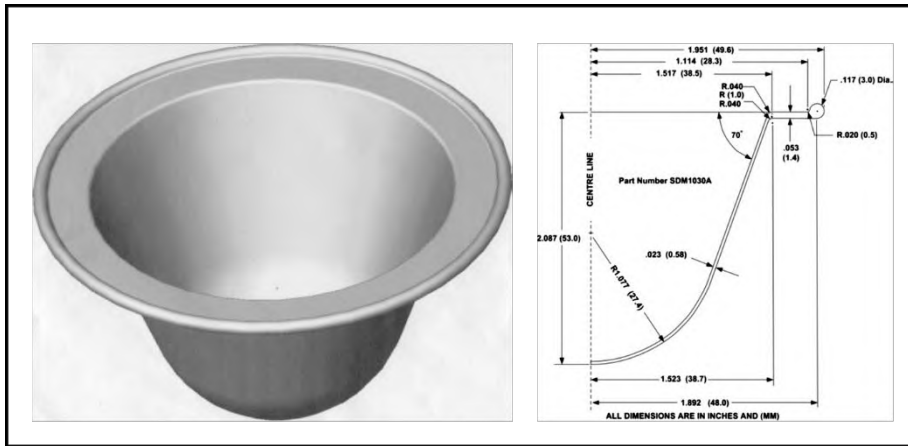


Figure 84: Geometry of the ViVitro left ventricular model [124].

For the manufacturing of each model, a kernel is developed and used as mold to produce the actual model. The kernel is designed according to the geometry of the Type-I ViVitro ventricular model [124] via Computer Aided Design (CAD), as illustrated in Figure 84. It comprises a truncated ellipsoid shape and is equipped with an integrated O-ring for sealing. In this way, the anisotropic left ventricular model is compatible with the ViVitro cardiovascular simulator (ViVitro Systems Incorporated, Victoria, BC, Canada) and enables a straightforward integration into a conventional Type-I system.

For the correct positioning of the fiber arrangement, the kernel is equipped with a specific groove pattern at the inner side, which serves as a reference during manufacturing. As shown in Figure 85 (CAD models), each of the fiber patterns comprises of 24 grooves which are spirally arranged around the circumference of the left ventricular model. These 24 spirals follow an anti-clockwise path to mimic the natural clockwise torsional motion of the natural left ventricle during systole of the model. The spiral path is defined perpendicular to the model surface and with a constant angle with respect to the left ventricular long axis of 45° , 35° , and 20° , respectively. The number of fibers is set to 24 for a sufficiently dense fiber distribution to obtain a homogenous wall deformation.

7. MODELLING THE TORSIONAL MOTION OF THE LEFT VENTRICLE
BY INTEGRATION OF ANISOTROPIC MATERIAL PROPERTIES

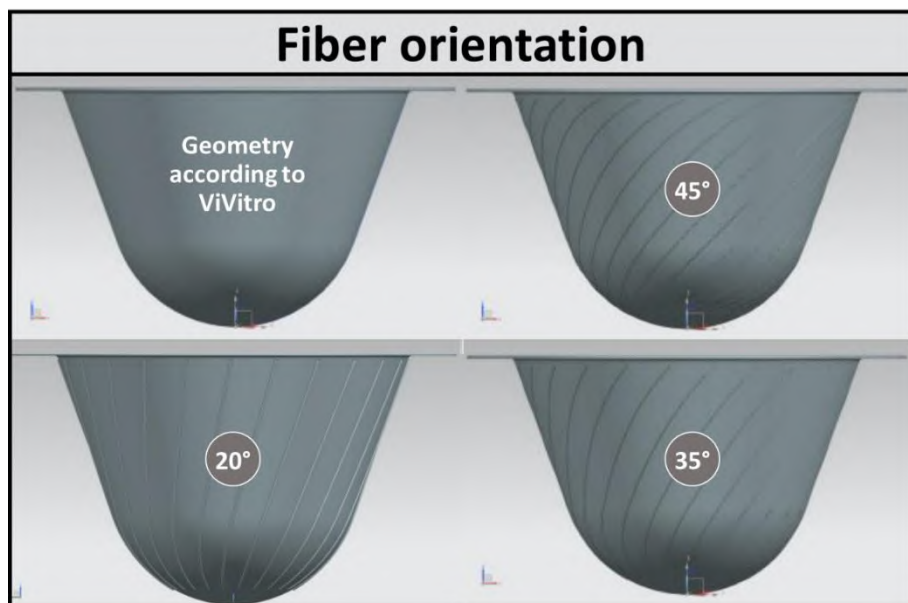


Figure 85: Grooved patterns in CAD models of the LV3 model.



Figure 86: Design of the kernel according to the ViVitro left ventricular model geometry, which is used as a mold for the manufacturing of the actual model. The 24 fiber grooves at the inner side are clearly visible to enable accurate deposition of the fibers.

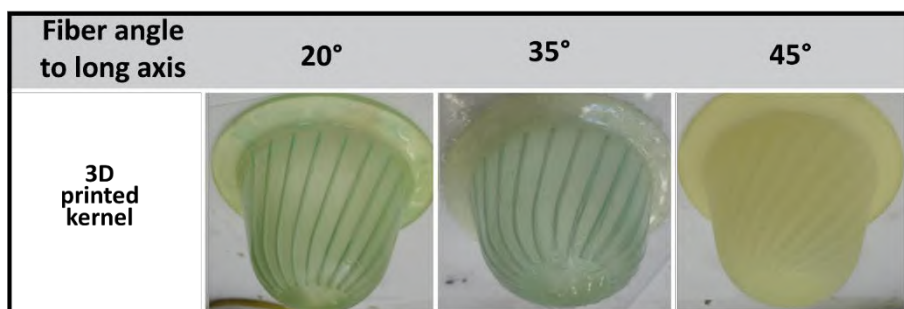


Figure 87: 3D printed LV3 kernels before (model 45°) and after (models 20° and 35°) colored PVA coating.

7.5 MATERIALS AND METHODS

The three kernels are 3D printed and used for the realization of the actual models via a dip-coating process as well as the deposition of fibers according to the reference fiber pattern. First, the kernel is 3D printed by the PolyJet technology (Objet Eden 350V, Stratasys, Rehovot, Israel) with a layer thickness of 16 μ m, as shown in Figure 87. After printing, the kernel is polished and coated with a Polyvinyl Alcohol (PVA) to enhance model release from the kernel and to provide a glossy finish of the actual model inner surface. This coating is applied for both the inner and outer surface. To obtain improved visibility of the groove pattern, a color is added to the PVA. This, in combination with the thin walled design (mm) and the transparent 3D printed material (FullCure®720), allows for a good visibility of the reference fiber pattern during the fiber deposition. In order to obtain a uniform distribution of the PVA, the kernels are subjected to a randomized rotation and 2 layers of PVA are applied.

After the PVA coatings are finished, the kernel is ready for the production of the actual anisotropic left ventricle model. These anisotropic left ventricular models are realized by a 3-layer composition. The first and the third layers are made of a flexible material and represent the flexible matrix component of the composite. These layers are responsible for the elastic properties of the left ventricular model and function as a watertight barrier between the two compartments of the Type-I model. The middle layer comprises polymer fibers and determines the direction in which wall deformation is constrained.

We selected silicone (HT 33 TRANSPARENT, Zhermack SpA, Italy) for the flexible matrix material because of its semi-transparent and flexible

properties, and Nylon multifilament yarns for the fiber component. Each model is equipped with 24 yarns and each yarn contains about 50 monofilaments (diameter) to maximize strength and minimize bending rigidity. The composite structure is thus realized by the deposition of the fibers between two layers of flexible material. The first silicone layer is applied by dipping and subsequently submitted to a randomized rotation to enhance a uniform layer thickness upon drying. After that, the multifilament yarns are moisturized by liquid-state silicone and manually deposited onto the first silicone layer according to the predefined fiber orientation pattern in the kernel, with an estimated accuracy of 1° . Then, the model is exposed to vacuum conditions during the curing process to eliminate air bubbles inclusion between the yarn filaments, which might cause local weaknesses of the actual model. Finally, the left ventricular model is finished by applying the second silicone layer and after curing, the actual model is easily removed from the kernel due to the PVA coating. The ventricular model is now ready to be mounted into the ViVITro system.

7.6 PRELIMINARY EXPERIMENTS AND RESULTS

As shown in Figure 88, the three models are mounted into the ViVITro cardiovascular simulator (ViVITro Systems Incorporated, Victoria, BC, Canada) and the interventricular model volume is adjusted. For experiments with the conventional ViVITro system, the EDV of a ViVITro left ventricular model is usually set to its equilibrium volume, which is 127 ml. However, because this anisotropic model only induces torsion during stretching of the membrane, the equilibrium volume (127 ml) is set as ESV. The stroke volume is set to 80 ml and the torsional angle of the model is obtained by video recording of a marker at the model's apex (Figure 88 right panel). The recordings are then post processed and the torsion angle is obtained by measuring the rotation difference of a marker at the apex with a goniometer (accuracy of 1°) at the time of end systole and end diastole. During the experiments, longitudinal, circumferential, as well as torsion is observed for each model. For the three models with fiber orientation angles of 45° , 35° and 20° , torsional angles of 26° , 22° and 17° are generated, respectively.

7.7 DISCUSSION

In this chapter, we have demonstrated that it is feasible to integrate well-defined anisotropic wall properties to generate torsional motion in a conventional Type-I cardiovascular simulator, such as the ViVITro system.

7. MODELLING THE TORSIONAL MOTION OF THE LEFT VENTRICLE
BY INTEGRATION OF ANISOTROPIC MATERIAL PROPERTIES

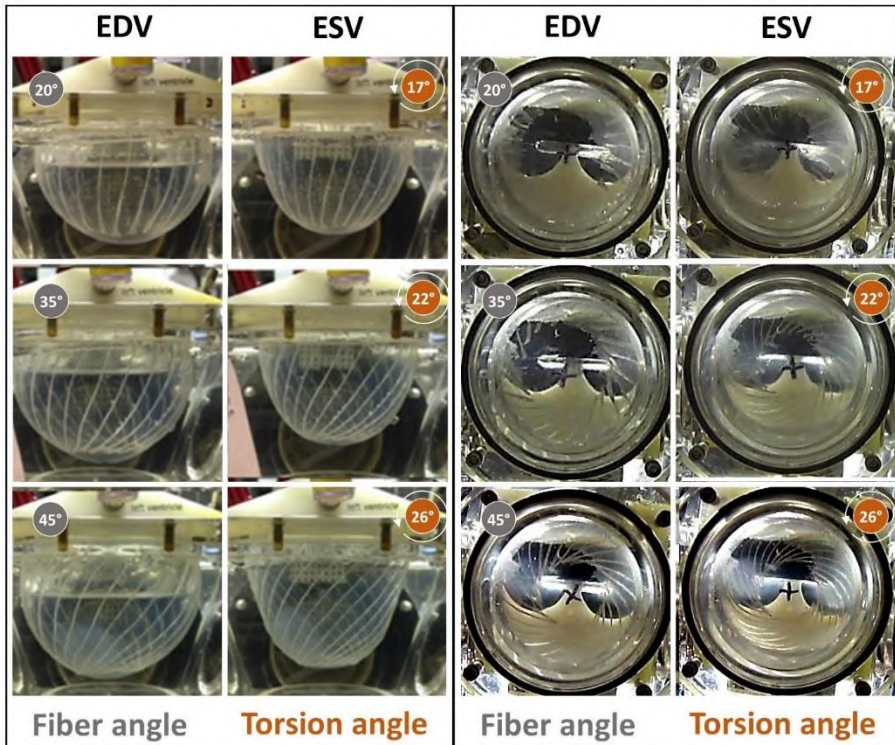


Figure 88: LV3 models (fiber orientation 20° , 35° , and 45°) display torsional motion (17° , 22° , and 26° , respectively) as well as longitudinal and circumferential wall deformations by a given stroke volume of 80 ml. Left panel shows the front view of the model, while the right panel illustrates the view from the apex towards the base. Index: EDV: end diastolic volume and ESV: end systolic volume.

As can be seen in Figure 88, the implementation of 24 evenly arranged fiber yarns results in a homogenous wall deformation with torsional, circumferential, as well as longitudinal wall motions.

From the experiments with different fiber orientation angles, it can be deduced that the degree of torsion clearly relates to the fiber orientation angle. Within the fiber orientation range from 45° to 20° , it is observed that higher fiber orientation angles result in higher torsional angles, with a maximum value of 26° for the model with fiber orientation angle of 45° . However, a wider fiber orientation range is required to get a more accurate approximation of the absolute maximum torsional angle. Also, we notice that torsion is positively related to the left ventricular volume. Furthermore, the experiments show that the physiological torsional angle of 17° is generated by the model with fiber orientation angle of 20° .

As described in Chapter 6, the Type-II model is also able to generate torsional motion. However, the maximum torsion angle was limited to approximately 13° in our experiments, which is low in comparison with the physiological mean value of about 17° . Although the deformation mechanism is inspired by this Type-II contraction mechanism, this anisotropic model is able to generate torsional angles which are far beyond the 13° because the deformable component of the wall is able to transcend the maximal lengthening of the Type-II model (which is limited to the periphery minus the diameter of the inflatable cells).

A mathematical or numerical simulation of this anisotropic wall behavior as a function of fiber orientation, model geometry and volume change during the heart cycle should be of great value to fully establish this more naturally accurate approach of ventricular modelling. As such, in-vitro left ventricular models could be optimized to generate physiological and patient specific values of torsion as well as of the circumferential and longitudinal deformations.

Although the anisotropic wall properties in the real heart vary along the muscle wall, the anisotropy in our model is constant with a fixed angle relative to model long axis. However, this novel way of ventricular modelling would allow for locally adjusting of the anisotropy, which enables modelling of the anisotropic variation within the heart muscle wall to obtain a more detailed imitation of the natural as well as patient specific wall deformation patterns. Also, this fiber-based approach opens the possibility to locally include stiff zones which are present in the real heart after myocardial infarction.

Since we applied this technique for a simple and smooth model geometry with a large enclosed volume, we estimate the wall interaction with blood flow patterns of this torsional motion rather limited. A more accurate approximation of interventricular blood flow patterns is expected by integration of an anatomically correct geometry including the protruding structures such as the papillary muscles and trabeculae.

Obviously, this technique might also be applicable to other chambers of the heart.

7.8 LIMITATIONS

We opted for setting the equilibrium volume as the ESV, which has the advantage of generating a homogenous and much more natural wall deformation, in contrast to the unpredictable squeezing of models in which the

equilibrium volume is set to EDV. On the other hand, applying this approach involves higher model wall stresses, and consequently a lower model durability. Nevertheless, during the few experiments we conducted, we did not observe any damage, but we did not intensively test the models to quantify model durability.

In the context of the practical guidelines set out in Chapter 3 (Table 2), the LV model of this chapter is shaped according to the ViVitro LV model and the natural shape is not yet incorporated. This simplified LV geometry comprises an EDV of 127 ml. However, to enable the torsional motion, the LV model is needed to be stretched and therefore the equilibrium volume of 127 ml is set for this torsional model to be ESV. This results in rather non-physiological values for ESV and EDV (127 ml and 207 ml) and an ejection fraction of 38%. This limitation is not an important issue in this conceptual phase but, when interventricular flow patterns are of relevance, physiological values of EDV and ESV need to be respected. This issue will be further addressed in the LV models of Chapters 10 and 11 which are based on patient-specific geometries (ESV 57 ml). Also, the thick-walled approach (**PG1**) as well as the integration of active contractile wall elements (**PG3**) have not been taken into account in this model, but are addressed in Chapters 5 and 6 for **PG1**, and Chapter 6 for **PG3**.

Another limitation, which is typical for Type-I models, is the fixed valve plane which not only disables the downward motion (**PG8**) but also limits the ventricular torsion to act only in one direction, whereas in the natural ventricle the total torsional angle is composed of an apical and a basal component, as described in Chapter 1 (see § 1.3.3.2). If these components are of relevance for the study approach, one must consider making use of the Type-II model, which allows the use of the more nature-like approach of a ‘floating’ type of valve plane.

7.9 CONCLUSION

In this chapter, we have described an innovative approach that allows for a more accurate modelling of left ventricular torsional, longitudinal and circumferential deformation patterns.

The novel left ventricular model comprises a flexible wall in which fibers are spirally arranged around the left ventricular model circumference. As a consequence of this slant directed anisotropy, the model wall is forced to deform in a twisting manner. A nature-like - clockwise during the ejection phase - torsional angle of 17° was obtained with an anticlockwise fiber orientation angle of 20° .

7. MODELLING THE TORSIONAL MOTION OF THE LEFT VENTRICLE BY INTEGRATION OF ANISOTROPIC MATERIAL PROPERTIES

Apart from the practical guidelines **PG1**, **PG3**, **PG4c** and **PG8** (as mentioned in the limitations section), this model is able to meet the other guidelines, namely: the anisotropic wall properties are included (combining an elastic with an fiber component) (**PG2**), mimicking the global ventricular wall deformation patterns such as longitudinal and circumferential deformation (**PG4**), and inclusion of the twisting motion (**PG5**). Because of its compatibility to existing cardiovascular systems, we expect that this concept will be highly useful for further ventricular torsion-related research.

Part III

In-vitro modelling of the mitral (and venous) valve

Modelling the mitral valve using a fiber-based composite material

This chapter describes the design of two mitral valve models (MV1 and MV2) which have a similar material composition (embedding fibers into a flexible matrix) as the LV3 model which is described in the previous chapter. However, in this case, this fiber-based material composition is not applied to induce deformation patterns, but to obtain nature-like leaflet properties, which combines a firm leaflet structure to withstand the high blood pressures with leaflet bend flexibility to diminish transvalvular flow resistance.

The MV2 model will be implemented into the integrative left heart models presented in Chapters 10 and 11.

8.1 INTRODUCTION

As emphasized in Chapter 3 (see § 3.3), there are - to the best of our knowledge - no in-vitro mitral valve models that include all elementary features of the natural mitral valve available to date. In this study, we propose a novel approach of modelling mitral valves that (1) makes use of a fiber-based composite material and (2) provides a valve with a (simplified) natural mitral valve geometry. This approach enables us to include core anatomical structures of the mitral valve such as the flexible and saddle-like annulus, the

anterior (AML) and posterior leaflets (PML), the chordae tendineae as well as the anterolateral papillary (ALPM) and posteromedial papillary muscles (PMPM).

This final model is the result of an optimization process by which we gradually improved design criteria such as model design, production process, and material properties. This chapter has the objective to introduce the design, characteristics, and practical realization of the mitral valve model. It focuses on two in-vitro mitral valve models that mainly differ in leaflet geometry and material composition. The first model (MV1) generates pathological-like values, whereas the second model (MV2) mimics normal values of physiological function. Later on in this dissertation, these two mitral valve models are incorporated and tested in an integrative left heart model (see Chapters 10 and 11 for more information). In Chapter 10, we will further elaborate on the experimental results of the performance of this mitral valve within the integrated left heart model. In the current chapter, we give an introduction and a brief summary of these results in order to provide a first evaluation of the valves' functionality.

8.2 MODEL DESIGN

In order to enable the accommodation of the valves within the physical left heart model, we based the mitral valve geometry of the two models on that of the 3D Zygote heart model (Zygote Media Group Inc., UT, USA). The SolidWorks (Dassault Systèmes SolidWorks Corp., Concord, MA) version of this left heart CAD model formed the basis of the physical left heart model. While evaluating the 3D Zygote heart model, we noticed that its mitral valve geometry resembles a stenotic-like valve type, even though this was not the developers' objective. As the geometry of MV1 (Figure 89 top panel) is based upon Zygote's original mitral valve geometry, this first model also reflects more stenotic-like valves. We slightly modified the Zygote's leaflet geometry by extending the leaflet tips to obtain a coaptation length of 4 mm.

For MV2, we adapted the geometry of MV1 towards a more optimized leaflet shape in order to obtain a more accurate imitation of the physiologically healthy mitral valve (see Chapter 1). The saddle-like annulus is kept identical to the Zygote model, with a short axis of 32 and a long axis of 48 mm. As illustrated in Figure 89 (bottom panel), we used the following parameters (see § 1.4.2.2) [51, 54]: (1) the PML comprises $\frac{2}{3}$ and the AML $\frac{1}{3}$ of the annulus perimeter, (2) the PML contains $\frac{1}{3}$ and the AML $\frac{2}{3}$ of the valve surface, (3) the AML is $\frac{2}{3}$ of the PML leaflet length at the level of the middle section, (4) the PML is oriented at an angle of 50° with respect to the general annulus

plane, and, as in MV1 and (5) the coaptation length is set to 4 mm with a total valve height of 20 mm.

8.3 MODEL COMPOSITION

The natural mitral valve leaflets are mainly composed of collagen and elastin fibers. These fibers are well-arranged over the surface of the leaflets and merge into the chordae tendineae. This anatomical fiber pattern results in a firm structure which can withstand the high blood pressures while demonstrating low bending resistance, enabling the leaflets to smoothly open and close with only a minimum of energy losses. In our modelling approach, we mimicked these physiological material properties by embedding strong fibers (mimicking the collagen fibers) into a flexible matrix (mimicking the elastin fibers) by a three-layered structure that includes a fiber layer which is sandwiched between two layers of elastic material. The leaflet fibers are oriented radially with respect to the annulus and continue beyond the leaflets, as such, modelling the chordae tendineae which will be in a later stage attached to the corresponding papillary muscles of the left heart model. In addition to the radially-oriented fibers, we provided the mitral valve model with a parallel-oriented fiber at the level of the leaflet tips to avoid rupture of the leaflets along the radial fibers during valve closure. This MV model fiber pattern is illustrated in Figure 90 C.

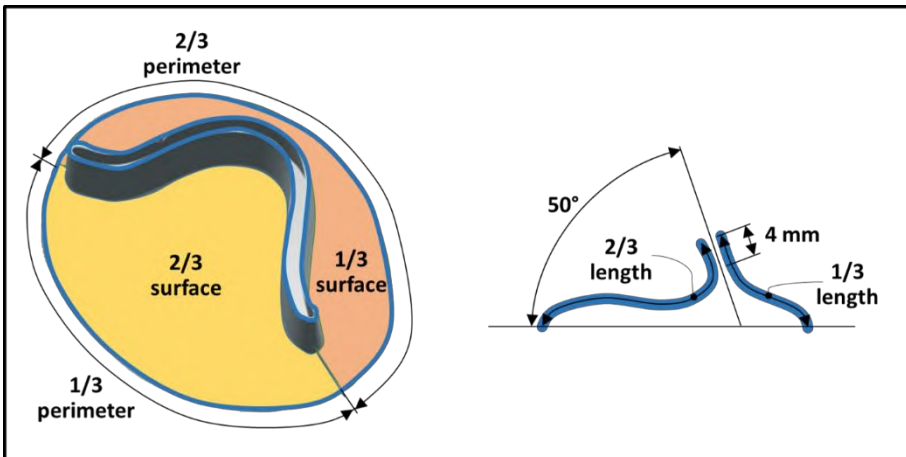


Figure 89: Geometrical design of MV2 with an identical mitral annulus of the Zygote CAD model.

8.4 MATERIALS AND METHODS

The production of the models includes a six-step procedure which is based on a dip coating process [89, 95, 96], extended with the implementation of the fiber component. First, an aluminum matrix (Figure 90 B) is produced using a 5-axis milling machine (DMU 50 eVolution, Deckel Maho Gildemeister, Pfronten, Germany) according to the two geometrical designs presented earlier (STEP 1) (Figure 90 A). Then, the aluminum mold is finished by a polishing treatment to obtain a glossy mold surface that guarantees a smooth inner surface of the actual model leaflets later in the process (STEP 2). After finishing the aluminum mold, the actual mitral valve model is produced by building up three layers. The first layer is formed by the silicone coating (HT 33 Transparent, Zhermack SpA, Italy) of the aluminum mold (STEP 3). After the first silicone layer is cured, the second layer is realized by the deposition of the fibers (STEP 4). This includes two radial fibers at the anterior and posterior commissures, four fibers which are evenly distributed along the anterior and posterior leaflet surfaces, and one parallel fiber at the level of leaflet tips which are deposited on top of the radial fibers. These fibers are first submerged in silicone to facilitate fiber deposition and to enhance adhesion between the fibers and the silicone material. This submerging process is performed under vacuum conditions for the elimination of air inclusions. After this second layer is finished, the third layer is realized by repeating STEP 3 (STEP 5). In the final step, the mitral valve model is removed from the aluminum mold (STEP 6), as shown in Figure 90 C.

We used two fiber types for these models. The first are ordinary cotton sewing threads which we used for the radial fibers of both models, as well as for the parallel tip fiber of MV1. We opted for a garish thread color (dark green) to enhance model visibility, to enable visual inspection during the experiments where the valve model is integrated in the left heart model. The second fiber types are Nylon multifilament yarns, which are much thinner (0.1 mm) than the cotton threads (1.0 mm). This fiber type is used for the parallel tip fiber of MV2 as we reasoned that this would likely result in better leaflet bending properties and a reduction of leakage during valve closure. The total leaflet thickness ranged for both models from about 0.3 mm between the fibers to about 1.0 mm at the level of the threads. The leaflet tip thickness of MV2 is reduced from 1.0 mm to about 0.4 mm.

After production finalization, these in-vitro mitral valve models were subsequently integrated into the left heart model, as briefly illustrated in Figure 91.



Figure 90: (A) Geometry, (B) aluminum matrix, and (C) in-vitro mitral valve models of mitral valve MV1 (left) and MV2 (right), respectively.

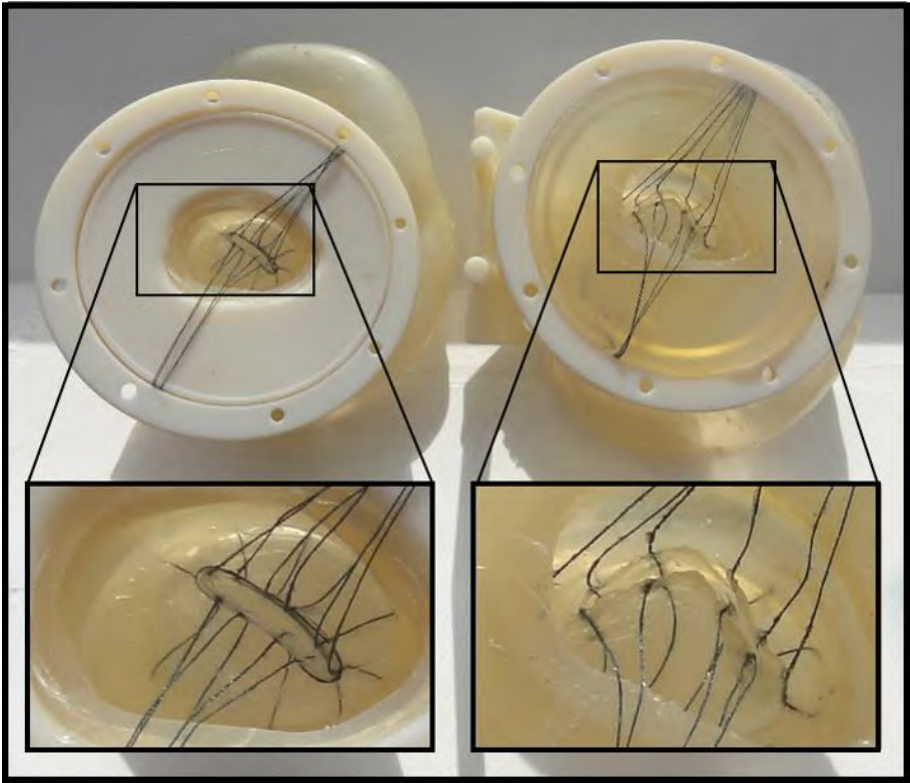


Figure 91: Integration into the left heart model and close up of MV1 (left) and MV2 (right), respectively.

8.5 EXPERIMENTS AND RESULTS

The two models have been validated by two experiments. First, before being integrated into the left heart model, they have been subjected to static pressure tests providing a quick qualitative assessment. Second, after integration of the valve models into the left heart models, validation was obtained via dynamic tests in a circulatory mock loop. More details about the integration of the mitral valve models, the experimental setup and preliminary results are described in Chapter 10 (§ 10.4 and § 10.5). In this section, we only provide a short summary of those results reflecting the mitral valve's functionality.

For the static pressure tests, the mitral valve models are built into a custom-made valve plane where both the annulus and the chordae tendineae are held in a fixed position. Valves were subjected to a backpressure of 140 mmHg, which is a slightly higher value than the normal end systolic pressure of 120 mmHg. These experiments showed that both valves were able to resist

the pressure, even though MV1 showed a substantial degree of regurgitation (100 ml/min). One reason of this valve leakage can be found in the relative high bending resistance of the leaflet tips, which prohibits the full closure of the valve model at the level of the commissures. This bending resistance is substantially reduced in MV2 by using the multifilament yarns instead of the relative thick treads, leading to a much lower leaflet tip thickness of 0.4 mm (instead of 1 mm).

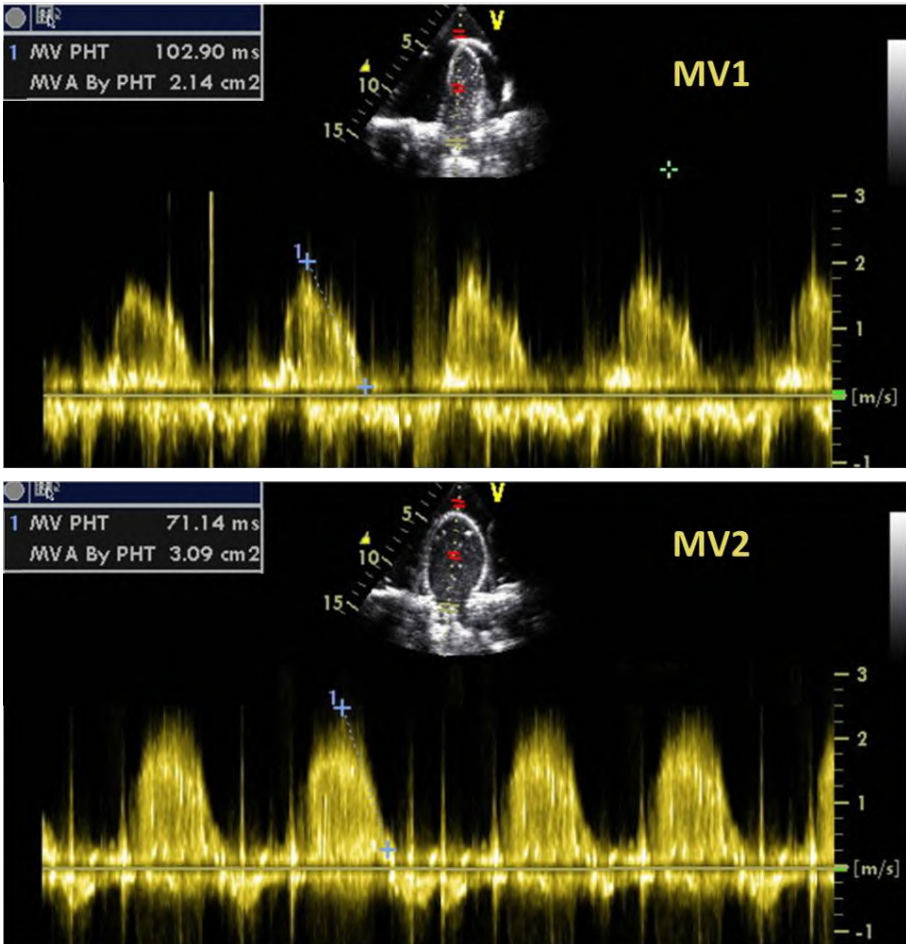


Figure 92: Transmittal valve continuous wave Doppler signals show a Mitral Valve Pressure Half Time (MV PHT) of 102.90 and 71.14 ms and a (derived) EOA of 2.14 and 3.09 cm² for MV1 and MV2, respectively.

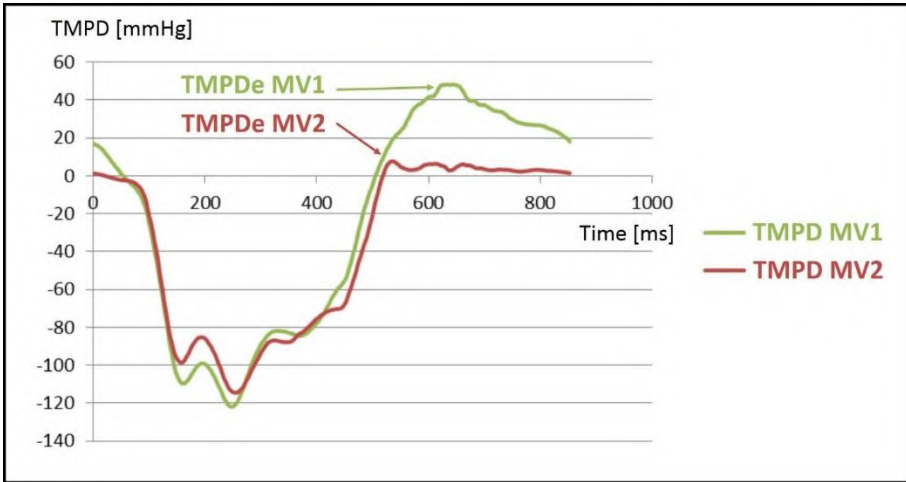


Figure 93: Transmittal pressure differences during early diastole (TMPDe) of MV1 and MV2.

Second, the mock loop experiments include an ultrasonic investigation (Vivid 7, GE, Vingmed, Horten, Norway) and pressure measurements using a sensor catheter (SPR-721, Millar Instruments; Houston, TX, USA). These results (also described in Chapter 10) show an Effective Orifice Area (EOA) of 2.28 and 3.04 cm² for valve 1 and 2, respectively (Figure 92). The Trans Mitral Pressure Difference during early diastole (TMPDe) averaged over the diastolic phase, for a cardiac output of 5.6 l/min and a heart rate of 70 beats/minute, was 28.58 (SD = 12.6) and 3.66 (SD = 1.66) mmHg for MV1 and MV2 respectively Figure 93. Durability tests have not been performed deliberately, but the two valves have lasted the extensive experiments of Chapters 10 and 11, which comprised about 4600 and 2000 cycles for MV1 (Chapters 8 and 10) and MV2 (Chapters 10 and 11), respectively.

8.6 DISCUSSION AND CONCLUSION

The described approach enables the mimicking of a natural mitral valve while including its most elementary features and geometrical shape, which is - to the best of our knowledge - unique. The integration of fibers into a flexible matrix and the three-layer composition models respect the architecture of the biological mitral valve. Furthermore, our methodology allows for the integration into a left heart model, as will be elaborated on in Chapter 10, providing reasonable performance in terms of effective orifice area and transmitral pressure gradients for MV2.

We realized two working prototypes. The first one demonstrated the proof of concept of the production process, whereas the second one is a further optimized version of the valve model in terms of geometry and leaflet tip fiber. While MV2 meets our goal to generate more physiology-like values of mitral valve performance, MV1 is also interesting as it turns out to be a model of a stenosed mitral valve, exhibiting high TMPDe, low EOA, and regurgitation. Overall, these mitral valve prototypes demonstrate that this new approach can be used to model normal as well as pathological mitral valves.

As summarized in Table 8, this model partly meets the practical guidelines of a basic in-vitro mitral valve as a reproducible mitral valve apparatus model with a parametrized geometry and including all basic feature of the mitral valve apparatus, such as the anterior (A) and posterior (P) leaflets (**PG6a**) which are hinged in a saddle-like annulus (**PG6b**) and made of a fiber-based flexible material (**PG6c**) and including the chordae tendineae (**PG6d**). However, the integration into the valve plane (**PG7**) and the connection with the papillary muscles (**PG6e**) are further discussed in Chapters 10 and 11. Because of the absence of such a model to date, we expect that this concept will be highly useful for future in-vitro mitral valve modelling.

8.7 LIMITATIONS AND FUTURE DIRECTIONS

Some limitations of this approach should be noted. First, the orientation of leaflet fibers is radial relative to the annulus. A more physiological approach could be attained by incorporating a parallel fiber orientation (see § 1.4.2.2). Second, the fibers in our approach have been modelled as a small number of relative thick threads, whereas a more nature-like and more durable approach would be achieved by using a large number of homogeneously distributed thin fibers. A third limitation is more production-related. Even though the silicone dip coating of an aluminum core is a straightforward and generally used technique, an unwanted side effect is that there are inherent local wall thickness variations. Fourth, our models do not completely capture the complexity of the human mitral valve as we shaped our model should be conceived as merely a generalization of reality. Finally, in this conceptual phase of the work, we used ordinary cotton sewing threads and a general purpose silicone. There is a large range of flexible and advanced fiber materials that can be explored to further optimize the mitral valve model leaflet characteristics.

Nevertheless, the described approach can be considered a major step forward for the in-vitro modelling of mitral valves and has great potential in the context of evolving digital technologies. The very fast advances in medical imaging and 3D printing technology will enable the realization of

even more realistic mitral valve models in the next few years. Today, highly detailed patient specific geometries can be obtained by the segmentation of high-resolution medical images. The combination of these techniques with the current approach may enable the production of patient-specific in-vitro models. Major revolutions can also be expected from the 3D printing technology where multiple research efforts are directed to high resolution printing with flexible materials. If this endeavor could be combined with the deposition of multiple thin fibers according to the anatomical fiber orientation of a natural mitral valve, great advances in in-vitro valve modelling can be anticipated.

Innovative design of a PIV compatible venous valve model

This chapter is based on “Innovative design of a venous valve intended for PIV measurements”, published as a proceeding in the ASME Summer Bioengineering Conference (2011) by Van Der Smissen B., Van Canneyt K., Vermeulen M., Bayley M., Narracott A., Kaminsky R., Van Ransbeeck P., Verdonck P. and Segers P. [189].

At first sight, venous valves models (VV) are out of the scope of left heart modelling. However, it is worthwhile to include this chapter into this dissertation because the approach we developed to build a PIV compatible venous valve model for optimizing in-vitro modelling research in the context of hemodialysis is directly applicable to our ideas towards building PIV compatible models of the left ventricle (LV5) and even of the full heart (FH2). We will discuss this pathway for future research in the final chapter of this dissertation (see § 12.2).

9.1 INTRODUCTION

Today, hemodialysis is a common therapy to treat people with severe chronic kidney disease. This therapy strongly relies upon the vascular access

that connects the patient's circulation to the artificial kidney and which is obtained by surgically creating an arteriovenous fistula in the arm. However, due to the high flows involved at the venous side and elevated venous pressures, the functioning of venous valves in the arm is significantly disturbed, which too often bring about serious dysfunctions or complications in the patient [190, 191]. To this end, research is done to improve the outcome of vascular access in patients on hemodialysis therapy by means of computational modelling [192]. One crucial challenge, however, is experimental validation of these computer models, preferably by using Particle Image Velocimetry (PIV) for simulations of flow fields. Yet, the task of modelling the venous valve is daunting because this valve functions at very low physiological pressure differences. Moreover, PIV requires an experimental model to be fully transparent. To our best knowledge, no such in-vitro models have been developed to date.

In the framework of this dissertation (see § 3.5; Table 8), we identify the need for such a PIV compatible venous valve model for the validation of CFD models as **NEED4**. Ideally, **such a model should be transparent for use in PIV simulations while keeping its functionality at low pressure difference**. This can be defined as a ninth and final practical guideline (**PG9**). In this study, we propose an innovative design of a PIV compatible venous valve model which has the ability to function at minimal pressure differences and which is able to generate valuable PIV data.

9.2 MATERIALS AND METHODS

9.2.1 Practical guidelines for building the venous valve model

In order to build a venous valve model for PIV validation, we chose to start from a very thin, highly transparent, plastic sheet with a thickness of 0.03 mm. Although it is not straightforward to build a 3D venous valve starting from a 2D sheet, we preferred this strategy for two main reasons. The first reason is the minimal bending stiffness of a thin film to ensure well-functioning of the valve model at minimal pressure differences. The second reason is the advantage of no restriction to match the refractive index of the structure and fluid material. In order to perform PIV measurements, the refractive index of structure and fluid need to be matched. Knowing that its importance is relative to the distance through which the light passes through, light deviation is limited in a very thin structure. Therefore, it can reasonably be assumed that the refractive index match can be neglected with the given refractive indices of the fluid 1.42 and the valve model material 1.59 [193].

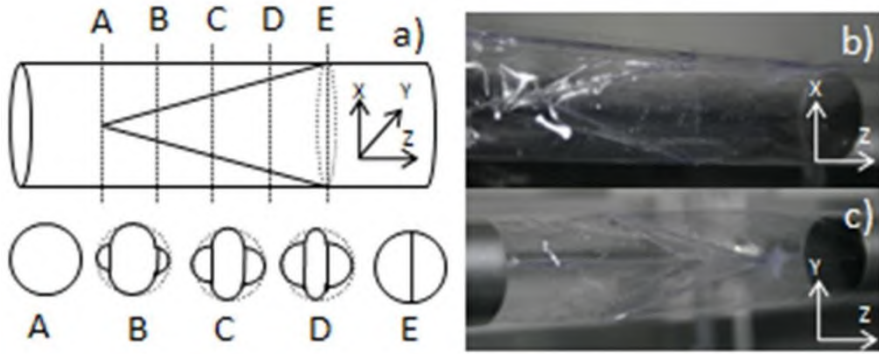


Figure 94: a) Drawing of the valve model (VV) with different sections in the XY plain and pictures in open air at b) XZ and c) YZ position.

The conversion of the two-dimensional thermoplastic polymer film to a three-dimensional venous valve model was realized by welding, using a household vacuum sealer (Krupps Vacupack 2 Plus, Krups, Peoria, IL, USA). The welding time and pressure were adjusted by trial and error in order to obtain qualitative welds. Although the biological venous valve is better represented using a curved line leaflet attachment to the wall, we assumed a straight weld line attachment, which resulted in a more simple constructing procedure, depicted in Figure 94.

To build the cylindrical three-dimensional venous valve, starting from the two-dimensional sheet, a step-by-step plan can be followed. First, draw the parametric pattern depicted in Figure 95 on a highly transparent thermoplastic film, e.g., a polystyrene film (as often used for flower or present packing). Then, cut out the rectangle and the two triangles, representing the lumen wall and the two leaflets respectively. After that, position the leaflet line W1 to lumen wall line W1 and weld them together. Next, position leaflet line W2 to the lumen wall line W2 by keeping the leaflet flat and at the same time folding the lumen wall part according to Figure 95. This folding is necessary because the triangle leaflet basis, being π , differs from that of the lumen wall, being $2r$ (with r 12.5 mm). After the first leaflet is attached to the lumen wall, the second one is performed likewise. Finally, in order to obtain a cylindrical three-dimensional venous valve model, fold the lumen wall to a cylinder, match W5 at the left side and W5 at the right side of the primary lumen wall rectangle and weld the two sides of the lumen wall together to obtain a sealed vessel wall. The venous valve model is now ready for experiments.

9.2.2 Experimental setup

In order to test this new design of the valve, we built a scaled model with a diameter of 25 mm. Testing of the valve included a functional as well as a PIV experiment.

The functional experiment involved a vertically positioned valve with a long outflow tube appended. In this tube, water was slowly added to a height of 1.5 m to test for leakage and pressure resistance. The PIV experiment encompassed a horizontally positioned valve (see (Figure 96 a) which was connected to a hydraulic mock loop. The fluid was directed by a steady flow pump, first through a long inlet tube of 1 meter, then through the valve, and subsequently through the outlet tube into an open reservoir which was again connected to the pump. For the test fluid, we used 42/58 water/glycerin mass percentage mixture seeded with polyamide microspheres particles (diameter 57 μ m). A Standard 2D normal speed PIV system (ILA GmbH, Juelich, Germany) was employed to perform the flow analyses and a double pulsed Nd:YAG laser (max. 120mJ) was used as a light source. A CCD Sencicam QE camera (PCO, Kelheim, Germany) with a resolution of 1376 x 1040 pixels was used to record image pairs at 8Hz. Post processing of the images was performed with commercial VidPIV 4.6 software (ILA GmbH, Juelich, Germany). In the region of interest, in plane velocity vectors and magnitudes were computed by averaging 500 instantaneous flow field measurements.

9.3 RESULTS

For the functional experiment, the filling of the space behind the leaflets was sufficient to close the valve after a minor modification of the design by adding an extra weld at W6 (see Figure 95). The valve kept closed when more water was added, up to a height of about 1.5 m, which indicates that the valve model could well resist these higher pressure differences (approx. 110 mmHg).

While calibrating the PIV measurements, we did not notice light distortion due to the difference of refractive index between the test fluid and the valve material. Also, when the model was immersed in water/glycerin mixture, the valve model could hardly be differentiated from the surrounding fluid, confirming our hypothesis that the use of a thin sheet does not require special precautions with respect to refractive index matching. Figure 96 b shows the PIV results of the stationary flow with a parabolic flow profile showing a maximum velocity of 1.6 m/s for a Reynolds number of 689.

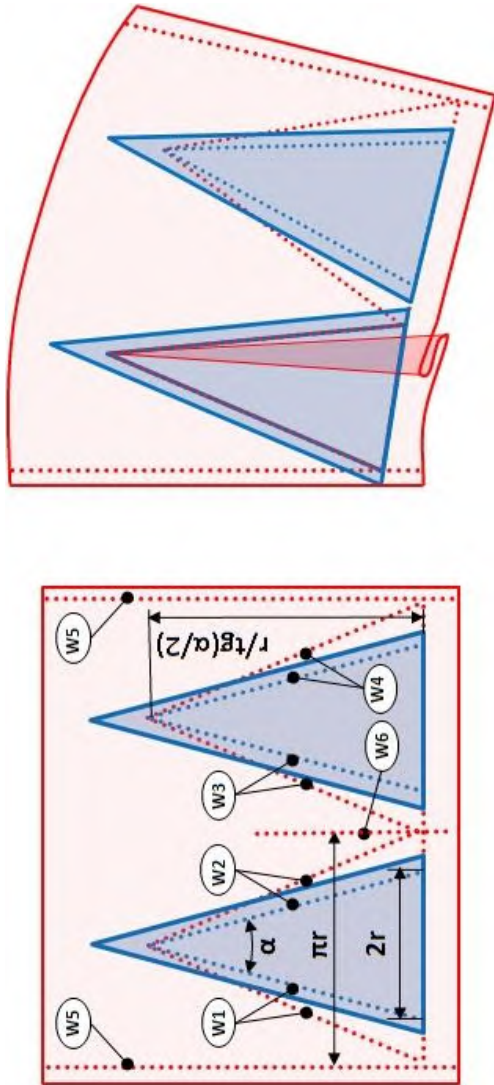


Figure 95: Step-by-step plan to build the cylindrical three-dimensional VV model starting from a two-dimensional sheet.

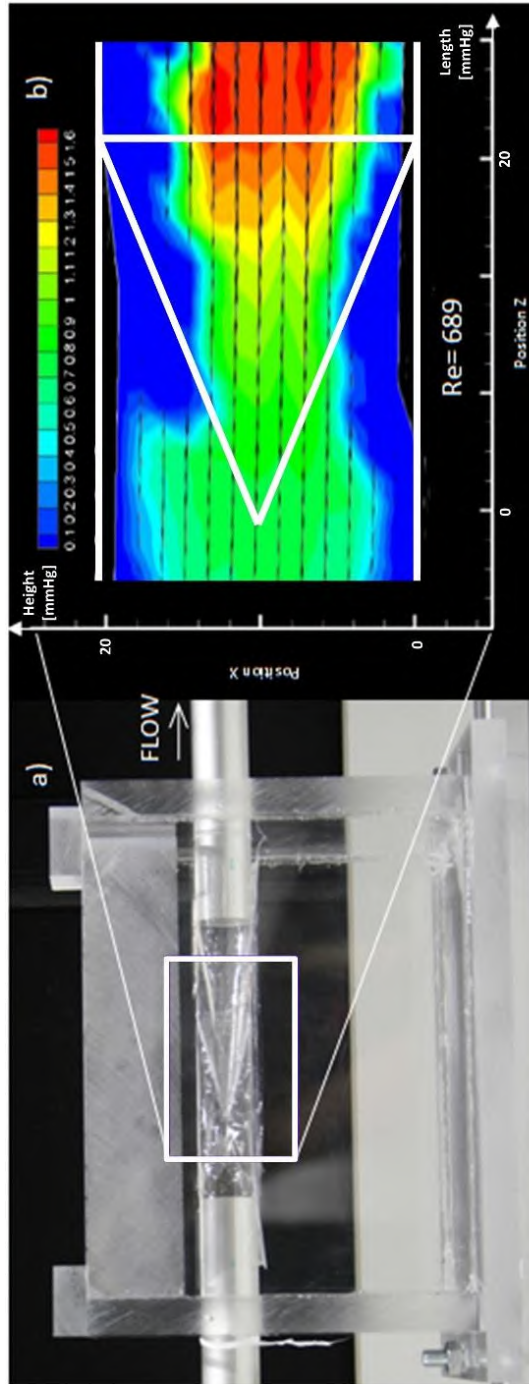


Figure 96: a) PIV setup of the valve model in a transparent box in open air, and b) the according PIV results.

9.4 DISCUSSION AND CONCLUSION

Although the experimental venous valve model clearly remains a work in progress, this novel valve design signifies an important step forward. To the best of our knowledge, this is one of the first functional venous valve models that is compatible with PIV. Our innovative design using the transparent and pliable features of polymer film resulted in an operational valve that is sensitive for fluid motion and able to function at low pressure differences (**PG9**, Table 8). Moreover, these preliminary results show that PIV measurements are not only available for flow patterns adjoining the valve but also within the valve itself. This opens the intriguing possibility to experimentally assess and examine intra-valvular flow patterns. Taken together, this valve design appears a promising tool for use in experimental validation studies of computational models of valve configurations.

9.5 LIMITATIONS AND FUTURE RESEARCH

Future challenges to be incorporated in the model can be noted. In order to obtain a simple construction procedure, we assumed a straight weld line attachment, although the biological venous valve would be better represented using a curved line leaflet attachment to the wall [194]. Also, we did not take into account the elasticity of a natural venous valve. Given that the construction procedure allows for a wide choice of thermoplastic materials, one might pursue a material that more closely resembles the properties of the biological venous valve tissue. Further research could also address the versatility of this valve design to mimic other cardiovascular valves.

Part IV

Modelling the left heart: an integrative approach

Modelling the left heart by a monolithic approach

In Part IV, two left heart models, namely LH1 and LH2, are realized by integrating different innovative elements from previous chapters, as well as some new features. As such, in Chapter 10, a nature-like geometry (including papillary muscles as new features) is added to a traditional thin walled left ventricular model and combined with the mitral valve MV2 (Chapter 8). Then, in Chapter 11, this model is extended by the anisotropic wall properties described in Chapter 7.

Chapter 10 focuses on the model design aspect by means of a monolithic left heart model version, whereas Chapter 11 focuses on the study of LV wall deformation patterns by means of a bilithic version including a number of modular LV models. In both chapters, the left heart model is mounted into an existing pulse duplicator system [100, 103, 119, 124, 184], which is described in the state-of-the-art of in-vitro models (Chapter 2).

10.1 INTRODUCTION, DESIGN AND COMPOSITION

As extensively discussed in Chapter 3, a key objective of in-vitro modelling is to mimic anatomical features as realistic as possible. In this chapter, we describe our novel approach of modelling the left heart (LH1) which leads to

a closer approximation of real anatomic features. It outperforms existent cardiovascular simulators in at least four ways.

First, most currently used cardiovascular simulators are made of rigid components (Chapters 3 and 4), while the real heart consists only of soft tissue (Chapter 1). In our approach, a more nature-like representation of the soft tissue is attained by assembling the new left heart model using flexible materials.

Second, current in-vitro cardiovascular models are much bulkier in volume compared to the natural heart. This relates to the fact that many setup components (e.g., left atrium, mitral valve, left ventricle) have to be modular to suit multiple experimental set-ups. However, in our design, the left atrium, mitral valve and left ventricular assembly are made in one single piece which results in a more compact and more nature-like model.

Third, we aim to mimic the left heart's working as a complex cooperation of various cardiovascular compartments. The new model includes the left atrium, mitral valve, left ventricle, (mechanical) aortic valve as well as the aortic arch. In the atrium, we also modelled the entrances of the four pulmonary veins (the left and right superior, and left and right inferior pulmonary veins) to mimic the blood flow from the lungs into the left atrium. Also, by integrating the mitral valve model MV2 (§ 8.2), our model is one of the first to include multiple mitral valve components at once, such as the flexible and saddle-like annulus, the anterior (AML) and posterior leaflets (PML), and the chordae tendineae which are connected to the left ventricle via the two papillary muscles.

A fourth asset of this model is that it draws its geometry directly from medical images of a real heart. Furthermore, similar to several other existing left heart models, our new model also shows compatibility with conventional clinical evaluation techniques such as ultrasound and pressure catheters. Figure 97 gives an overview of the left heart components which are included in the LH1 model.

It is worth mentioning that the left ventricle model is based upon the ordinary thin walled flexible models, which are able to generate the longitudinal and circumferential deformation patterns (**PG4a-b**). However, the integration of the papillary muscles and the connection with a mitral valve model are innovative aspects.

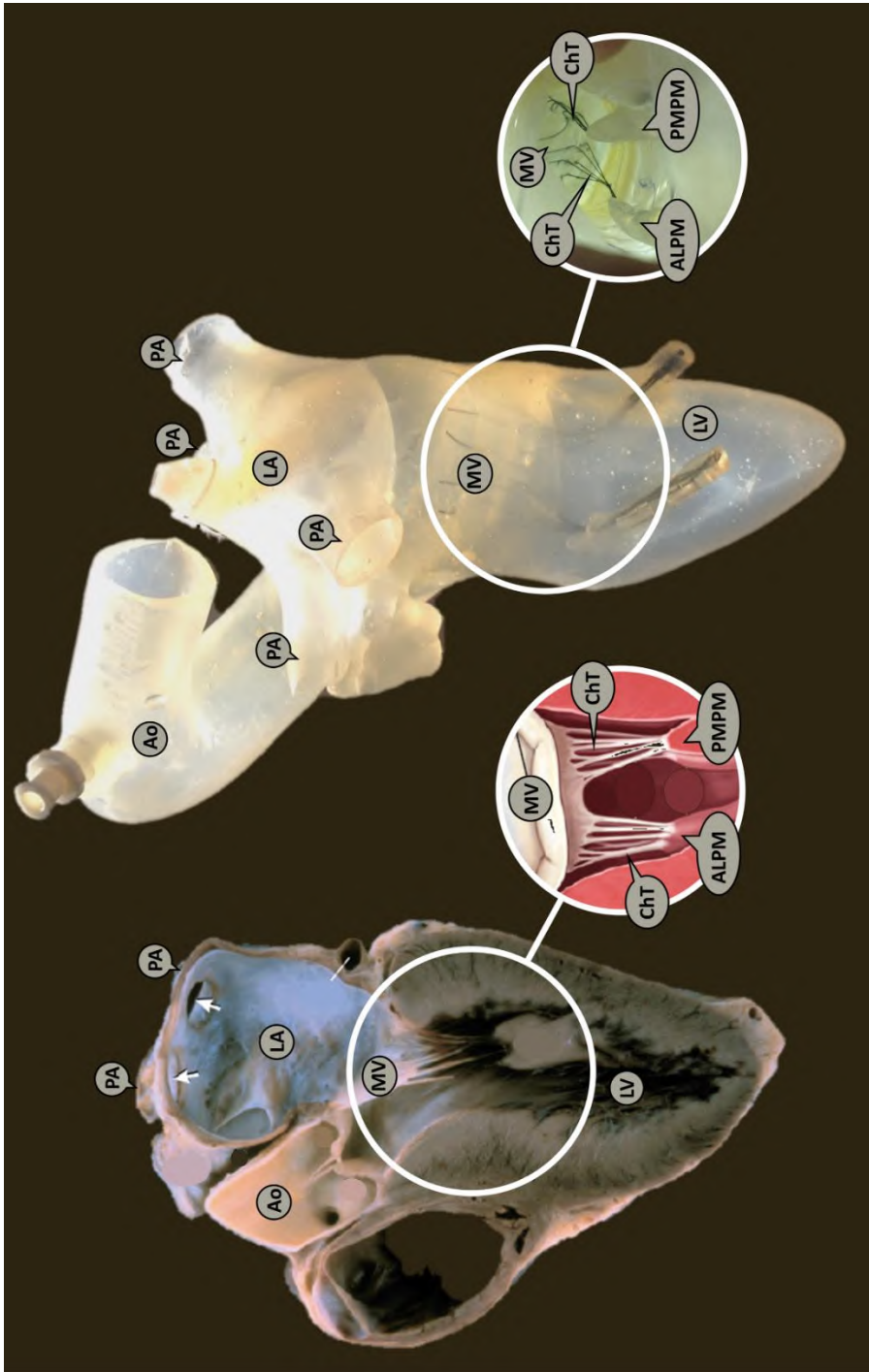


Figure 97: The components of the natural left heart (left panel) and the final LH1 model (right panel) with chordae tendineae (ChT) and pulmonary artery (PA).

10.2 REALIZATION OF THE MONOLITHIC LEFT HEART MODEL

The manufacturing of this in-vitro monolithic left heart model is a complex task as it requires taking into account a combination of critical fabrication criteria. First, the relatively complex shape of the left heart is a difficult aspect in the context of generating a monolithic model. Second, integrating the mitral valve model in this monolithic left heart model is not straightforward because it simultaneously requires an accurate positioning, a flexible annulus and valve plane suspension, as well as a firm attachment to the surrounding components. Moreover, also the chordae tendineae need to be firmly attached to the left ventricular wall via the papillary muscles. In this section, we describe the method we developed to realize this functional left heart model while accounting for these criteria.

A schematic overview of the fabrication procedure of the left heart model is presented in Table 4 and Figure 98. In short, this procedure involves eight steps which will be further discussed in detail in the subsequent section. First, a 3D solid heart model has been created from actual medical images (STEP 1). Next, the geometries of the left atrium and left ventricle were extracted by means of CAD (Computer-aided design) software (STEP 2) and subsequently *3D printed* (STEP 3). These printed models were then used to produce silicone molds (STEP 4) which served later in the process for creating hollow wax models (STEP 5). These models then functioned as sacrificial cores, which were fabricated by a *rotational molding* technique. After that, we manually positioned the MV model between the two wax models of the left atrium and left ventricle. In this way, a matching LA-MV-LV set was formed by the unique fit between the different parts (STEP 6). Next, while the whole assembly is kept in fixed position, the left heart assembly was coated by a number of silicone layers until the required thickness is achieved (STEP 7). During the silicone curing periods, the model was consequently exposed to a quasi-random three-dimensional rotation in order to obtain uniform layer thickness, using a custom-made rotation system specifically built for this purpose. These silicone layers covered the left atrium as well as the left ventricular wax models, hence representing the left atrium and left ventricular walls of the final model. These silicone layers also merge with the annulus of the MV model, hence resulting in a monolithic, flexible left heart model. Finally, after the silicone coatings were fully cured, the sacrificial cores were carefully broken into small pieces and subsequently removed from the silicone model (STEP 8). The remaining result is a flexible thin-walled model of the left heart, ready for the next phase, which is the connection with the ViVitro system. In the following paragraphs, we provide more details on this eight-step manufacturing procedure.

Fabrication procedure of the one-piece flexible LH1 model

STEP 1	Create a 3D solid heart model based upon actual medical images.
STEP 2	Extract the geometries of the left atrium and left ventricle by means of CAD.
STEP 3	3D print the left atrium and left ventricle CAD models.
STEP 4	Produce silicone molds from these prints.
STEP 5	Create hollow wax models of the left atrium and left ventricle by rotational molding.
STEP 6	Manually positioned the MV model between the two wax models to form a matching LA-MV-LV set.
STEP 7	Coat the left heart assembly by a number of silicone layers to form the one-piece left heart model. During the silicone curing, expose the coated assembly to a quasi-random three-dimensional rotation.
STEP 8	Carefully crush the sacrificial cores into small pieces and subsequently remove these from the silicone model.

Table 4: Fabrication procedure of the LH1 model.

10.2.1 Preparation of the CAD heart model

STEP 1 – To obtain an anatomically accurate model, we sought for a virtual 3D heart geometry, acquired by the detailed processing of medical images obtained by CT or MRI scanners. The Zygote 3D heart model (Zygote Media Group Inc., UT, USA) was considered the best option for providing the geometry of the left heart model in our study. This virtual model of an entire heart was developed from CT (GE Light Speed 64 slice) data from a healthy, middle-aged Caucasian male. Acquisition and reconstruction of the data was performed during 70% diastole. The model contains a smoothed heart shape, while keeping relevant anatomical structures, such as the auricles and papillary muscles, making it most interesting for our study. This virtual model was made commercially available for use in SolidWorks (Dassault Systèmes SolidWorks Corp., Concord, MA).

STEP 2 – Starting from this Zygote heart model, we used SolidWorks to extract LA, MV and LV geometries of the left heart, according to the following protocol. First, the blood cavity of the left heart is extracted, consisting of the LA and LV cavities which, at this point, forms one single part. Then, this part is divided into two parts by a Boolean subtraction by the mitral valve MV1, which results in the left atrial and ventricular (including the aorta) cavity geometries. This way of defining the geometry is of importance later in the production process to realize an accurate position of the left atrium and ventricle together with the mitral valve model in between. It should be emphasized that because the focus of this study is on mitral valve

modelling, we did not model a nature-like aortic model. Instead, we made use of a mechanical prosthetic aortic valve for the experiments. Finally, the CAD files of the left atrium and left ventricle were converted to an STL format and were sent to the 3D printer Objet 3D PolyJet (Objet Eden 350V, Stratasys Ltd., Rehovot, Israel).

10.2.2 Production of a sacrificial core by rotational molding

STEP 3 – The manufacturing of the mold was realized in three steps. First, the virtual models of the left atrium and ventricle were 3D printed into solid objects using the Objet 3D PolyJet (Objet Eden 350V, Stratasys Ltd., Minnesota) using a layer thickness of 16 μm (*high quality* modus). Second, the printed parts were carefully taken off the building platform of the 3D printer. Support material (i.e., jelly material providing spatial support while 3D printing) was removed by a high pressure water cleaner (Powerblast, 20-120 bar, Balco, UK). Finally, support material residuals were removed by chemical and ultrasonic cleaning (Sonic Industrial Bath, Alpha, Ghent, Belgium).

STEP 4 – Subsequently, we realized the fabrication of the silicone molds of the left atrium and the left ventricle (including the aortic arch). For this step, the 3D printed parts were suspended in an open box with a distance of 2 cm from the walls and from the bottom. A two- component Silicon (Essil 291, Axson Technologies, Saint-Ouen-l’Aumône, France) was then poured into the box, until the whole model was immersed for 2 cm. Next, air inclusions were removed by placing the box in a vacuum system (MCP 4/01, HEK-GMBH, Lübeck, Germany). After the silicone was cured, the silicone block was taken out of the box and was subsequently divided by means of a surgical scalpel, according to well-specified incisions. The 3D printed parts were carefully taken out and the silicone block was assembled back together to provide a casting mold. In this casting mold, a runner was included to allow wax casting.

The selection of optimal incisions to open the silicone block has been of utmost importance, especially for attaining models of complex geometries, such as the left heart. On the one hand, the incisions needed to be long enough to smoothly remove the 3D printed parts. Also, these incisions must allow to smoothly remove, after wax casting, the fragile hollow wax parts without breaking them. Thus, the more complex the casting parts are, the more section lines are needed to allow a successful extraction. On the other hand, the incisions and the according section lines needed to be confined enough to permit a tight-fitting reassembling of the silicone mold. It is of vital significance that the different parts of the silicone block fit well together in order to restore the mold in its original shape. Shifting of the different parts of

the mold relative to each other may lead to geometrical defects of the internal cavities and the resulting casted product. Moreover, attention needed to be directed to the fact that section lines in the silicone mold would result in scars on the casted model. In order to take into account these prerequisites, we opted to only apply partial cuts, so that the silicone mold remained in one piece at all times. In this way, section lines could be limited in length and the correct reassembling of the silicone mold is enhanced. For the left atrium silicone mold, the silicone block was cut according to one section line, first going along the aortic arch, then via the mitral annulus and the left ventricle and towards the apex. Whereas for the more complex LV-aorta part, the silicone mold was provided with two section lines, the first going along the four pulmonary veins and the second first along the auricle and then towards the mitral annulus.

STEP 5 – The next step involved the fabrication of the hollow wax replicas. After the silicone mold is opened and the printed parts are removed, the mold is folded back in its original position. Then, a limited fraction of heated wax is casted into the mold. Immediately afterwards, the mold is subjected to a three-dimensional rotation which causes the melted wax to cover the complete wall surface of the internal mold cavity. During this process, liquid wax solidifies and forms a hollow wax replica of the mold's internal geometry. Finally, after the solidification is complete, the wax part is carefully removed from the mold.

Two critical parameters in the process of hollow wax replica production are worth mentioning: (1) the wax casting temperature, and (2) the liquid wax volume fraction. Wax casting temperature is inversely related to the wax viscosity and hence determines the coating behavior. Obtaining a careful balance between these two parameters has been a challenge. On the one hand, higher casting wax temperatures lead to lower wax viscosities and bring about local lower wall thicknesses during wax solidification. This results in regional fragility of the hollow wax model, rendering the model susceptible to cracking when it is taken out of the mold. On the other hand, lower wax casting temperatures lead to higher wax viscosities, higher wall thicknesses, and a shorter solidification time. Too short solidification times lead to uncoated regions, which finally result in incomplete hollow wax parts. An optimal temperature results in a wall thickness that is high enough to keep the hollow wax model intact during removal from the silicone mold and small enough to allow the crushing and removal of the wax model from the final silicone left heart model (see STEP 6-8). In this study, wax (Green Casting Wax, Kerr Ltd, Peterborough, UK) is heated to 85°C and casted into the mold (at room temperature 21°) with liquid wax volume fractions of 50 and 70 ml for the left atrium and left ventricular models, respectively.

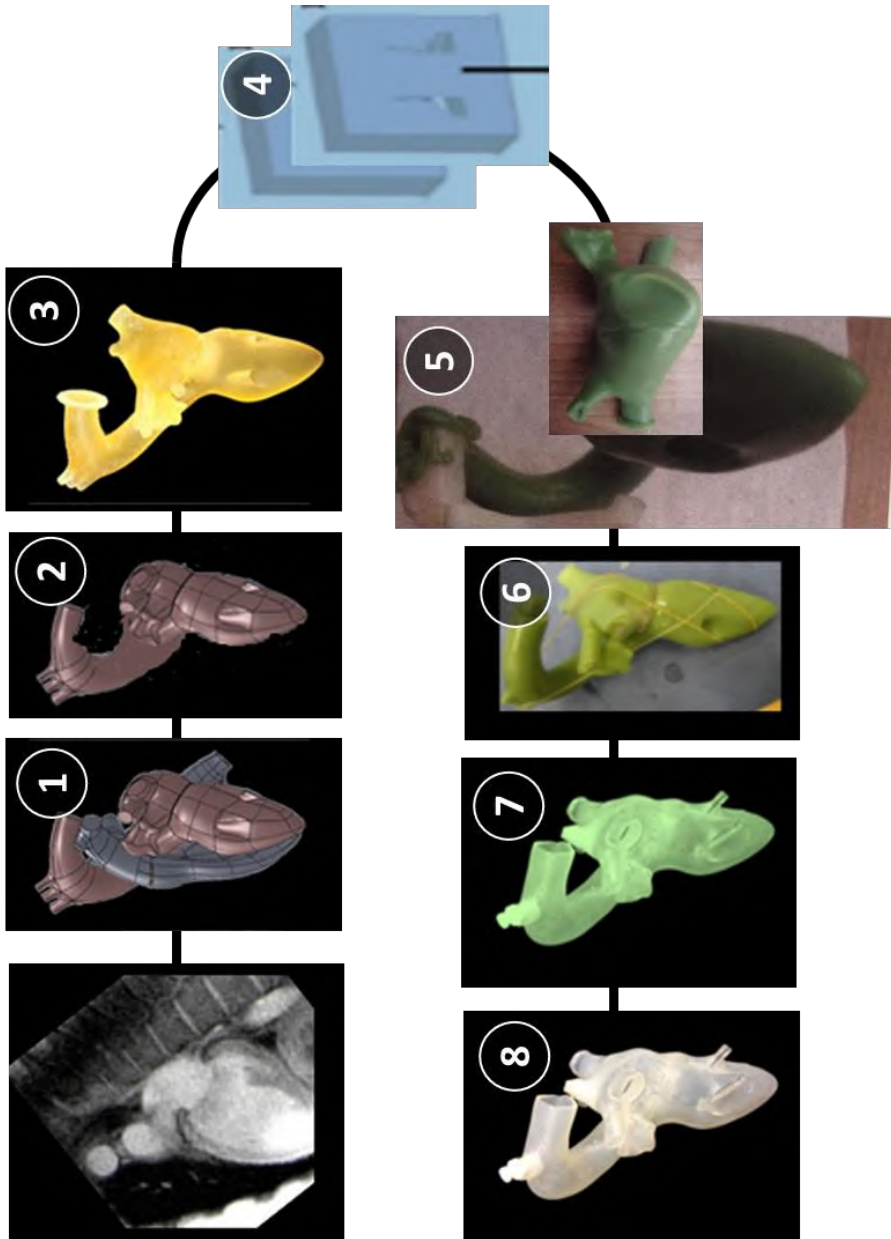


Figure 98: Schematic overview of the manufacturing procedure of the LH model: 1) the creation of a virtual 3D model from medical images, 2) the extraction of the left atrial and ventricular cavities using CAD (Computer-aided design) software, 3) the building of the physical left heart parts using 3D printing, 4) the production of the silicone molds, 5) the fabrication of the wax replica of the 3D printed parts with rotational molding, 6) the assembly of LV, LA and MV, 7) the creation of the thin-walled flexible left heart model by a custom-made rotation system, and finally 8) the removal of the wax cores to obtain the flexible thin-walled, monolithic left heart model.

10.2.3 Creation of the left heart model and integration of the mitral valve model

The creation of the thin-walled flexible left heart model is finalized in STEP 6 to 8. First, the thin-walled wax replicas of the left atrium and the left ventricle are assembled together and the mitral valve MV2 (as described in more detail in Chapter 8) is carefully positioned in between these two wax replicas (STEP 6). Then, the actual left heart model is created by a silicone coating procedure (STEP 7). In a final step, the wax replicas are removed from the model (STEP 8).

STEP 6 – For the assembly of the wax replicas, the mitral valve model is first mounted on top of the left ventricular wax replica and the connection of the chordae tendineae with the corresponding papillary muscles is realized. The chordae tendineae of the MV model (MV1, as described in Chapter 8) are first brought into the wax left ventricular wax model at MV tip region and then brought out back again at the corresponding papillary muscle end region. In our model, we equally divided the chordae tendineae over the two papillary muscles. After the careful positioning of the MV model, the left atrial wax replica is mounted on top of the mitral valve-left ventricle-assembly. A proper orientation of these three parts is achieved by the mutual unique fit which is set during the CAD design process. In order to keep these matching parts in position during the further process, we provided a local silicone sealing at the mitral annulus region. Subsequently, Luer fittings are attached to the wax replica assembly at the aortic arch, left atrium and left ventricle positions.

STEP 7 – After this local silicone coating, the complete left heart assembly is ready for a global coating. This process will then lead to the creation of the left atrium and ventricular walls of the final model. First, the left heart hollow wax assembly is fully submerged in silicone (HT 33 Transparent, Zhermack SpA, Italy) and is subsequently subjected to a slow 3D random rotation to enhance uniform layer thickness. This procedure is repeated until the required thickness is achieved. For our model, three layers are applied which corresponds to a global wall thickness of the model was 1.0 ± 0.3 mm. For the realization of this slow and controlled rotational motion, a custom-made rotating system (Figure 99) was built [195]. Hereby, the randomized rotation was approached by a gear ratio of 16/25 (two times) which requires 625 rotations before getting back in its original position.

STEP 8 – When the silicone coating process is finished, the thin-walled wax replicas are crushed inside the silicone model. The crushed wax can then be carefully removed from the silicone left heart model via the aorta and

pulmonary vein holes, hence accomplishing the flexible thin-walled model of the left heart.

10.2.4 Model realizations

The final result, the monolithic flexible left heart model, is further illustrated in Figure 100, this shows the model in five positions while it is rotated around the left ventricular long axis and provides a view on the different features that are incorporated in the model. Figure 101 is a picture taken from the inside of the left ventricle. This picture clearly shows the attachment of the mitral valve model leaflets to the papillary muscles via the chordae tendineae.

In this final model, we achieved a global wall thickness of the model of 1.0 ± 0.3 mm. However, higher and lower values are observed for local convex (up to 5 mm) and concave regions (down to 0.3 mm), which is inherent to the rheological characteristics of unpolymerized silicon. The thinner regions were locally provided with extra silicone layers to achieve the global wall thickness.

Overall, these results show that the described eight-step production process is successful in producing a monolithic, flexible, and geometrically complex model of the left heart.



Figure 99: Custom-made rotation system: left panel CAD design, middle panel realization and right panel reduction and gears.



Figure 100: The flexible monolithic LH1 model is demonstrated in different positions.

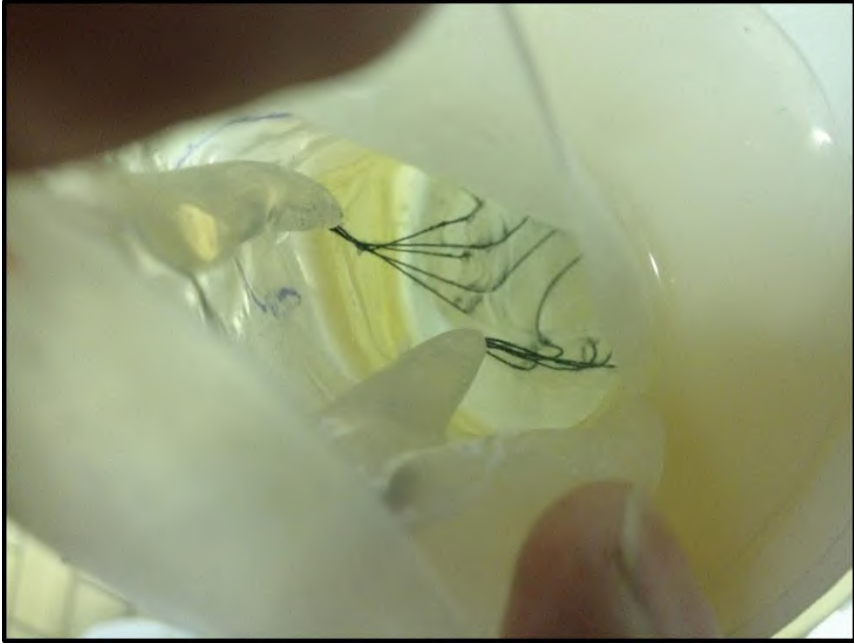


Figure 101: Attachment of the chordae tendineae of MV2 (Chapter 8) to the papillary muscles of the LH1 model.

10.3 CONNECTION WITH THE ViVITRO SIMULATOR

To turn the anatomically correct left heart model into a functional pumping chamber, it was connected to an actuator system as well as to a mock circulatory loop, in order to simulate the left heart function. We chose to incorporate our left heart model into an existing heart simulator, the ViVITRO Pulse Duplicator (ViVITRO systems Inc., Victoria, BC, Canada). As described in Chapter 2 (Figure 32), the ViVITRO cardiovascular simulator is an FDA approved and widely used cardiovascular simulator which is commonly used for the testing of cardiovascular devices [82, 83, 104, 105, 120]. The system is available in our lab and was used in our study as a testing platform for the testing of our new left heart model. The connection of our left heart model with the ViVITRO system is realized at (1) the pump system, (2) the venous, and (3) the arterial regions. Before we describe how our new model is connected, we explain how these connections have been worked out for the original ViVITRO system. Then, we describe how we designed and developed a new suspension system, enabling a functional fit between the new left heart model and the ViVITRO simulator.

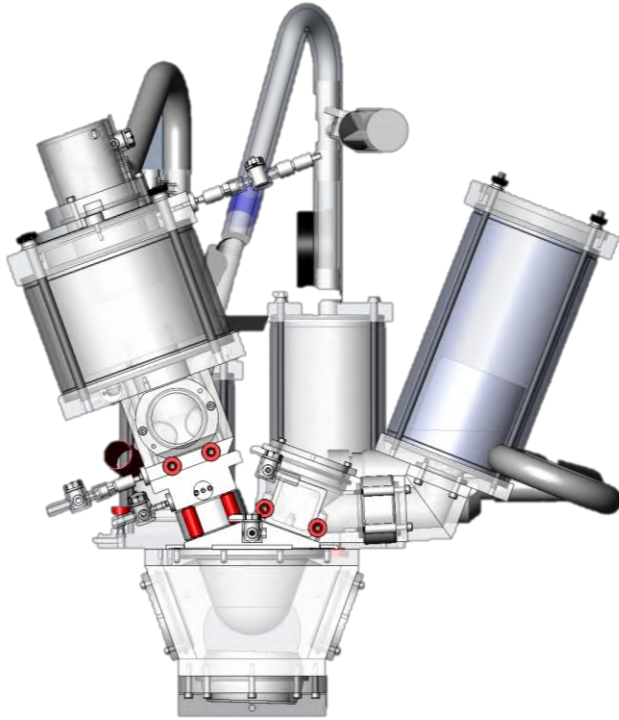


Figure 102: The ViVitro left heart model and components of the mock loop. Adapted from [196].

10.3.1 Configuration of the original ViVitro suspension system

The original ViVitro's suspension system design is based upon three crucial design criteria (DC). First, a durable connection of the left heart model with the piston pump needs to assure that the system can resist the pulsatile pressures generated by the piston pump (DC1). Second, water sealing during the heart cycle needs to be guaranteed (DC2). Finally, a modular design is highly recommended (DC3). In the original ViVitro system (Figure 102), these three design criteria are fulfilled by a combination of different components.

As depicted in Figure 114 (top panel), the original ViVitro-ventricular model (5) (a simple silicon bag, as described in Chapter 2) is suspended in the hydraulic chamber (4) and fixed by the rigid valve plane (6). This left ventricular model is made of a flexible material (Silicone Rubber Type GE/Bayer #LIM6040 D2 900) and is equipped with the integrated O-ring (5) which is positioned between the hydraulic chamber, the rigid valve plane, and the ventricular base ring (6). The watertight sealing is realized by a tightening

of eight screws (2). This results in a downwards displacement of the four ventricular base clamps (3) and of the rigid valve plane, but also a squeezing of the O-ring (shown in the orange zoomed view). This type of sealing avoids leakage between the mock loop and pump circuit fluids.

10.3.2 Design and realization of a new suspension system

In order to enable the integration of our new left heart model into the existing ViVitro simulator, the design of a new suspension system was required. Therefore, we specified three additional design criteria. A first design criterion (DC4) is that the new suspension system should account for patient-specific geometries of the new left heart model. This geometry comprises a more complex shape and hence also a greater challenge to attain a durable suspension and an overall water tightness during testing. A second design criterion (DC5) is that the new system should be fully compatible with the ViVitro simulator, so that the modifications of the experimental setups (and the conversion to the ViVitro original configuration) are straightforward and easy. Finally, as a third added design criterion (DC6), we specified the valve plane with flexible properties to be compatible with the mitral valve model which is featured with a flexible annulus. Table 5 summarizes the original ViVitro as well as our newly developed design criteria for the design of the new suspension assembly.

Following these six design criteria, we designed and developed a new suspension system that enabled a functional fit of the left heart model and the ViVitro simulator. As depicted in middle panel of Figure 114, this new system consists of six components which are assembled in the following manner. First, a customized sealing ring (6) (shown in the orange zoomed view) and the ventricular base ring (7) are positioned into the hydraulic chamber of the ViVitro system (5). Then, the left heart model, including the suspension upper (1) and the suspension lower (8) plates and the suspension flexible plate (2) sandwiched in between, is placed on top of the sealing ring. Finally, the compression ring (4) (which is a substitute for the four ventricular base clamps of the ViVitro left heart model) is mounted on top and secured by eight screws (8).

Each of these components features specific functionalities in order to meet the complete set of design criteria. In this section, we describe in more detail what the specific challenges (and solutions) were to fulfill the six design criteria.

Design Criteria (DC) of the suspension assembly for the connection to the ViVidro pump system	ViVidro System	Left Heart Model
DC1 To enable a durable connection of the left heart model with the piston pump	v	v
DC2 To guaranty watertightness during the heart cycle	v	v
DC3 To be modularly designed to straightforwardly allow setup changes	v	v
DC4 To be adapted for a patient specific geometry as well as radial contraction		v
DC5 Setup conversion to its original configuration need to be straightforwardly		v
DC6 The flexible properties of the valve plane need to be maintained		v

Table 5: A summary of the design criteria for the suspension system of the original ViVidro system and the LH1 model.

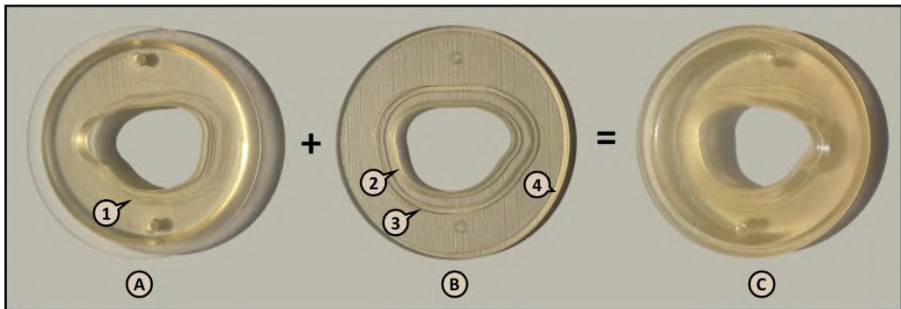


Figure 103: The upper (A) and lower (B) rigid suspension plates are equipped with opposite extensions (1-3) to ensure a durable connection with the flexible LH1 model. These two parts are placed on top of each other (C) and sandwiches the flexible material of the left heart. Also, the upper suspension plate is equipped with a circular extension (4) which pressurizes the O-ring part of the sealing ring.

The first design criterion (DC1) ensures a durable connection of the left heart model with the piston pump in order to resist the pulsatile pressures that are acting on the left heart model and the suspension plates. In this process, two key aspects are involved. A durable suspension should be realized by a strong connection between the left heart model and the suspension plates (DC1.1), and by restraining model displacements due to the pulsatile pressures (DC1.2). In our newly built suspension system, we realized DC1.1 by means of a mechanical anchoring of the flexible plate. This flexible

plate (see (2) of Figure 114, middle panel) is sandwiched between the upper and lower suspension plates (see (1) and (8) of Figure 114, middle panel). This is realized by designing the CAD model of the lower suspension plate with two extensions (thickness 0.5 mm, width 2 mm and shaped with an offset to the left ventricular model of 3 and 11 mm, respectively), while the upper suspension plate is provided with one extension (thickness 0.5 mm and an offset of 7 mm), as depicted in Figure 103 and Figure 104. These opposite extensions are gripped into corresponding cut-outs of the flexible plate and, in this way, realizes a durable sealing. In addition, we realized DC1.2 (limited displacements of the suspension plate) by selecting a relatively rigid plate material (Objet VeroWhite, Stratasys Ltd., Minnesota - tensile strength 58 MPa and modulus of elasticity 2500 MPa), and sufficient wall thicknesses of the suspension plates (set to 8 mm for the upper plate and to 3 mm for the lower plate). The above described local plate-extensions additionally benefit the plates' stiffness, because they function as local reinforcements. During the experiments, with normal values of pressure (80-120mmHg) and cardiac output (5.6 l/min), maximal suspension plate displacements of only 2 mm were observed.

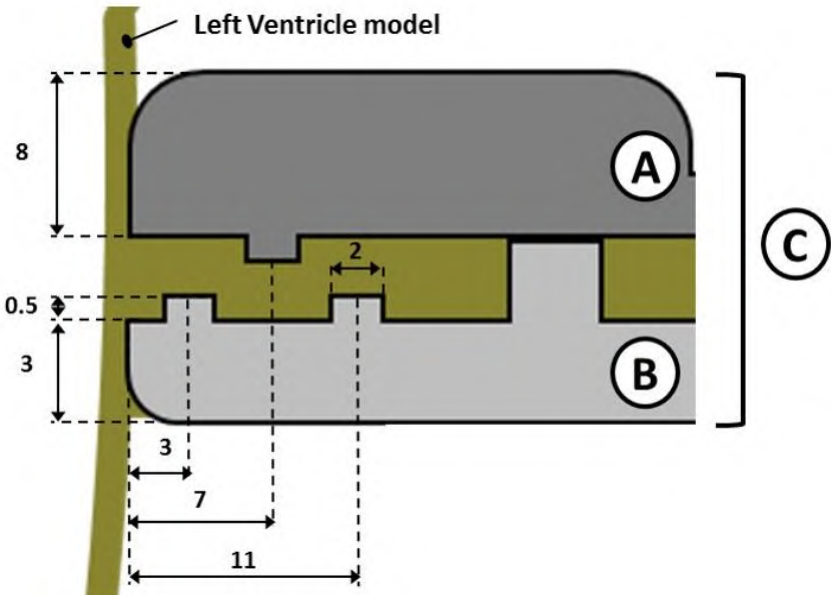


Figure 104: Dimensions of the LH1 suspension system (C) including the upper (A) and lower (B) rigid suspension plates and the flexible plate in between (green) which is joined with the left ventricle model.

The second design criterion (DC2) comprises durable watertight sealing. In the suspension assembly, this should be realized at three levels: between the hydraulic chamber and the lower suspension plate (DC2.1), between the suspension plates and the flexible plate (DC2.2), and between the flexible plate and the left heart model (DC2.3). This was realized as follows. First, we used a similar sealing between the hydraulic chamber and the lower suspension plate (DC2.1) as the original of the ViVitro system between the hydraulic chamber and the valve plane: eight screws are tightened and hence are pushing the connection plate towards the transparent ViVitro box. As depicted in Figure 105, the geometry of the sealing ring in our suspension model is identical to the ViVitro ventricular model (also shown in Figure 84), apart from the ventricular part which is excluded in our model, and is also equipped with an integrated O-ring. We also designed the CAD model of the lower plate with a circular extension (identical to that of the ViVitro valve plane, see Figure 114) which then compresses the O-ring part of the sealing ring. By doing this, the actual sealing is realized. Second, a durable sealing between the suspension plates and the flexible plate (DC2.2) is based on a watertight bond which is created during the production of the flexible plate. This bond is realized by applying the liquid state silicone the suspension plates which makes the silicone to adhere to the suspension plates. Third, a durable and watertight sealing between the flexible plate and the left heart model (DC2.3) is realized by a local 2 mm thick silicon layer between these parts. This local widening of the left heart at the valve plane region affects the suspension plates' dimensions, so this aspect was already taken into account during the CAD design phase and the value of 2 mm was set by trial and error during the prototype phase. This tight adhesion of the flexible plate to the left heart model was realized by using the same type of silicone material of the left heart model (HT 33 TRANSPARENT, Zhermack SpA, Italy).

The third design criterion (DC3) refers to the modular design. Thanks to this newly designed suspension system configuration, (dis)assembly and setup modifications are straightforward.

The fourth design criterion (DC4) implies the compatibility with patient-specific geometries. The newly designed suspension system accounts for this criterion because patient-specific geometries are applied for (1) the inner opening of the suspension upper, lower and flexible plates, and (2) the corresponding extensions. 3D print technology allows for a straightforward way of manufacturing these models including patient-specific geometries.

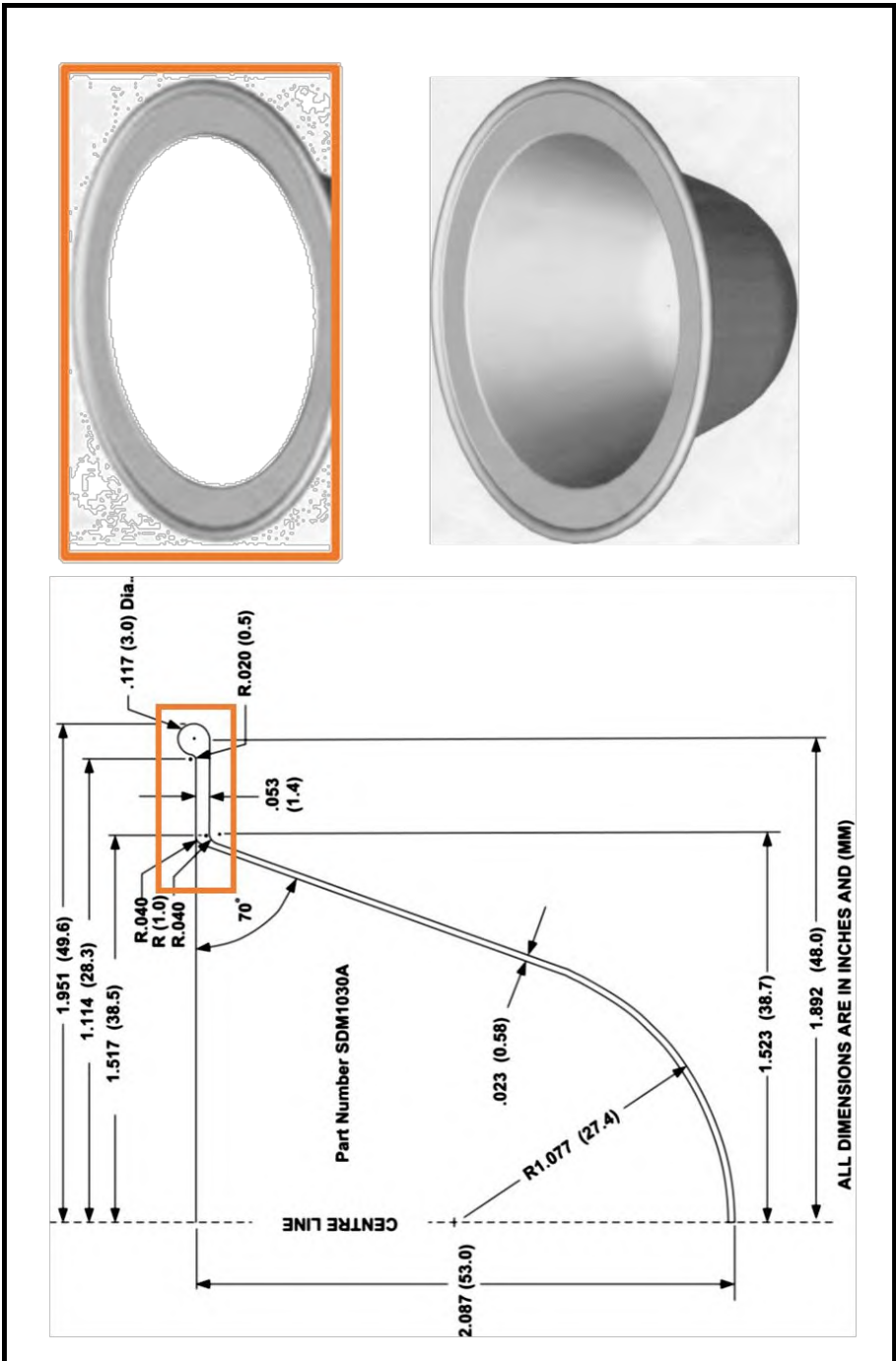


Figure 105: Customized sealing ring (left bottom) is equipped with an integrated O-ring and a flat part. Its geometry is based on that of the ViVibro left ventricular model (left upper and right) [124].

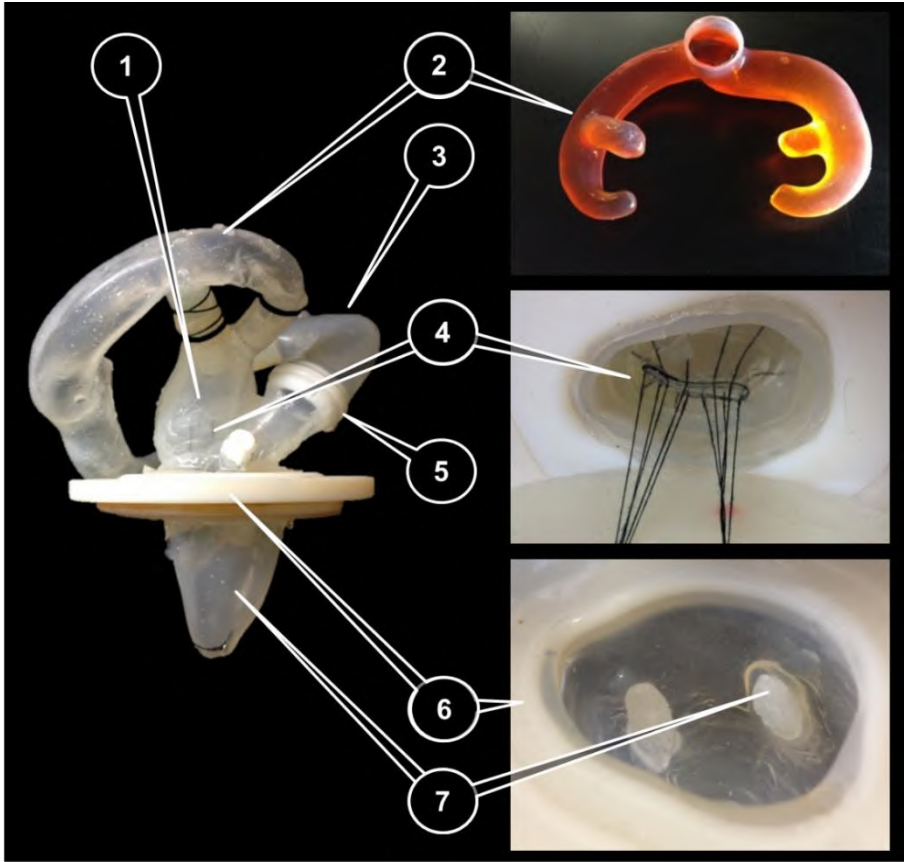


Figure 106: This figure shows the LH1 model including the suspension system (6) and the venous site adapter (2). More details are given such as the LA (1), the aorta (3), the mitral valve (MV1) (4), the aortic valve (5), and the LV model including the papillary muscles (7).



Figure 107: Incorporation of the mechanical bi-leaflet aortic valve into the aorta by a 3D printed valve plane ring (white).

The fifth design criterion (DC5), a straightforward conversion of the modified set ups to the original ViVitro set up, is realized by tuning multiple part dimensions of the new system to correspond with the original ViVitro parts, such as the O-ring, the lower plate circular extension and the position of the eight holes in the left heart compression ring for the screws. In addition, original parts of the ViVitro system (Figure 114) are integrated as much as possible, such as the hydraulic chamber, the eight screws and the ventricular base ring. Switching between the new and the ViVitro's original configuration (see also DC5) is possible within half an hour.

Finally, the sixth criterion (DC6) is to maintain the flexible valve plane properties. In our suspension model, we opted to suspend the left heart model not at the level of the left heart base, but at a slightly lower level (offset of 10 mm from the original valve plane, in the direction of the LV long axis and towards the apex).

10.3.3 Connection to the ViVitro mock circulatory loop

Subsequently, as shown in Figure 106, the LH1 model with its newly developed suspension system (6) is connected to the ViVitro mock circulatory loop via a *venous site adapter* (2) which functions as a manifold given that its geometry is designed to smoothly distribute the flow from the ViVitro atrial reservoir to each of the four pulmonary vein entrances of the left atrial model. Analogous to the other flexible parts of the LH1 model, this part is made of a silicone material (HT 33 TRANSPARENT, Zhermack SpA, Italy). The production process of the manifold proceeded in a similar fashion as the fabrication process of the left heart model, as described in § 10.2. This venous site adapter is also applied for the LH2 model of the next chapter.

10.4 EXPERIMENTAL TEST SETUP

As shown in Figure 108, the experimental setup consists of the new left heart model, which is mounted into the ViVitro cardiovascular simulator (StarFish Medical, Victoria, B.C.) based upon the new suspension system and connecting procedure described in § 10.3. This new left heart model also incorporates a flexible polymeric mitral valve model in addition to a bi-leaflet mechanical aortic valve. More details about the mitral valve model development and initial testing is described in Chapter 8, while its integration into the left heart model is explained in § 10.2.3. The mechanical aortic valve is placed into the flexible aorta and kept in position by a custom made 3D printed valve plane ring, as illustrated in Figure 107.

The ViVITro system includes a Superpump and a ViViGen Waveform Generator (Vivitro Systems Inc., Victoria, B.C.) to drive the test liquid through the mock loop. The programmable waveform of the generator is set to the standard wave form ‘FDA’ with a 35/65 systole/diastole ratio. Physiologically normal values are set for arterial pressure (120/80 mmHg), for stroke volume (80 ml), and for heart rate (70 bpm). Arterial pressure was measured using a pressure transducer delivered with the ViVITro system (Deltran® Pressure Transducer Model PT43-604, Utah Medical Products, Inc.).

To check the proof of concept, the left heart model is subjected to a test of 4200 beats (1 hour) under these conditions. The test fluid within the mock loop is a blood analog consisting of a 30/70% glycerin/water mixture ($\rho = 1060 \text{ kg/m}^3$ and $\mu = 3.5 \text{ mPa}\cdot\text{s}$ at room temperature). Echographic investigations are performed using a Vivid 7 system (GE, Vingmed, Horten, Norway).

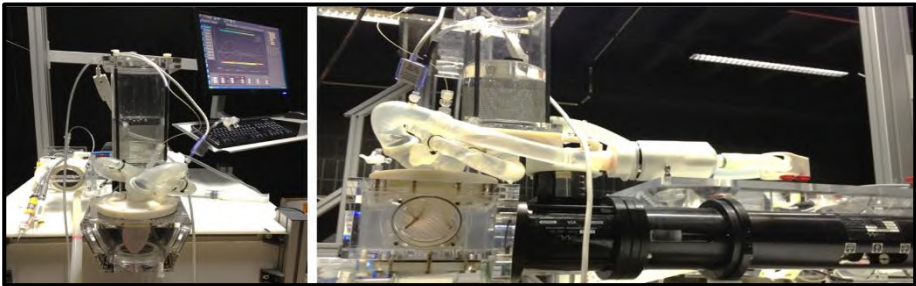


Figure 108: Experimental setup of the LH1 model which is built into the ViVITro system.

10.5 PRELIMINARY RESULTS

Our experimental results show that this novel left heart model is able to generate realistic data in terms of end-systolic volume (54 mL) and pressure (120 mmHg), end-diastolic volume (134 mL) and pressure (80 mmHg), stroke volume (80 mL), ejection fraction (60 %), mean outflow (5.6 L/min) and heart rate (70 bpm). This test also confirmed that the newly developed suspension assembly enabled a proper connection of the left heart model with the rigid parts of the ViVITro system, while maintaining the flexible properties of the left heart features, such as the mitral valve annulus. During the experiments, we noticed a maximal up and downward displacement of the suspension system valve plane of about 2 mm. Also the mitral valve model functions well in terms of durability (at least 4200 beats) under normal conditions, given that

there were no signs of mitral valve prolapse nor chordae tendineae or leaflet rupture.

In addition to the hydrodynamic performance, the echocardiographic examination of the left heart model (Figure 109 left panel) shows relatively good similarity to the anatomy of a human left heart (Figure 109 right panel), such as the left ventricular wall and the anterior (AML) and posterior mitral valve leaflets (PML). Also, the anterolateral papillary (ALPM) and posteromedial papillary muscles (PMPM) are visible during this examination. The color Doppler measurements of our model (Figure 110) also exhibit vortex formation during filling, which is also observed in a natural heart. In the in-vitro model, the test fluid flows from the atrium through the mitral valve and enters the left ventricle towards the probe (red region) and makes a 180° turn at the apex level and flows away from the probe (blue region) towards the aortic valve.

In general, these preliminary experimental and echocardiographic results support the proof of concept of the newly developed models of the left heart, mitral valve, and suspension system. Moreover, relatively realistic hydrodynamic performance results and similarities to human physiology are obtained.

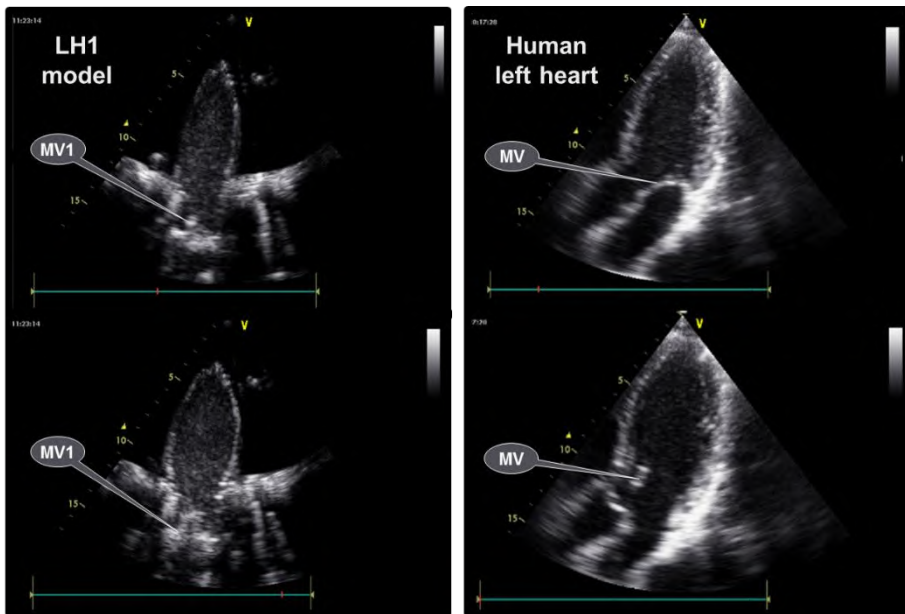


Figure 109: At the left side, the results of an echocardiographic examination is shown of the LH1 model, that incorporates the physiologically normal-like mitral valve model (MV1) at the time of end systole (top) and end diastole (bottom). For the purpose of comparison, results of a healthy human left heart (male, 32 years old) are depicted at the right side.

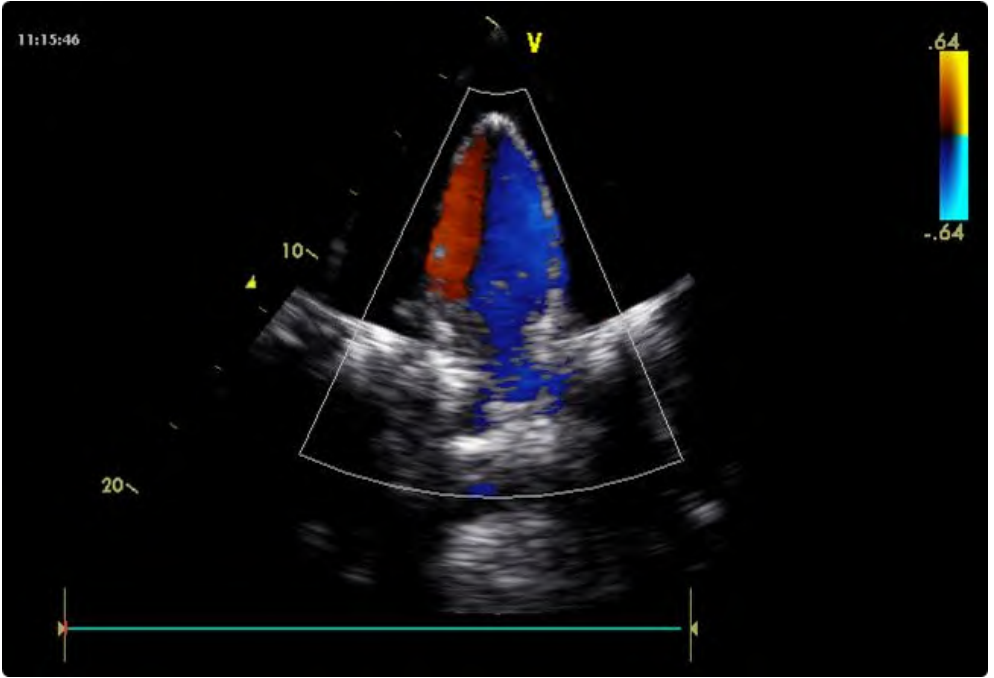


Figure 110: Color Doppler measurements of the LH1 model at the time of ventricular filling. Blue colors represent blood flowing towards the probe, while red colors correspond to blood flowing away from the probe.

10.6 DISCUSSION AND CONCLUSION

In this chapter, we elaborated on the design and development of the innovative monolithic left heart model LH1 that incorporates the flexible fiber-based mitral valve model MV2 (Chapter 8). Next, we described the design and development of tailored suspension and connection systems that enabled the integration and experimental testing of the left heart model with the ViVitro mock circulatory loop. Finally, we reported preliminary but promising results of our left heart model based upon hydrodynamic and echocardiographic measurements.

Overall, this novel approach of left heart modelling more closely approximates real anatomic features in multiple ways. Firstly, the geometry of the in-vitro left heart model is based on medical images from a real heart, and includes the left ventricle, left atrium and the aortic arch, but also more detailed features, such as the auricle and the entrances of the four pulmonary veins. Secondly, the previously described mitral valve apparatus MV2 (Chapter 8) has been integrated into the model, which adds even more anatomical-like structures (PG6a-e). Thirdly, the left heart model is made of

silicon and fiber materials to mimic the mechanical as well as the ultrasonic characteristics of the biological soft tissue of the heart. Fourthly, the innovative production process enabled the realization of this complex model in one single piece, resulting in a more anatomical-like and compact left heart model and discarding the need to connect components, which often introduces rigid zones and structures into the model. Fifthly, the newly developed suspension system ensures compatibility with a standard (Type I) cardiovascular simulator, while preserving its flexible appearances and the complex anatomical-like shape of the valve plane region (**PG7**). Finally, the preliminary benchtop experiments show that (1) the model is able to generate normal values of left heart performance, (2) the structures are visible using ultrasound, and (3) the model generates physiological-like intraventricular flow patterns that can be observed via color Doppler. Taken together, these multiple strengths of our integrative monolithic approach can be considered as a significant step forward in in-vitro modelling of the left heart.

10.7 LIMITATIONS AND FURTHER DIRECTIONS

Despite the aforementioned substantial strengths, the current approach is still subject to certain limitations that should be addressed in future research. A first limitation of our approach lies in the modelling of the papillary muscles. In reality, papillary muscles vary in the number of heads and exact position in the ventricle and are generally categorized in two main groups comprising the anterior and posterior papillary muscles. In this study, these two groups were simplified into only one head. Also, the active papillary muscle contractions of the real heart are not taken into account in the current approach.

A second limitation relates to the left heart model's geometry. Although the LH1 model geometry is unique as it is based on real medical images, it should be noted that a rather global smoothed geometry of the Zygote CAD-model stood model for the in-vitro replica. This eliminates smaller anatomical details which may have an effect on the intraventricular blood flow patterns. Therefore, a more anatomically correct geometry is still desirable in future research in order to attain a more accurate approximation of interventricular blood flow patterns by the integration of rough trabeculae structures.

A third limitation pertains to the integrative, all-in-one character of the model. As the left heart model is made in one single piece, it has the disadvantage that replacing defect parts or components is not possible. Instead, the whole model needs to be replaced. Nevertheless, it can be noted that the direct 3D printing of sacrificial cores makes the building of a new model much more straightforward.

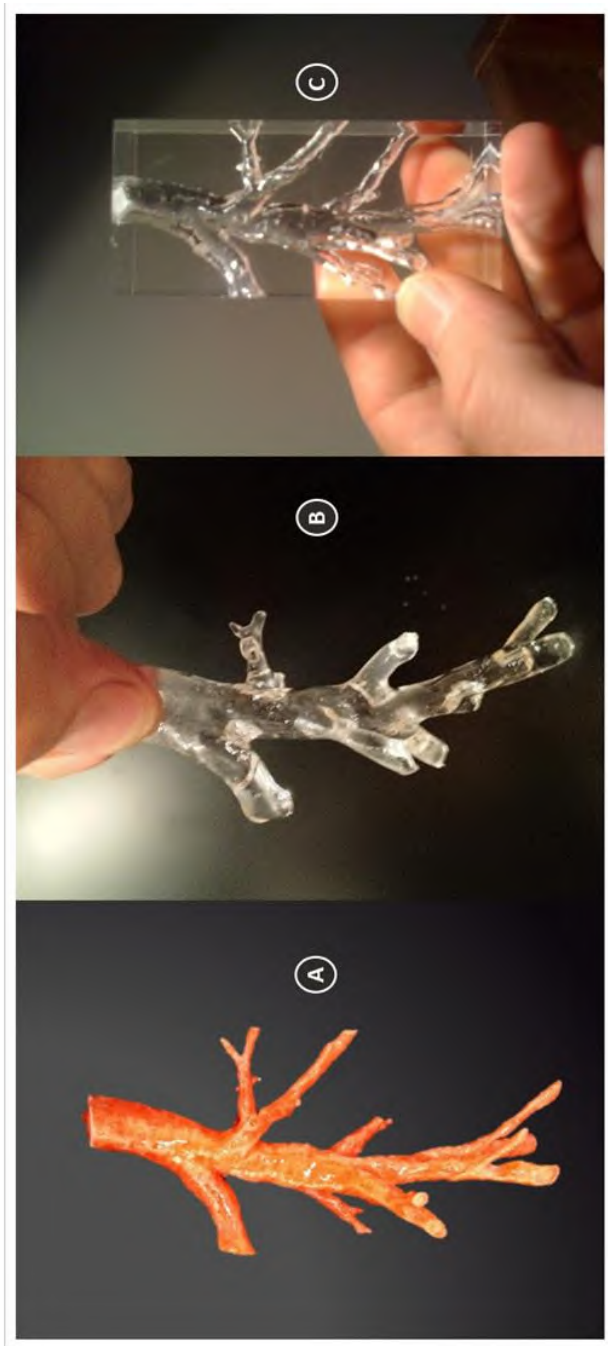


Figure 111: Starting from a 3D printed kernel (A), flexible thin-walled (B) and rigid transparent highly detailed models (C) are realized of the upper human airways. The red appearance of the kernel is due to the pigmented PVA coating to facilitate kernel removal and optimize surface smoothness.

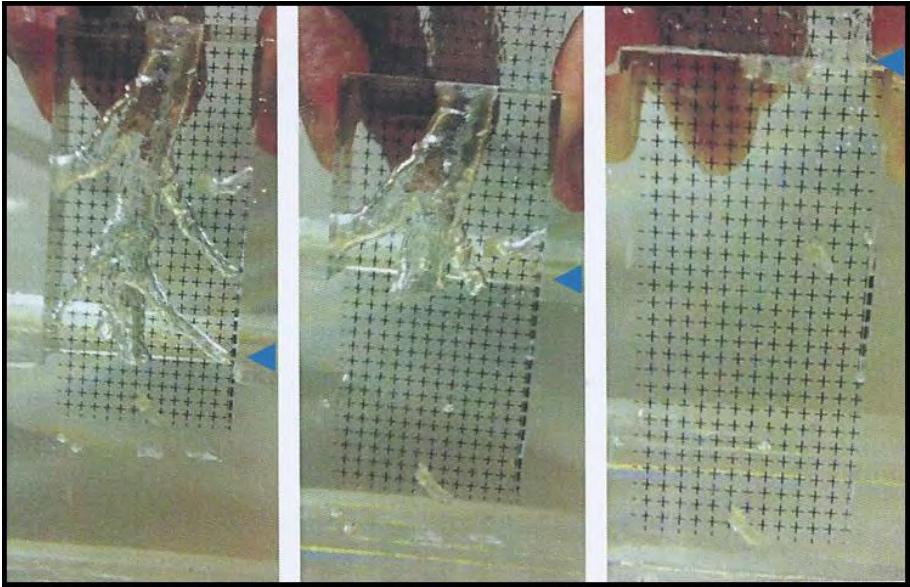


Figure 112: The PMMA model visually disappears when submerging it in a refractive index matched fluid. A transparent film with cross marks is placed at the backside of the model to check optical refraction. The blue arrow indicates the liquid level.

A fourth limitation concerns the fabrication process. Even though the currently applied fabrication techniques enables the modelling of more anatomical details, two major limitations can still be noted: (1) part of the production process still depends upon manual techniques, hence reducing geometrical accuracies, and (2) the production of the sacrificial cores by wax casting into silicone molds also poses limitations to the geometrical complexity. In future work, higher anatomical detail and geometrical accuracy is likely to be obtained by skipping intermediate steps in the production process. In this regard, we started developing a new technique to 3D print cores in a more direct manner by using a PolyJet 3D printer (Objet Eden 350V, Stratasys Ltd., Minnesota). In short, this technique can be described as follows. While in the current study, the objects are first 3D printed as solid pieces that then serve to produce the silicon molds to ultimately attain the wax sacrificial cores, the new technique aims to directly print the objects as thin-walled (0.3 mm) objects. Because the 3D printer is programmed to support the actual part by providing support material beneath over-heeling part sections, closed thin-walled objects will be filled up - by default - with support material. In this way, it is possible to 3D print a sacrificial core made of a rigid shell, in combination with a soft support material (Figure 111 A). After finishing the silicone coating procedure of the sacrificial core, the support material is then easily removed, followed by the fragmentation of the thin rigid shell. By this

approach, the sacrificial core is obtained in a fully digital way (no manual actions are involved). Even more complex geometrical models can be produced and this with an ever higher accuracy. We experimented successfully with this technique to produce two patient-specific PIV compatible models of the main branches of the human airways (up to the 3rd bifurcation). The first model is a flexible thin-walled model (Figure 111 B) made of a highly transparent silicone material (Sylgard 184, Dow Corning, Midland, MI) while the second is a rigid model (Figure 111 C) made of polymethyl methacrylate (PMMA - Plexiglas). As demonstrated in Figure 112, the PMMA model visually disappears while submerging in a refractive index matched fluid (aqueous sodium iodide solution, 60% concentration) without distortion of the cross marks at the background. This preliminary result demonstrates that this technique was successfully applied to realize a PIV compatible model of the upper human airways.

Finally, the fifth and major limitation of the described left heart model is that it still does not generate a torsional motion (**PG5**). In the next chapter, we address this limitation by integrating the anisotropic left heart model introduced in Chapter 7 in our in-vitro left heart model, and, as such, enabling various left ventricular wall deformation and torsion patterns.

Modelling the left heart by a bilithic approach: Feasibility study of the effect of torsion on intracardiac diastolic pressure parameters

In this chapter, the left heart model LH1 (Chapter 10) is transformed from a monolithic to a modular bilithic model LH2, with the built-in ability to straightforwardly change different LV models. Based upon the anisotropic model LV3 (Chapter 7), different deformation patterns are modelled and related with diastolic pressure parameters in this study.

11.1 INTRODUCTION

We consider the hydraulic left heart model LH1 presented in Chapter 10 as an important step forward in accomplishing a more realistic in-vitro modelling of the left heart by implementing a patient-specific geometry, a mitral valve apparatus, and a flexible valve plane suspension. Nonetheless, looking back at the practical guidelines postulated in Chapter 3 (Table 2), one has to conclude that some essential recommendations for in-vitro model optimization are still missing. Most importantly, just like most of the current cardiovascular simulators (see Chapter 3, Table 3), the described model does not implement the anisotropic wall properties of the natural ventricular wall

(**PG2**). As a consequence, it does also not allow controlling ventricular wall deformation patterns, such as longitudinal, circumferential, and radial deformation (**PG4**). Moreover, the twisting motion (**PG5**), which is a fourth deformation pattern of the natural left heart, cannot be replicated with the previously described cardiovascular simulator.

As extensively discussed in Chapter 3 (Table 2), there remains a great challenge but also an urgent need for new left heart models to mimic global wall deformation patterns (**PG4**) and, even more, to simulate the natural torsion motion (**PG5**). The realization of these two practical guidelines for in-vitro model optimization is necessary to achieve a more accurate mimicking of the physiological events of the natural left ventricle as ventricular torsion presumably has a pivotal role for normal ventricular function. In 2011, Buckberg and colleagues wrote “Ventricular torsion and untwisting are essential for normal ventricular function and their mechanisms are related to the temporal responses of the helical and circular muscle fibers that comprise cardiac architecture” [197]. However, little is still known about the effect of LV torsion and of wall deformation on intraventricular flow patterns.

Benchmark models accounting for torsion would be very useful to reveal the role and importance of the mechanisms behind these complex interactions because of their controllable hydrodynamic conditions. However, to the best of our knowledge, no adequate left heart model including torsional motion as well as a realistic mitral valve model exists to date.

Therefore, in this chapter, we describe the development of an innovative left heart model LH2, which combines (1) the unique kinematic abilities of the anisotropic model LV3 (Chapter 7), with (2) the anatomical-like mitral valve model of Chapter 8, and (3) the suspension system of Chapter 10, allowing the connection to a well-approved standard cardiovascular simulator. Moreover, by modifying the monolithic to a modular bilithic left heart model with a separate and demountable ventricular component, we were able to build an innovative, experimental set-up enabling a comparison of five various wall deformation patterns. Two models with predominantly longitudinal or circumferential deformation, and two models with different degrees of torsion, are compared to a general model with no deformation patterns. To this end, five different ventricular models were built based upon different anisotropic properties, and mounted successively into our bilithic left heart model.

An in-vitro technique of examining blood flow patterns is PIV; however, there is no PIV compatible torsional LV model available yet. Such a model could be developed in the near future by manufacturing the LV2 model (Chapter 6) according to the procedure of the PIV compatible venous

valve model VV (Chapter 9) and will likely result in detailed insights of intraventricular flow patterns in relation to LV torsion (see § 12.2.3). Meanwhile, there are other parameters which give a more global general measure of the intraventricular flow, such as pressure differences.

As described in Chapter 1 (§ 1.2.3.1), it has been shown that pressure differences play an important role in the acceleration/deceleration of the blood flow [9, 12]. Briefly, during the early filling phase, the elastic recoil of the myocardium causes a swift drop within the left ventricle. This decrease in LV pressure causes a pressure difference [10] which begins from the LA (left atrium) and then spreads towards the LV apex [11]. This pressure difference accelerates the blood coming from the LA and causes a rapid flow which is carried on towards the left ventricular apex and then again upwards, opening the mitral valve. Therefore, this diastolic pressure difference ($p_{LA} - p_{apex}$) has been regarded as a measure of left ventricular filling [3].

In this study, two components of this early diastole pressure difference are measured, namely the transmitral ($TMPDe = p_{LA} - p_{base}$) and intraventricular pressure differences ($IVPDe = p_{base} - p_{apex}$). The exact locations of the pressure points p_{LA} , p_{base} and p_{apex} are shown in Figure 118. This chapter not only describes the design and development of this experimental design but also reports initial experimental measurements of how global wall deformations and torsion affect the transmitral (TMPDe) and intraventricular pressure differences during early diastole (IVPDe).

11.2 LEFT HEART MODEL DESIGN

In this study, we developed the LH2 on the basis of the monolithic left heart model of Chapter 10, which has the advantages that it is flexible, compact, shaped with an anatomically-like geometry and equipped with the nature-like mitral valve model of Chapter 8. Besides these features, four new features are added to the model. Figure 113 shows the design and the composition of the LV2 model.

The first added feature is the torsional motion which is realized by applying the anisotropic material properties and its accompanying twisting mechanism of the left ventricular model (described in Chapter 7) to the more anatomically-like geometry of the ventricle in the monolithic left heart model (described in Chapter 10). Multiple left ventricular models with different anisotropic characteristics were constructed to generate different wall deformation patterns (see § 11.4 for more details).

The second unique feature of this model is that we adapted our design of the monolithic approach to become a modular bilithic approach. In this bilithic model, we separated the ventricular model from the other left heart components in a modular design, to enable a straightforward switch of the different left ventricular models during experiments.

The third feature of this model is that the aortic arch of our monolithic model is replaced by the original aortic model of the ViVitro system (ViVitro Systems Incorporated, Victoria, BC, Canada) which allows a wider range of options in controlling the arterial compliance. This connection is realized by an extra part, namely the *arterial site adapter* (see Figure 113 (1)). This supports the ViVitro aortic model by two supporting pins and is also made from a rigid 3D printed material (VeroWhite, Objet Eden 350V, Stratasys Ltd., Minnesota). The venous valve site adapter is identical to the one of Chapter 10 (see Figure 113 (3)).

The final and fourth added feature of this model compared with the LV models of Chapter 7, is that we respect the physiological-like end systolic volume (ESV) value of 54 ml. This ESV is much more natural than the abnormal high value of 127 ml, which is the default setting for the original ViVitro left ventricle model which was used for the left ventricle model of Chapter 7.

11.3 LEFT VENTRICULAR MODEL DESIGN

In general, the production process of the left ventricular models for this study is strongly similar to the process used to produce the anisotropic left ventricular model of Chapter 7. However, building the patient-specific geometry and the modular composition to switch the left ventricular models implied more advanced building techniques. A comparison between the monolithic and bilithic model suspension system is illustrated in the middle and bottom panel of Figure 114, respectively. The modular, bilithic approach (Figure 114, bottom panel) is realized by separating the LV model from the left heart model at the level of the suspension system. The suspension system of the LH1 model is divided in the middle and hence consists of two flexible parts instead of one, namely an upper (2) and a lower (9) flexible plate.

11. MODELLING THE LEFT HEART BY A BILITHIC APPROACH: FEASIBILITY STUDY OF THE EFFECT OF TORSION ON INTRACARDIAC DIASTOLIC PRESSURE PARAMETERS

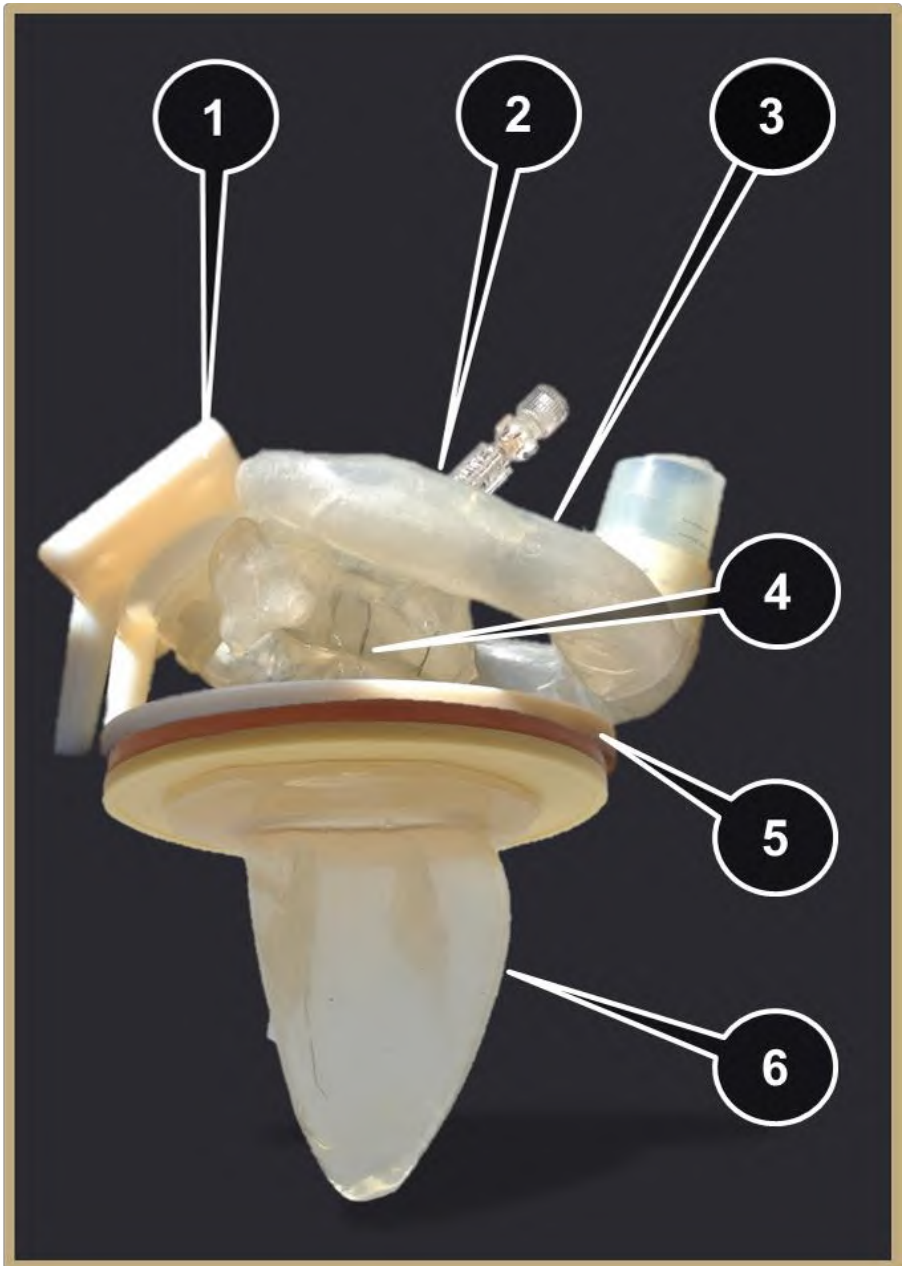


Figure 113 Design and composition of the modular LH2 model with the arterial site adapter (1), the LA (2), the venous site adapter (3) (similar to the LH1 model), the MV2 of Chapter 8 (4), the suspension system (5), and the LV model (6).

All the left ventricular models used in this study, except for the general model G (see below), are realized by a three-layer composition. The first and the third layer are made of silicone (HT 33 Transparent, Zhermack SpA, Italy) and represent the matrix fraction of the composite. These layers are responsible for the elastic properties of the left ventricular model, for the embedding of the fibers, and for the watertight barrier between the circulatory loop and the piston pump circuit. The middle layer, then, is the layer where Nylon multifilament yarns are inserted to mimic the function of cardiac muscle fibers. The arrangement of these fibers determines the direction in which wall deformation is constrained.

The production process of such a left ventricle model incorporates the following steps. First, the suspension lower plate (8) and ventricular kernel are 3D printed in a rigid material (Objet FullCure®720, Stratasys Ltd., Minnesota) and subsequently positioned with a mutual offset of 2 mm. Then, silicone is poured out over the left ventricular kernel. This forms the first layer of the left ventricular model as well as the lower flexible plate (9). These steps are also applied for the creation of the suspension upper plate (1) and the upper flexible plate (2) which are attached by the silicone to the left heart model. To avoid air bubbles during the curing process, the system is exposed to vacuum conditions. Subsequently, polymer filament yarns are moistened with silicone and imposed onto the first silicone layer. The placement of these filaments proceeds according to the required fiber pattern. This fiber pattern is designed during the CAD process and implemented into the 3D printed ventricular kernels in the form of small cut-outs, which are then visualized by ink to enhance correct positioning of the fibers according to the method described in Chapter 7 (see Figure 87). Also for the realization of this second layer, vacuum conditions are applied during silicone curing to eliminate air inclusions between the fiber filaments. Afterwards, the third layer is applied by pouring out the silicone mixture, for the second time, to make the different components a whole. This pouring not only fully embeds the polymer fibers but also makes strong connections with the first layer as well as with the suspension lower plate. Finally, after the curing of the silicone, the ventricular kernel is removed from the ventricle model. To enhance loosening and surface smoothness of the left ventricular kernel, we made sure the left ventricular kernel has been coated with polyvinyl alcohol (PVA). The reference model, model G, is fabricated in the same manner, except that it doesn't include the middle layer (i.e., no polymer filaments).

11. MODELLING THE LEFT HEART BY A BILITHIC APPROACH: FEASIBILITY STUDY OF THE EFFECT OF TORSION ON INTRACARDIAC DIASTOLIC PRESSURE PARAMETERS

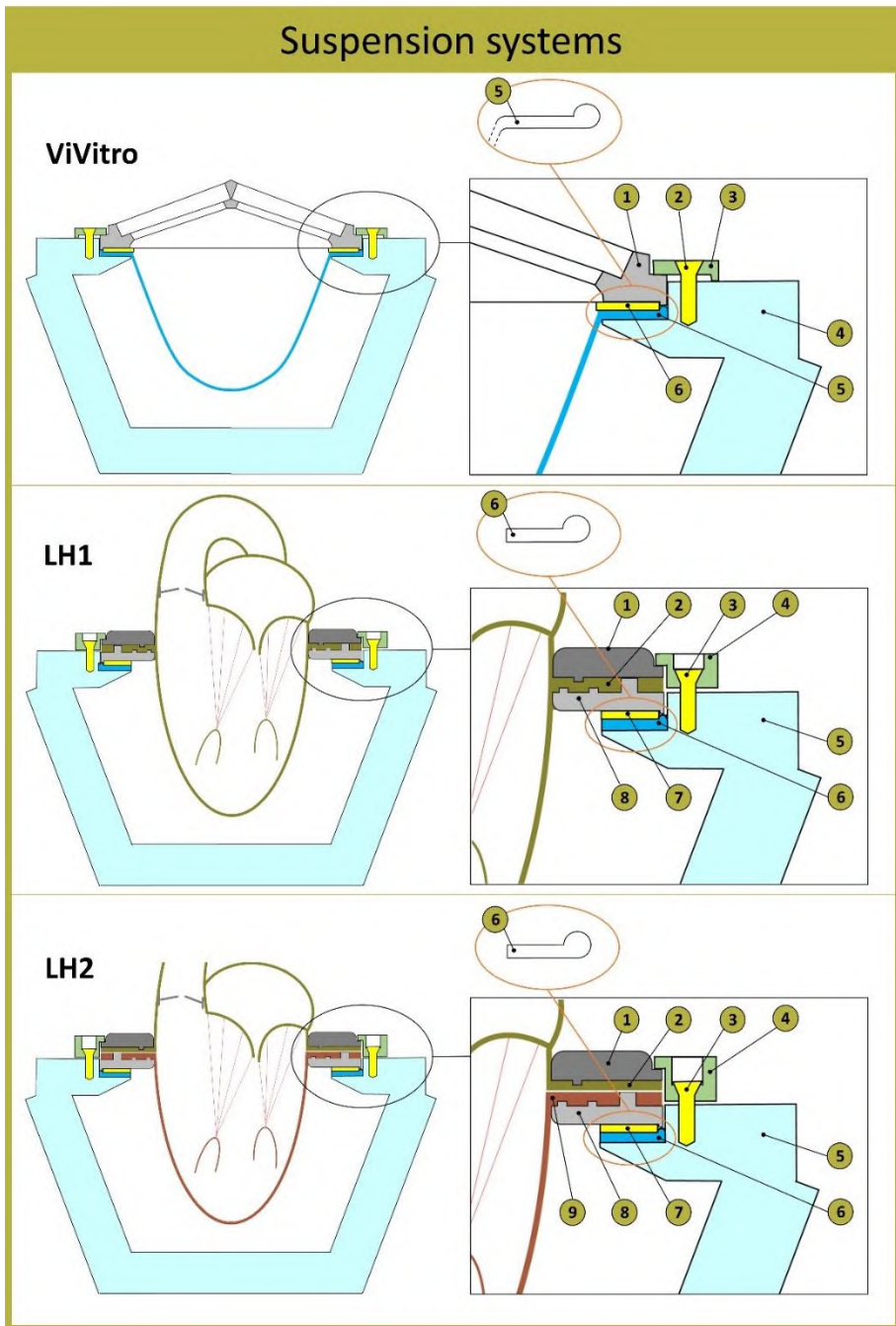


Figure 114: Design (left side) and suspension systems (right side) of the ViVitro system (§ 10.3.1) and left heart models LH1 (§ 10.3.2) and LH2 (§ 11.3). See text for explanation of the numbers.

11. MODELLING THE LEFT HEART BY A BILITHIC APPROACH: FEASIBILITY STUDY OF THE EFFECT OF TORSION ON INTRACARDIAC DIASTOLIC PRESSURE PARAMETERS

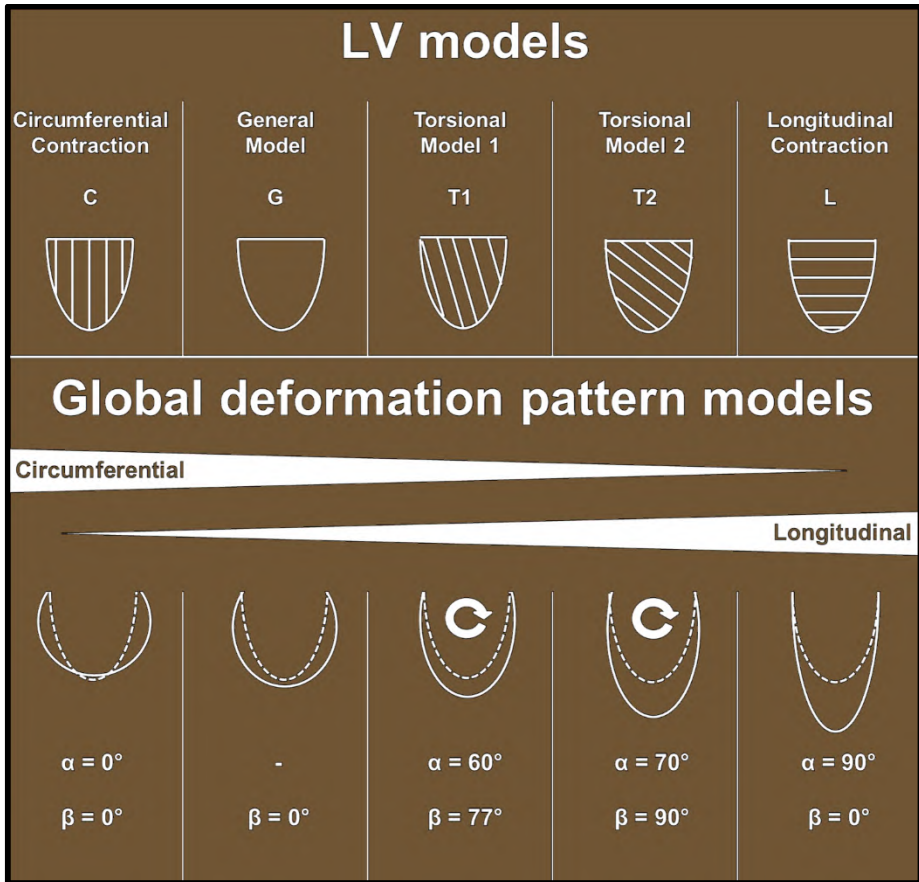


Figure 115: Design of the five LV models and the corresponding expected global wall deformation with α , the fiber angle (with respect to the LV long axis) and β , the torsional angle.

11.4 EXPERIMENTAL PROTOCOL

Five different left ventricular models are mounted into the left heart model: a General model (G), a Longitudinal deformation (L), a Circumferential deformation (C), and Torsional models 1 (T1) and 2 (T2). The design of the models is illustrated in Figure 115, while the actual models are shown in Figure 116 (front view) and Figure 117 (top view). The L and C models include fibers with an orientation angle of 0° and 90° with respect to the left ventricular long axis, resulting in a predominantly longitudinal and a circumferential deformation pattern, respectively. The Torsional models 1 (T1) and 2 (T2) are also equipped with fibers, but with a fiber angle of 60° and 70° , resulting in a torsional motion of 77° and 90° , respectively, and both in a combination of longitudinal as well as a circumferential deformation

11. MODELLING THE LEFT HEART BY A BILITHIC APPROACH: FEASIBILITY STUDY OF THE EFFECT OF TORSION ON INTRACARDIAC DIASTOLIC PRESSURE PARAMETERS

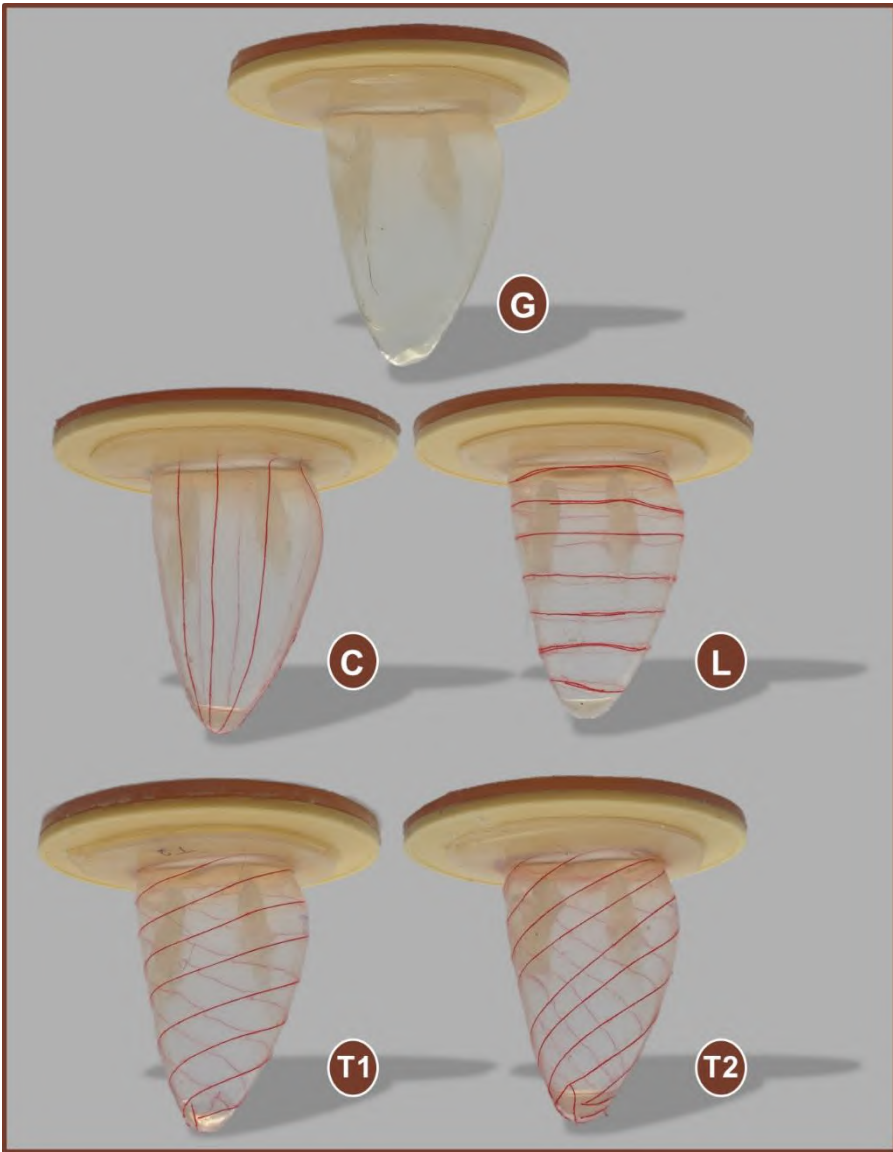


Figure 116: Front view of the five LV models: the General model (G), the Longitudinal deformation (L), the Circumferential deformation (C), and the Torsional models 1 (T1) and 2 (T2).

patterns. As already noted, model G is the reference model in our study and does not contain any fibers. This latter model can be considered as similar to the typically existing cardiovascular simulators, except that this model includes the papillary muscles, has a more nature-like anatomic geometry, and a smaller and more realistic ESV. All the five left heart models are mounted on the same upper part of the left heart model. This upper part is equipped with a modified version of the mitral valve MV2 of Chapter 8. This valve was modified due to mitral valve model repair after leaflet rupture (caused by erroneous overloading in previous experiments). This modification results in higher values of transvalvular pressure differences in comparison with the mitral valve MV2 described in Chapter 8, and therefore, the mitral valve model of this study resembles a stenotic-like valve type.

Each model is tested in a circulatory mock loop similar to the experimental setup described in Chapter 10, with three different heart rhythms (HR = 50, 65 and 80 bpm) and stroke volumes (SV = 50, 65 and 80 ml). End systolic (ESP) and end diastolic pressure (EDP) are kept constant to about 80 and 120 mmHg. The test fluid within the mock loop is a blood analog consisting of a 30/70 % glycerin/water mixture ($\rho = 1060 \text{ kg/m}^3$ and $\mu = 3.5 \text{ mPa}\cdot\text{s}$ at room temperature). Left atrial and left ventricular pressures are measured by a Mikrotip® intravascular dual pressure transducer (SPR-721, Millar Instruments, Houston, TX, USA) and the aortic pressure by a pressure transducer of the ViVitro pressure measuring system (Deltran® Pressure Transducer Model PT43-604, Utah Medical Products, Inc.) at a sample rate of 200 Hz. Torsional angles are acquired by video recording (30 frames/second) of a marker at the model's apex.

In this study, early diastolic pressure differences are measured at two positions, as depicted in Figure 118. For the first set of experiments, TransMitral Pressure Differences (TMPDe) are measured, whereas for the second set of experiments IntraVentricular Pressure Differences (IVPDe) are measured. TMPDe is defined as $p_{\text{atrium}} - p_{\text{base}}$ (Equation 1, see § 1.2.3.1) whereas IVPDe is defined as $p_{\text{base}} - p_{\text{apex}}$ (Equation 2, see § 1.2.3.1). During post-processing, a Savitzky-Golay smoothing filter (sgolayfilt, MATLAB) is applied for all signals (with a polynomial order 3 and a frame size of 31). Because previous studies in the literature reported an effect of IVPDe with end systolic volume (ESV) (Firstenberg et al. [24]) and with preload (Popovic et al. [198] and De Mey et al. [17]), these values are kept approximately constant in the current study. We set the ESV to 60 ml and used a relative constant water column of 15 cm (11mmHg) for the preload. Given that we mounted five different ventricular models in the left heart, and compared three heart rhythms, three stroke volumes, and two pressure measurements configurations, this study provides information about 60 experimental configurations in total.

11. MODELLING THE LEFT HEART BY A BILITHIC APPROACH: FEASIBILITY STUDY OF THE EFFECT OF TORSION ON INTRACARDIAC DIASTOLIC PRESSURE PARAMETERS

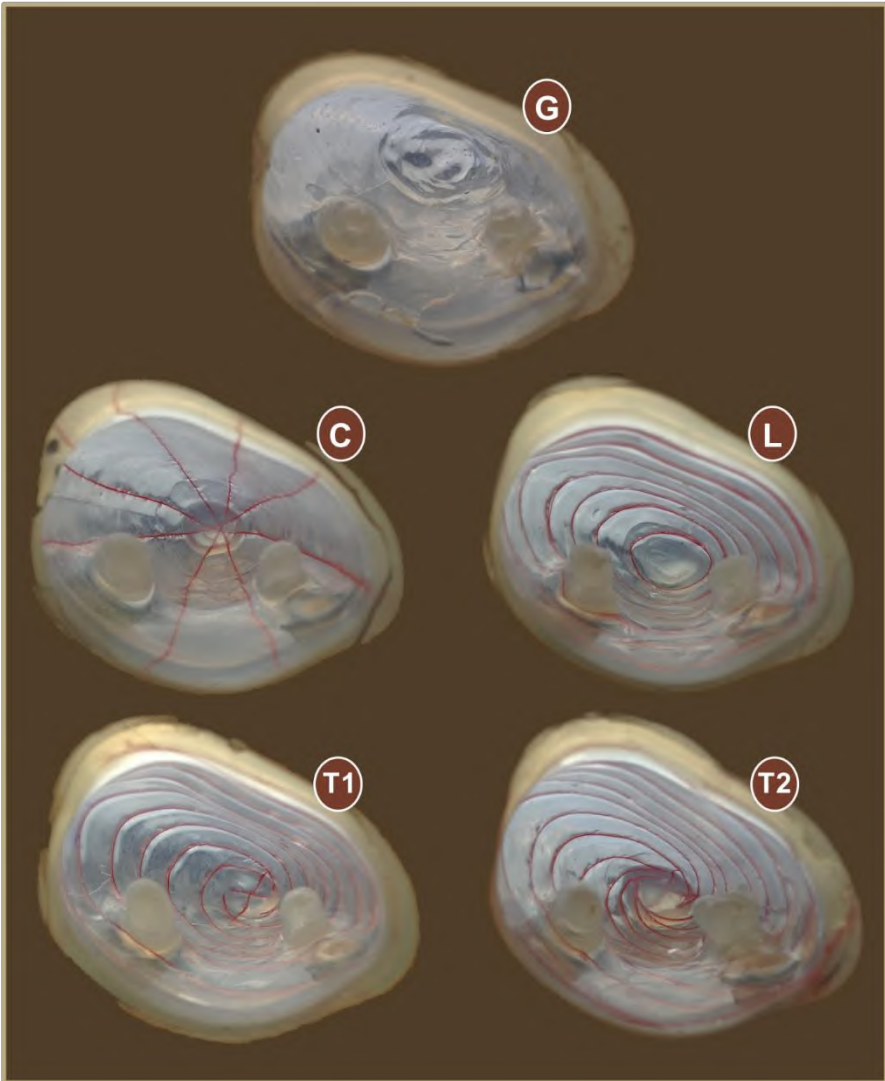


Figure 117: The five LV models shown from the inside (top view).

11.5 PRELIMINARY RESULTS

11.5.1 Transmitral pressure differences during early diastole

As shown in Figure 119 and Table 6, TMPDe values range from 9.9 mmHg for model T2 (SV 50 ml and HR 65 bpm) up to 23.8 mmHg for model G (SV 65 ml and HR 80 bpm). Compared with the reference model G, the mean TMPDe values are 2.1 %, 7.5 %, 20.2 % and 28.3 % lower for the C, L, T1 and T2 models, respectively. Furthermore, TMPDe is positively related with HR and SV.

SV	HR	TMPDe [mmHg] (SD)				
		G	L	C	T1	T2
65	50	16.4 (0.2)	14.4 (0.2)	16.2 (0.2)	12.7 (0.1)	10.5 (0.2)
	65	19.1 (0.1)	17.4 (0.3)	19.2 (0.2)	14.8 (0.3)	13.9 (0.5)
	80	20.3 (0.5)	20.3 (0.4)	20.1 (0.3)	16.7 (0.3)	14.6 (0.2)
50	50	13.3 (0.1)	12.6 (0.2)	13.9 (0.1)	10.5 (0.2)	9.9 (0.2)
	65	19.1 (0.1)	17.4 (0.3)	19.2 (0.2)	14.8 (0.3)	13.9 (0.5)
	80	23.8 (0.2)	21.5 (0.2)	21.4 (0.2)	20.1 (0.3)	17.6 (0.7)
Comparison		Reference	-7.5%	-2.1%	-20.2%	-28.3%

Table 6: Overview data of TMPDe varying SV while keeping HR constant (panel 1) and varying HR while keeping SV constant (panel 2). The mean values and SD's per model are given for TMPDe

11.5.2 Intraventricular pressure differences during early diastole

As shown in Figure 120 and Table 7, IVPDe values range from 1.0 mmHg for models G and C (SV 65 ml and HR 50 bpm) up to 3.9 mmHg for model T2 (SV 65 ml and HR 80 bpm). Table 7 also shows that, in comparison with the reference model G, the mean IVPDe values are 22.4 % lower for the C model and 6.9 %, 23.5 % and 42.3 % higher for the T1, L and T2, respectively. Furthermore, IVPDe is also positively related with HR and SV.

11. MODELLING THE LEFT HEART BY A BILITHIC APPROACH: FEASIBILITY STUDY OF THE EFFECT OF TORSION ON INTRACARDIAC DIASTOLIC PRESSURE PARAMETERS

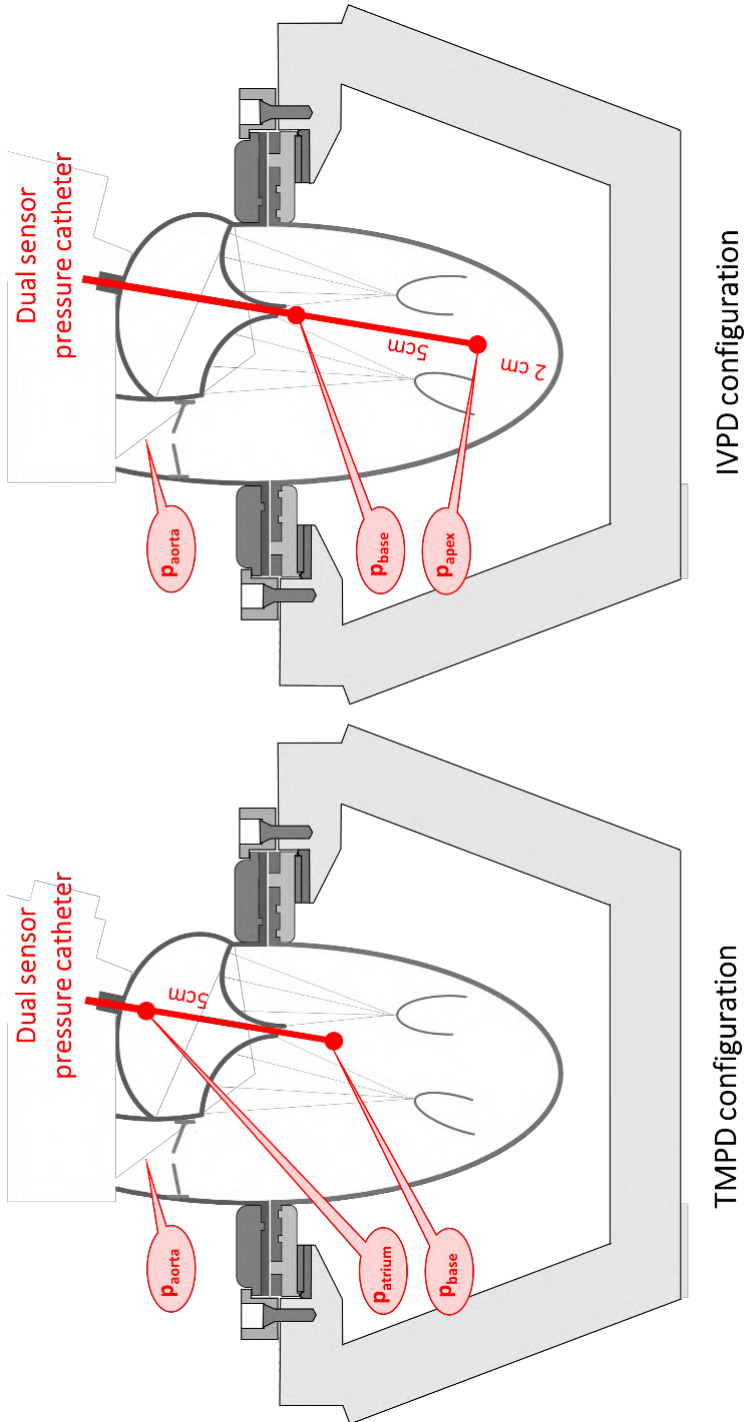


Figure 118: Position of the dual sensor catheter in the LH2 model for the transmitral and intraventricular pressure difference measurements.

11. MODELLING THE LEFT HEART BY A BILITHIC APPROACH: FEASIBILITY STUDY OF THE EFFECT OF TORSION ON INTRACARDIAC DIASTOLIC PRESSURE PARAMETERS

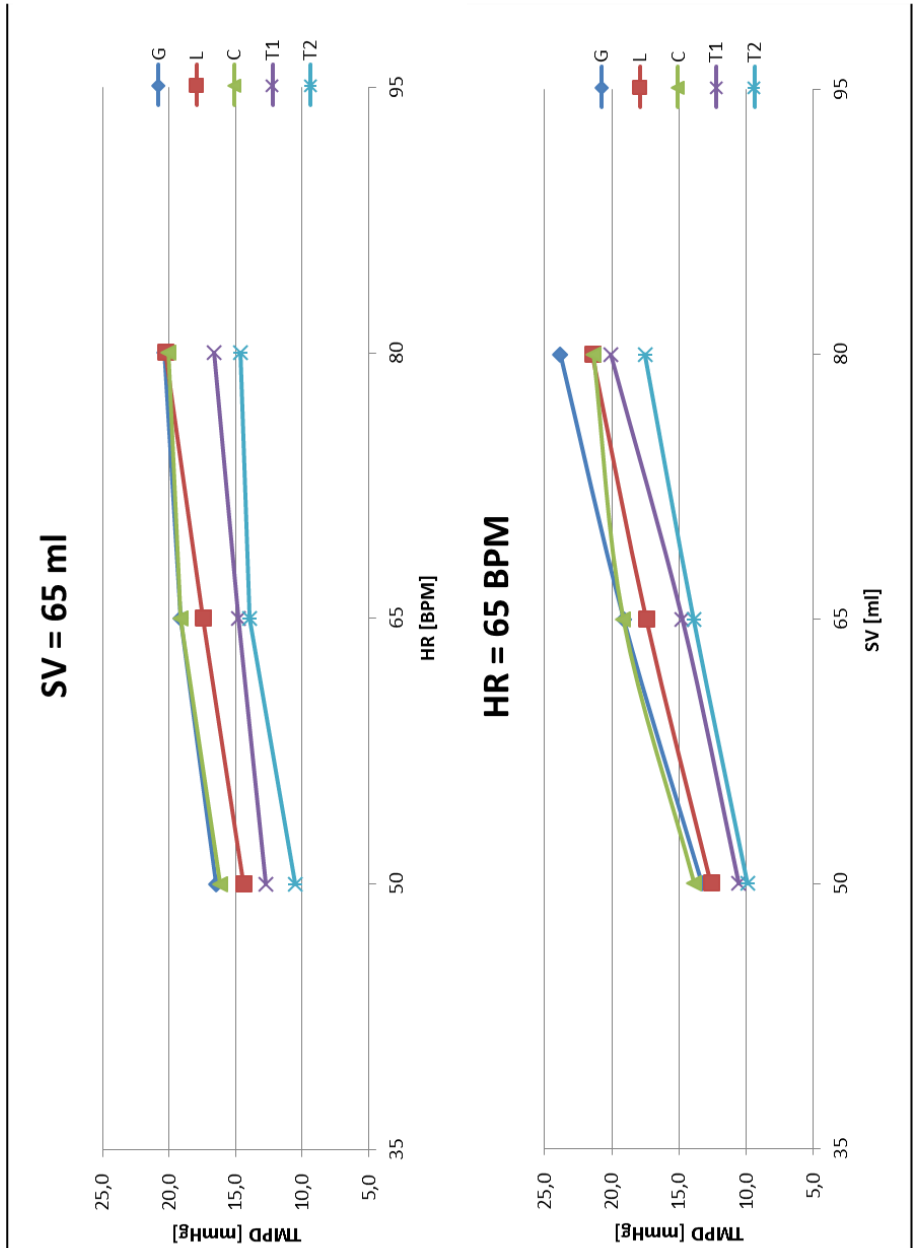


Figure 119: TMPDe values in function of SV (top panel) and HR (bottom panel)

11. MODELLING THE LEFT HEART BY A BILITHIC APPROACH: FEASIBILITY STUDY OF THE EFFECT OF TORSION ON INTRACARDIAC DIASTOLIC PRESSURE PARAMETERS

SV	HR	IVPDe [mmHg] (SD)				
		G	L	C	T1	T2
65	50	1.7 (0.1)	2.3 (0.2)	1.3 (0.1)	2.1 (0.4)	2.7 (0.2)
	65	2.0 (0.1)	2.9 (0.3)	1.7 (0.2)	2.2 (0.3)	3.2 (0.3)
	80	2.5 (0.2)	3.0 (0.4)	1.9 (0.4)	3.5 (0.4)	3.9 (0.5)
50	65	1.0 (0.1)	1.3 (0.1)	1.0 (0.1)	1.1 (0.1)	1.2 (0.1)
65		2.0 (0.1)	2.9 (0.3)	1.7 (0.2)	2.2 (0.3)	3.2 (0.3)
80		3.6 (0.2)	3.3 (0.3)	2.4 (0.4)	2.4 (1.6)	3.9 (0.4)
Comparison		Reference	23.5%	-22.4%	6.9%	42.3%

Table 7: Overview data of IVPDe varying SV while keeping HR constant and varying HR while keeping SV constant. The mean values and SD's per model are given for IVPDe

11.6 DISCUSSION OF RESULTS

Transmitral pressure differences

As anticipated, the pressure difference magnitude across the valve is dependent on the flow rate across the valve, with TMPDe increasing with higher values of HR and SV (see Figure 119 and Table 6). The magnitude of TMPDe values (about 10-24 mmHg) of this study is within the range of severe mitral stenosis (10-30 mmHg) [55], which is much higher compared to normal values (a few mmHg), which is inherent to the stenotic-like valve type model of this study as a consequence of the valve repair.

More interesting is the impact of the different wall deformation models on these pressure differences. As such, by normal conditions (SV 65 ml and HR 65 bpm) and compared with the reference model G (19.1 (0.1) mmHg), these results show that TMPDe is not significantly affected by a predominant circumferential wall deformation (model C with 19.2 (0.2) mmHg), while lower TMPDe values are noticed by applying a predominant longitudinal wall deformation (model L with 17.4 (0.3) mmHg). Moreover, higher TMPDe values are observed up to 28.3 % with increased torsional left ventricular motion (i.e., models T1 and T2).

Intraventricular pressure differences

The IVPDe values of this study by normal conditions (SV 65 ml and HR 65 bpm) vary from 1.7 (0.2) to 3.2 (0.3) and are close to the normal range of adults as reported by Rovner et al. 2.6 mmHg (0.21) [199], by Popovic et al. 2.4 (0.18) [198] and by Yotti et al. 2.5 (0.18) [200].

11. MODELLING THE LEFT HEART BY A BILITHIC APPROACH: FEASIBILITY STUDY OF THE EFFECT OF TORSION ON INTRACARDIAC DIASTOLIC PRESSURE PARAMETERS

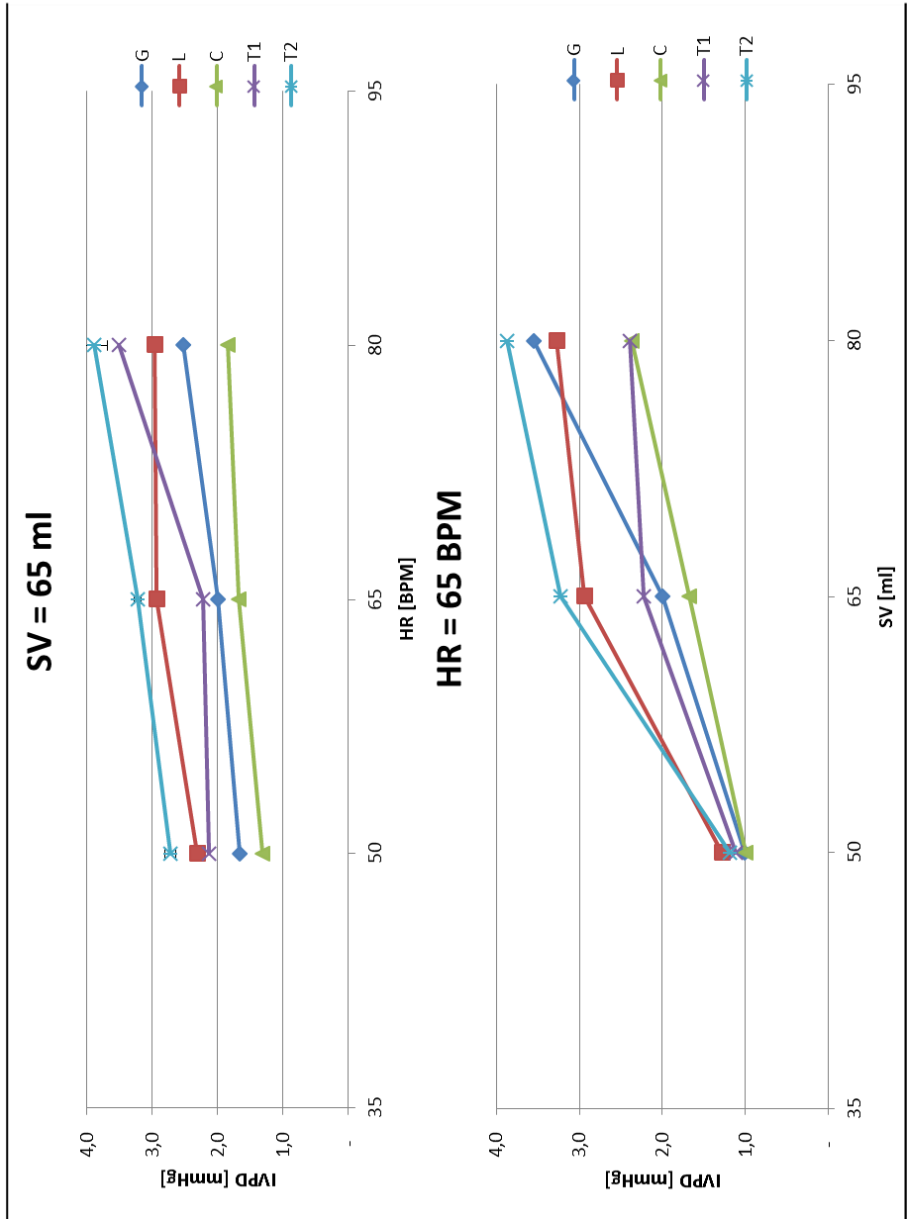


Figure 120: IVPDe values in function of SV (top panel) and HR (bottom panel)

Previous studies have shown that during infusion of isoproterenol (an agent which induces positive inotropic and chronotropic effects) the IVPDe's are accentuated [201-203]. This finding is in good agreement with the results of the present study, since IVPDe positively relates with increased values of SV (which is related to inotropy) and HR. This relation is valid across the complete set of left ventricular models.

Compared with the reference model, these results also show that IVPDe is diminished by 22.4 % for predominant circumferential deformation, while clearly augmented IVPDe values up to 23.5 % are observed by applying predominant longitudinal wall deformations (exclusive torsion).

Moreover, an even stronger augmentation of IVPDe values are observed with increased torsional left ventricular motion, with 6.9 % for T1 and 42.3 % for T2. This finding could be referred to the hypothesis that increased values of torsion could play a role as compensation mechanism to maintain normal filling [204].

11.7 CONCLUSIONS

This study demonstrates a novel in-vitro left heart model LH2 which adds the anisotropic LV wall properties of LV3 (Chapter 7) to the left heart model LH1 (Chapter 10). By this integrative approach, this unique model achieves the greatest number of practical guidelines compared to models of previous chapters (see Table 8) and exceeds existing approaches (as described in Chapter 3, Table 3) in the following ways. First, this model is able to generate versatile wall deformation patterns by the anisotropic wall properties (**PG2**) in terms of torsional motion (**PG5**) as well as longitudinal (**PG4a**) and circumferential deformations (**PG4b**). Second, the integrated mitral valve model includes all basic features of the mitral valve apparatus MV2 (Chapter 8) (**PG6a-e**). Finally, the mitral valve apparatus is integrated into a flexible valve plane (**PG7**). This wide range of more realistic characteristics bears promise to make this in-vitro left heart model an indispensable tool for revealing insights of mitral valve- and torsional-related physiological events.

The LH2 model has been used in this study to obtain more insights into the relationship between LV torsion and the diastolic parameters TMPDe and IVPDe. The experiment protocol included different hydrodynamic conditions (HR 50/65/80 bpm and SV 50/65/80 ml) and five different LV models with different wall kinematics: (1) a reference model, (2) predominant circumferential and (3) longitudinal deformation, and (4-5) two torsional models.

Compared to a thin walled silicone membrane model G, which is currently the most widely used model to mimic the left ventricle, this study shows that left ventricular torsion is related with diminished TMPDe values (down to 28.5 %) and augmented IVPDe values (up to 42.3%). Also, this study shows that the model with predominant circumferential wall deformation leads to a reduction of IVPDe by 22.4% while the model with predominant longitudinal model leads to a decrease of TMPDe by 7.5 % and an increase of IVPDe by 23.5 %. The lower TMPDe and higher IVPDe values of the torsional models are partly due to its longitudinal component, but because this longitudinal deformation component is lower than that of the L model, these results may suggest that the torsional motion has indeed additional effects on top of the longitudinal deformation component.

11.8 LIMITATIONS AND FURTHER DIRECTIONS

The main limitation of this study is the repeatability of the measurements. This feasibility study concentrates on the proof of concept of the left heart model and its results are merely indicative. More reliable results can be obtained by more extensive experiments and measurements.

Another limitation relates to the model setup, which is a volume controlled cardiovascular simulator to generate a pulsatile flow. However, IVPDe's are part of a complex interaction between pressure waves which travel within the left ventricle [205], and because of the sensitivity of this parameter (ranges within of a few mmHg), a volume controlled pump is not the best option. A pressure controlled system could be a more robust way to generate this pulsatile flow and measuring IVPDe's.

The total rotational angle of models T1 and T2 of 77° and 90° are much higher than the 17° in the human left ventricle. Also, the rough trabecular wall structures, which promote the flow-structure interaction, are not yet included in our model. In this study, an assumption is made that these higher values of torsion in our model are set to partly compensate for the inadequately flow-structure interaction.

In this study, the atrium is modelled by a passive silicon sac. However, a more physiological-like approximation can be obtained by modelling the active atrium contraction.

Part V

Conclusions and future directions

Conclusions and future perspectives

This chapter provides a general discussion of the results of the studies described with regard to the research goals. It also addresses important methodological considerations, along with the innovations and suggestions for future research.

12.1 GENERAL DISCUSSION

In the introduction of this dissertation, we formulated the three research goals that guided the development of this PhD work. As a first goal, we aimed to define practical guidelines for more realistic in-vitro left heart modelling in terms of anatomical and physiological likeness. The second goal was to design and develop more realistic models of the left ventricle and the mitral valve. The third and final goal was to integrate these novel components to attain a more nature-like model of the left heart. A general overview of our models is shown in Figure 121 and placed in the context of the practical guidelines in Table 8. In this chapter, we summarize the key findings related to each research goal, as well as some methodological considerations, the innovation of this work, and future perspectives.

12.1.1 Key findings

Goal 1: Defining practical guidelines for more realistic in-vitro left heart modelling in terms of anatomical and physiological likeness.

In **Chapter 2**, we reviewed the 55 year history of cardiovascular simulator development. This state-of-the-art overview clearly illustrates the wide range of approaches as well as the accompanying challenges in order to attain more realistic in-vitro modelling of the left heart. These approaches and accompanying challenges are summarized in Table 3. From our overview, it becomes evident that current cardiovascular models account for only a few of the anatomical features and physiological events, which underscores the need for designing and developing more naturally accurate left heart models. As such, from the various limitations described in **Chapter 3**, we isolated three general needs related to cardiovascular in-vitro modelling:

- *there is a need for more naturally correct left ventricular models (**NEED 1**);*
- *there is a need for in-vitro mitral valve models including the basic anatomical features (**NEED 2**);*
- *there is a need for in-vitro left heart models integrating these models of the left ventricle, mitral valve, incorporating a flexible valve plane (**NEED 3**).*

In **Chapter 3**, we translated these limitations into corresponding practical guidelines that should be targeted in order to attain more realistic cardiovascular models. Regarding **NEED 1**, five practical guidelines were defined in the context of LV modelling: the implementation of a thick wall (**PG1**), and inclusion of the anisotropic wall properties of the natural ventricular wall (**PG2**), to invent left ventricular models that are equipped with an active contractile wall containing contractile elements (**PG3**), mimicking the global ventricular wall deformation patterns (**PG4**) including longitudinal (**PG4a**), circumferential (**PG4b**) as well as radial deformation (**PG4c**) and finally, to include the twisting left ventricular motion (**PG5**). Evaluating **NEED 2** brought about a sixth practical guideline which concerns with the modelling of the mitral valve apparatus by a parametrized geometry (**PG6**) which includes elementary features of the mitral valve apparatus, such as the anterior and posterior leaflets (**PG6a**) which are hinged by a saddle-like annulus (**PG6b**) and made of a fiber-based composite material (**PG6c**), chordae tendineae (**PG6d**) and corresponding anterolateral and posteromedial papillary muscles (**PG6e**).

With reference to **NEED 3**, two additional guidelines were proposed regarding left heart modelling, more specifically, to the optimization of the valve plane. The seventh practical guideline states that a more naturally

correct valve plane approach for mitral valve modelling is obtained by implementing a flexible instead of a rigid mitral annulus while the valve plane is needed to be suspended in the rigid hydraulic chamber of the ViVtiro system (PG7). Finally, the eighth practical guideline (PG8) recommends that a left heart model would be more naturally correctly represented by allowing the motion of the valve plane by the invention of novel ways of ventricle actuation mechanisms. This full set of practical guidelines is crucial for the invention, design and optimization of cardiovascular in-vitro models and has high potential to bring cardiovascular modelling to a next level.

Goal 2: Designing more realistic models of the left ventricle and the mitral valve apparatus.

Based on the practical guidelines set out in Goal 1, new in-vitro models of the left ventricle (Chapters 5 to 7), the mitral valve (Chapter 8) and the venous valve (Chapter 9) were designed, realized and tested. In **Chapter 5**, a first thick-walled (PG1) LV model was proposed which included flexible bars that connect the LV wall with an external frame in order to attain exerted control on the LV wall deformation. In this way, control of the longitudinal (PG4a) and the circumferential (PG4b) components of wall deformation is realized, a feature which is absent from current in-vitro approaches. **Chapter 6** presents a second thick-walled (PG1) LV model with the addition of anisotropic (PG2) and contractile (PG3) wall elements. This LV model is able to generate the full set of deformation patterns (PG4a-c), the LV torsional motion (PG5) as well as the valve plane motion (PG8) which is typical for the natural heart. **Chapter 7** describes the third LV model which is thin-walled and equipped with spirally arranged fibers. These fibers induce anisotropic wall properties (PG2) which forces the wall to deform in a twisting manner (PG5). Besides this left ventricular torsion, two components of the global LV wall deformation patterns are included, the longitudinal (PG4a) as well as the circumferential component (PG4b). **Chapter 8** presents a mitral valve model which includes the most elementary features and geometrical shape of the natural valve, as suggested by PG6. As such, this valve model includes the two main leaflets (PG6a) and a saddle-shaped annulus (PG6b). Also, the leaflets are composed of a three layer composite layer structure (PG6c) which allows normal valve function and a tight connection with its chordae tendineae (PG6d). Finally, as a side project, a PIV compatible venous valve is proposed in **Chapter 9**. This chapter starts with the identification of an additional need (NEED 4) of a PIV compatible venous valve model for the validation of Computational Fluid Dynamics (CFD) models. In this regard, an additional practical guideline was added (see Table 8) stating that a relevant venous valve model needs to combine functionality, especially at low pressure differences, with transparency to allow optical access for PIV measurements (PG9). Then,

this chapter presents the development of such a PIV compatible venous valve model which is sensitive for fluid motion and is able to function at low pressure differences (**PG9**).

***Goal 3:** Integration of these novel components to attain a more nature-like model of the left heart.*

In Chapters 10 and 11, two left heart models are developed by assembling the components of Goal 2 to model also the interactions between these individual components. By its integrative approach, the first left heart model (**Chapter 10**) closely mimics real anatomical features in three main ways. First, its geometry is based on medical images and includes besides larger features (such as the left ventricle which mimics the longitudinal (**PG4a**) and circumferential deformation patterns (**PG4b**), left atrium, valve plane and aorta), also smaller features such as the auricle and the entrances of the four pulmonary veins. Second, the mitral valve model MV2 (**Chapter 8**) adds even more anatomical components (**PG6a-d**) and is joined with the left ventricle via the chordae tendineae to the two main papillary muscles (**PG6e**). Third, these different features are all assembled in a monolithic entity which results in a more compact and more nature-like model of the left heart. A tailored suspension system enables the connection with a standard cardiovascular simulator while preserving the flexible appearance and complex shape of the valve plane region (**PG7**). This model is made compatible with ultrasound and has shown to be able to reproduce physiological-like intraventricular flow patterns. The second left heart model (**Chapter 11**) also accounts for the practical guidelines of the first left heart model, but adds the anisotropic material properties of the left ventricular model as developed in **Chapter 7** (**PG2**). As a result, this left heart model is able to mimic the natural left ventricular torsional motion (**PG5**). This wide range of more realistic characteristics bears promise to make this latter in-vitro left heart model an indispensable tool for expanding our knowledge of mitral valve- and torsional-related physiological events in in-vitro experimental studies.

12.1.2 Methodological considerations

Despite the strengths of these key findings, the approaches described in this thesis are still subject to certain limitations which should be addressed by future research. The limitations of our work can be described in relation to three themes.

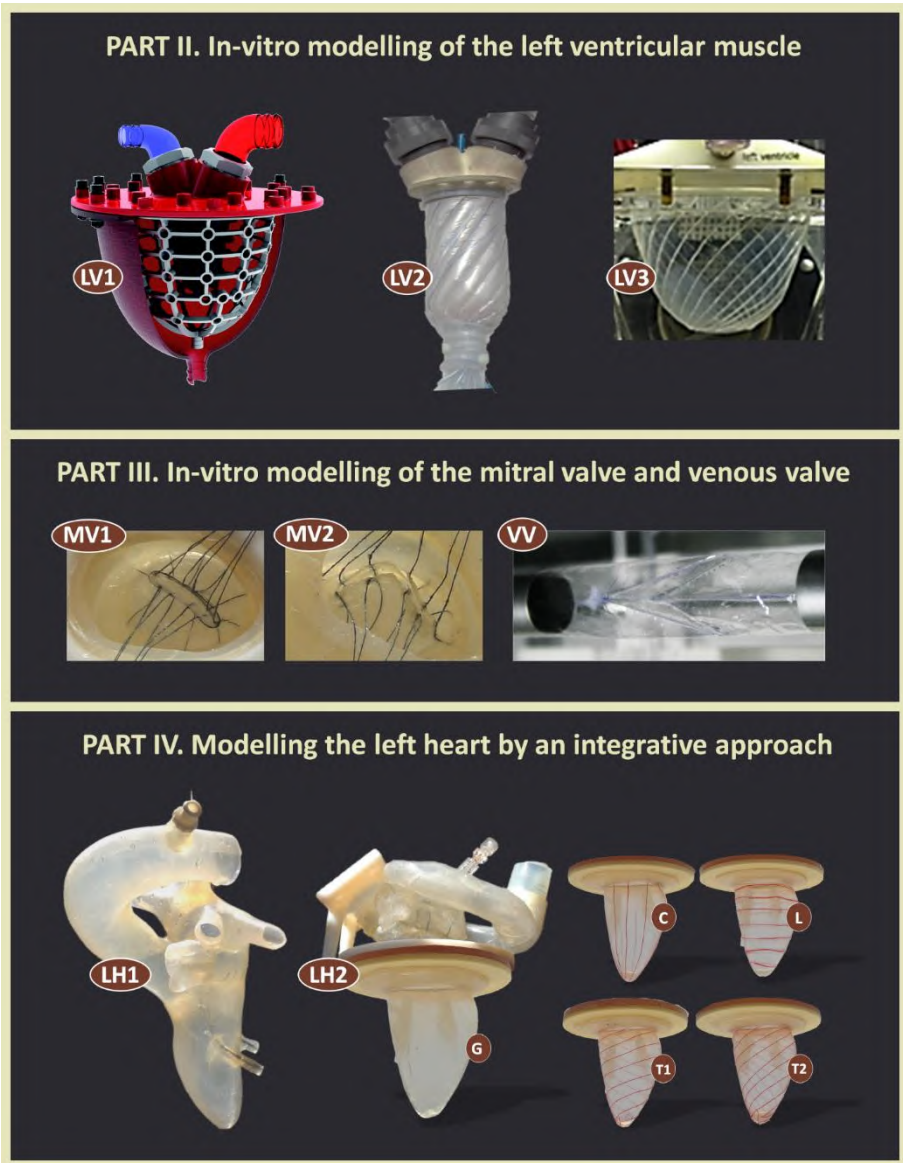


Figure 121: Overview of the in-vitro models developed in this dissertation.

12.1.2.1 Physiological events

Although many challenges of current in-vitro approaches have been targeted in this dissertation, there are at least three practical guidelines which remain open for further investigation and resolution. The first limitation deals about the modelling of the valve plane motion (**PG8**). Even though this guideline was successfully addressed by the active LV wall model (Chapter 6), it was not integrated into the integrative left heart models (Chapters 10 and 11). We acknowledge that, in reality, the valve plane is constantly in motion along the LV long axis by an up and downward as well as a rotating movement, while the apex is also subjected to a partial torsional motion but is otherwise relatively static. Whereas our final left heart model (Chapter 11) adds the torsional LV motion to current in-vitro approaches, we emphasize that its valve plane is still fixed, even though the apex freely moves up and downward to account for the full rotational movement. Although this valve plane motion plays an important role in the pump function of the heart, this item has not been well-covered in the in-vitro research literature and has also not been implemented in the integrative left heart models of this dissertation.

The second limitation in attaining the practical guidelines is about the modelling of the contractile myocardial wall (**PG3**). In the LV2 approach (Chapter 6), the contractile elements have been modeled by an artificial muscle concept with inflatable cells, which is a major step forward in comparison with the current passive membrane models. However, in this approach, the actual myocardial fibers as well as the papillary muscles of the biological heart are not modelled yet.

As a third limitation, we acknowledge the current absence of optical accessibility of all developed left heart models towards PIV measurements. Although we started to develop a procedure to realize PIV compatible thin-walled three dimensional structures (such as the venous valve model described in Chapter 9 or the model of the human airways briefly described in Chapter 10), we haven't applied these techniques for the left heart model despite its great potential. In the Future directions section below, we propose new more detailed ideas how these latter three limitations can be addressed in future research.

In addition to these three practical guideline limitations, there are other physiological events which are not implemented in our models so far. For example, we did not yet incorporate the atrial muscle contraction which is especially important during diastolic filling. To attain this goal, existing functional atrium models from the literature [88, 95-97] could be

In-Vitro Modelling of the Left Heart																	
PART I. The left heart: from nature to model (GOAL 1)																	
Chapter	The left heart structure and function	LV model						MV model						VP model			
		Thick wall	Anisotropic wall	Contractile elements	Longitudinal deformation	Circumferential deformation	Radial deformation	Twisting motion	Posterior & anterior leaflets	Saddle-like annulus	Fiber-based leaflets	Chordae tendineae	Papillary muscles	Flexible annulus & valve plane	Longitudinal valve plane motion	VP model NEED 3	VP model NEED 4
Chapter 1	In-vitro modelling of the left heart: State-of-the-art	PG1	PG2	PG3	PG4a	PG4b	PG4c	PG5	Type	PG6a	PG6b	PG6c	PG6d	PG6e	PG7	PG8	PG9
Chapter 2	Needs and practical guidelines (PGs)	PG1	PG2	PG3	PG4a	PG4b	PG4c	PG5		PG6a	PG6b	PG6c	PG6d	PG6e	PG7	PG8	PG9
Chapter 3	Design methodology	PG1	PG2	PG3	PG4a	PG4b	PG4c	PG5		PG6a	PG6b	PG6c	PG6d	PG6e	PG7	PG8	PG9
Chapter 4		PG1	PG2	PG3	PG4a	PG4b	PG4c	PG5		PG6a	PG6b	PG6c	PG6d	PG6e	PG7	PG8	PG9
PART II. In-vitro modelling of the left ventricular muscle (GOAL 2)																	
Chapter 5	LV1: Thick-walled left ventricle model	v	-	-	-	-	-	-	M	-	-	-	-	-	-	-	-
Chapter 6	LV2: Contractile cell left ventricle model	v	v	v	v	v	v	v	M	v	v	v	v	v	v	v	v
Chapter 7	LV3: Anisotropic left ventricle model	-	v	-	v	v	v	v	M	-	-	-	-	-	-	-	-
PART III. In-vitro modelling of the mitral (GOAL 2) and the venous valve (side project)																	
Chapter 8	MV1, MV2: Composite models of the mitral valve								IV	v	v	v	v	v	v	v	v
Chapter 9	VV: PIV-compatible venous valve model																v
PART IV. Modelling the left heart by an integrative approach (GOAL 3)																	
Chapter 10	LH1: Monolithic left heart model (inclusion of MV2)	-	-	-	-	-	-	-	IV	v	v	v	v	v	v	v	-
Chapter 11	LH2: Bilithic left heart model (inclusion of LV3 and MV2)	-	v	-	v	v	v	v	IV	v	v	v	v	v	v	v	-
PART V. Future directions (suggestions)																	
Chapter 12	LV4: Myocardial fiber left ventricle model	v	v	v	v	v	v	v		v	v	v	v	v	v	v	v
	LV5: PIV-compatible contractile cell LV model (VV + LV2)	v	v	v	v	v	v	v		v	v	v	v	v	v	v	PIV
	FH1: Myocardial band full heart model 1 (LV4 + MV2)	v	v	v	v	v	v	v	IV	v	v	v	v	v	v	v	v
	FH2: Myocardial band full heart model 2 (VV + LV2 + MV2)	v	v	v	v	v	v	v	IV	v	v	v	v	v	v	v	v

Table 8: A general overview of this dissertation is given. Index: ‘-’ absent, ‘v’ present, ‘~’ present but limited, ‘ ’ not applicable, M: mechanical mitral valve and IV: in-vitro mitral valve.

implemented, as well as the active muscle model LV2 (Chapter 6). Furthermore, papillary muscle contraction which is a key role player in mitral apparatus function is also not yet taken into account in the current PhD work. In addition, it should be emphasized that because of the focus on mitral valve modelling (in Chapters 8 and 10 to 11) in the current thesis, we made use of a mechanical prosthetic aortic valve for the experiments. A final physiology-related limitation is that although heart function is based upon underlying chemical and electrical mechanisms, these physiological events are also not yet taken into account in the approaches described in this dissertation.

12.1.2.2 Anatomical structures

Even though we added much more anatomical detailed structures to current in-vitro approaches, we acknowledge that more accurate geometrical approximations of the real heart can be obtained. As such, one limitation is about the papillary muscles which anatomically differ in the number of heads as well as in exact location, and which are usually grouped in two main groups. In our left heart model, we implemented a simplification of reality as each group of papillary muscles was represented by only one head. Also, more anatomically detailed geometry is desirable in future models in order to obtain more correct approximations of the interventricular blood flow patterns. For example, one can attempt to incorporate the rough trabeculae structures which promote flow-structure interactions. Lastly, our mitral valve models do not completely capture the complexity of the human mitral valve as we shaped our model according to a relatively simplified design and hence should be conceived as only a generalization of reality.

12.1.2.3 Proof of concept

This dissertation concentrated on demonstrating the proof of concepts of the proposed models and not on full-fledged validations. As a consequence, it cannot be overemphasized that the experimental results reported in this PhD work are merely indicative. More reliable results are definitely needed and can be obtained by more extensive experiments and measurements before these models can be utilized in experimental-clinical settings, such as testing surgical or interventional cardiovascular innovations or in research settings, such as advancing knowledge on cardiovascular functioning. In this regard, future research on these models should aim to realize this fundamental requirement for an experimental model to be valid: the model and its mock circuit have to behave similarly with the biological system they are simulating. Another limitation of this conceptual phase is the general choice of some materials. As such, we made use of a general purpose silicone as flexible material, universal thermoplastic films as sheet material, and non-treated

polymer multifilament yarns or ordinary cotton sewing threads as fiber material. Although these materials are suitable for experiments for this conceptual phase, there is a wide range of advanced flexible, sheet and fiber materials available that can be explored and investigated to further optimize the left heart model material characteristics. Also the fiber architecture and distribution within the flexible matrix of the composite material is rather preliminary in this study and can be supplementary explored in order to obtain a higher durability and a more detailed imitation of normal left heart dynamics, or even of pathological events due to local wall stiffness after myocardial infarction. In summary, there is opportunity for future research in material optimization which will likely result in more repeatable and extensive testing to obtain more reliable results.

12.1.3 Innovations

The innovative aspect of this dissertation primarily applies to the novel concepts and designs which tackle complex issues by means of a broad range of techniques and materials. As such, we distinguish three major novelties: by complexity, by innovation and by its broad character.

12.1.3.1 Novel by complexity

In-vitro simulation of the human cardiovascular system has become a valuable instrument to enhance cardiovascular insights, to advance procedures, and to develop medical devices. Through its 55 year history, these bench models have continuously been developed to mimic the complex anatomical and physiological conditions as accurately as possible. The wide variety of heart models and accompanying model limitations emphasize that - even in these advanced technological times - it is still extremely challenging to accurately simulate the complex physiological conditions that occur in the human left heart with an in-vitro simulator. We did not circumvent these current limitations but brought up solutions for modelling left heart components, even for the most complex architectural structures, such as the mitral valve apparatus. Integrating these interrelated components to form one compact monolithic left heart model which is able to mimic the natural anatomical elementary structures, physiological wall deformation patterns and ultrasonic tissue properties, appeared to be rather complex in concept, building strategy, as well as in realization. Bringing up ideas that meet individual practical guidelines (as achieved in Chapters 5 to 9) is a challenge in itself, however, fulfilling a combination of multiple practical guidelines in one concept (as realized in Chapters 10 to 11) is even more exciting and challenging. As such, the model LH2 (Chapter 11) exceeds all current in-vitro models by attaining

at least nine aspects of the proposed practical guidelines (**PG4a, PG4b, PG5, PG6a, PG6b, PHG6c, PG6d, PG6e, and PG7**).

12.1.3.2 Novel by innovation

A first innovation of this study in cardiovascular modelling is the application of fiber-silicone based composite structures. On the one hand, this material composition allows anisotropic wall properties of LV3. This causes the substrate to deform in a predefined direction, resulting in global LV wall deformation patterns such as exclusive or combined longitudinal, circumferential, as well as torsional components (Chapters 7 and 11). On the other hand, this approach is also applied to mimic the native mitral leaflet properties of MV1 and MV2 (Chapter 8) by a well-designed arrangement of strong fibers into a flexible matrix over the leaflet surface, which resulted in a firm structure that can withstand the high blood pressures while demonstrating low bending resistance, enabling the leaflets to smoothly open and close with only a minimum of energy losses. Also, these leaflet fibers served to merge into the chordae tendineae and - at the end - to merge into the papillary muscle heads, as such ensuring that the mitral valve leaflets could be firmly connected to the LV wall.

A second novelty is the invention of an artificial cardiac muscle LV2 (Chapter 6) which, by inclusion of contractile cells, captures the full set of natural LV wall deformation patterns, including torsion and valve plane motion. This model exceeds all current in-vitro LV models by attaining at least seven aspects of the proposed practical guidelines (**PG1, PG3, PG4a, PG4b, PG4c, PG5 and PG8**). In this model, the torsional motion is generated by the shortening of a range of parallel oriented inflatable cells which are slantly oriented along the circumference of the LV model.

A third aspect of innovation lies in the proposed production procedures for making these benchtop models. Three novel methods are especially worth mentioning in this conclusion as they are focused on realizing complex-shaped benchtop models. The first procedure is developed for the creation of flexible thin-walled models through hollow wax cores and is applied for the realization of the flexible part of the monolithic left heart model LH1 (see description in Chapter 10). The other two procedures are based on the direct 3D printing of tailored cores and are invented for realizing even more detailed structures. We described and applied these procedures for the creation of a thin-walled flexible and thick-walled rigid models of the upper human airways, respectively (described in Chapter 10). These procedures may be especially of great value for realizing benchtop models that are compatible for PIV modelling.

A fourth novelty put forward in this dissertation is the venous valve model design VV (described in Chapter 9) which was also developed in the perspective of compatibility with PIV measurements. Its design is based on the folding and welding of a transparent and pliable polymer film to a three-dimensional valve that is sensitive for fluid motion and low pressure differences, while it is able to withstand physiologically high pressure drops. This approach opens the intriguing possibility to experimentally assess and examine intra-valvular flow patterns. It may also prove to be a promising tool for use in experimental validation studies of computational models of cardiovascular configurations.

12.1.3.3 Novel by broadness

Each proposed new concept is the result of a broad collection of ideas, designs and concepts that became before (see also Chapter 4). It is broad because of the wide range of production techniques and materials that have been applied and because of the wide range of challenges that have been addressed. It is also broad because of the variety in applications of the left heart models and by its compatibility to other cardiovascular setups. As such, this dissertation work can be considered as an important step forward in innovating the field of left heart models. Since the FDA stated that clinically relevant benchtop models are urgently needed for in-vitro testing and that the best are preferred [2], we hope that our simulators will be widely used for cardiovascular applications in the future.

12.2 FUTURE DIRECTIONS

Bringing together the cardiovascular simulation history and the approaches developed in this dissertation, we define a three-fold ambition which can bring – in our opinion - benchtop modelling to the next level of innovation. The first challenge is to ‘*go for an active wall*’. This recommendation denotes that future cardiovascular simulators should account for the contractile muscle cells. In our opinion, the integration of contractile elements is the most promising way to combine the full range of LV physiological events, including the valve plane motion. The second aim is to ‘*go for an integrative approach*’. This recommendation reflects our opinion that an integrative approach of modelling an entire left heart is to be preferred above modelling separate left heart components. As well discussed in this dissertation, the mitral valve, for instance, is part of the valve plane but is also well connected to the left ventricle. Hence, its function can only be completely modelled by taking into account the co-operation between these different components. In sum, we thus believe that the heart physiology is more accurately represented

by the incorporation of all interrelated elements into one single model, even though this signifies a major challenge for the manufacturing process. Finally, the third ambition for future in-vitro modelling is to ‘*go for a transparent model*’. This recommendation points to the importance of attunement of cardiovascular simulators to be compatible with PIV investigations. Realizing this PIV compatibility bears the promise to enable experimental assessments and examinations of intra-cardiac flow patterns which are of great value for revealing insights of physiological events and for medical device testing. However, realizing this aspect increases the complexity of in-vitro modelling because it narrows the range of applicable materials, and on top of that, it demands more advanced production processes. It is noteworthy to mention that another experimental technique to assess these flow patterns is by MRI examinations. In this case, other design criteria apply to account for the MR-compatibility, such as the absence of ferrous metals in model components.

To close this dissertation, we formulate three suggestions – developed during our thinking and design process for the current PhD work - that may help to accomplish this three-fold ambition to ‘*go for an active wall, go for an integrative approach and go for a transparent model*’ in future in-vitro modelling research.

12.2.1 To go for an active wall

First, to account for contractile elements in cardiovascular models, we designed a new artificial muscle which is able to mimic the actual muscle fiber contraction, namely LV4. The contractile muscle fiber is based on an exterior braided sleeving and an inner elastic tube. By applying pressure, the elastic tube tends to expand while forcing the exterior braid to widen its diameter. As a result of this diameter increase, the actuator shortens in length and mimics thereby the actual contraction of the natural muscle fiber. This idea was inspired by the deployment of a woven self-expandable stent which likewise increases in diameter while shortening in length. We researched the literature and noted that this approach is not entirely new, as a similar concept was invented in the 1960’s in the context of an orthotic appliance for polio patients by J. L. McKibben [206]. Based on this actuator concept, we developed LV4 by arranging multiple of these artificial muscle fibers spirally around the circumference of the LV (Figure 122). After investigation of recent literature, we found that a similar type of LV model was developed using a bioinspired soft actuated material [207], as it is composed of McKibben actuators which are slantly oriented along the circumference of the model. This model is able to generate the torsional motion as well as a limited pump function. This model is able to pump and generate torsion, however, the ejection fraction is suboptimal [208], which is the same observation we made from preliminary

tests of our developed LV4 model. The reason can be found in the mechanism of diameter increase of the individual fibers which induces an unwanted side effect, i.e., circumferential widening instead of circumferential narrowing. This partially neutralizes the effect of fiber contraction. In our opinion, this might be resolved by impeding the unnatural circumferential widening either by adding a pericardial sac around the fiber model or by adding more artificial muscle fibers layers according to the natural LV muscle wall. This latter solution is implemented in the first full heart approach (FH1), as described further in this chapter, as well as recently applied in an implantable heart assist sleeve [208], including two layers of soft actuated material, leading to normal values of ejection fraction. An optimization of these artificial muscle models, together with the other active wall model LV2 (Chapter 6), will be able to generate torsional motion by the integration of contractile elements and as such, these two models can be considered as stepping stones to fully account for the first challenge, to ‘*go for an active wall*’.

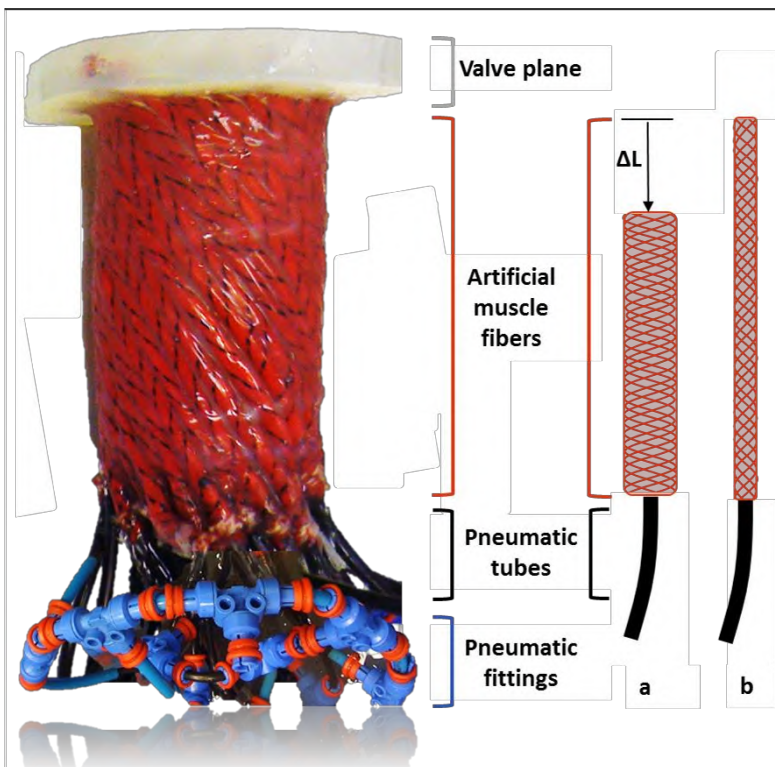


Figure 122: Active left ventricular muscle LV4 including a series of spirally arranged artificial muscle fibers (b). By applying pressurized air, an outer braid fiber structure is expanded in radial direction by an internal flexible tube and meanwhile shortens in length (ΔL) (a).

12.2.2 To go for an integrative approach

Second, we acknowledge that the integrative approach can go beyond on that what was developed for this dissertation. Whereas our study was focused on modelling the left heart, it is possible to translate these concepts to the right side of the heart and by integrating both sides, forming a model of the four-chambered heart. To realize such a total heart model, the concept of Torrent-Guasp et al. [37-40] which explains the architecture and function of myocardial macrostructure could be an interesting source of inspiration, as illustrated in Figure 123. As such, one could start with integrating contractile elements into the geometry of the unwrapped myocardial band (a Torrent-Guasp rubber model is commercially available [209] and might be an interesting tool for this endeavor) with respect to the natural fiber arrangement. Contractile elements could either be the inflatable cells of the LV2 or the artificial muscle fibers of the lastly proposed new LV4 actuator model. Once the artificial myocardial band has been developed, this continuous muscle can then be helically folded to form the right as well as the left ventricular muscle structure according to Torrent-Guasp's concept of the natural heart. Adding the valves (including MV2) and atria according to the previous described concepts, this approach might likely end in the realization of the first active, in-vitro full heart models FH1 and FH2, respectively, which fully fulfills the second ambition for future research, namely to '*go for an integrative approach*'.

12.2.3 To go for a transparent model

The third aim, to '*go for a transparent model*' and to account for the PIV compatibility, can be considered as the icing of the cake in future in-vitro heart modelling. We believe that also this ambition is not too far from now. As a functional PIV compatible venous valve model VV (Chapter 9) has been realized by using a transparent pliable polymer sheet material, we suggest that this method can also be applied for building the contractile LV2 model, which is also made by welding of polymer sheets. By applying a fluid - instead of air - for the actuation of the cells and matching its refractive index to both, the blood substitute of the mock loop and the applied polymer sheet material, this new idea of left ventricle model (LV5, see Figure 124) has clear potential to soon become the first PIV compatible torsional LV model. Furthermore, if research is able to realize to wrap such a transparent artificial muscle according to the helical myocardial band, this even bears promise to become the first PIV compatible model of the entire heart (FH2, see Figure 123).

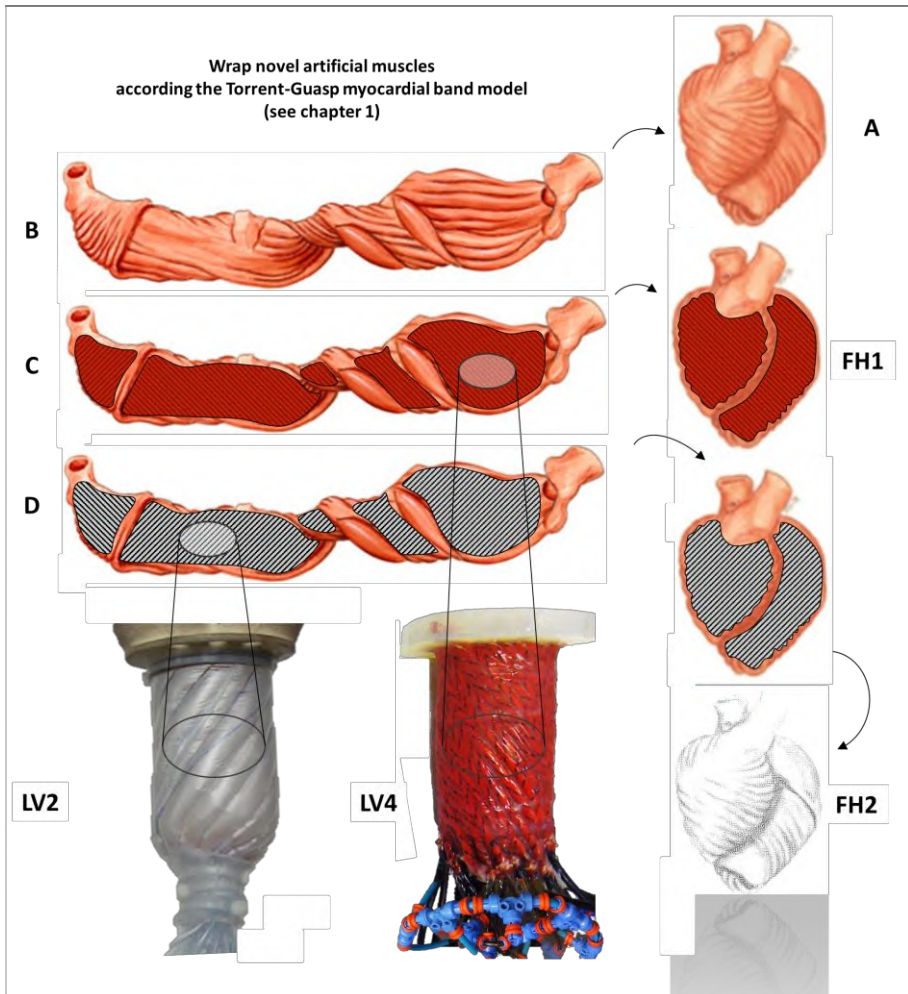


Figure 123: Illustration of the FH1 and FH2, ideas for future in-vitro models of the total heart.

This image shows the heart (A) which can be unwrapped to form a continuous ventricular myocardial band (B) according to the Torrent-Guasp concept [32]. Likewise, artificial muscle bands (C and D) can be constructed according to the LV2 or LV4 muscle designs and subsequently wrapped to form the in-vitro full heart models FH1 and FH2, respectively.

Similar to the VV model, transparent sheet materials could be used to account for PIV compatibility.

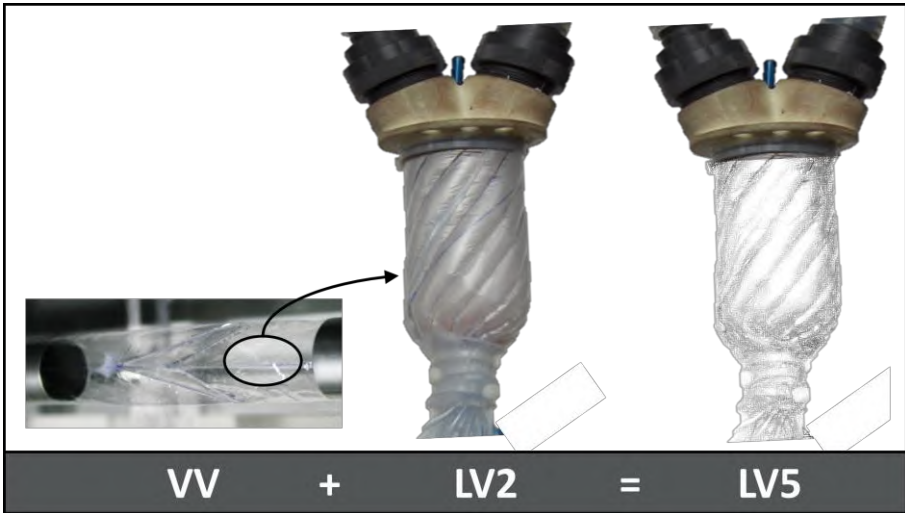


Figure 124: Illustration of the LV5, an idea for a future PIV compatible active LV model.

Hence, by implementing the innovative approaches proposed in this dissertation and in this discussion, we believe that it is feasible for future research to accomplish the three-fold ambition to ‘*go for an active wall, go for an integrative approach and go for a transparent model*’, even though we acknowledge that the production and manufacturing processes will remain challenging. Realizing such in-vitro models will likely give birth to a multitude of more advanced physiological insights as well as a more accurate platform to test medical devices. Nevertheless, even though this would signify a major step forward in comparison to the currently used in-vitro approaches, we should still humbly acknowledge that these in-vitro models will always be simplifications and approximations of reality, which are still far away from the complex anatomical and physiological events and features of the human heart.

References

1. Mendis, S., P. Puska, and B. Norrving, *Global atlas on cardiovascular disease prevention and control*. 2011: World Health Organization.
2. FDA, *Draft Guidance for Industry and Food and Drug Administration Staff, Investigational Device Exemptions (IDE) for Early Feasibility Medical Device Clinical Studies, Including Certain First in Human (FIH) Studies, November 10, 2011*.
3. Little, W.C. and J.K. Oh, *Echocardiographic Evaluation of diastolic function can be used to guide clinical care*. *Circulation*, 2009. **120**(9): p. 802-809.
4. Nagueh, S.F., et al., *Recommendations for the evaluation of left ventricular diastolic function by echocardiography*. *European Journal of Echocardiography*, 2009. **10**(2): p. 165-193.
5. Rausch, M., *Development and validation of an in-vitro platform for the study of mitral valve function under normal and pathologic conditions with particular emphasis on isolated annular dilatation*. 2009, University of Stuttgart.
6. Purves, W.K., et al., *Life: The Science of Biology: Volume III: Plants and Animals*. Vol. 3. 2003: Macmillan.
7. Yellin, E., *The momentum of mass, the momentum of ideas, and diastolic function*. *Systolic and diastolic function of the heart*, 1995 (IOS Press, Amsterdam).
8. Bell, S.P., et al., *Alterations in the determinants of diastolic suction during pacing tachycardia*. *Circulation Research*, 2000. **87**(3): p. 235-240.
9. Cheng, C.P., et al., *Effect of Loading Conditions, Contractile State, and Heart-Rate on Early Diastolic Left-Ventricular Filling in Conscious Dogs*. *Circulation Research*, 1990. **66**(3): p. 814-823.
10. Ling, D., et al., *Regional Diastolic Mechanics of the Left-Ventricle in the Conscious Dog*. *American Journal of Physiology*, 1979. **236**(2): p. H323-H330.
11. Courtois, M., S.J. Kovacs, and P.A. Ludbrook, *Transmitral Pressure-Flow Velocity Relation - Importance of Regional Pressure-Gradients in the Left-Ventricle During Diastole*. *Circulation*, 1988. **78**(3): p. 661-671.
12. Klabunde, R., *Cardiovascular Physiology Concepts*. <http://cvphysiology.com/Heart%20Disease/HD001.htm>, accessed on 10/12/2009.
13. Katz, L.N., *The role played by the ventricular relaxation process in filling the ventricle*. *Am J Physiol*, 1930. **95**: p. 542-553.

14. Lissauskas, J.B., et al., *Chamber properties from transmitral flow: prediction of average and passive left ventricular diastolic stiffness*. Journal of Applied Physiology, 2001. **91**(1): p. 154-162.
15. Little, W.C., et al., *Determination of Left-Ventricular Chamber Stiffness from the Time for Deceleration of Early Left-Ventricular Filling*. Circulation, 1995. **92**(7): p. 1933-1939.
16. Marino, P., et al., *Early mitral deceleration and left atrial stiffness*. American Journal of Physiology-Heart and Circulatory Physiology, 2004. **287**(3): p. H1172-H1178.
17. De Mey, S., *Diastology: Insights from Model Studies and Clinical Observations using Color M-Mode Doppler Echocardiography*. Proefschrift, 2002.
18. Verdonck, P., et al., *In vivo validation of a fluid dynamics model of mitral valve M-mode echocardiogram*. Medical & Biological Engineering & Computing, 1996. **34**(3): p. 192-198.
19. Chemla, D., et al., *Mechanics of relaxation of the human heart*. Physiology, 2000. **15**(2): p. 78-83.
20. Courtois, M., S.J. Kovacs, and P.A. Ludbrook, *Physiological Early Diastolic Intraventricular Pressure-Gradient Is Lost During Acute Myocardial-Ischemia*. Circulation, 1990. **81**(5): p. 1688-1696.
21. Firstenberg, M.S., et al., *Relationship between early diastolic intraventricular pressure gradients, an index of elastic recoil, and improvements in systolic and diastolic function*. Circulation, 2001. **104**(12): p. I330-I335.
22. Gillebert, T.C., A.F. LeiteMoreira, and S.G. DeHert, *The hemodynamic manifestation of normal myocardial relaxation - A framework for experimental and clinical evaluation*. Acta Cardiologica, 1997. **52**(3): p. 223-246.
23. Lenihan, D.J., et al., *Mechanisms, Diagnosis, and Treatment of Diastolic Heart-Failure*. American Heart Journal, 1995. **130**(1): p. 153-166.
24. Firstenberg, M.S., et al., *Relationship between ventricular contractility and early diastolic intraventricular pressure gradients: A diastolic link to systolic function*. Journal of the American Society of Echocardiography, 2008. **21**(5): p. 501-506.
25. Simons, M., *Section of Cardiovascular Medicine*. http://www.med.yale.edu/intmed/cardio/echo_atlas/references/graphics/heart_anatomy.gif, accessed on 02/01/2010.

26. Grégoire, L., *Inleiding in de Anatomie/Fysiologie van de mens, tweede druk*. http://www.med.yale.edu/intmed/cardio/echo_atlas/references/graphics/hear_t_anatomy.gif, accessed on January 1, 2010: p. Thieme Meulenhoff, Module 2, hoofdstuk 1, deel 5, p. 117.
27. Anatomy, D. accessed on March 21, 2016; Available from: <https://www.pinterest.com/delgas/anatomy/>.
28. Silbernagl, S.D.A., *Atlas van de fysiologie*. 2007: Sesam
29. Huxley, H., *Sliding filaments and molecular motile systems*. J Biol Chem, 1990. **265**(15): p. 8347-8350.
30. College study guide, accessed on March 21, 2016; Available from: <https://www.studyblue.com/notes/n/pre-ap-biology-study-guide-2012-13-mrsedward/deck/9722162>.
31. Klabunde, R.E. *Cardiovascular Physiology Concepts*. accessed on March 21, 2016; Available from: <http://www.cvphysiology.com/Cardiac%20Function/CF020.htm>.
32. Buckberg, G., et al., *Structure and function relationships of the helical ventricular myocardial band*. The Journal of thoracic and cardiovascular surgery, 2008. **136**(3): p. 578-589. e11.
33. Sabadini, R., Sale, . *Animation de la contraction musculaire*. Website Centre Nationale de la recherche scientifique, La cellule animale. Voyage au coeur du vivant accessed on April 3, 2006; Available from: <http://www.cnrs.fr/cw/dossiers/doscel/imgAr/animtheq/page.htm>.
34. Robb, J.S. and R.C. Robb, *The normal heart: anatomy and physiology of the structural units*. American Heart Journal, 1942. **23**(4): p. 455-467.
35. Rushmer, R.F., D.K. Crystal, and C. Wagner, *The functional anatomy of ventricular contraction*. Circulation Research, 1953. **1**(2): p. 162-170.
36. Streeter, D.D., et al, *Fiber orientation in the canine left ventricle during diastole and systole*. Circulation research, 1969. **24**(3): p. 339-347.
37. Torrent-Guasp, F., *Sobre morfologia y funcionalismo cardiacos*. Rev Esp Cardiol, 1967. **20**(1).
38. Torrent-Guasp F, B.M., Buckberg GD, Carreras F, Flotats A, Carrio I, Ferreira A, Samuels and L.a.N. J, *Spatial orientation of the ventricular muscle band: physiologic contribution and surgical implications*. Thorac Cardiovasc Surg, 2001. **122**: p. 389-392.
39. Torrent-Guasp F, K.M., Corno A, Komeda M, Cox J, Flotats A, Ballester-Rodes M and and C.-C. F., *Systolic ventricular filling*. Eur J Cardiothorac Surg, 2004. **25**: p. 376-386.

40. Torrent-Guasp F, K.M., Corno AF, Komeda M, Carreras-Costa F, Flotats A, Cosin-Aguillar J and a.W. H., *Towards new understanding of the heart structure and function*. Eur J Cardiothorac Surg, 2005. **27**: p. 191-201.
41. Anderson, R.H., et al., *The three-dimensional arrangement of the myocytes in the ventricular walls*. Clinical Anatomy, 2009. **22**(1): p. 64-76.
42. Nasiraei-Moghaddam, A. and M. Gharib, *Evidence for the existence of a functional helical myocardial band*. American Journal of Physiology-Heart and Circulatory Physiology, 2009. **296**(1): p. H127-H131.
43. Sengupta, P.P., et al., *Left ventricular form and function revisited: applied translational science to cardiovascular ultrasound imaging*. J Am Soc Echocardiogr, 2007. **20**(5): p. 539-51.
44. Carreras, F., et al., *Left ventricular torsion and longitudinal shortening: two fundamental components of myocardial mechanics assessed by tagged cine-MRI in normal subjects*. The international journal of cardiovascular imaging, 2012. **28**(2): p. 273-284.
45. Abraham, T.P., V.L. Dimaano, and H.-Y. Liang, *Role of tissue Doppler and strain echocardiography in current clinical practice*. Circulation, 2007. **116**(22): p. 2597-2609.
46. Notomi, Y., et al., *Measurement of ventricular torsion by two-dimensional ultrasound speckle tracking imaging*. Journal of the American College of Cardiology, 2005. **45**(12): p. 2034-2041.
47. Zacek, P., J. Dominik, and P. Kubis, *Interactive Cardiac Surgery*. ANNALS-ROYAL COLLEGE OF SURGEONS OF ENGLAND, 2006. **88**(1): p. 84.
48. Maharaj, N., et al., *Left ventricular twist in a normal African adult population*. European Heart Journal-Cardiovascular Imaging, 2012: p. jes208.
49. Helle-Valle, T., et al., *New noninvasive method for assessment of left ventricular rotation speckle tracking echocardiography*. Circulation, 2005. **112**(20): p. 3149-3156.
50. Kocabay, G., et al., *Normal left ventricular mechanics by two-dimensional speckle-tracking echocardiography. Reference values in healthy adults*. Revista Española de Cardiología (English Edition), 2014. **67**(8): p. 651-658.
51. Fuster, V., R. Walsh, and R. Harrington, *Hurst's the Heart: Volume One*. 13th edition. 2011: McGraw Hill Professional.
52. Castillo, J.G. and D.H. Adams, *Mitral Valve Repair and Replacement*. Valvular Heart Disease: A Companion to Braunwald's Heart Disease, 2014: p. 326.

53. Gammie, J.S., et al., *Influence of hospital procedural volume on care process and mortality for patients undergoing elective surgery for mitral regurgitation*. *Circulation*, 2007. **115**(7): p. 881-887.
54. Vanhercke, D., *Personal Communication*. 2012: Ghent, Belgium.
55. Collier, P., D. Phelan, and B.P. Griffin, *Mitral Valve Disease: Stenosis and Regurgitation*.
56. Edwards, W., *Applied anatomy of the heart*. *Cardiology Fundamentals and Practice*, 1987. **1**: p. 47-112.
57. Gammie, J.S., et al., *Trends in mitral valve surgery in the United States: results from the Society of Thoracic Surgeons Adult Cardiac Database*. *The Annals of thoracic surgery*, 2009. **87**(5): p. 1431-1439.
58. Levine, R.A., *Dynamic mitral regurgitation—more than meets the eye*. *N Engl J Med*, 2004. **351**(16): p. 1681-1684.
59. Levine, R.A., et al., *Three-dimensional echocardiographic reconstruction of the mitral valve, with implications for the diagnosis of mitral valve prolapse*. *Circulation*, 1989. **80**(3): p. 589-598.
60. Noack, T., et al., *New concepts for mitral valve imaging*. *Annals of cardiothoracic surgery*, 2013. **2**(6): p. 787.
61. Carpentier, A., D.H. Adams, and F. Filsoufi, *Carpentier's reconstructive valve surgery*. 2011: Elsevier Health Sciences.
62. Ranganathan, N., et al., *Morphology of the human mitral valve II. The valve leaflets*. *Circulation*, 1970. **41**(3): p. 459-467.
63. Dent, J.M., et al., *Mechanism of mitral leaflet excursion*. *American Journal of Physiology-Heart and Circulatory Physiology*, 1995. **269**(6): p. H2100-H2108.
64. Lam, J., et al., *Morphology of the human mitral valve I. Chordae tendineae: a new classification*. *Circulation*, 1970. **41**(3): p. 449-458.
65. Edwards, W., *Cardiac anatomy and examination of cardiac specimens*. *Moss & Adams' Heart Disease in Infants, Children, and Adolescents*, 1995. **1995**: p. 70-105.
66. Björk, V., F. Intonti, and A. Meissl, *A mechanical pulse duplicator for testing prosthetic mitral and aortic valves*. *Thorax*, 1962. **17**(3): p. 280-283.
67. Langendorff, O., *Untersuchungen am überlebenden Säugethierherzen*. *Pflügers Archiv European Journal of Physiology*, 1895. **61**(6): p. 291-332.
68. Chinchoy, E., et al., *Isolated four-chamber working swine heart model*. *The Annals of thoracic surgery*, 2000. **70**(5): p. 1607-1614.

69. de Weger, A., et al., *Direct endoscopic visual assessment of a transcatheter aortic valve implantation and performance in the physioheart, an isolated working heart platform*. Circulation, 2010. **121**(13): p. e261-e262.
70. Leopaldi, A., *Multifunctional passive-heart platforms for in vitro hemodynamic studies*. 2014.
71. McMillan, I., *Aortic stenosis: A post-mortem cinephotographic study of valve action*. British heart journal, 1955. **17**(1): p. 56.
72. Davila, J.C., et al., *A simple mechanical pulse duplicator for cinematography of cardiac valves in action*. Annals of Surgery, 1956. **143**(4): p. 544-551.
73. Duran, C., A. Gunning, and T. McMillan, *A simple versatile pulse duplicator*. Thorax, 1964. **19**(6): p. 503-506.
74. Hashim, S.R., et al., *A three-component force vector cell for in vitro quantification of the force exerted by the papillary muscle on the left ventricular wall*. Journal of biomechanics, 1997. **30**(10): p. 1071-1075.
75. Gabbay, S., et al., *In vitro hydrodynamic comparison of mitral valve prostheses at high flow rates*. The Journal of thoracic and cardiovascular surgery, 1978. **76**(6): p. 771-787.
76. Gabbay, S., et al., *In vitro hydrodynamic comparison of mitral valve bioprostheses*. Circulation, 1979. **60**(2): p. 62-70.
77. Fisher, J., I. Reece, and D. Wheatley, *In vitro evaluation of six mechanical and six bioprosthetic valves*. The Thoracic and cardiovascular surgeon, 1986. **34**(03): p. 157-162.
78. Cochrane, T., et al., *Validation of the orifice formula for estimating effective heart valve opening area*. Clinical Physics and Physiological Measurement, 1991. **12**(1): p. 21.
79. Akutsu, T., *Hydrodynamic performance of mechanical prosthetic heart valve*. 1985, University of British Columbia.
80. Bellhouse, B.J., *Fluid mechanics of a model mitral valve and left ventricle*. Cardiovascular Research, 1972. **6**(2): p. 199-210.
81. Bellhouse, B. and F. Bellhouse, *Fluid mechanic performance of five prosthetic mitral valves*. The Mitral Valve. A Pluri-disciplinary Approach. edited by Kalmanson D. Acton, Mass, Publishing Sciences Group Inc, 1976.
82. Scotten, L., D. Walker, and R. Brownlee, *Construction and evaluation of a hydromechanical simulation facility for the assessment of mitral valve prostheses*. Journal of medical engineering & technology, 1979. **3**(1): p. 11-18.
83. Walker, D., et al., *In vitro assessment of mitral valve prostheses*. The Journal of thoracic and cardiovascular surgery, 1980. **79**(5): p. 680-688.

84. Lee, C., *Fluid mechanical study of mitral valve motion*, in *Mechanical Engineering Dept.* 1977, University of California: Berkeley
85. Lee, C. and L. Talbot, *A fluid-mechanical study of the closure of heart valves*. *Journal of Fluid Mechanics*, 1979. **91**(01): p. 41-63.
86. Reul, H., *Cardiovascular simulation models*. *Life support systems: the journal of the European Society for Artificial Organs*, 1984. **2**(2): p. 77.
87. Knott, E., et al., *In vitro comparison of aortic heart valve prostheses. Part I: Mechanical valves*. *The Journal of thoracic and cardiovascular surgery*, 1988. **96**(6): p. 952-961.
88. Mouret, F., et al., *A new dual activation simulator of the left heart that reproduces physiological and pathological conditions*. *Medical and Biological Engineering and Computing*, 2000. **38**(5): p. 558-561.
89. Tanné, D., et al., *Assessment of left heart and pulmonary circulation flow dynamics by a new pulsed mock circulatory system*. *Experiments in Fluids*, 2010. **48**(5): p. 837-850.
90. Kheradvar, A., et al., *An in vitro study of changing profile heights in mitral bioprostheses and their influence on flow*. *ASAIO Journal*, 2006. **52**(1): p. 34-38.
91. Carson, D.J. *The Vascular Simulations Replicator* 2014; Available from: <http://www.vascularsimulations.com/>.
92. Little, S., *Patient-Specific Cardiovascular Models for Medical Device Testing*. 2012.
93. Baeck, K.L., P.; Verschuere, P., *Material characterization of HeartPrint® models and comparison with arterial tissue properties*. White paper, 2014.
94. *The Heartbeat Simulator*. accessed on 2014/12/27; Available from: <http://biomedical.materialise.com/heartbeat-simulator>.
95. Verdonck, P., et al., *Computer-controlled in vitro model of the human left heart*. *Med Biol Eng Comput*, 1992. **30**(6): p. 656-9.
96. Verdonck, P., *Studie van de bloedstroom doorheen de mitraalklep*, in *Faculty of Applied Sciences*. 1993, Ghent University: Ghent.
97. Carson, D.J., et al., *Cardiac Simulation Device*. 2013, US20130196301 A1, Google Patents.
98. Claessens, T., P. Segers, and P. Verdonck. *A new thick-walled hydraulic model of the left heart for the assessment of blood-wall interaction using ultrasound*. in *Computers in Cardiology, 2004*. 2004. IEEE.
99. Segers, P., *Biomechanische Modelleren van het Arterieel Systeem voor de niet-invasieve bepaling van de Arteriële Compliantie*, in *Faculty of Applied Sciences*. 1997, Ghent University: Ghent

100. ViVITro Labs Inc., *The ViVITro Heart Simulator*. 1992: Victoria, BC, Canada.
101. Rinaldi, J.E. and S.W. Smith, *Anthropomorphic cardiac ultrasound phantom*. 1990, Google Patents.
102. Reul, H. and N. Talukder, *Fluid mechanics of the natural mitral valve*. Journal of biomechanics, 1981. **14**(5): p. 361-372.
103. ViVITro Labs Inc. *ViVITro Labs product description of the pulse duplicator* 2014 2014; Available from: <http://vivitrolabs.com/product/pulse-duplicator/>
104. Kaminsky, R., et al., *In Vitro 3D High Speed Piv Measurements Behind An Aortic Artificial Heart Valve*. ASAIO Journal, 2006. **52**(2): p. 4A.
105. Kaminsky, R., et al., *Flow Visualization Through Two Types of Aortic Prosthetic Heart Valves Using Stereoscopic High-speed Particle Image Velocimetry*. Artificial organs, 2007. **31**(12): p. 869-879.
106. Wiggers, C.J., *The innervation of the coronary vessels*. American Journal of Physiology--Legacy Content, 1909. **24**(4): p. 391-405.
107. Larsen, V., *An apparatus for measuring the effect of drugs on the coronary vessels in the isolated heart*. Acta pharmacologica et toxicologica, 1948. **4**(1): p. 1-18.
108. Ryser, H. and W. Wilbrandt, *Die Wirkung von Recosen auf den Coronarwiderstand des nach Langendorff perfundierten Meerschweinchenherzens und ihre Deutung im Sinne eines Verdrangungsantagonismus*. Archives Internationales de Pharmacodynamie et de Therapie, 1953. **96**(2): p. 131-160.
109. Luduena, F., E. Miller, and W. Wilt, *A new perfusion apparatus for the study of the effects of drugs on the coronary vessels*. Journal of the American Pharmaceutical Association, 1955. **44**(6): p. 363-366.
110. Schaefer, E., *Do the coronary vessels possess vasomotor nerves?* Arch Sci Biol, 1904. **2**: p. 251-257.
111. de Hart, J., et al., *An ex vivo platform to simulate cardiac physiology: a new dimension for therapy development and assessment*. The International journal of artificial organs, 2011. **34**(6): p. 495-505.
112. Hill, A.J., et al., *In vitro studies of human hearts*. The Annals of thoracic surgery, 2005. **79**(1): p. 168-177.
113. Granegger, M., et al., *Investigation of hemodynamics in the assisted isolated porcine heart*. The International journal of artificial organs, 2013. **36**(12): p. 878-886.
114. Laske, T.G., N.D. Skadsberg, and P.A. Iaizzo, *A novel ex vivo heart model for the assessment of cardiac pacing systems*. Journal of biomechanical engineering, 2005. **127**(6): p. 894-898.

115. Shiose, A., et al., *Cardioscopy-guided surgery: Intracardiac mitral and tricuspid valve repair under direct visualization in the beating heart*. The Journal of thoracic and cardiovascular surgery, 2011. **142**(1): p. 199-202.
116. Tuzun, E., et al., *Assessment of aortic valve pressure overload and leaflet functions in an ex vivo beating heart loaded with a continuous flow cardiac assist device*. European Journal of Cardio-Thoracic Surgery, 2014. **45**(2): p. 377-383.
117. Schuster, A., et al., *An isolated perfused pig heart model for the development, validation and translation of novel cardiovascular magnetic resonance techniques*. J Cardiovasc Magn Reson, 2010. **12**(53,429).
118. Bateman, M.G. and P.A. Iaizzo, *Comparative imaging of cardiac structures and function for the optimization of transcatheter approaches for valvular and structural heart disease*. The international journal of cardiovascular imaging, 2011. **27**(8): p. 1223-1234.
119. ViVITRO Labs Inc., *Product and Service Brochure (Revision 2)*. 2009: Victoria, BC, Canada.
120. Annerel, S., et al., *Validation of a numerical FSI simulation of an aortic BMHV by in vitro PIV experiments*. Medical engineering & physics, 2014. **36**(8): p. 1014-1023.
121. Yoganathan, A.P., et al., *Bileaflet, tilting disc and porcine aortic valve substitutes: In vitro hydrodynamic characteristics*. Journal of the American College of Cardiology, 1984. **3**(2s1): p. 313-320.
122. Jensen, M.Ø., A.A. Fontaine, and A.P. Yoganathan, *Improved in vitro quantification of the force exerted by the papillary muscle on the left ventricular wall: three-dimensional force vector measurement system*. Annals of biomedical engineering, 2001. **29**(5): p. 406-413.
123. Padala, M., et al., *Cleft closure and undersizing annuloplasty improve mitral repair in atrioventricular canal defects*. The Journal of thoracic and cardiovascular surgery, 2008. **136**(5): p. 1243-1249.
124. ViVITRO Labs Inc., *Model Left Heart Operating Manual, Model SD 2001-1*. 2001: Victoria, BC, Canada.
125. Yoganathan, A.P. *Georgia Tech Left Heart Simulator 2013*; Available from: <http://groups.bme.gatech.edu/groups/cfmg/group/Infrastructure.html>.
126. Reul, H., et al., *Comparative in vitro evaluation of porcine and pericardial bioprostheses*. Zeitschrift fur Kardiologie, 1985. **75**: p. 223-231.
127. Reul, H., et al., *In vitro comparison of bileaflet aortic heart valve prostheses. St. Jude Medical, CarboMedics, modified Edwards-Duromedics, and Sorin-Bicarbon valves*. The Journal of thoracic and cardiovascular surgery, 1993. **106**(3): p. 412-420.

128. Hasenkam, J., M. Giersiepen, and H. Reul, *Three-dimensional visualization of velocity fields downstream of six mechanical aortic valves in a pulsatile flow model*. Journal of biomechanics, 1988. **21**(8): p. 647-661.
129. Giersiepen, M., et al., *Velocity and shear stress distribution downstream of mechanical heart valves in pulsatile flow*. The International journal of artificial organs, 1989. **12**(4): p. 261-269.
130. Akutsu, T. and V. Modi, *Unsteady fluid dynamics of several mechanical prosthetic heart valves using a two component laser Doppler anemometer system*. Artificial organs, 1997. **21**(10): p. 1110-1120.
131. Akutsu, T. and D. Higuchi, *Effect of mechanical prosthetic heart valve orientation on the flow field inside the simulated ventricle: comparison between St. Jude Medical valve and Medtronic-Hall valve*. Journal of Artificial Organs, 1999. **2**(1): p. 39-45.
132. Akutsu, T. and D. Higuchi, *Flow analysis of the bileaflet mechanical prosthetic heart valves using laser Doppler anemometer: effect of the valve designs and installed orientations to the flow inside the simulated left ventricle*. Journal of Artificial Organs, 2001. **4**(2): p. 113-125.
133. Akutsu, T. and T. Masuda, *Three-dimensional flow analysis of a mechanical bileaflet mitral prosthesis*. Journal of Artificial Organs, 2003. **6**(2): p. 112-123.
134. Akutsu, T. and T. Fukuda, *Time-resolved particle image velocimetry and laser Doppler anemometry study of the turbulent flow field of bileaflet mechanical mitral prostheses*. Journal of Artificial Organs, 2005. **8**(3): p. 171-183.
135. Akutsu, T., T. Fukuda, and J. Saito. *Time resolved PIV ventricular flow field study of differently designed contemporary bi-leaflet mitral valves*. in *International Journal of Artificial Organs*. 2007.
136. Akutsu, T., et al., *Dynamic particle image velocimetry study of the aortic flow field of contemporary mechanical bileaflet prostheses*. Journal of Artificial Organs, 2008. **11**(2): p. 75-90.
137. Akutsu, T., et al., *Correlation between ventricular flow field and valve closing sound of mechanical mitral prostheses*. Journal of Artificial Organs, 2008. **11**(2): p. 67-74.
138. Akutsu, T. and T. Suzuki. *In vitro dynamic PIV flow field analyses of the mechanical bi-leaflet valves: influence of pulse waveform and working fluid viscosity*. in *International Journal of Artificial Organs*. 2008.
139. Akutsu, T., et al. *Influence of the several mechanical bi-leaflet prosthetic valve designs of the three dimensional flow field inside the simulated aorta*. in *International Journal of Artificial Organs*. 2009.

140. Akutsu, T., H. Takahashi, and Y. Kamoshita. *Influence of the mechanical bileaflet prosthetic valve designs on the flow field and accumulated stress inside the simulated aorta*. in *International Journal of Artificial Organs*. 2011.
141. Bishop, W.F., *Hydrodynamic performance of mechanical and biological prosthetic heart valves*. 1990.
142. Modi, V., *Unsteady fluid dynamics of three contemporary heart valves using a two component LDA system*. *Artif Organs*, 1991. **14**: p. 103-107.
143. Barbara, V., et al., *In vitro evaluation of prosthetic heart valves: towards comparable testing*. *Journal of medical engineering & technology*, 1992. **16**(1): p. 10-14.
144. Conti, J.C. and E.R. Strobe, *Evaluating the in situ loading and accelerated durability of barbs located on bifurcated aorto-iliac stent-grafts*. *Biomedical sciences instrumentation*, 1999. **36**: p. 93-98.
145. Inc., D.L. *The Dynatek MP4 Robotic Cardiovascular Pulse Duplicator* 20/9/2014; Available from: www.dynatekdalta.com.
146. Black, M., et al., *In vitro heart valve testing: steady versus pulsatile flow*. *The Journal of heart valve disease*, 1994. **3**(2): p. 212-215.
147. Segers, P., *Biomechanische modellering van het arterieel systeem voor de niet-invasieve bepaling van de arteriële compliantie*. Gent: Universiteit Gent, 1997.
148. Verdonck, P., G. Van Nooten, and Y. Van Belleghem, *Pulse duplicator hydrodynamics of four different bileaflet valves in the mitral position*. *Vascular*, 1997. **5**(6): p. 593-603.
149. Verdonck, P.R., et al., *Mock Loop Testing of On-X Prosthetic Mitral Valve with Doppler Echocardiography*. *Artificial organs*, 2002. **26**(10): p. 872-878.
150. Dumont, K., et al., *Omnicarbon 21 mm aortic valve prosthesis: in vitro hydrodynamic and echo-Doppler study*. *The International journal of artificial organs*, 2002. **25**(8): p. 783-790.
151. Segers, P., et al., *Role and relevancy of a cardiovascular simulator*. *Cardiovascular Engineering*, 1998. **3**: p. 48-56.
152. Vandenberghe, S., et al., *In vitro evaluation of the PUCA II intra-arterial LVAD*. *The International journal of artificial organs*, 2003. **26**(8): p. 743-752.
153. Vandenberghe, S., et al., *In vitro assessment of the unloading and perfusion capacities of the PUCA II and the IABP*. *Perfusion*, 2004. **19**(1): p. 25-32.
154. Narine, K.K., et al., *Hydrodynamic evaluation of kangaroo aortic valve matrices for tissue valve engineering*. *Artificial organs*, 2006. **30**(6): p. 432-439.

155. Segers, P. and P. Verdonck, *Role of tapering in aortic wave reflection: hydraulic and mathematical model study*. Journal of biomechanics, 2000. **33**(3): p. 299-306.
156. Swillens, A., et al., *Effect of an abdominal aortic aneurysm on wave reflection in the aorta*. Biomedical Engineering, IEEE Transactions on, 2008. **55**(5): p. 1602-1611.
157. Matthys, K.S., et al., *Pulse wave propagation in a model human arterial network: assessment of 1-D numerical simulations against in vitro measurements*. Journal of biomechanics, 2007. **40**(15): p. 3476-3486.
158. Claessens, T.E., *Model-Based Quantification of Systolic and Diastolic Left Ventricular Mechanics*, in *Faculty of Applied Sciences*. 2006, Ghent University: Ghent
159. Evin, M., et al., *Localized Transvalvular Pressure Gradients in Mitral Bileaflet Mechanical Heart Valves and Impact on Gradient Overestimation by Doppler*. Journal of the American Society of Echocardiography, 2013. **26**(7): p. 791-800.
160. Pierrakos, O., P.P. Vlachos, and D.P. Telionis, *Time-resolved DPIV analysis of vortex dynamics in a left ventricular model through bileaflet mechanical and porcine heart valve prostheses*. Journal of biomechanical engineering, 2004. **126**(6): p. 714-726.
161. Pierrakos, O. and P.P. Vlachos, *The effect of vortex formation on left ventricular filling and mitral valve efficiency*. Journal of biomechanical engineering, 2006. **128**(4): p. 527-539.
162. *The Virginia Tech Left Heart Model*. 2009; Available from: <http://www.research.vt.edu/resmag/2009summer/flowpix03.html>.
163. Falahatpisheh, A. and A. Kheradvar, *High-speed particle image velocimetry to assess cardiac fluid dynamics in vitro: From performance to validation*. European Journal of Mechanics-B/Fluids, 2012. **35**: p. 2-8.
164. Kheradvar, A., et al., *Echocardiographic particle image velocimetry: a novel technique for quantification of left ventricular blood vorticity pattern*. Journal of the American Society of Echocardiography, 2010. **23**(1): p. 86-94.
165. Kheradvar, A. and A. Falahatpisheh, *The effects of dynamic saddle annulus and leaflet length on transmitral flow pattern and leaflet stress of a bileaflet bioprosthetic mitral valve*. Journal of Heart Valve Disease, 2012. **21**(2): p. 225.
166. Kheradvar, A. and M. Gharib, *On mitral valve dynamics and its connection to early diastolic flow*. Annals of Biomedical Engineering, 2009. **37**(1): p. 1-13.

167. Rasponi, M., et al., *A reliable method for prototyping flexible physiologic-like behaving left ventricles for studying mitral valve surgical corrections*. Journal of Mechanics in Medicine and Biology, 2006. **6**(1): p. 101-107.
168. Materialise NV., *HeartPrint® for cardiovascular anatomical models*. 2014 2014/12/27]; Available from: <http://biomedical.materialise.com/HeartPrint-FAQ>.
169. Jimenez, J.H., et al., *Mitral valve function and chordal force distribution using a flexible annulus model: an in vitro study*. Annals of biomedical engineering, 2005. **33**(5): p. 557-566.
170. Jimenez, J.H., et al., *Effects of a saddle shaped annulus on mitral valve function and chordal force distribution: an in vitro study*. Annals of biomedical engineering, 2003. **31**(10): p. 1171-1181.
171. Verdonck, P., *Personal Communication*. 2006: Ghent, Belgium.
172. Van Nooten, G. and F. De Somer, *Personal Communication*. 2011: Ghent, Belgium.
173. Mester, D., *Personal Communication*. 2011: Victoria CA.
174. Council, D. *Double diamond design process*. Accessed on June 14, 2016; Available from: [http://www.designcouncil.org.uk/sites/default/files/asset/document/ElevenLessons_Design_Council%20\(2\).pdf](http://www.designcouncil.org.uk/sites/default/files/asset/document/ElevenLessons_Design_Council%20(2).pdf).
175. Howard, T.J., S.J. Culley, and E. Dekoninck, *Describing the creative design process by the integration of engineering design and cognitive psychology literature*. Design studies, 2008. **29**(2): p. 160-180.
176. Council, D. *Mission British Design Council*. accessed on June 17, 2016; Available from: <http://www.city.ac.uk/news/2013/may/design-council-funds-city-university-london-scholarship-to-develop-new-products-and-services-for-uks-ageing-population>.
177. Council, D. *Figure of the double diamond design process*. Accessed on June 14, 2016; Available from: <https://innovationenglish.sites.ku.dk/files/2013/12/double-diamond-stor1.png>
178. Han, H.-C., *An echocardiogram-based 16-segment model for predicting left ventricular ejection fraction improvement*. Journal of theoretical biology, 2004. **228**(1): p. 7-15.
179. Van Der Smissen, B., et al., *Modelling the left ventricle using rapid prototyping techniques*. IRBM, 2013. **34**(3): p. 226-234.
180. Van Der Smissen, B., et al., *SolidWorks heeft ook hart voor u!*, in *design solutions update*. 2008, Design Solutions B.V. p. 2-3.

181. Massie, B.M. and N.B. Shah, *Evolving trends in the epidemiologic factors of heart failure: rationale for preventive strategies and comprehensive disease management*. Am Heart J, 1997. **133**(6): p. 703-12.
182. Verdonck, P.R., G.J. Van Nooten, and Y. Van Belleghem, *Pulse duplicator hydrodynamics of four different bileaflet valves in the mitral position*. Cardiovasc Surg, 1997. **5**(6): p. 593-603.
183. Dumont, K., et al., *Omnicarbon 21 mm aortic valve prosthesis: in vitro hydrodynamic and echo-Doppler study*. Int J Artif Organs, 2002. **25**(8): p. 783-90.
184. Scotten, L.N. and D.K. Walker, *New laboratory technique measures projected dynamic area of prosthetic heart valves*. J Heart Valve Dis, 2004. **13**(1): p. 120-32; discussion 132-3.
185. Kheradvar, A. and M. Gharib, *On mitral valve dynamics and its connection to early diastolic flow*. Ann Biomed Eng, 2009. **37**(1): p. 1-13.
186. De Mey, S., et al., *Assesment of LV diastolic filling using color M-mode Doppler echocardiography: validation in new hydroualic model*. Biomech Model Mechanobiol, 2004. **2**(3): p. 127-38.
187. Han, H.C., *An echocardiogram-based 16-segment model for predicting left ventricular ejection fraction improvement*. J Theor Biol, 2004. **228**(1): p. 7-15.
188. Van Der Smissen, B., et al., *Design of an artificial left ventricular muscle: an innovative way to actuate blood pumps?* Artificial organs, 2009. **33**(6): p. 464-468.
189. Van Der Smissen, B., et al. *Innovative Design of a Venous Valve Intended for PIV Measurements*. in *ASME 2011 Summer Bioengineering Conference*. 2011. American Society of Mechanical Engineers.
190. Murphy, G., S. White, and M. Nicholson, *Vascular access for haemodialysis*. British journal of surgery, 2000. **87**(10): p. 1300-1315.
191. Paulson, W.D., S.J. Ram, and G.B. Zibari. *Vascular access: Anatomy, examination, management*. in *Seminars in nephrology*. 2002. [New York, NY]: Grune & Stratton,[c1981]-.
192. *ARCH – Developing patient-specific computer models for improvement of vascular access creation and care in patients on hemodialysis therapy. A specific targeted research project funded within the EU 7th Framework Programme (Project n. 224390)*.
193. Refractive Index of Polystyrene, P. accessed on June 18, 2016; Available from: <http://www.filmetrics.com/refractive-index-database/Polystyrene/PS>.

194. Hossler, F.E. and R.F. West, *Venous valve anatomy and morphometry: studies on the duckling using vascular corrosion casting*. American journal of anatomy, 1988. **181**(4): p. 425-432.
195. De Meulemeester, J.H., I, *Ontwikkeling van een productietechniek voor dunwandige patiëntspecifieke modellen*, in *Master in de industriële wetenschappen elektromechanica*. 2010, University College Ghent.
196. ViVitro Labs Inc., Personal communication. **2011**.
197. Buckberg, G., et al., *Ventricular torsion and untwisting: further insights into mechanics and timing interdependence: a viewpoint*. Echocardiography, 2011. **28**(7): p. 782-804.
198. Popovic, Z.B., et al., *Relationship among diastolic intraventricular pressure gradients, relaxation, and preload: impact of age and fitness*. American Journal of Physiology-Heart and Circulatory Physiology, 2006. **290**(4): p. H1454-H1459.
199. Rovner, A., et al., *Improvement in diastolic intraventricular pressure gradients in patients with HOCM after ethanol septal reduction*. American Journal of Physiology-Heart and Circulatory Physiology, 2003. **285**(6): p. H2492-H2499.
200. Yotti, R., et al., *A noninvasive method for assessing impaired diastolic suction in patients with dilated cardiomyopathy*. Circulation, 2005. **112**(19): p. 2921-2929.
201. De Mey, S., et al., *Regional Differences in Relaxation Time (τ): Its Relationship to Intraventricular Pressure Gradients in a Canine and Hydraulic Model*. Cardiovascular Engineering, 2002. **2**(4): p. 149-159.
202. Greenberg, N.L., et al., *Estimation of diastolic intraventricular pressure gradients by Doppler M-mode echocardiography*. American Journal of Physiology-Heart and Circulatory Physiology, 2001. **280**(6): p. 2507-2515.
203. Falsetti, H.L., et al., *Regional Pressure Differences in the Left-Ventricle*. Catheterization and Cardiovascular Diagnosis, 1980. **6**(2): p. 123-134.
204. Park, S.-J., et al., *Left ventricular torsion by two-dimensional speckle tracking echocardiography in patients with diastolic dysfunction and normal ejection fraction*. Journal of the American Society of Echocardiography, 2008. **21**(10): p. 1129-1137.
205. Verdonck, P., et al., *Left-ventricular pressure gradients: a computer-model simulation*. Medical & Biological Engineering & Computing, 1999. **37**(4): p. 511-516.
206. Nickel, V.L., J. Perry, and A.L. Garrett, *Development of useful function in the severely paralyzed hand*. J Bone Joint Surg Am, 1963. **45**(5): p. 933-952.

REFERENCES

207. Roche, E.T., et al., *A bioinspired soft actuated material*. *Advanced Materials*, 2014. **26**(8): p. 1200-1206.
208. Roche, E.T., *A Multi-faceted Approach to Cardiac Repair*. 2015.
209. Torrent-Guasp, F. *Ventricular myocardial band rubber model*. Accessed on March 22, 2016; Available from: <http://www.torrent-guasp.com/PAGES/Modelo-Elastico.htm>.

List of figures

- Figure 1: Composition of the heart with Right (RA) and Left Atrium (LA), the Right (RV) and Left Ventricle (LV), the Tricuspid Valve (TV), the Pulmonary Valve (PV), the Mitral Valve (MV) and the Aortic Valve (AV). Adapted from [5]..... 51*
- Figure 2: The blood flow through the four heart chambers. Adapted from [6]. 52*
- Figure 3: Ventricular pressure-volume relation during a cardiac cycle with ESPVR: end-systolic pressure-volume relation and EDPVR: end-diastolic pressure-volume relation. . 53*
- Figure 4: Changes in pressure, flow, and volume in the left heart during a cardiac cycle. The points A, B, C and D indicate the start of the following stages: A, isovolumic contraction; B, ejection; C: isovolumic relaxation; and D, filling. Adapted from [7]..... 54*
- Figure 5: Top panel: Pressure measurement at the level of the LV apex and in the LA.... 55*
- Figure 6: Left: Simultaneous intraventricular pressure measurement 2 and 5 cm away from the apex towards the base, respectively. Right: simultaneously measured transmitral pressures, in the middle of the atrium and the center of the ventricle, respectively. Adapted from [11]. 57*
- Figure 7: The cardiac wall comprises 1) the endocardium, 2) the myocardium, 3) the epicardium, and 4) the pericardium. Adapted from [25, 26]..... 60*
- Figure 8: Macrostructure of the cardiac wall. Adapted from [27]. 60*
- Figure 9: Microscopic structure of cardiomyocytes: mononuclear, striated muscle cells. Adapted from [26]..... 63*
- Figure 10: Myofibrils of the cardiomyocyte. Adapted from [29]..... 63*
- Figure 11: Myosin filaments are composed of myosin proteins; each protein has two heads that are connected via the neck to the tail portion. Actin filaments comprise three different types of protein: actin, tropomyosin, and troponin. Adapted from [31]. 64*
- Figure 12: The organization of actin and myosin filaments is represented by formation of cross-bridges in a myocyte. Adapted from [26, 32]. 66*
- Figure 13: Four concepts of myocardial fiber orientation are given: (1) by Robb et al. [34] with a superficial (1a) and deep bulbospiral (1b), by Rushmer et al. [35] with spiral muscles including opposite fiber orientation, (3) by to Streeter et al. [36] with helical fibers which forming doughnut-like surfaces and (4) by Torrent-Guasp et al. [37-40] including a continuous ventricular myocardial band, with (4a) a schematic version of the double-helix, (4c) the unwrapped version of (4b). Ao, Aorta and Pa, Pulmonary artery. Adapted from [33]. 68*
- Figure 14: A step-by-step procedure to unscroll a heart by dissection according to the Torrent-Guasp's myocardial band model. Starting from the intact heart (1), the Right Segment (RS) is first unwrapped (2), then the Left Segment (LS) (3) and subsequently, the Ascending Segment (AS). At the end, by unfolding the Descending Segment (DS) (4), the complete helical structure is outspread and forms a continuous myocardial band. Note*

the twisting nature of the oblique fold at the center of the junction of the basal as apical loops. Adapted from [33]...... 69

Figure 15: Global wall deformation patterns during systole and diastole. Adapted from [44-46]...... 70

Figure 16: The LV torsion during one heart beat in a normal healthy subject is illustrated. $LV_{torsion}$ (orange curve) is defined as $rotation_{apex}$ (yellow curve) minus $rotation_{base}$ (black curve). During the isovolumic contraction phase (1), the apex generates a small clockwise twist and the base a small counterclockwise twist. During ejection phase (2), the twisting directions alter and the LV torsion values are significantly higher. During the isovolumic relaxation phase (3) and the early diastolic filling phase (4), the twisting direction is changed again and torsional recoil takes place. Adapted from [43]...... 71

Figure 17: This diagram shows the fibrous cardiac skeleton or valve plane with the four annuli of the cardiac valves. The aortic annulus at the center is the keystone and its fibrous extensions support the other three annuli. Adapted from [51]...... 73

Figure 18: As shown in the drawing (left) and the real heart (right), the mitral valve (MV) apparatus is composed of five elementary components, the mitral annulus, mitral leaflets, chordae tendineae, papillary muscles, and the left ventricle (LV). During systole, the mitral apparatus brings the two leaflets together and establishes the coaptation zone (CZ). Adapted from [51, 61]...... 75

Figure 19: Both mitral valve leaflets have a clear zone (CZ) and a rough zone (RZ) and are separated by a closing edge (dotted line). Note the fanlike array of the commissural chordae tendineae (). Adapted from [51].*..... 75

Figure 20: Schematic diagram of the section across the dotted lines clarifies the association between the annulus, the closing edge (CE), the free edge and the left ventricle (LV) and atrium (LA). Also the clear zone (CZ) and the rough zone (RZ) are shown. Modified from [51]...... 76

Figure 21: Fiber orientation of the mitral valve. Adapted from [60]...... 76

Figure 22: This picture shows an isolated and unfolded mitral valve including the anterolateral (ALPM) and posteromedial papillary muscles (PMPM) with the chordae tendineae and leaflets. Note the commissures (C) of the posterior (P) and anterior leaflets (A). Adapted from [51]...... 77

Figure 23: Anatomical section shows the valve plane with the cardiac valves in systole and a detailed composition of mitral valve. The anterior (A) and posterior leaflets (P) are both subdivided into three segments (1 -3) and separated from one another by the anterior (AC) and the posterior commissures (PC). Adapted from [51, 61]...... 78

Figure 24: Pulse duplicator using a postmortem human heart actuated by a piston pump. (A) The reservoir, (B) the peripheral resistance, (C) aortic viewing chamber-outflow, (D) atrial viewing chamber-inflow, (E) postmortem heart with left ventricle connected to the pump outflow tube and (F) piston pump. Adapted from [72]...... 86

Figure 25: Pulse duplicator system of the Department of Thoracic Surgery at Sweden (1962). Left panel: The pulse duplicator with (A) left atrium, (B) mitral valve (C) left ventricle, (D) rigid container, (E) elastic container, (F) aortic valve, (G) aorta, and (H)

peripheral resistance. Right panel: The pulse duplicator at the time of end systole (top) and end diastole (bottom). Adapted from [66]...... 88

Figure 26: Cardiovascular simulator of the Engineering Science Group at Oxford (1972), including pulmonary veins (A), the left atrium (B), the mitral valve (C), the left ventricle model (D), the external pressure source (E), the aortic valve (F) and the aorta (G). Adapted from [80]...... 89

Figure 27: Schematic diagram of the left heart model and circulatory network of the Mechanical Engineering Group at Berkeley, California. Adapted from [85]...... 90

Figure 28: Flow patterns inside ventricle model to explore the nature of pulsatile flow (A) during diastolic filling and (B) just after mitral valve closure. The experiment was performed at a heart rate of 20 beats/min and a stroke volume 80 ml. Adapted from [85]...... 91

Figure 29. Pulse duplicator system of the Cardiothoracic Surgery Unit, New York [75]. 92

Figure 30: The Superpump system SPS 3891 of ViVitro Lab Inc. This pump was commercially available from the 1984 (top), for a period of almost 30 years (middle: latest version of the analog pump), until the electronic pump (bottom) came in place...... 93

Figure 31: The ViVitro Left Heart Simulator: version ‘Model SD 2001-1’ of 2009 (left panel) and version ‘AR Series’ of 2014 (right panel). Adapted from [103, 119]...... 94

Figure 32: The Heart Simulator according to ViVitro Labs Inc., Victoria (1992) [100]. The model is composed of a left atrial reservoir (1), mitral valve (2), left ventricle (3), aortic valve (4), the aorta (5), peripheral compliance (6), resistant (7), ventricle membrane model (8), wave form generator (9) and super pump system (10). Pressure sensors can be placed at mitral (11), aortic (12), left atrial, left ventricular, and aortic position. Electromagnetic flow sensors are positioned upstream the mitral (13) and aortic (14) valves. 95

Figure 33: The ViVitro electronic Superpump AR Series can be provided with a pump head including a ventricle membrane and two heart valves to simulate physiological flows. 95

Figure 34: Left panel shows the aortic valve test apparatus developed by Yoganathan in 1984 [121]. Right panel illustrates the left heart model build by Hashim and colleagues in 1997 [74], also called the “Georgia Tech Left Heart Simulator” [123]...... 96

Figure 35: Left, the original Georgia Tech Left Heart Simulator (2007) including a rigid left ventricle which is driven by a compressible bladder type pump. Right, the simulator revised by Rausch and colleagues (2009) including a flexible ventricle model which is driven by a ViVitro linear piston pump [5]...... 97

Figure 36: The latest version of the Georgia Tech Left Heart Simulator (2013). Adapted from [125]...... 98

Figure 37: Schematic overview is shown of the cardiovascular simulator of Reul and colleagues (A) and of Knott and colleagues (B). Panel (C) shows a photograph of Knott’s model. Adapted from [86, 87]...... 100

Figure 38: The cardiovascular simulator according to Akutsu (1985) with a conically shaped transparent ventricle [79]...... 101

Figure 39: The Dynatek MPI Pulse Duplicator (1990). The simulated circulatory loop 12 includes the following successively components: a reservoir 22, a variable compliance chamber (A), mitral valve port 18 including the mechanical prosthetic mitral valve 14, a

flexible left ventricular sac 10, aortic valve port 20 including the mechanical prosthetic aortic valve 16, flow meter 74, variable compliance chamber (A) and a variable resistance manifold (B). Adapted from [101]. 103

Figure 40: The Dynatek MP3 Pulse Duplicator: the circulatory system is given (left) together with a close-up of the left heart model (right). The ventricle model is not shown on the pictures. Adapted from [144]...... 104

Figure 41: The Dynatek MP4 Robotic Cardiovascular Pulse Duplicator [145]. 104

Figure 42: Schematic drawing of the Sheffield pulse duplicator (1991) consisting of the following components [78]: fluid container (R), electromagnetic flow meter (EMF) and flow straighteners at both mitral and aortic valve sites (S), left atrium (At) and a mitral valve plane (Mv), mitral chamber (M), left ventricle (V), mitral (MV) and aortic valve (AV), aorta (A), a model of the systemic circulation (SA). Systemic arterial compliance is realized by a volume of trapped air and the peripheral resistance is controlled by a flow control valve (FCV). 105

Figure 43: Photograph of the pulsatile flow simulator of Sheffield (1991) [78]...... 105

Figure 44: The cardiovascular left heart simulator of Verdonck and colleagues. The left panel shows a photograph and the top panel shows a technical drawing of the original pneumatically driven model (1992) and the right panel illustrates the revised hydraulically actuated model (2006). The system is equipped with (1) reservoir, (2) tube, (3) two pulmonary veins, (4) left atrium, (5) mitral valve, (6) left ventricle, (7) aortic valve, (8) aorta, (9) resistance, (10) volume measurement reservoirs and (11) ultrasound probes. Adapted from [95] and [154]...... 107

Figure 45: The extended version by Segers and colleagues (1997) comprises the left heart model of Verdonck and colleagues (at the outer left side) which is connected to an extensive model of the arteries (middle and right panel). The left heart model comprises 1) lung reservoir, 2) pulmonary veins, 3) left atrium, 4) left ventricle and a partial aorta. The arterial tree model includes 5) the larger part of the aorta, 6) aorto-iliac bifurcation, 7) peripheral model, 8) veins, 9) venous return conduit, 10) electromagnetic flow meter, 11) venous overflow, 12) buffering reservoir and 13) pump. Adapted from [99, 155]...... 108

Figure 46: Overview of the experimental setup of Claessens and colleagues: (1) Left ventricular phantom (close up right), (2) Doppler transducer, (3) mitral valve, (4) pressure transducer, (5) proportional valve, (6) valve, (7) PMMA chamber, (8) preload reservoir and (9) device to measure ventricular volume. Adapted from [98]. 109

Figure 47: The Dual Activation Simulator (DAS) setup (left panel) and the left heart model (right panel) of Mouret and colleagues (2000) [88]...... 110

Figure 48: Workflow to obtain an anatomical-shaped left atrial and a left ventricular model: first, medical images are segmented (A), then a virtual solid model is created (B), next an aluminum core is milled (C) and finally a silicone model is produced (D). Adapted from [89]. 110

Figure 49: Two versions of the cardiovascular simulator of Marseille are shown. Left panel illustrates the PIV compatible version (2010) and right panel demonstrates the ultrasound compatible version (2013). The following components are indicated: echocardiographic probe (EP), left ventricle (LV), mitral valve (MI) and left atrium (LA). Adapted from [89] (left) and [159] (right)...... 111

LIST OF FIGURES

Figure 50: The Virginia Tech heart simulator (2004), a schematic setup overview (left panel) [160] and a photo (right panel) of the left heart model are shown [162]. 112

Figure 51: The Caltech's left heart pulsed flow simulator system (2006): A) Composition of the in-vitro setup, B) left ventricular model suspended in a transparent box full of water, C) close up of the ventricular model, the aortic and mitral valves and the inflow and outflow tract. Intraventricular flow patterns which are visualized by fluorescent microparticles which are illuminated by a laser sheet. D) Intraventricular streamlines of a transmitral jet which are obtained by PIV. Figures A, B and C are adapted from [163] and D from [166]. 114

Figure 52. Design of a bi-leaflet mitral bioprosthesis (top panel) composed of a saddle shaped annulus made of Nitinol and two leaflets made of pericardial tissue (bottom panel). Adapted from [165]. 114

Figure 53: The left ventricular model of Rasponi and colleagues (2006). This figure illustrates the fair agreement between numerical model (left panel) and the ventricle prototype (right panel) at the end diastolic phase. A prominent longitudinal deformation is realized using reinforcement of the silicone wall by circumferential bands. Adapted from [167]. 115

Figure 54: The Vascular Simulations Replicator developed by Carson and colleagues (2013) with (A) left atrium assembly, (B) brachiocephalic artery, (C) right common carotid artery, (D) subclavian artery, (E) aortic arch, (F) aorta and (G) left ventricle assembly. Adapted from [91, 97]. 116

Figure 55: The left panel illustrates a transparent rigid anatomically realistic and accurate representation of a human heart. The right panel illustrates a printed calcified aortic valve. Adapted from [168]. 118

Figure 56: The left panel illustrates a functional multi-material 3D printed calcified aortic valve which was built in the Heart Beat Simulator. The right panel shows the MRI compatible set up including the software and actuator, the MRI-compatible dive shaft and the MRI-compatible flow loop. Adapted from [92]. 118

Figure 57: The Double Diamond engineering design process. The red dots represent the following critical points: 'Problem', 'Problem Definition' and 'Solution'. Adapted from [177]. 137

Figure 58: Global design strategy of this dissertation following the Double Diamond design logic..... 139

Figure 59: Hydraulic/Pneumatic Models of the general design approach as basis for the actuation mechanism of a LV model. 140

Figure 60: Electric and Thermal Models of the general design approach as basis for the actuation mechanism of a LV model. 141

Figure 61: Trade-off table shows the comparison and evolution in function of the design criteria. It starts from the Honeycomb model and designates the Frame model as most favorable model (which led to the LVI model of Chapter 5). 143

Figure 62: The Honeycomb model. 144

Figure 63: The Inner Tire model. 145

<i>Figure 64: The Sixteen Segment model</i>	146
<i>Figure 65: The PorQpine model</i>	147
<i>Figure 66: The Marionette model</i>	149
<i>Figure 67: The Frame model (LV1 of Chapter 5)</i>	151
<i>Figure 68: Render of the thick-walled left ventricular model LV1 [180]</i>	159
<i>Figure 69: Our model consists of two main parts: (a) a valve plane and (b) a thick wall</i>	161
<i>Figure 70: Illustrative drawing of a 16-segment left ventricle model representing the 16 segments, which is often used in echocardiography. The model consists of three slices: (1) the basal and (2) the mid-ventricular slices which are uniformly divided into six segments and (3) the apical slice which is split into four equal segments. Reproduced from Han, 2004 [15]</i>	162
<i>Figure 71: The ventricular part consists of (a) a thin membrane including (f) a sealing ring, (b) flexible bars, (c) a supporting frame, (d) an O-ring, (e) an external shell, (g) eye pins, (h) supporting points, (i) modular discs and (j) connection to the piston pump</i>	163
<i>Figure 72: The valve plane contains (e) a valve plane, (a) two gates and positions, (d) two mechanical valves. Leakage between valves and valve plane is prevented by using (c) O-rings which are pressed by (b) a compression nut</i>	165
<i>Figure 73: The eye pins are designed with (a) an eye to connect the flexible bars, (d) a perforated flange to assure embedding in a tight connection with the flexible thin membrane, (e) a centering pin to provide (c) a constant membrane thickness of 3mm and (b) guiding planes to align them perpendicular to the membrane</i>	166
<i>Figure 74: The modular discs are designed with (d) a hole and (a) a cut-away in which a transverse spill (Figure 76) fits to allow easy connection using different types of flexible bars, (c) a cut-away to facilitate tightening and loosening of the flexible bars and (b) an adjusting ring to fit them together (e)</i>	166
<i>Figure 75: The practical realization of (a) our model, (b) the valve plane, (c) an assembly of the supporting frame and membrane without the flexible bars, (d) the external shell, (e) the supporting frame and (f) the membrane containing the embedded eye pins</i>	167
<i>Figure 76: The practical realization of (b) the flexible bars (a) connecting the membrane and the supporting frame by the use of the eye pins and (c) a modular disc</i>	169
<i>Figure 77: The practical realization of (a) the valve plane. It contains (d) the valve plane, (a and e) two gates and positions, (b and g) two mechanical valves. Leakage between valves and valve plane is prevented using (f) O-rings which are pressed by (c and e) a compression nut</i>	171
<i>Figure 78: Once (a) our model was built, we activated it using (f) a piston pump and connected it to a lumped hydraulic windkessel model of the vascular system, including (b) compliance, (c) resistance, and (d) preload. After that, ventricular pressure (p_{ventr}) and aortic flow (Q_{aorta}) were measured. In order to create a closed circuit, (e) an overflow and a circulation pump were added</i>	172

Figure 79: Compared with physiological data (dashed line), the experimental results (solid line) show that the model is able to generate realistic data in terms of end-systolic pressure (120 mmHg). Due to the too high afterload resistance, the aortic flow in our model (solid line) was low compared to (human) physiological data (dashed line) with a mean aortic flow of 1.6 l/min. 173

Figure 80: Wall deformation patterns of our model were fairly nicely demonstrated in terms of circumferential and longitudinal deformation: end-systolic (white line) and end-diastolic wall-deformation (white dotted line)..... 173

Figure 81: The contraction principles of the biological and the new artificial LV (left ventricle) muscle are illustrated. The contraction (systole) and relaxation (diastole) of a biological muscle take place along the direction of the cardiac muscle fibers, while the contraction (inflation) and relaxation (deflation) in a single contractile chamber of this new artificial LV muscle (a) take place perpendicular to its long axis (L_m : shortening of a biological muscle and $L_{single\ cell}$: shortening of a single contractile chamber). An actual three dimensional (3D) artificial LV muscle can be created by folding the 2D rectangular artificial LV muscle (b) to a cylindrical artificial LV muscle (c). When pressurized air is applied, the muscle cells contract perpendicularly to their longitudinal axis and the rectangular contour transforms into a parallelogram contour (b) with an angle $\beta_{torsion}$, a decrease in length (ΔL_{circum}) and in height (ΔL_{long}). Analogously, if both ends of the artificial muscle are welded together, the 3D cylindrical artificial LV muscle which is initially inactivated, will display torsion (with an angle equal to $\beta_{torsion}$) as well as radial, circumferential, and longitudinal deformation when activated (c). 177

Figure 82 Panel I: Circumferential and radial deformation is obtained by directing the contractile cells parallel to the LV long axis (axis of symmetry). A physical cylindrical 3D model demonstrates circumferential and radial deformation, in top-view at diastole (blue) and systole (red)..... 179

Figure 83: Pump performance. A slightly modified (see text) artificial LV muscle, namely LV2, was built to test the performance of the design as a functional pump. After connecting it to a lumped hydraulic windkessel model of the vascular system (including compliance and resistance), we measured pressure and flow. Our experimental results show that the model is able to generate realistic data in terms of pressure, flow and pressure-volume relationship..... 181

Figure 84: Geometry of the ViVitro left ventricular model [124]..... 187

Figure 85: Grooved patterns in CAD models of the LV3 model. 188

Figure 86: Design of the kernel according to the ViVitro left ventricular model geometry, which is used as a mold for the manufacturing of the actual model. The 24 fiber grooves at the inner side are clearly visible to enable accurate deposition of the fibers. 188

Figure 87: 3D printed LV3 kernels before (model 45°) and after (models 20° and 35°) colored PVA coating..... 189

Figure 88: LV3 models (fiber orientation 20°, 35°, and 45°) display torsional motion (17°, 22°, and 26°, respectively) as well as longitudinal and circumferential wall deformations by a given stroke volume of 80 ml. Left panel shows the front view of the model, while the right panel illustrates the view from the apex towards the base. Index: EDV: end diastolic volume and ESV: end systolic volume. 191

Figure 89: Geometrical design of MV2 with an identical mitral annulus of the Zygote CAD model...... 201

Figure 90: (A) Geometry, (B) aluminum matrix, and (C) in-vitro mitral valve models of mitral valve MV1 (left) and MV2 (right), respectively...... 203

Figure 91: Integration into the left heart model and close up of MV1 (left) and MV2 (right), respectively...... 204

Figure 92: Transmitral valve continuous wave Doppler signals show a Mitral Valve Pressure Half Time (MV PHT) of 102.90 and 71.14 ms and a (derived) EOA of 2.14 and 3.09 cm² for MV1 1 and MV2, respectively...... 205

Figure 93: Transmitral pressure differences during early diastole (TMPDe) of MV1 and MV2...... 206

Figure 94: a) Drawing of the valve model (VV) with different sections in the XY plain and pictures in open air at b) XZ and c) YZ position...... 211

Figure 95: Step-by-step plan to build the cylindrical three-dimensional VV model starting from a two-dimensional sheet...... 213

Figure 96: a) PIV setup of the valve model in a transparent box in open air, and b) the according PIV results...... 214

Figure 97: The components of the natural left heart (left panel) and the final LH1 model (right panel) with chordae tendineae (ChT) and pulmonary artery (PA)...... 221

Figure 98: Schematic overview of the manufacturing procedure of the LH model:..... 226

Figure 99: Custom-made rotation system: left panel CAD design, middle panel realization and right panel reduction and gears...... 228

Figure 100: The flexible monolithic LH1 model is demonstrated in different positions. . 229

Figure 101: Attachment of the chordae tendineae of MV2 (Chapter 8) to the papillary muscles of the LH1 model...... 230

Figure 102: The ViVitro left heart model and components of the mock loop. Adapted from [196]...... 231

Figure 103: The upper (A) and lower (B) rigid suspension plates are equipped with opposite extensions (1-3) to ensure a durable connection with the flexible LH1 model. These two parts are placed on top of each other (C) and sandwiches the flexible material of the left heart. Also, the upper suspension plate is equipped with a circular extension (4) which pressurizes the O-ring part of the sealing ring...... 233

Figure 104: Dimensions of the LH1 suspension system (C) including the upper (A) and lower (B) rigid suspension plates and the flexible plate in between (green) which is joined with the left ventricle model...... 234

Figure 105: Customized sealing ring (left bottom) is equipped with an integrated O-ring and an flat part. It's geometry is based on that of the ViVitro left ventricular model (left upper and right) [124]...... 236

Figure 106: This figure shows the LH1 model including the suspension system (6) and the venous site adapter (2). More details are given such as the LA (1), the aorta (3), the mitral

valve (MV1) (4), the aortic valve (5), and the LV model including the papillary muscles (7).
 237

Figure 107: Incorporation of the mechanical bi-leaflet aortic valve into the aorta by a 3D printed valve plane ring (white). 237

Figure 108: Experimental setup of the LHI model which is built into the ViVitro system.
 239

Figure 109: At the left side, the results of an echocardiographic examination is shown of the LHI model, that incorporates the physiologically normal-like mitral valve model (MV1) at the time of end systole (top) and end diastole (bottom). For the purpose of comparison, results of a healthy human left heart (male, 32 years old) are depicted at the right side. 240

Figure 110: Color Doppler measurements of the LHI model at the time of ventricular filling. Blue colors represent blood flowing towards the probe, while red colors correspond to blood flowing away from the probe..... 241

Figure 111: Starting from a 3D printed kernel (A), flexible thin-walled (B) and rigid transparent highly detailed models (C) are realized of the upper human airways. The red appearance of the kernel is due to the pigmented PVA coating to facilitate kernel removal and optimize surface smoothness..... 243

Figure 112: The PMMA model visually disappears when submerging it in a refractive index matched fluid. A transparent film with cross marks is placed at the backside of the model to check optical refraction. The blue arrow indicates the liquid level..... 244

Figure 113 Design and composition of the modular LH2 model with the arterial site adapter (1), the LA (2), the venous site adapter (3) (similar to the LHI model), the MV2 of Chapter 8 (4), the suspension system (5), and the LV model (6). 251

Figure 114: Design (left side) and suspension systems (right side) of the ViVitro system (§ 10.3.1) and left heart models LHI (§ 10.3.2) and LH2. See text for explanation of the numbers. 253

Figure 115: Design of the five LV models and the corresponding expected global wall deformation with α , the fiber angle (with respect to the LV long axis) and β , the torsional angle..... 254

Figure 116: Front view of the five LV models: the General model (G), the Longitudinal deformation (L), the Circumferential deformation (C), and the Torsional models 1 (T1) and 2 (T2). 255

Figure 117: The five LV models shown from the inside (top view). 257

Figure 118: Position of the dual sensor catheter in the LH2 model for the transmitral and intraventricular pressure difference measurements. 259

Figure 119: TMPDe values in function of HR (top panel) and SV (bottom panel) 260

Figure 120: IVPDe values in function of HR (top panel) and SV (bottom panel) 262

Figure 121: Overview of the in-vitro models developed in this dissertation..... 273

Figure 122: Active left ventricular muscle LV4 including a series of spirally arranged artificial muscle fibers (b). By applying pressurized air, an outer braid fiber structure is

expanded in radial direction by an internal flexible tube and meanwhile shortens in length (ΔL) (a)..... 281

Figure 123: Illustration of the FH1 and FH2, ideas for future in-vitro models of the total heart. This image shows the heart (A) which can be unwrapped to form a continuous ventricular myocardial band (B) according to the Torrent-Guasp concept [33]. Likewise, artificial muscle bands (C and D) can be constructed according to the LV2 or LV4 muscle designs and subsequently wrapped to form the in-vitro full heart models FH1 and FH2, respectively. Similar to the VV model, transparent sheet materials could be used to account for PIV compatibility..... 283

Figure 124: Illustration of the LV5, an idea for a future PIV compatible active LV model. 284

List of tables

<i>Table 1: Values of LV torsion in healthy humans [47-50].....</i>	<i>70</i>
<i>Table 2: Overview of the practical guidelines for designing a more natural accurate in-vitro left heart model.</i>	<i>130</i>
<i>Table 3: An overview of cardiovascular simulators is given in the context of practical guidelines. Different types of mitral valves are applied, mechanical (M), bioprosthetic (B) and post-mortem (P), but no in-vitro valve model yet. Index: ‘-’ absent, ‘~’ present but limited, ‘v’ present, ‘ ’ not applicable.....</i>	<i>131</i>
<i>Table 4: Fabrication procedure of the LHI model.</i>	<i>223</i>
<i>Table 5: A summary of the design criteria for the suspension system of the original ViVtiro system and the LHI model.</i>	<i>233</i>
<i>Table 6: Overview data of TMPDe varying SV while keeping HR constant (panel 1) and varying HR while keeping SV constant (panel 2). The mean values and SD’s per model are given for TMPDe.....</i>	<i>258</i>
<i>Table 7: Overview data of IVPDe varying SV while keeping HR constant and varying HR while keeping SV constant. The mean values and SD’s per model are given for IVPDe .</i>	<i>261</i>
<i>Table 8: A general overview of this dissertation is given. Index: ‘-’ absent, ‘v’ present, ‘~’ present but limited, ‘ ’ not applicable, M: mechanical mitral valve and IV: in-vitro mitral valve.</i>	<i>275</i>

